BNWL-1736
UC-80

11A

MEASUREMENT OF TURBULENT VELOCITY, INTENSITY AND SCALE IN ROD BUNDLE FLOW CHANNELS

D. S. Rowe

Battelle
Pacific Northwest Laboratories
Richland, Washington 99352

MAY 1973

Prepared for the U.S. Atomic Energy Commission under Contract AT(45-1):1830

BNWL-1736

NOTICE

PACIFIC NORTHWEST LABORATORY
operated by
BATTELLE
for the
U.S. ATOMIC ENERGY COMMISSION
Under Contract AT(45-1)-1830

AEC-RL RICHLAND, WASH.

BNWL-1736
UC-80 Reactor
Technology

MEASUREMENT OF TURBULENT VELOCITY, INTENSITY AND SCALE IN ROD BUNDLE FLOW CHANNELS

by

D. S. Rowe

Fluid and Energy Systems Section
Mechanical Engineering Department

May 1973

BATTELLE
PACIFIC NORTHWEST LABORATORIES
RICHLAND, WASHINGTON 99352

MEASUREMENT OF TURBULENT VELOCITY, INTENSITY AND SCALE IN ROD BUNDLE FLOW CHANNELS

D. S. Rowe

ABSTRACT

An experimental study was performed to investigate the effect of flow channel geometry on fully developed turbulent flow in "clean" rod bundle flow channels. This information was sought to obtain a better understanding of crossflow mixing between rod bundle subchannels.

The experimental measurements of turbulence velocity were performed with a two-component laser-Doppler velocimeter in approximately twice size models of nuclear reactor fuel rod bundle flow subchannels. The experimental flow models considered pitch-to-diameter ratios of 1.25 and 1.125. Axial components of velocity, turbulence intensity and Eulerian autocorrelation function were the primary measurements. A limited amount of lateral component turbulence intensity data was also obtained. The autocorrelation function provided an indication of the dominant frequency of turbulence and an estimate of the longitudinal macroscale by using Taylor's hypothesis. The experiments were performed in water with a Reynolds number range from 50,000 to 200,000.

The experimental results show that rod gap spacing (pitch-to-diameter ratio) is the most significant geometric parameter affecting

the flow structure. Decreasing the rod gap spacing increased the turbulence intensity, longitudinal macroscale, and the dominant frequency of turbulence. These turbulence parameters were found to be rather insensitive to Reynolds number. The turbulence parameters within a rod gap were found to be insensitive to the shape of adjacent subchannels and only slightly affected by the amount of lateral freedom allowed by the various size and shape of flow models considered in this study.

The results indicate that macroscopic flow processes exist adjacent to the rod gap. This includes secondary flows and increased scale and frequency of flow pulsations when the rod gap spacing is reduced. By considering the eddy diffusion coefficient to be related to the product of intensity and macroscale, the results show a compensating increase in eddy diffusion for a decrease in rod gap spacing. When interpreted in terms of crossflow mixing, the results are consistent with present crossflow mixing correlations.

TABLE OF CONTENTS

1.0 Introduction 1

2.0 Theoretical Aspects and Literature Survey 3

2.1 Turbulent Transport Processes 3

2.1.1 Diffusion by Lagrangian Turbulence Parameters 5

2.1.2 Eulerian Turbulence Parameters 7

2.1.3 Relationships Between Lagrangian and Eulerian Parameters 9

2.1.4 Classical Mixing Length Theory 11

2.1.5 Recent Developments in Turbulence Models 13

2.2 Turbulent Flow in Rod Bundles. 14

2.2.1 Crossflow Mixing 14

2.2.2 Rod Bundle Turbulence 20

3.0 Laser-Doppler Measurement Technique 30

3.1 Principles of Laser-Doppler Velocity Measurement . . . 30

3.2 Abilities and Limitations 34

3.2.1 Transit Time Broadening. 37

3.2.2 Aperture Broadening 37

3.2.3 Velocity Gradient Broadening 38

3.2.4 Temporal Turbulence Broadening 38

3.2.5 Spatial Turbulence Broadening 38

4.0 Experimental Program 40

4.1 Description of Test Section 40

4.2 Laser-Doppler Velocimeter 46

4.2.1 Optical System. 46

4.2.2 Traversing System. 49

4.2.3 Electronic Readout 49

4.3 Signal Processing. 55

4.4 Method of Data Acquisition. 58

4.5 Method of Data Reduction 61

5.0 Experimental Results 65

5.1 Subchannel Flow Structure 66

5.1.1 Maps of Velocity and Intensity 67

5.1.2 Effect of Rod Gap Spacing 76

5.1.3 Effect of Reynolds Number 86

5.1.4 Effect of Flow Model Size 95

5.2 Flow Structure in Rod Gap 100

5.2.1 Effect of Subchannel Shape 100

5.2.2 Effect of Lateral Freedom 105

5.2.3 Effect of Rod Gap Spacing 112

5.3 Channel Friction Factors 115

6.0 Discussion of Results 118

6.1 Comparison with Other Experimental Data 118

6.2 Secondary Flow Patterns. 136

6.3 Macroscale and Correlation Functions 147

6.4 Implications Regarding Crossflow Mixing 151

7.0 Accuracy of Experimental Data 158

7.1 Sample Volume Size and Location 159

7.2 Mean Velocity 162

7.3 Turbulence Intensity. 165

7.4 Turbulence Scale 169

7.5 Reproducibility 171

8.0 Conclusions and Recommendations. 173

9.0 Nomenclature 176

10.0 Bibliography 180

APPENDIX A - Data Reduction Computer Program 186

APPENDIX B - Tabulation of Reduced Data 193

MEASUREMENT OF TURBULENT VELOCITY, INTENSITY AND SCALE IN ROD BUNDLE FLOW CHANNELS

1.0 INTRODUCTION

The subchannel analysis method (48) has become an important tool for predicting the thermal hydraulic performance of rod bundle nuclear fuel elements. This "lumped-parameter" method considers a rod bundle to be a continuously interconnected set of parallel flow subchannels such as those shown in Figure 1.1. The subchannels are assumed to contain one-dimensional flow and are coupled to each other by crossflow mixing. For single-phase flow, turbulent crossflow mixing is dominant and is usually assumed to be an eddy diffusion process. By applying the conservation equations of mass, energy, and momentum to the interconnected flow channels, a set of coupled differential equations can be derived to describe the mass and thermal transport in the rod bundle. The resulting set of equations are usually solved by using a digital computer (8,55,56).

One of the important empirical inputs to the subchannel analysis method is the turbulent crossflow mixing. This is usually defined by experiment because a definitive correlating equation for crossflow mixing has not been developed. While several correlations exist (15,22,29,45,47,48,52,53) none have been proven to apply generally to all rod bundle geometries. The primary difficulty seems to be their inability to include geometric parameter effects on crossflow mixing.

This involves parameters such as rod gap spacing, subchannel shape and subchannel size. The development of a universal correlation, if there is one, is hampered by the incomplete description of turbulent transport processes in rod bundles and how it is affected by the bundle geometry. Flow processes from simple channels such as round tubes are often extrapolated to rod bundles with only partial success (47,48). There is a definite need to obtain a more fundamental understanding of the turbulent flow structure in bundles so that an improved understanding of crossflow mixing processes can be developed.

The objective of this work is to investigate experimentally the turbulent flow behavior in rod bundle subchannels and in particular those turbulence parameters of interest to the crossflow mixing process. As shown in the subsequent discussion those parameters are the intensity and scale of turbulence.

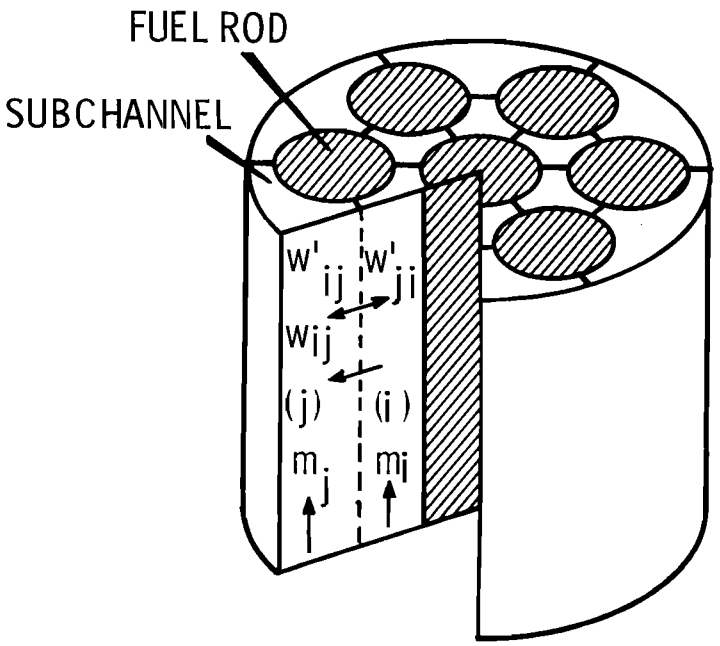

Figure 1.1. Method of subchannel selection.

2.0 THEORETICAL ASPECTS AND LITERATURE SURVEY

The following sections review two topics related to the objectives of this research. The first is a discussion of turbulent flow processes and those parameters of interest to the description of crossflow mixing processes in rod bundles. The second section presents a review of recent literature concerned with natural mixing in bundles and summarizes the present thinking concerning the turbulent crossflow mixing processes in bundles.

2.1 TURBULENT TRANSPORT PROCESSES

Two-dimensional scalar transport in the absence of sources or sinks can be described (23, p.25) by the equation

$$u \frac{\partial \Gamma}{\partial x} + v \frac{\partial \Gamma}{\partial y} = \frac{\partial}{\partial x} \left(D_\gamma \frac{\partial \Gamma}{\partial x} \right) + \frac{\partial}{\partial y} \left(D_\gamma \frac{\partial \Gamma}{\partial y} \right) \tag{2.1}$$

where Γ is the scalar quantity being transported and D_γ is the molecular diffusion coefficient. Instantaneous values of u, v, and Γ can be defined in terms of the time averages and fluctuating components

$$\Gamma = \bar{\Gamma} + \gamma \tag{2.2}$$

$$u = \bar{u} + u' \tag{2.3}$$

$$v = \bar{v} + v'. \tag{2.4}$$

By substituting these definitions into Equation (2.1) and performing a time average gives

$$\bar{u} \frac{\partial \bar{\Gamma}}{\partial x} + \bar{v} \frac{\partial \bar{\Gamma}}{\partial y} = \frac{\partial}{\partial x} \left(D_\gamma \frac{\partial \bar{\Gamma}}{\partial x} - \overline{u'\gamma} \right) + \frac{\partial}{\partial y} \left(D_\gamma \frac{\partial \bar{\Gamma}}{\partial y} - \overline{v'\gamma} \right) \tag{2.5}$$

This is identical to Equation (2.1) except for the added transport terms. Thus, the distribution of Γ by the mean motion is affected not only by the molecular diffusion but also by the turbulent convective motions defined by the double correlations $\overline{u'\gamma}$ and $\overline{v'\gamma}$.

Now consider the distribution of the scalar in the x direction, under conditions of $\bar{v} = 0$ and without axial mixing. Under these conditions Equation (2.5) becomes

$$\bar{u}\frac{\partial \Gamma}{\partial x} = \frac{\partial}{\partial y}\left[(D\gamma + \varepsilon_\gamma)\frac{\partial \bar{\Gamma}}{\partial y}\right] \qquad (2.6)$$

where the eddy transport coefficient ε_γ has been introduced by assuming that $\overline{v'\gamma}$ can be approximated by a gradient diffusion term. This is the form of the scalar transport equation often used as the basis for formulating lumped parameter crossflow mixing coefficients for the subchannel analysis method. The quantity in brackets represents the flux of transported scalar Γ. In this example and for further discussion, ε_γ is assumed to be a scalar quantity; however, in general it could be a tensor of the second order. At the present time Equation (2.5) cannot be effectively applied to the analysis of turbulent transport processes because of the incomplete description of ε_γ.

Eddy diffusion coefficients have classically been defined in terms Lagrangian turbulence parameters (23, p.42). Unfortunately it is difficult to measure the Lagrangian turbulence parameters since the measurements must be referred to a moving coordinate system following the fluid motion. There are, however, analogous Eulerian turbulence parameters (23,49) that can be measured in a fixed coordinate system.

While exact relationship between these two types of parameters do not presently exist, the measurement of Eulerian parameters can provide considerable insight into the turbulent flow processes. Eddy diffusion coefficients can also be represented in terms of classical mixing length theory (23, p.277,63). While mixing length theory has its limitations, it provides a "physical feel" for the mixing process. The following sections discuss these topics in more detail and discuss some recent work concerning new models for turbulence.

2.1.1 Diffusion by Lagrangian Turbulence Parameters

An estimate of the eddy diffusion coefficient can be made in terms of Lagrangian turbulence parameters by following Taylor's (61) treatment of turbulent diffusion by marked particles as reported by Hinze (23, p.45). The distance traveled in the y direction by a particle in homogeneous turbulence during time t can be expressed as

$$y(t_o+t) = \int_o^t v(t_o+t')\, dt' \qquad (2.7)$$

where v is the Lagrangian velocity and t_o is the starting time. By assuming that the flow field is homogeneous and by averaging with respect to a large number of particles with different starting times, the variance of y is

$$\overline{y^2(t)} = \frac{1}{T} \int_o^T y^2(t_o+t)\, dt_o. \qquad (2.8)$$

By substituting Equation (2.7) Equation (2.8) can be eventually written as

$$\overline{y^2(t)} = 2\, v'^2 \int_o^t \int_o^{t'} R_L(\tau)\, d\tau\, dt' \qquad (2.9)$$

where the Lagrangian correlation function is defined by

$$R_L(\tau) = \frac{\overline{v(t)v(t+\tau)}}{v'^2} \tag{2.10}$$

Equation (2.9) can be integrated partially to give

$$\overline{y^2(t)} = 2\, v'^2 \int_0^t (t-\tau)\, R_L(\tau)\, d\tau. \tag{2.11}$$

For short times $R_L(\tau) \simeq 1$ and $\sqrt{\overline{y^2(t)}} \simeq v't$, thus diffusion proceeds proportionally with time. For long time $R_L(\tau) \to 0$ as $\tau \to \infty$. Under these conditions Equation (2.11) becomes

$$y_2^2(t) \simeq 2\, v'^2 T_L t \tag{2.12}$$

where the Lagrangian macrotime scale is defined by

$$T_L = \int_0^\infty R_L(\tau)\, d\tau. \tag{2.13}$$

This is usually considered to be a measure of the longest time during which, on the average, a particle's motion persists in a given direction. For long diffusion times it is customary to define an eddy diffusion coefficient in analogy to diffusion of particles in a gas (23, p.48). The turbulent eddy diffusion coefficient is therefore defined as

$$\varepsilon = \frac{\overline{y^2(t)}}{2t} \tag{2.14}$$

or

$$\varepsilon = v'\Lambda_L \tag{2.15}$$

where the space macroscale is defined as

$$\Lambda_L = v' \, T_L \tag{2.16}$$

The product[1] of the Lagrangian fluctuating velocity and space macroscale defines the eddy diffusion coefficient.

Unfortunately, the Lagrangian parameters v', T_L and Λ_L are difficult to measure since they must be determined with respect to a moving flow field. They are usually inferred from turbulent diffusion experiments (1). It is natural to seek a relationship between these Lagrangian parameters and similar Eulerian parameters since the latter are measured with respect to a fixed coordinate system. Unfortunately a relationship between the two representations has not been found. Only by making rather gross simplifications and assumptions can some approximate relations be obtained.

2.1.2 Eulerian Turbulence Parameters

The longitudinal Eulerian spatial correlation coefficient is defined (23, p.37) by

$$f(x) = \frac{\overline{u' \, (x_o) u' \, (x_o + x)}}{\overline{u'^2}} \tag{2.17}$$

and the corresponding macroscale is defined as

$$\Lambda_f = \int_0^\infty f(x) \, dx \tag{2.18}$$

---

[1] It is worth noting that the introduction of a mixing promotor for the purpose of increasing the overall rate of mixing may not always serve this purpose. Such a mixing promotor must not be too fine, because the reduction in the coefficient of eddy diffusion by the decrease in the scale is often greater than the increase in value caused by the augmented intensity of turbulence.

where Λ_f is usually taken to be the longest connection distance between eddies. This could also be taken as the size of the largest eddies. Similar relationships exist for macroscales in other component directions.

It is also possible to define an Eulerian time correlation (23, p.39) as

$$R_E(\tau) = \frac{\overline{u'(t)\, u'(t-\tau)}}{\overline{u'^2}} . \tag{2.19}$$

The macro time scale is defined as

$$T_E = \int_0^\infty R_E(\tau)\, d\tau . \tag{2.20}$$

A convenient, but approximate, relationship exists between the longitudinal space and Eulerian time correlations (23, p.41). If the flow field is homogeneous, and if it has a constant mean velocity $\bar{u}$ in the x direction and if $u' << \bar{u}$ then

$$f(x) = R_E(\tau)$$

where

$$|x - x^o| = \bar{u}|t - t^o| \tag{2.21}$$

In other words, the space and time Eulerian correlations are equivalent and the macro scales can then be related by

$$\Lambda = \bar{u}\, T_E \tag{2.22}$$

This approximation, called "Taylor's hypothesis", greatly simplifies measuring procedures since $R_E(\tau)$ can be easily measured by using a signal correlator with a single input velocity signal. To distinguish between the true macroscale Λ_f the symbol Λ is used throughout the remainder of the discussion to denote the product $\bar{u}T_E$.

2.1.3 Relationships Between Lagrangian and Eulerian Parameters

It would be very helpful to have a relationship between Eulerian and Lagrangian turbulence parameters. This would allow data from Eulerian experiments to be transferred to a Lagrangian description of the flow. Unfortunately not much is known (23, p.52) about relationships to define the Eulerian equivalents for v', T_L and Λ_L. The situation for v' is not too bad for homogeneous turbulence where the value of v' could be set equal to the lateral component of turbulence velocity (23, p.49). In nonhomogeneous turbulence this would not be true but v' could be expected to be of the same order as u'.

Relationships between Λ_L and Λ_f are believed to exist; however, even for isotropic turbulence, such relationships apparently have not been found theoretically. According to Hinze (23, p.323), experimental evidence has shown that, at least at large Reynolds numbers, the overall shapes of the Langrangian correlation coefficient $R_L(\tau)$ and the longitudinal spatial correlation coefficient f(r) can be approximated by the exponential functions $\exp(-\tau/T_L)$ and $\exp(-r/\Lambda_f)$, respectively. Thus, these correlations have the same functional form. If this is assumed true, then the Lagrangian and Eulerian

integral scales must be proportional. Experiments referred to by Hinze (23, p.324) have shown that Λ_f/Λ_L ranges from about 0.5 up to about 0.8 for grid produced isotropic turbulence and in the case of pipe flow.

Baldwin and Walsh (1) discuss a relationship between what is called the Eulerian space-time correlation $R_E(x,\tau)$ and $R_L(\tau)$ where $x = \bar{u}\tau$. In this case $R_L(\tau)$ represents the decay of the peak values of $R_E(x,\tau)$ as x proceeds at the fluid velocity.

The Russian literature (2-7,27-28,59,60) contains some interesting work relating Lagrangian and Eulerian scales for temperature fluctuations by using space-time correlations. Bobkov, et al. (7), write the Lagrangian correlation for temperature fluctuations as

$$R_L(\tau) = R_E(\delta,\tau) \tag{2.23}$$

where δ and τ are related by

$$\delta = 0.8\ v'\tau \tag{2.24}$$

By assuming

$$R_E(\delta,\tau) = R_E(\delta,0)\ R_E(0,\tau) \tag{2.25}$$

and

$$R_E(\delta,0) = \exp\ (-\delta/L_E) \tag{2.26}$$

$$R_E(0,\tau) = \exp\ (-\tau/T_E), \tag{2.27}$$

The Lagrangian correlation can be written as

$$R_L(\tau) = \exp\left[-\left(\frac{1}{T_E} + \frac{0.8\ v'}{L_E}\right)\tau\right] \tag{2.28}$$

and the Lagrangian time macroscale is

$$T_L = \frac{1}{\frac{1}{T_E} + \frac{0.8\ v'}{L_E}} \tag{2.29}$$

where T_E is the time macroscale obtained from an autocorrelation function and L_E is the transverse space macroscale. This can be rearranged to give

$$\frac{T_L}{T_E} = \frac{1}{1 + \frac{0.8\ v' T_E}{L_E}} \tag{2.30}$$

Equation (2.30) has been found to apply to the central part of a tube for Reynolds numbers up to 216,000. The values of T_L/T_E are weakly dependent upon Reynolds number and have values on the order of 0.8.

Bobkov, et al. (5), extend the basic ideas given above to define eddy diffusion in noncircular channels.

2.1.4 Classical Mixing Length Theory

Mixing length theory has been used rather extensively in the past to model the transport properties of a turbulent flow. Even with the known deficiencies of mixing length theory, it provides a valuable physical description of turbulence transport processes. Consider the classical mixing length theory for scalar transport presented by Welty, et al. (63, p.323). Assume that a packet of fluid retains its mean value $\bar{\Gamma}$ while moving a distance L normal to the flow from its point of origin. Upon reaching its destination, the packet will differ

from its surroundings by an amount $\bar{\Gamma}|_{y\pm L} - \bar{\Gamma}|_y$. By assuming the mixing length is small this difference may be expressed by the approximation

$$\bar{\Gamma}|_{y\pm L} - \bar{\Gamma}|_y = \pm L \frac{\partial \bar{\Gamma}}{\partial y}\Big|_y \tag{2.31}$$

Now let the instantaneous scalar be written as

$$\Gamma = \bar{\Gamma} + \gamma \tag{2.32}$$

Since the fluctuating quantity γ is responsible for the scalar transfer in Equation (2.31),

$$\gamma = \pm L \frac{\partial \bar{\Gamma}}{\partial y} \tag{2.33}$$

The cross product term can be written as

$$\overline{v'\gamma} = \overline{v'L \frac{\partial \bar{\Gamma}}{\partial y}} \tag{2.34}$$

or

$$\overline{v'\gamma} = \overline{v'L} \frac{\partial \bar{\Gamma}}{\partial y} \tag{2.35}$$

From Equation (2.35) the product $\overline{v'L}$ is recognized as the eddy diffusion coefficient. The product of intensity and scale is the same result as obtained from Taylor's diffusion by continuous movements where L would be equivalent to the Lagrangian macroscale. The advantage of the mixing length representation is that L physically represents the lateral distance traveled by the fluid packet moving at velocity v'. This distance is determined by the turbulence scale and more specifically by the lateral macroscale. It could be expected that this scale

would also be of the same order but probably smaller than the size of longitudinal eddies in the turbulent core away from the wall.

2.1.5 Recent Developments in Turbulence Models

With the increased use of high speed digital computers for solving the transport equations, there has been considerable effort devoted to the formulation of turbulence models. Ng and Spalding (40) present a brief review of turbulence models where they show a progression of model developments that started with Kolmogoroff (34) who characterized the local properties of turbulence by formulating a partial differential equation for the energy of the fluctuating motion and the average frequency of this motion. Prandtl (43,44) proposed a somewhat simpler model where only the differential equation for the turbulence energy was solved while deducing the local average length scale from an empirically derived algebraic relation. Rotta (49) proposed obtaining a length scale from a differential equation while also using a differential equation to obtain the turbulent shear stress. Several other models are mentioned that consider variations on the above methods. Ng and Spalding's (40) approach to turbulence modeling is to consider the eddy viscosity to be the product of two characteristic local quantities of turbulence, namely, the product of the turbulence kinetic energy, defined as $k' = 1/2\ (\overline{u'^2} + \overline{v'^2} + \overline{w'^2})$, and an integral scale of turbulence. They develop two differential equations - one for the product and another for the kinetic energy of turbulence only. Their computations for the configurations of a flat-plate boundary-layer, pipe-flow,

flow in a plane-walled channel and a plane wall-jet compare quite well with experimental data. The important point brought out by their approach is that both scale and turbulence energy are fundamental parameters necessary for the understanding of turbulent flows. These quantities can also be defined in terms of equations that describe their generation, transport and dissipation.

2.2 TURBULENT FLOW IN ROD BUNDLES

The previous section has shown that eddy diffusion and therefore crossflow mixing is closely related to the turbulence intensity and scale. Unfortunately not much is known about the details of these parameters in rod bundles. What is known has been inferred from crossflow mixing experiments and from studies of turbulent flow in simple ducts. Only very recently have there been any data concerning turbulence in rod bundles.

2.2.1 Crossflow Mixing

Turbulent crossflow mixing is very important to the thermal-hydraulic performance of rod bundles as it provides an important mechanism to equalize temperatures throughout the bundle. Crossflow mixing is measured experimentally and then correlated by using appropriate dimensionless parameters. Although these semiempirical correlations are usually quite accurate for a particular experimental configuration, no definitive general correlation has been developed for crossflow mixing in spite of the many recent publications on the subject (48).

The subchannel analysis method is used to incorporate the effects of crossflow mixing into the analysis of rod bundles. The mixing between subchannels is usually assumed to be of the eddy diffusion type as defined by Equation (2.6) where the scalar transport per unit length can be written in terms of the difference equation

$$\rho s\varepsilon \frac{\partial \bar{\Gamma}}{\partial y} = \rho s\varepsilon \frac{\Delta \bar{\Gamma}}{\Delta y} \tag{2.36}$$

and the turbulent crossflow mixing per unit length is defined as

$$w' = \frac{\rho s\varepsilon}{\Delta y} \quad . \tag{2.37}$$

Dividing Equation (2.37) by GD gives

$$\frac{w'}{GD} = \left(\frac{\varepsilon}{UD}\right)\left(\frac{s}{\Delta y}\right) \tag{2.38}$$

This dimensionless equation gives the mixing parameter w'/GD in terms of the inverse turbulent Peclet (ε/UD) number and a geometric ratio parameter ($s/\Delta y$). The group w'/GD has been called the mixing Stanton number based on hydraulic diameter. Many correlations use gap spacing for this dimension which gives the equivalent form

$$\frac{w'}{Gs} = \left(\frac{\varepsilon}{UD}\right)\left(\frac{D}{\Delta y}\right) \tag{2.39}$$

An early assumption (48,56) regarding crossflow mixing was that the right side of Equation (2.39) was nearly constant or weakly dependent upon Reynolds number with the implication that w' was proportional to gap spacing. While the form was valid for a single experiment, it was not found to be valid for different rod gap spacings. Experiments

in water by Rowe and Angle (50-52) showed that mixing between two parallel subchannels was about the same for a gap spacing of 0.020 inches and 0.085 inches for 0.563 inch diameter rods. Thus experimental observation contradicted the assumption that mixing was proportional to gap spacing. The authors concluded (52, p.36) that "some phenomena in addition to eddy diffusion is responsible for the weak influence of spacing on subchannel mixing rates". These experiments also showed that mixing was less between square-square subchannels as compared to square-triangular subchannels. This observation supported the concept of eddy diffusion because reduced mixing would be expected if the diffusion length was longer.

At about the same time Rapier (45) independently arrived at similar experimental results for mixing through a single gap and multiple gaps. For a rounded gap entrance as in a rod bundle he did not find a detectable reduction of mixing with reduction of gap size. For experiments with sharp edge (slit orifice) gap he found only a factor of 2 reduction in mixing for a factor of 8 reduction in gap width.

In 1968 Rogers and Todreas (48) presented a comprehensive review of crossflow mixing in rod bundles. Their paper summarized the results of many prior studies and put the various proposed mixing correlations on a common basis by using consistent terminology and nomenclature. A portion of their paper was devoted to the effect of gap spacing on mixing in rod bundles. The correlation forms available at that time generally considered eddy diffusivity to be expressed in the form

$$\frac{\varepsilon}{\nu} \propto Re\sqrt{f} \tag{2.40}$$

from which it is seen that

$$\frac{\varepsilon}{UD} \propto \sqrt{f} \tag{2.41}$$

Since the friction factor was weakly dependent upon Reynolds number, so was the inverse turbulent Peclet number. The correlations also dealt with a geometry factor[2] $D/\Delta y$ in several different ways. The result of the more successful correlations was that Δy changed about as fast as the gap spacing thus giving a mixing rate that was weakly dependent upon gap spacing. No correlation was considered to be definitive for all rod bundle configurations.

Since the paper of Rogers and Todreas, several additional experiments have been performed and correlations prepared. Skinner, et al. (58) investigated gas mixing in a 7-rod bundle. Although they did not vary gap spacing, they found (58, p.272) "the rate of transfer of nitrous oxide through the gap is greater than can be accounted for by turbulent diffusion alone." Away from the gap Skinner found that (58, p.272) "the behavior could be explained by turbulent diffusion using an acceptable value of eddy diffusivity. The higher rate of diffusion in the gap region is attributed to a secondary flow."

Galbraith (14) performed a mixing experiment where he varied gap spacings over a range from 0.011 to 0.220 inches for 1 inch diameter

---

[2] z_{ij}/d using Rogers and Todreas notation.

rods. He found a significant reduction in mixing at the 0.011 spacing; however, at spacings of 0.028 and above, mixing increased only modestly with increased gap spacing. At a Reynolds number of 30,000 mixing increased by 60% for a nearly 8 fold increase in gap spacing.

There has been some attempt to obtain a better mixing correlation based upon the emerging physical description of the mixing process. Rowe (54) used the observations from his experiments to formulate a correlation of the form

$$\frac{w'}{GD} = \frac{\varepsilon}{UD} \quad \frac{\Delta y^*}{\Delta y} \quad \frac{s^*}{\Delta y^*} \tag{2.42}$$

where the ratio $\Delta y^*/\Delta y$ is the centroid (diffusion) length ratio (1.0 for square-square; 0.79 for square-triangular) and $s^*/\Delta y^*$ is ratio of the effective gap spacing to the centroid distance. The value of s^* can be larger than s which is also the assumption made by Rapier (45). Rowe and Angle found that (52, p.35) "eddy diffusion could explain the effect of subchannel shape, but it could not explain their weak gap spacing effect". This is the basis of the $(\Delta y/\Delta y^*)$ term. They also postulated the existence of macroscopic transverse flow fluctuations which would augment eddy diffusion near the gap. They assumed a mixing mechanism where the eddy diffusion in the subchannel was controlling and the gap was relatively nonrestrictive because of the assumed macroscopic flow processes. By using Equation (2.42) all of their previous mixing data for three independent experiments can be correlated well by using a single value for $(s^*/\Delta y^*)$ and $\varepsilon/UD \propto R_e^{-0.1}$. No other data are considered for this correlation.

Ingesson (29,30) and his coworkers formulated a mixing correlation based upon their work and much of the available mixing data including the recent data of Galbraith (14,15), Hetsroni (22), and Van der Ross and Bogaardt (62). The form of Ingesson's correlation is

$$\frac{w'}{GD} = \left(\frac{\varepsilon}{UD}\right)\left(\frac{s}{\Delta y}\right) Y \qquad (2.43)$$

where Y is a correction factor, Δy is the centroid distance, s is the gap spacing and

$$\frac{\varepsilon}{\nu} = \frac{R_e}{20}\sqrt{f/2} \; . \qquad (2.44)$$

The correction factor Y corrects for the assumed eddy diffusivity correlation and the ratio of the centroid distance to some diffusion length. His correlating variable $Y \to \infty$ as $p/d \to 1$ and decays rapidly as p/d increases. The combination of $s\,Y/\Delta y$ therefore results in a mixing rate that is at most modestly affected by gap spacing and channel geometry.

Rogers and Rosehardt (47) recently evaluated their earlier mixing correlations in light of the previously described data. They found it necessary to use two equations to correlate the available data. One is for bundle geometries and the other for simple geometries. In either case their correlation contains the features described previously for Ingesson's correlation. The mixing rate is rather insensitive to the gap spacing but depends upon the shape of the channel in a way related to the centroid-to-centroid distance.

Rogers and Rosehardt (47) also make some inferences regarding structure of turbulence in the gap regions of fuel bundle. By defining eddy diffusivity as $\varepsilon = v'\Lambda_L$ and by using their correlation, they conclude that the ratio of Λ_L/s is only a function of gap spacing and subchannel equivalent diameter. For s/d above 0.1, Λ_L is essentially proportional to the gap spacing. Their reasoning is based upon the assumption that the gap region controls the mixing between channels. This is somewhat contradictory to the features of their correlation. If centroid-to-centroid distance is an important parameter and gap spacing is not, it would seem to indicate that diffusion through the gap is not controlling.

Although the recent and more accurate correlations for crossflow mixing show a weak dependence of mixing rate with gap spacing, a satisfactory explanation of this phenomena has not been demonstrated by experimental data. This is due to the lack of understanding of the turbulence structure in rod bundles.

2.2.2 Rod Bundle Turbulence

The presently incomplete understanding of turbulent flow and crossflow mixing in bundles is largely due to the lack of experimental measurements of turbulence in rod bundles. Most of what is known has been inferred through analysis of measured velocity distributions and mixing experiments of the type previously discussed.

One of the earliest analyses of turbulent flow through rod bundles was performed by Diessler and Taylor (11). They applied expressions for eddy diffusivity of momentum, which were verified in tubes, to

calculate velocity profiles normal to a wall. One of their primary assumptions was to neglect circumferential eddy diffusion. With this assumption the analysis was limited to channels with slowly varying shape. Calculations based on this method deviated considerably from experimental data in channels of rapidly varying shape. Wall shear stress was overpredicted because of the smoothing effect of large circumferential turbulence is neglected.

Ibragimov, et al. (26), proposed a procedure similar to that of Diessler and Taylor for calculating wall shear stress and velocity profiles in complex channels; however, they considered two momentum terms in a manner similar to that reported by Hinze (23, p.288). The first was a gradient transfer of momentum due to molecular friction and small-scale turbulent eddies. The second was a convective transfer of momentum due to large-scale motion of eddies. The turbulent transverse shear was given by

$$\rho \overline{u'v'} = - (D + \varepsilon) \frac{\partial \bar{u}}{\partial y} + \rho \overline{u'V'} \qquad (2.45)$$

where V' is the pulsation velocity of large eddies in the y direction. These authors state that (26, p.733) "These two forms of momentum transfer differ considerably. Whereas the gradient transfer is determined by the local characteristics of the flow, the convective transfer depends mainly on the geometric features of the channel as a whole.

In complex channels the effect of large-scale eddies on the velocity field should appear most strongly in the directions in which the

velocity varies slowly (along the channel perimeter). Along the normal to a channel perimeter, however, convective transfer plays a small part since the velocity gradient is very high and hence so is the gradient of momentum.

Convective transfer should appear more strongly in channels with a sharply varying cross-sectional shape (e.g. close-packed rods), when exchange between eddies of considerably different velocities may occur."

The above comments are interesting as they offer an independent view concerning the possible existence of macroscopic turbulent flow processes in complex channels. By using these concepts the authors develop a computational method for calculating wall shear stress and velocity distribution. They show excellent agreement with experimental data.

Subboten, et al. (60), recently published a paper that experimentally reinforces the concept of transverse macroscopic flow processes. They measured velocity profiles in a pair of triangular pitch flow channels for p/d of 1.05, 1.10 and 1.20. They performed the measurements in air by using small pitot tubes. The velocity profiles at p/d = 1.05 showed distinct curvature of isovels (lines of constant velocity) due to the existence of secondary flows as shown in Figure 2.1. This behavior was not observed at p/d of 1.10 and 1.20. This tends to be consistent with the ideas of Ibragimov because the shape varies more rapidly at p/d = 1.05 than for p/d of 1.10 or 1.20. It is interesting that the inferred secondary flow patterns are not symmetric about all lines of symmetry in the flow model.

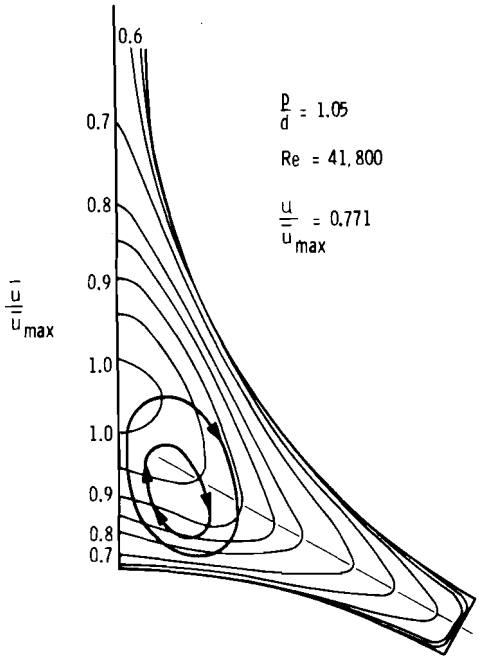

Figure 2.1. Secondary flow pattern indicated from the data of V. I. Subbotin, et al.

Subsequent to the completion of the experimental work reported herein, Kjellström (32,33) reported what is believed to be the first known measurements of rod bundle turbulence parameters available in the open literature. He performed an experimental and theoretical study of turbulent flow in a rod bundle of triangular array with a pitch-to-diameter ratio of 1.217. The experiments included measurements of pressure drop and local distributions of axial and secondary velocities, turbulence intensities, Reynolds stresses and wall shear-stress. The results of the turbulence measurements were used for calculation of local eddy diffusivities. He found that the eddy diffusivity (momentum) is strongly nonisotropic - the diffusivity in

the peripheral direction being a factor 5 to 1.5 higher than that in the radial direction. The higher value applies to the wall region and the lower one to the core of the flow. His theoretical studies included the calculation of the distributions of the axial velocity and the kinetic energy of turbulence. A modified version of Prandtl's energy length model (44) in combination with Buleev's (10) method was used for estimating the turbulent length scale. The report presents an extensive review of previous studies for predicting velocity distributions in rod bundles.

The experiments performed by Kjellström investigated the turbulent flow in an enlarged flow channel formed by nine 4.77 inch diameter tubes on a triangular array. Most of the experimental measurements were made in air with a hot wire anemometer just upstream from the discharge plane located at 129 channel average hydraulic diameters from the inlet.

The experimental observations of secondary flows and turbulence intensity are of particular interest to this study. Secondary flow velocities were found to be less than 1% of the axial velocity, although the data had considerable scatter. The secondary flow pattern midway between the gap and subchannel center generally showed flow moving along the centerline toward the gap and away from the gap along the rod surface. No significant secondary flows were observed in the gap or near the subchannel center.

Figure 2.2 shows the measured turbulence intensities and compares the results with the data of Laufer (36,37). The data compare quite well when normalized to the shear velocity defined by

$$u^* = \sqrt{\tau_w/\rho} \tag{2.46}$$

where τ_w is the wall shear stress which can be defined through the relationship

$$f = \frac{8\,\tau_w}{(\rho U^2)} \quad . \tag{2.47}$$

Combining Equations (2.46) and (2.47) gives the relationship

$$\frac{u^*}{U} = \sqrt{\frac{f}{8}} \tag{2.48}$$

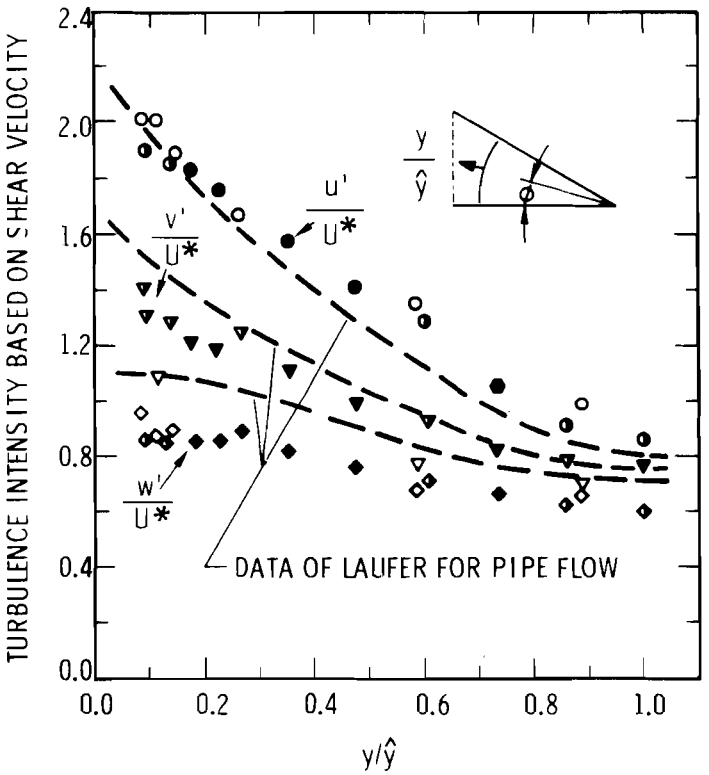

Figure 2.2a. Experimental turbulence intensity data of Kjellström at $\phi = 0$ compared to the data of Laufer.

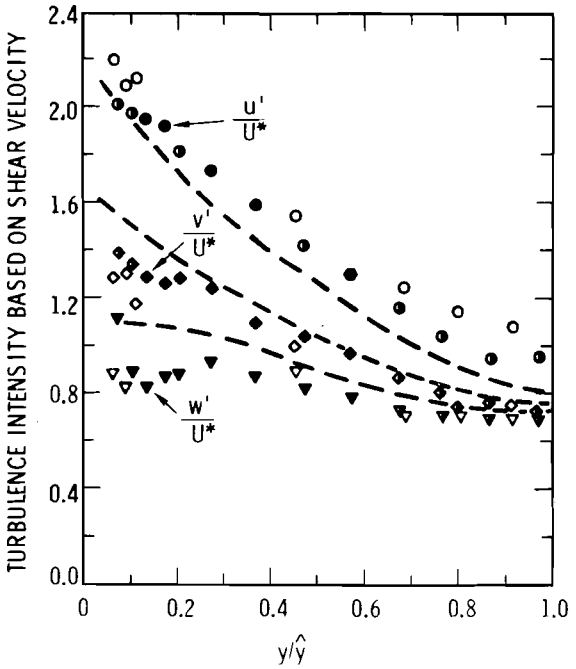

Figure 2.2b. Experimental turbulence intensity data of Kjellström at ϕ = 18° compared to the data of Laufer.

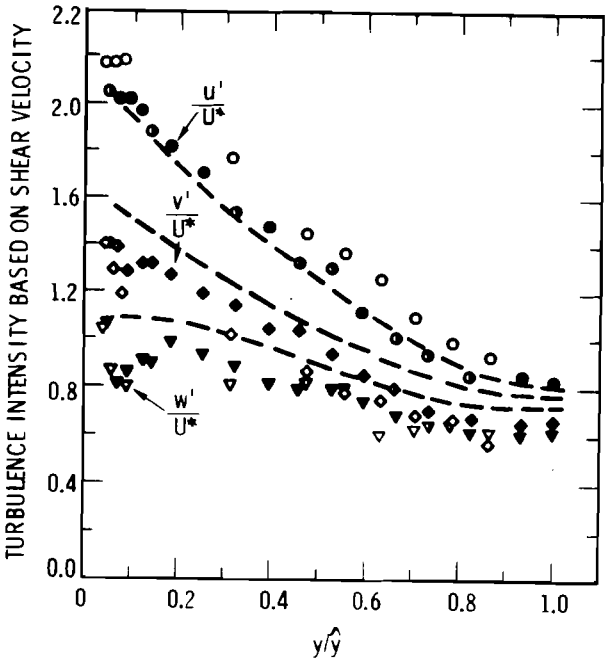

Figure 2.2c. Experimental turbulence intensity data of Kjellström at ϕ = 30° compared to the data of Laufer.

Kjellström also compared his measured velocity profiles with the analytical predictions by Eifler and Nijsing (13) and found excellent agreement with the universal velocity distribution proposed by Eifler. The experimental data also indicate secondary velocities on the order of 0.25% of the axial velocity with a pattern the same as assumed by Eifler and Nijsing. This secondary flow moved toward the rod gap along a centerline and back along the rod surfaces then out to the central part of the subchannel.

The results of Kjellström's study could not explain the high mixing factors recommended by Ingesson and Hedberg (29). The experimental data indicated a value of Y = 1.6 whereas Ingesson and Hedberg's correlation would indicate Y = 7.9 for the geometry considered.

Kjellström has also undertaken a rather ambitious project to develop a mathematical description of turbulent flow in rod bundles. He has formulated a set of three-dimensional transport equations for the flow field by using an eddy diffusion model based on Prandtl's model where the eddy diffusion is represented by

$$\varepsilon = K \ell \quad k' \tag{2.49}$$

where k' is the kinetic energy of turbulence and ℓ is a length scale defined by using the semiempirical model of Buleev (10). Various values of K are used for the different coordinate transport directions. The length scale ℓ is assumed to be known from purely geometric considerations. This contrasts with the approach of Ng and Spalding (40)

where ℓ is a property of the turbulent flow. Kjellström has had partial success in actually performing numerical calculations of the flow field. His results are generally promising as far as the distribution of turbulence kinetic energy and axial velocity are concerned. However, the axial velocity tends to be too low in some regions which is attributed to a coarse grid size near the wall. The calculations were also only possible (convergent) when the secondary velocities were held to zero.

No actual experimental data are known to exist concerning turbulence scale in rod bundles. Several theoretical calculations of scale in noncircular channels have been performed. Kjellström (32,33) estimated the length scale of turbulence by using the assumption of Buleev (10) which gives a scale estimate of

$$\frac{1}{\ell} = \frac{1}{2} \int_0^{2\pi} \frac{1}{y} \, d\phi \tag{2.50}$$

where y is the distance from the point under consideration to the wall. For pipe flow the above equation gives $\ell = D/2\pi = 0.16\ D$. An estimate for tubes as reported by Kjellström, is given by Prandtl's equation

$$\frac{\ell}{D} = 0.07 - 0.04 \left(\frac{2r}{D}\right)^2 - 0.03 \left(\frac{2r}{D}\right)^4 \tag{2.51}$$

which gives $\ell/D = 0.07$ at the center of a pipe. Kjellströms estimates for tricusp channels were generally on the order of $\ell/D = 0.05$.

Kashcheev and Nomofilov (31) performed theoretical estimates of turbulence scale in closely packed rods. Their estimates were

generally of the magnitude $\ell/D = 0.03$. The calculated distribution was nearly cosine which was not flat as indicated by their comparison with two data points of Buleev, et al. (10).

All of the above estimates of scale are considerably less than the size of the flow channel characteristic diameter D. Estimates of the longitudinal macro space scale are made in the present study by using Taylor's hypothesis. Since the lateral and longitudinal scales in tubes are known to be quite different because of elongation in the direction of flow, similar results could be expected in bundles.

3.0 LASER-DOPPLER MEASUREMENT TECHNIQUE

Since the laser-Doppler technique is new to fluid flow research in rod bundles, this chapter gives a brief account of its theory and applications.

The recent development of laser-Doppler technique for measuring fluid velocity provides a new and important tool for performing fluid flow research. Since the velocity measurement is performed with light beams, no probe disturbs the flow. Furthermore, the fluid volume over which the measurement is performed is very small. The measurement point can also be put into very small spaces and measurements can be performed where the laser beams can pass through the flow channel without distortion.

3.1 PRINCIPLES OF LASER-DOPPLER VELOCITY MEASUREMENT

The laser-Doppler velocity measurement technique uses the principle that coherent laser light scattered from a moving particle experiences a frequency shift (65). This phenomena, known as the Doppler shift, is detected by optical heterodyne mixing of the scattered light with the reference light from the same laser. The resulting heterodyne or "beat" frequency is equal to the difference of the frequencies of the reference and scattered beams. The velocity can be calculated directly by measuring this frequency shift with a given geometric arrangement of the optical detection apparatus.

Several authors have discussed derivation of the basic Doppler shift equation. Using a variety of approaches (30), they all derive

the same equation for the condition that the particle velocities are much less than the velocity of light.

The equation relating the Doppler shift to the velocity and geometry is given by

$$f_D = \frac{1}{2\pi} \bar{K} \cdot \bar{V} \tag{3.1}$$

where f_D is the Doppler shift frequency and $\bar{V}$ is the velocity. $\bar{K}$ is the scattering vector given by

$$\bar{K} = \frac{2\pi n}{\lambda_o} (\bar{r}_s - \bar{r}_o) \tag{3.2}$$

where $\bar{r}_s$ is the unit vector for scattered light, $\bar{r}_o$ is the unit vector for the reference light and λ_o is the "in vacuo" wavelength of the laser light. Combining Equation (1) and (2) gives

$$f_D = \frac{n}{\lambda_o} \bar{V} \cdot (\bar{r}_s - \bar{r}_o) \tag{3.3}$$

which is a more convenient equation for computation. The Doppler shift is seen to depend upon the "in vacuo" wavelength of the laser light, the index of refraction of the medium, the velocity and the optical geometry. While a variety of optical schemes can be used to perform the optical heterodyning presently required to detect the Doppler shift, the basic idea is shown in Figure 3.1. The laser beam is focused to a point in the fluid. The light passing directly through the fluid is not scattered and is therefore available as the reference light. Light scattered within a solid angle centered at angle θ is gathered by a lens and is combined with the reference light at the photomultiplier tube by adjusting the appropriate mirrors, lenses and beam splitters.

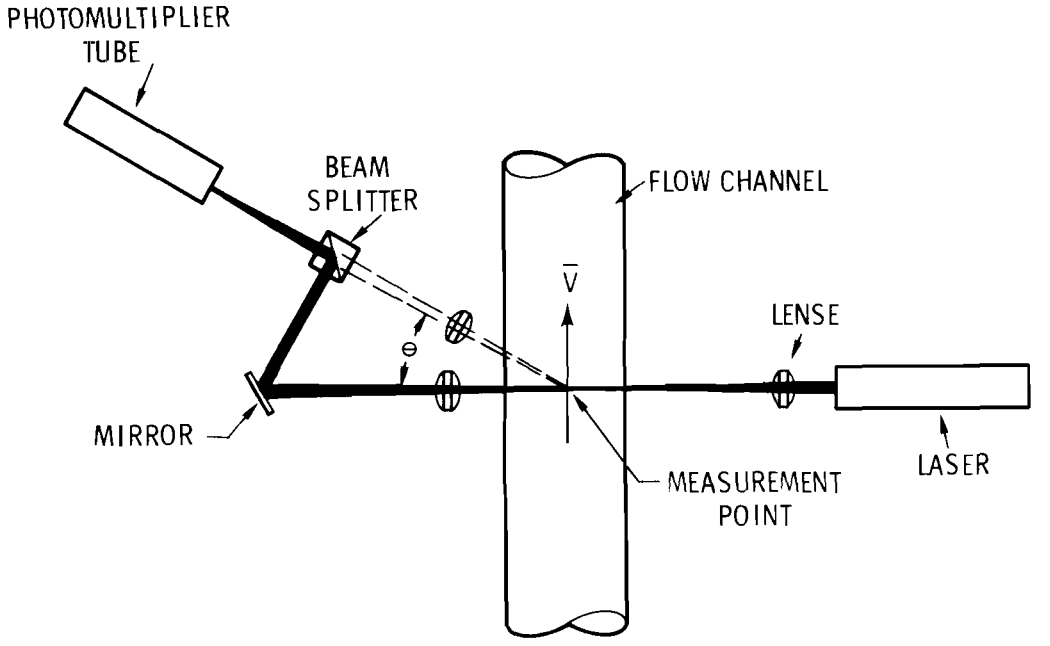

Figure 3.1. Laser-Doppler velocimeter optical system.

The light intensity of the two beams is optimized for efficient heterodyning by using an attenuating filter to reduce the reference beam intensity before optical mixing.

The Doppler signal measured by the photomultiplier tube can be determined by considering the reference and scattered light to be monochromatic with angular frequency ω_1 and ω_2, respectively. Let their electric field be given by

$$E_1 = E_{10} \cos \omega_1 t \tag{3.4}$$

$$E_2 = E_{20} \cos \omega_2 t \tag{3.5}$$

The current from the photomultiplier tube is proportional to the square of the electric field incident upon it; therefore,

$$i \alpha (E_1 + E_2)^2 \tag{3.6}$$

or

$$i \alpha (E_{10} \cos \omega_1 t + E_{20} \cos \omega_2 t)^2 \tag{3.7}$$

Expanding this gives

$$i \alpha \frac{E_{10}^2 + E_{20}^2}{2} + \frac{E_{10}^2}{2} \cos 2 \omega_1 t + \frac{E_{20}^2}{2} \cos 2 \omega_2 t + E_{10} E_{20} \cos (\omega_1 + \omega_2)t + E_{10} E_{20} \cos (\omega_1 - \omega_2)t \tag{3.8}$$

The first term represents the dc component of the signal. The three middle terms contain frequencies about twice that of the laser light. Since the photomultiplier can only respond to frequencies up to a few hundred MHz, these high frequency terms do not contribute to the current. The last term represents the Doppler frequency and is the ac part of the photomultiplier tube current. For most applications it ranges from a few kHz up to maybe 100 MHz.

Several methods may be used to measure the Doppler frequency as detected by the photomultiplier tube. The simplest is to observe the Doppler signal on an oscilloscope and determine the frequency from the scale calibration. This is of limited value because the signal cannot be read with an accuracy greater than about 10%. The scope is an indispensable accessory, however, because it can be used to aid optical alignment, to perform quick velocity surveys of the flow field, to help optimize the Doppler signal and to indicate relative levels of turbulence. The most common method for measuring the mean Doppler

frequency is to analyze the photomultiplier tube output with a spectrum analyzer. The peak of the Doppler spectrum is taken to be the mean frequency. The Doppler spectrum also contains information concerning turbulence and Brownian motion; however, no satisfactory method has been devised to extract this information directly from the output of a spectrum analyzer. Considerable effort has been directed toward obtaining a direct Doppler frequency-to-voltage conversion since this provides instantaneous values of velocity that are analogous to those obtained from hot-wire anemometers. Several successful schemes are in operation and are commercially available; however, they all have operational limitations. They must be able to process very noisy Doppler signals that contain broadening due to frequency, amplitude and phase modulation. The noise originates from both electronic noise and from light scattering process itself.

3.2 ABILITIES AND LIMITATIONS

The laser-Doppler velocity measuring technique has the advantage of not disturbing the flow field. This is a significant improvement over previous methods such as hot-wire anemometers and pitot tubes.

The laser-Doppler technique also allows the sample volume to be positioned easily in the flow channel by traversing the optical components. Measurements can be made in regions where an undisturbed optical path exist between the laser and the receiving optics. This requires that flow channel windows be flat and clean.

The laser-Doppler technique can also provide very fine spatial resolution through the selection of suitable optics. The optical resolution of the laser-Doppler velocimeter is determined by the intersection of the scattered and reference light beams. An estimate of the effective diffraction limited beam diameter at the focal point is given by

$$d = 2\sigma = \frac{2}{\pi}\frac{\lambda f}{D} \tag{3.9}$$

where σ is the standard deviation of intensity, D is the beam diameter at the $1/e^2$ intensity points of a Gaussian beam at the lens and f is the focal length of the lens. Small beam diameters are achieved by small values of f/D. This means a short focal length lens produces a small beam diameter thus a small sample volume.

The angular position of the reference and scattered light beams also affects the size of the sample volume. The smallest volume is achieved when the scattered light is detected at right angles to the reference beam. Since the light is primarily forward scattered, this arrangement is not always satisfactory because of low scattered light intensity. Most laser-Doppler systems operate with forward light scattering with the angle θ less than about 45°. This gives a sample volume elongated in the direction of the laser beam. Mathews and Rust (39) have shown that additional elongation also occurs because of the refractive index effect in water.

Although very small sample volumes can be obtained through a suitable choice of optical parameters this is often not desirable.

George and Lumley (16,17,18) have shown that an optimum sample volume exists for turbulence measurements, however, regardless of the volume size there is a limit to the possible resolution of turbulence with a laser-Doppler velocimeter. According to the theory developed by George and Lumley, the Doppler ambiquity broadening causes a constant noise base level on the power density spectrum of turbulence energy as illustrated in Figure 3.2. The determination of turbulence intensity (or energy) therefore depends upon the importance of the noise tail at high frequency. If the base level is made low by using an optimum sample volume size then it may be of little concern. If it is not,

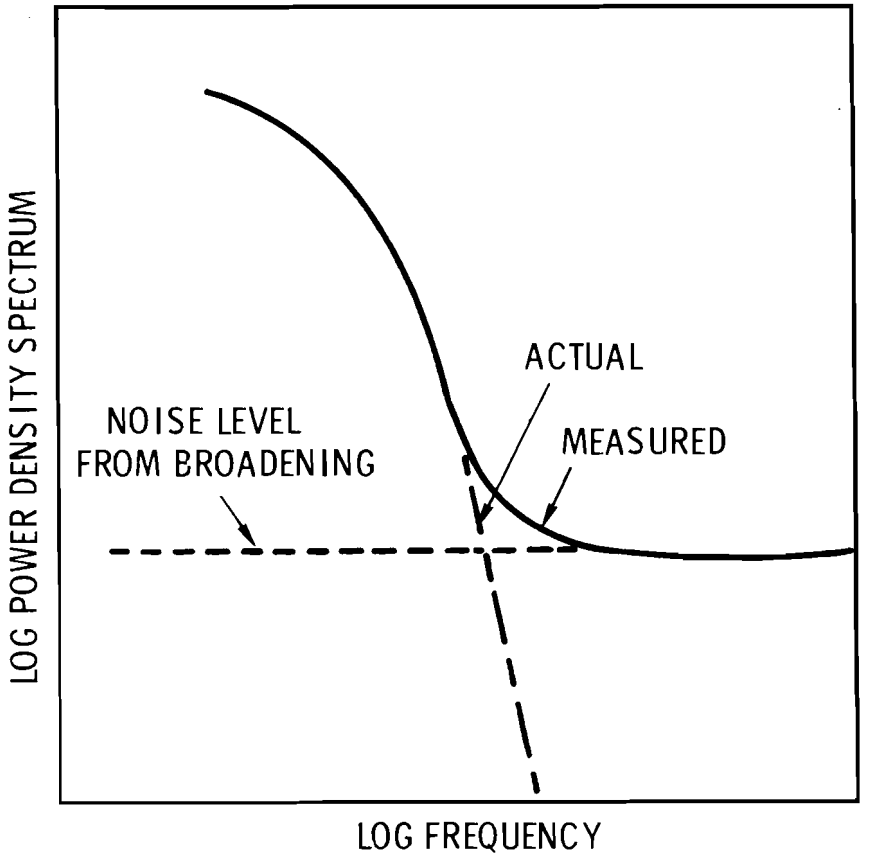

Figure 3.2. Power density spectrum of turbulence showing the effect of laser-Doppler signal broadening.

its effect on the measurements can be reduced by "cutting off" the high frequency components with a low pass electronic filter prior to processing the turbulence signal.

Signal broadening can originate from several sources.

3.2.1 Transit Time Broadening

The finite transit time of the scattering centers through the sample volume causes a broadening of the Doppler frequency. This phenomenon has also been called the "Radar Ambiguity" (42). In general its effect is to produce a spectral broadening that is inversely proportional to the size of the sample volume. This broadening can be expressed as

$$\frac{\Delta\omega}{\omega} = \frac{\bar{u}}{\omega\, 2\sigma_{min}} \tag{3.10}$$

where σ_{min} is the minimum standard deviation of the intensity distribution within the sample volume. The above equation shows that the frequency broadening increases as the inverse transit time through the sample volume. This equation has been derived and verified experimentally by several investigators (12,16,42). This broadening is also considered to be the time rate of change of phase in the sample volume as the particles enter and leave. As the sample volume decreases this rate of change increases.

3.2.2 Aperture Broadening

Receiving aperture broadening has also been attributed to the uncertainty of the scattering angle defined by the beam divergence or

receiver aperture size. This effect has been shown to be equivalent to finite transit time broadening by Edwards, et al. (12).

3.2.3 Velocity Gradient Broadening

Velocity gradients across the sample volume are also a source of broadening. This can be expressed as

$$\frac{\Delta\omega}{\omega} = \frac{2\,\sigma}{\bar{u}} \frac{\partial \bar{u}}{\partial x} \tag{3.11}$$

where the combination of steepest velocity gradient and maximum effective sample volume dimension must be considered. A theoretical study of velocity gradient broadening by Edwards, et al. (12), shows that the velocity gradient also introduces a skew in the Doppler spectrum and decreases the mean frequency slightly. Data obtained in regions of steep velocity gradients should be treated with caution.

3.2.4 Temporal Turbulence Broadening

Temporal broadening refers to the time variation of the Doppler frequency. Doppler frequency is proportional to velocity, therefore, the temporal turbulence broadening can be expressed as

$$\frac{\Delta\omega}{\omega} = \frac{u'}{\bar{u}} \tag{3.12}$$

This is the quantity to be measured in studies of turbulent flow by using the laser-Doppler technique.

3.2.5 Spatial Turbulence Broadening

Spatial turbulence broadening is caused by variation of velocity across the finite sample volume. George and Lumley (16,17,18) have investigated this theoretically to show that this broadening can be

related to the turbulence intensity, microscale and sample volume size. As a limiting case using George's asymptote formula, the broadening can be expressed as

$$\frac{\Delta\omega}{\omega} = \frac{2\sigma}{\lambda}\frac{u'}{\bar{u}} \tag{3.13}$$

where σ is the effective maximum sample volume size and λ is the microscale. For this term to be small, the sample volume must be smaller than λ. This can be interpreted physically by noting that u'/λ is a measure of maximum velocity gradients produced by turbulence. With this interpretation, only the small scale turbulence would be significant in this term. Large scale turbulence would be associated with the temporal broadening.

The previous discussion identifies some of the abilities and limitation of laser-Doppler measurements. Generally the size of the sample volume limits the resolution of the instrument for measuring small scale turbulence. Small sample volumes are desirable for high resolution and to minimize broadening due to velocity gradients and spatial turbulence. Small sample volumes, however, cause transit time broadening. Lumley and George show that there is an optimum size for minimum broadening however, it is somewhat difficult to choose it prior to actually performing an experiment. In many cases of moderately high turbulence, the sample volumes can be made quite small before the transit time broadening begins to dominate.

4.0 EXPERIMENTAL PROGRAM

The experiments were performed in Battelle-Northwest's Thermal-hydraulic Laboratory located in the 189-D Building on the Hanford Atomic Project near Richland, Washington. All experimental work was done in the Hydraulics Loop which is an isothermal recirculating flow loop with flow capability of 900 gpm at temperatures up to 200°F. Turbulent velocity measurements were made within a rod bundle test section by using a two-component laser-Doppler velocimeter. The following sections describe the test section, the laser-Doppler velocimeter and the method of data acquisition.

4.1 DESCRIPTION OF TEST SECTION

Figure 4.1 shows a view of the test section use for the experimental program. Flow entered the bottom of the flow housing, flowed vertically up through the test, emerged at the top of the flow housing, and returned to the flow loop. Rubber expansion bellows were used to help isolate the flow housing from the normal vibrations of the flow loop.

Figure 4.2 shows a detailed view of the test section construction. It consisted of a front and back plate and flow housing body. The back plate contained the inlet and outlet nozzles and was permanently installed in the flow facility. The front plate was bolted to the back plate with the flow housing body placed between them. A continuous "O-ring" sealed the joint between the plates and the flow housing body. Dimensions of the rectangular cavity within test section were maintained

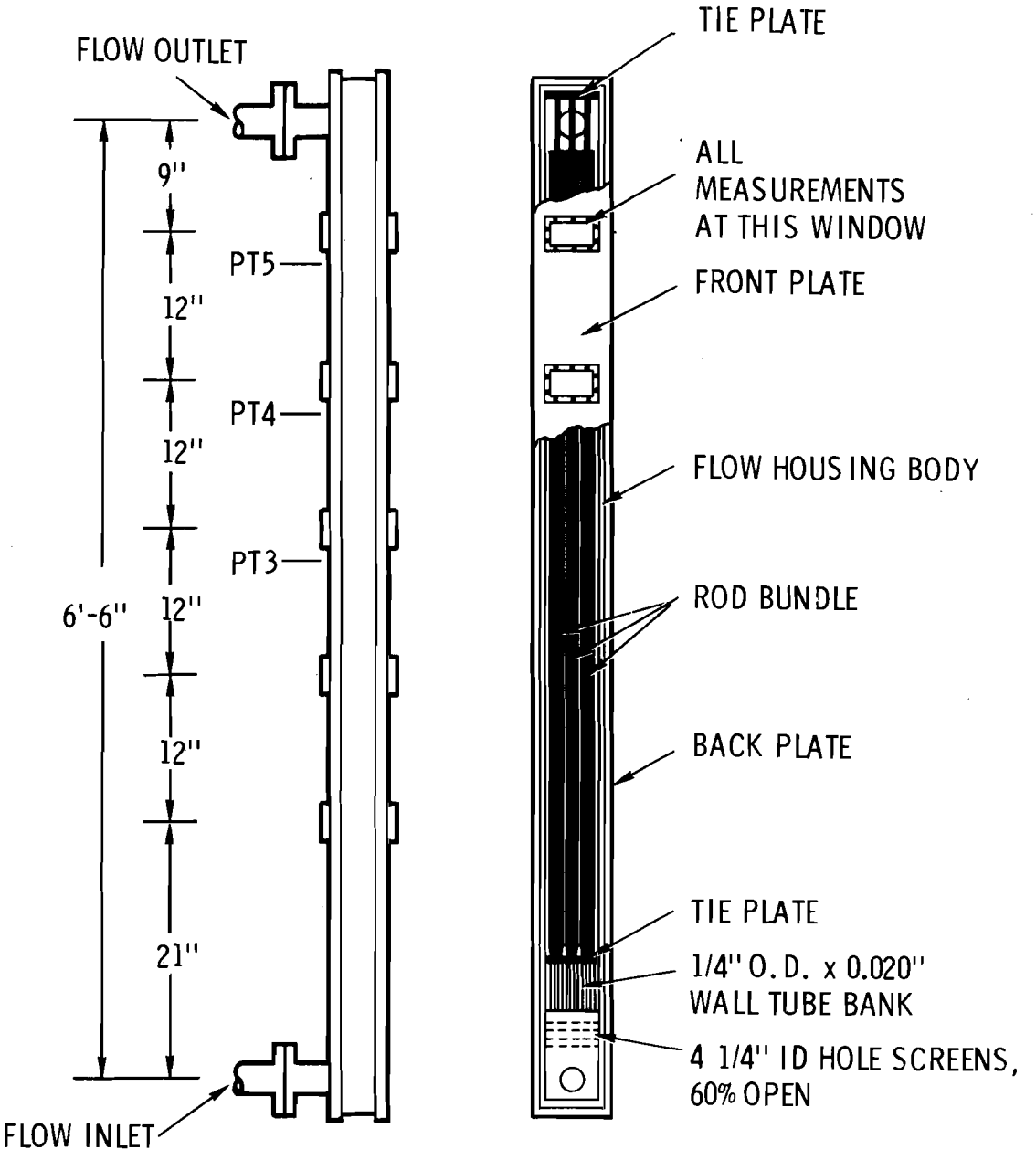

Figure 4.1. Flow housing arrangement.

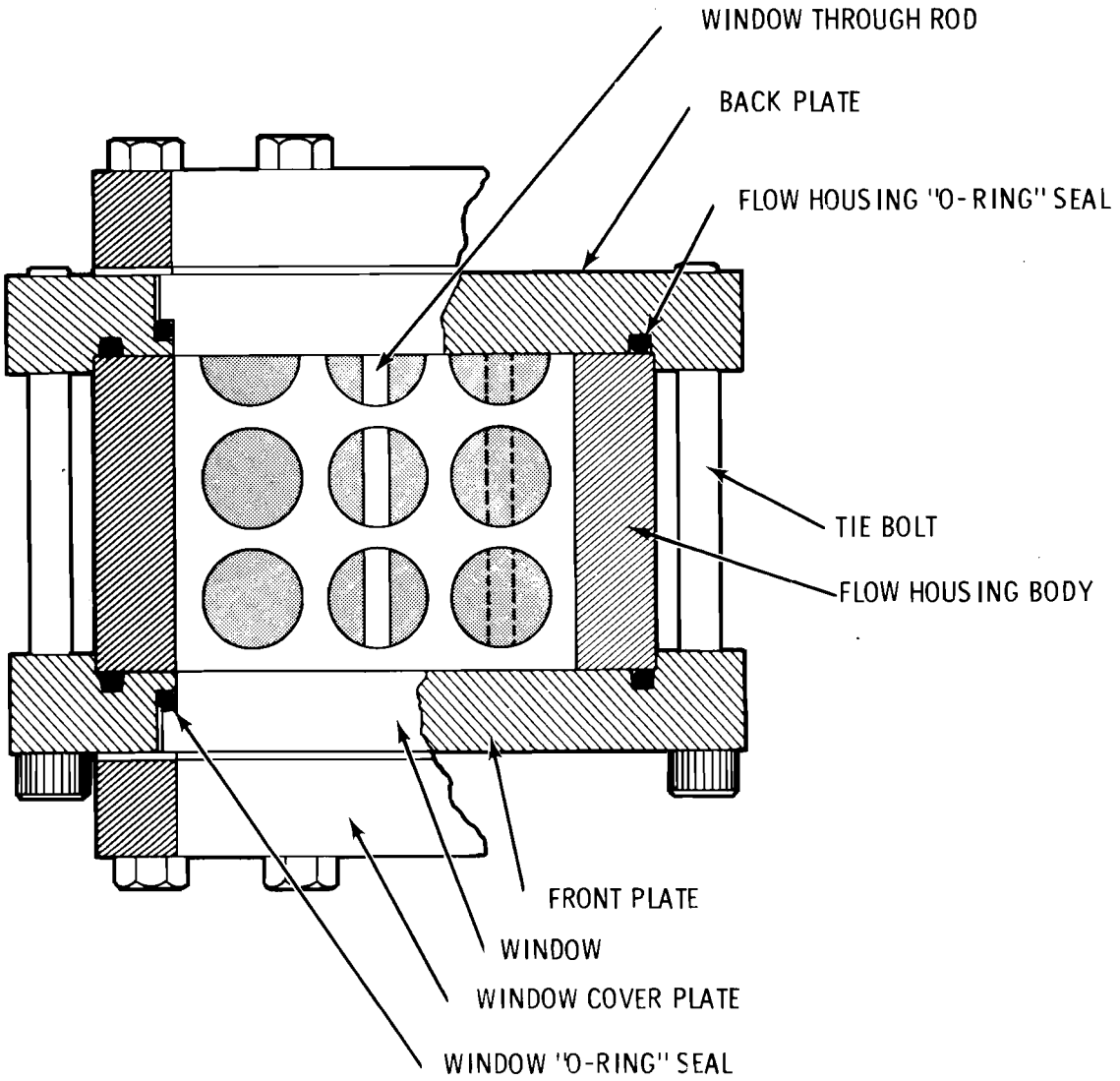

Figure 4.2. Test section construction details.

by the restraining shoulder next to the "O-ring" groove on the front and back plates. To assure that the insert rested against this shoulder during experiments, the bolts were only brought snug during assembly. Then with the system under pressure the insert was forced against the shoulder and the bolts were torqued to 10 ft-lb. This type of construction allowed quick access to the test section for changing internals. It also allowed the size of the test section to be changed by only fabricating a new flow housing body to be inserted between the front and back plates. The entire test section was fabricated from 300 series stainless steel.

The front and back plate each contained 5 window ports 2 inches high by 4 inches wide for entrance and exit of the laser beam. Optically flat ($\lambda/4$) view windows were fabricated from quartz. The windows were sealed by "O-ring" and were held in place by thick cover plates. A shim was placed between the window and cover plate to position the window to be "flush" with the inner surface of the flow housing (± 0.001 inch).

To obtain flow channels that were typical of nuclear reactor rod bundles filler blocks consisting of rectangular sections and sectors of rods were placed within the test section. Figure 4.3 shows the fillers that were necessary to obtain the flow channels considered in this study. Table 4.1 summarizes the geometric parameters for each flow channel. The rod sectors for some flow channels contained small windows so that the laser beam could pass through the rods. These

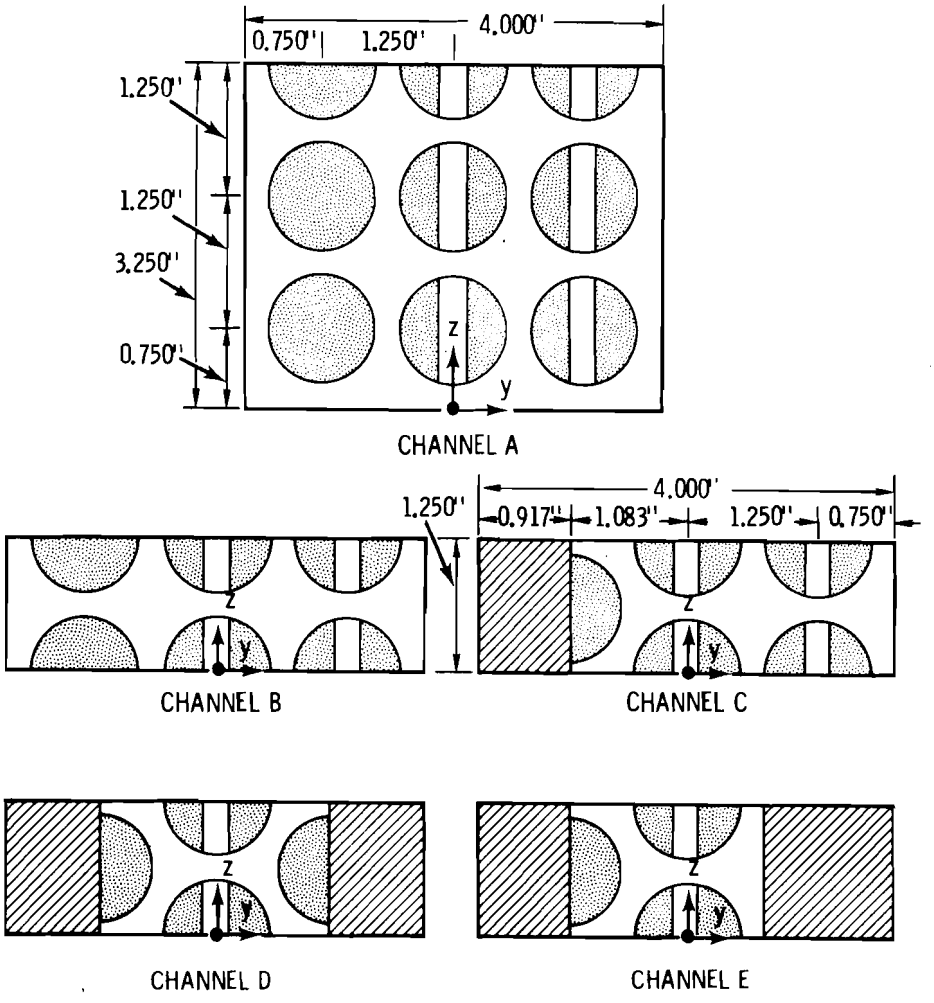

Figure 4.3. Flow channel internal arrangements showing nominal dimensions.

TABLE 4.1. Geometric Parameters of Test Sections

Test Section	Rod Diameter (inches)	Flow Area $(inches)^2$	Wetted Perimeter (inches)	Hydraulic Diameter $(inches)^2$
A	1.000	7.110	35.06	0.8111
A	1.125	5.545	37.63	0.5894
B	1.000	2.644	13.92	0.7595
C	1.000	1.890	11.52	0.6563
D	1.000	1.137	9.115	0.4990
E	1.000	1.113	7.878	0.5651

windows and their rods had 1/8 inch wide flats to eliminate distortion of the laser beam. All rods and sectors were 1 inch diameter except for the 1-1/8 inch diameter rods used for the experiment in Channel A with reduced rod gap spacing. The full round rods were made from aluminum and the half rods were made from stainless steel. Stainless steel was selected for the half rods to minimize differential thermal expansion at elevated temperatures. To maintain a clean geometry no spacing devices were used in the subchannels. The solid rods in Channel A were supported at the ends only. Paint was applied to the rods to help reduce light reflections.

An 8 inch long flow straightening section was placed at the inlet of each flow channel. This consisted of a "bell" entry from the inlet nozzle plenum, followed by a flow conditioner. The flow conditioner consisted of four eccentric screens (60% open) with 1/4 inch holes in a triangular array followed by a bank of 1/4 inch 0.020 inch thick wall tubes 3-1/4 inch long. The screens tended to equalize the inlet velocity distribution and the tubes helped to establish a fixed scale of turbulence and straighten the flow. The inlet ends of the rods and rod sectors has 60° taper to minimize further disturbances of flow due to flow area change upon entering the rod section. The flow straightening abilities of this section were verified by velocity measurements in the rectangular flow channel prior to inserting the rods and rod sectors.

The exit from the rod section was an abrupt expansion to the plenum at the discharge nozzle. This was about 9 inches above the measurement plane at the top window. All measurements were made at the top window which was over 60 L/D from the inlet for all rod bundle flow configurations. This long entrance length was considered sufficient to achieve fully developed turbulent flow.

Pressure taps 1/32 inch diameter were drilled into the back plate two inches below the three upper window ports to allow measurement of pressure drop.

4.2 LASER-DOPPLER VELOCIMETER

A two-component laser-Doppler velocimeter manufactured by Laser Systems and Electronics was used to perform measurements of turbulent velocities. The velocimeter consisted of optical, mechanical and electrical systems.

4.2.1 Optical System

The optical arrangement shown in Figure 4.4 was used for all one component velocity measurement. For this arrangement, the equation for the Doppler frequency obtained from Equation (3.3) was

$$f_D = \frac{n}{\lambda} \left[u \sin \theta + w \, (1-\cos \theta)\right] \qquad (4.1)$$

Since the contribution of the w component was small for $\theta = 10°$ and $w \ll u$, Equation (4.1) could be satisfactory approximated by

$$f_D = \frac{n}{\lambda} u \sin \theta \qquad (4.2)$$

for $\lambda = 0.6328 \times 10^{-6}$ m and n = 1 (air), $u = 11.93 \, f_D$ where u is the velocity in ft/sec and f_D is the frequency in MHz.

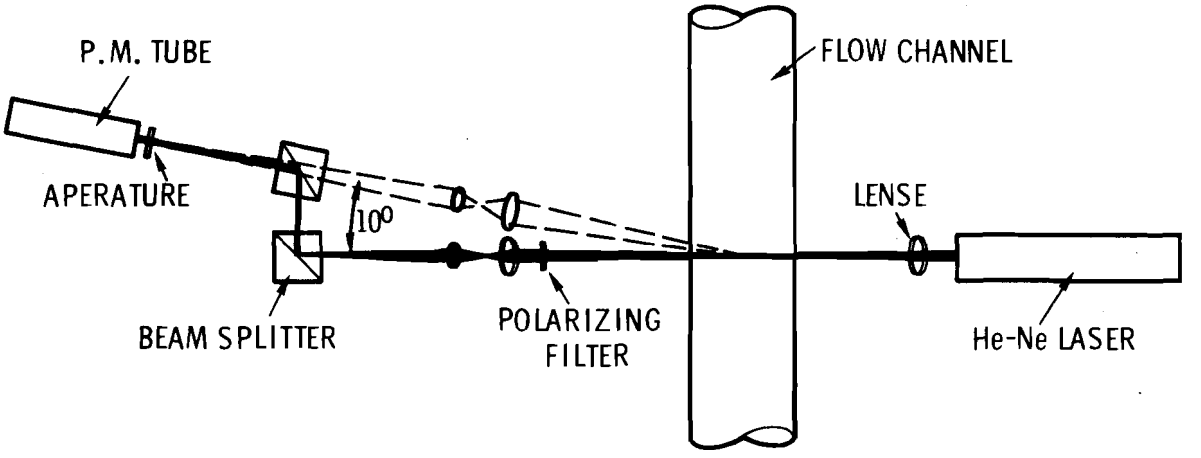

Figure 4.4. One-component laser-Doppler velocimeter optical arrangement.

The beam from a Spectra Physics Model 124 He-Ne laser was focused to a point within the flow channel by using a 237 mm focal length lens. The beam passing through test section was used as the reference beam and was routed to the photomultiplier tube by a polarized filter, a 42 mm focal length combination lens, a mirror, a second polarized filter, a second beam splitter and a 0.030 inch diameter aperture. The reference light was gathered at an angle of 10° by a 42 mm focal length combination lens with an aperture of 16 mm. The scattered light passed through a beam splitter and on to the photomultiplier tube where it was optically mixed with the reference light to produce the Doppler signal. The alignment of the reference and scattered light was achieved visually

by adjusting the beam splitters with the small aperture and photomultiplier tube removed. The aperture and photomultiplier tube were then replaced and the polarized filters adjusted to give the optimum Doppler signal.

For two-component velocity measurements the optical arrangement shown in Figure 4.5 was used. This was essentially two single-component optical arrangements located at right angles to each other. The position of the optics was rotated 45° about the laser beam axis for two-component measurement; therefore, the Doppler signals corresponded to the two velocity components each located 45° from vertical. These two velocities were resolved into the axial and lateral velocity components.

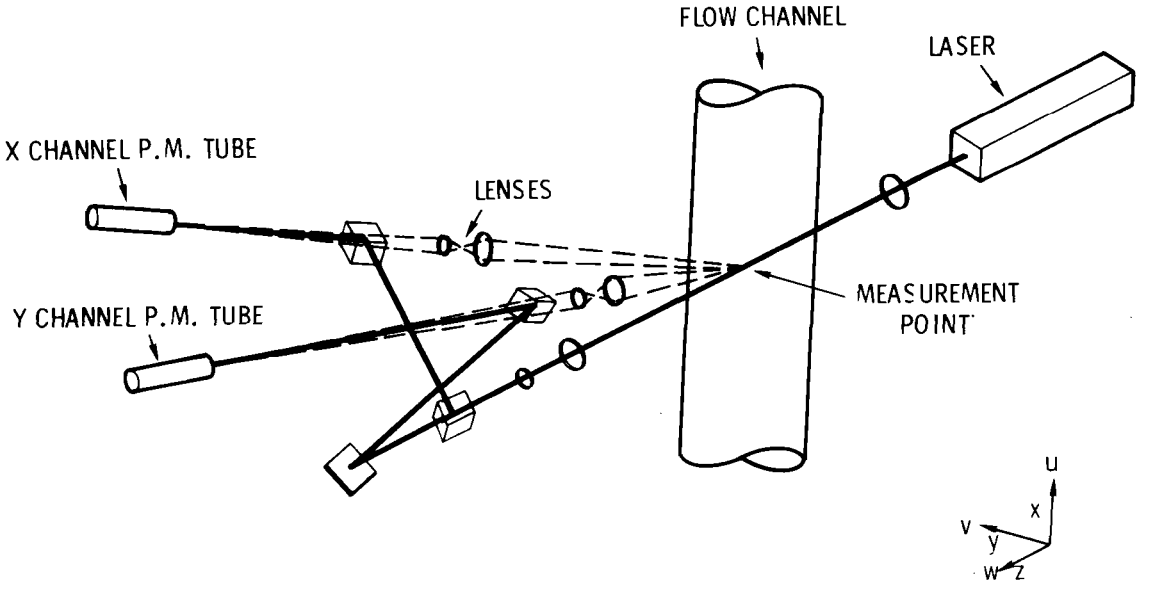

Figure 4.5. Two-component laser-Doppler velocimeter optical arrangement.

In principle, taking two-component data would be similar to taking one-component data; however, this was not the case when turbulence data was to be obtained. In this case the location of each sample volume had to intersect sufficiently close to allow proper resolution of velocity. This meant that each receiving optics channel had to view essentially the same point on the laser beam to assure valid resolution of the measured turbulent velocity into the u and v components. Since this could not be done exactly, an acceptable tolerance of 0.010 inches was selected. This distance was acceptable because it was about half the size of the sample volume longitudinal dimension.

4.2.2 Traversing System

The measurement point was positioned within the flow channel by using a traversing system that moved the laser and receiving optics as an integral unit. The traversing system was supported on a precision linear ball bearings and was driven by variable-speed servo-motors. The motor speed control and position readout could locate the measurement point to within 0.001 inch in both the z and y directions in a horizontal plane.

4.2.3 Electronic Readout

A Laser Systems and Electronics readout system was used to measure local instantaneous velocity consisting of the time average value plus the fluctuating component. The basic elements of the readout system are shown in Figure 4.6. The signal from the photomultiplier tube entered a 10 MHz low pass filter to eliminate high frequency noise. An

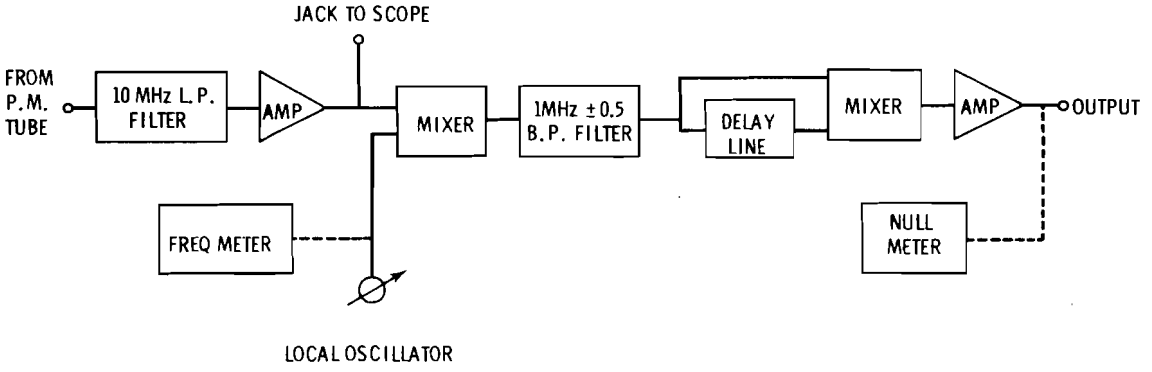

Figure 4.6. Electronic readout system schematic.

amplifier increased the signal level from about 10 mV to about 1 volt. The signal was then mixed with the output from a local oscillator whose frequency was measured with a digital frequency meter. The band-pass filter with a center frequency of 1 MHz rejected the upper side-band of the mixed signal. The lower side-band was frequency detected by the signal correlator which consisted of a delay-line and a mixer. The outputwas short-time integrated by the operational amplifier. The output was connected to a null meter where, at null, the local oscillator frequency was related to the average Doppler frequency. The output provided an analog signal that was proportional to the fluctuating component of velocity.

The method by which this system extracts turbulent velocity information from the Doppler signal can be shown by considering the electronic signal in the form

$$E_o(t) = e(t) \cos \omega_D t + n(t) \tag{4.3}$$

where e(t) is a random amplitude, ω_D is the radial frequency of the Doppler signal and n(t) is noise. Mixing this signal with the local oscillator signal gives

$$E_1(t) = e(t) \cos \omega_D t \cos \omega_o t + n(t) \tag{4.4}$$

where the amplitude of the oscillator signal is assumed to be unity. Expanding this by using a trigonometric identity and by taking the lower side-band (difference frequency), the output from the band pass filter is

$$E_2(t) = \frac{e(t)}{2} \left[\cos (\omega_o - \omega_D)t + n(t)\right] \tag{4.5}$$

Delaying this signal by time τ gives

$$E_2(t-\tau) = \frac{e(t-\tau)}{2} \cos \left[(\omega_o - \omega_D)\ (t - \tau)\right] + n(t - \tau) \tag{4.6}$$

If this is now multiplied by the undelayed signal, the result is

$$E_3(t) = \frac{e(t)\ e(t-\tau)}{4} \left\{\cos (\omega_o - \omega_D)t + n(t)\right\} \left\{\cos \left[(\omega_o - \omega_D)\ (t - \tau)\right] + n(t - \tau)\right\} \tag{4.7}$$

Expanding this by using trigonometric identities gives

$$\begin{aligned} E_3(t) = \frac{e(t)\ e(t-\tau)}{8} \Big\{ & \cos (\omega_o - \omega_D)\tau + \cos \left[(\omega_o - \omega_D)\ (2t - \tau)\right] \\ & + \cos\ (\omega_o - \omega_D)t\ \ n(t - \tau) \\ & + \cos\ (\omega_o - \omega_D)\ (t - \tau)\ \ n(t) \\ & + n(t)\ n(t - \tau)\Big\} \end{aligned} \tag{4.8}$$

All terms in brackets, except the first, are of high frequency. The noise term is high frequency because of the high center frequency of the band pass filter. By integrating over a short time with the operational amplifier, but for a time significantly larger than τ, the high frequency components can be filtered leaving as the output

$$E_4(t) = \frac{\overline{e(t)\ e(t-\tau)}}{8} \cos\ \left[(\omega_o - \omega_D)\tau\right] \qquad (4.9)$$

The term $\overline{e(t)\ e(t-\tau)}$ can be expressed as

$$\overline{e(t)\ e(t-\tau)} = \frac{1}{T}\int_0^T e(t)\ e(t-\tau)dt \qquad (4.10)$$

This is an autocorrelation function of the amplitude modulation in the Doppler signal for $T \to \infty$. If T is less than the period of the highest frequency turbulent fluctuations and larger than the period of the lowest frequencies of amplitude modulation, then $\overline{e(t)\ e(t-\tau)}$ is essentially constant. The value of T in the readout system is about 0.8×10^{-4} sec which permits measurement of turbulence with frequencies up to about 12 kHz. This time is two orders of magnitude greater than the delay time $\tau = 0.25 \times 10^{-6}$ sec.

Equation (4.9) shows that the time average output signal is proportional to cos $(\omega_o - \omega_D)$. The first zero crossing occurs when $(\omega_o - \omega_D) = \pi/2$. Since the center frequency of 1 MHz is used in the readout system, a value of $\tau = 0.25 \times 10^{-6}$ is required. Thus, when $f_o - f_D = 1$ MHz the average output of the readout is zero, or null. For other values of $(\omega_o - \omega_D)\tau$ within the width of the band pass filter the average value of $E_4(t)$ is shown in Figure 4.7. At high frequency

there is no output. As the frequency is decreased a swing in voltage is observed at the edge of the band pass. A linear frequency to voltage conversion takes place within the band pass by using electronic linearizing circuits to shape the cosine function. At low frequency the output is zero because the frequency is below the lower side of the band pass filter. From this frequency-to-voltage characteristic the average Doppler frequency is measured from $f_D = f_o - 1$ (MHz) where f_o is the local oscillator frequency that produces the null voltage.

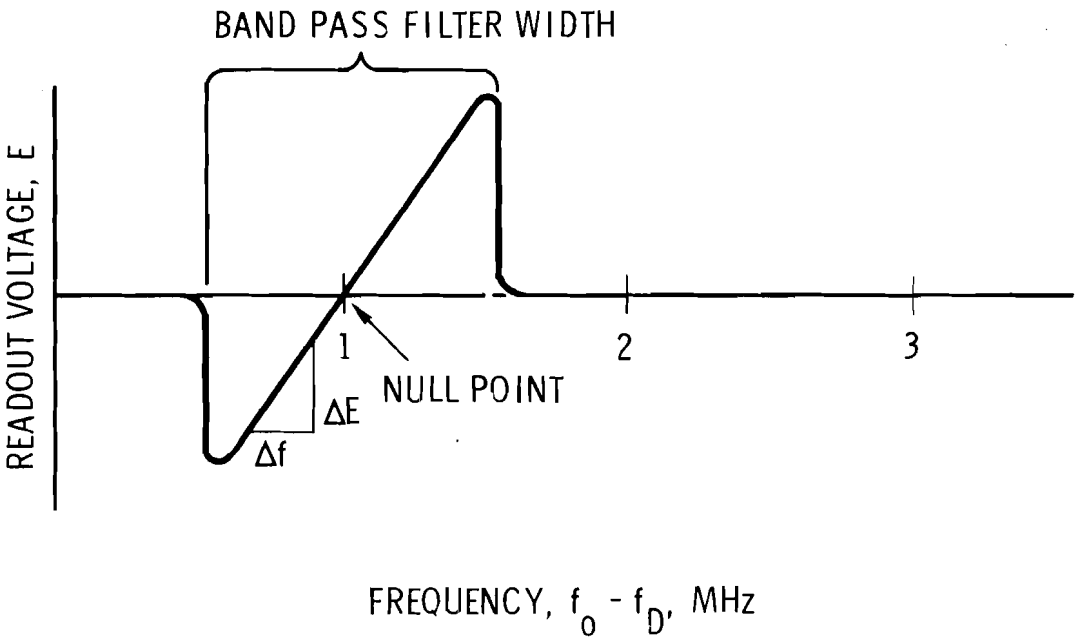

Figure 4.7. Frequency-to-voltage characteristic of readout system.

The width of the band pass filter puts a lower limit on the velocity and an upper limit on the band width of turbulence. Considering the instantaneous Doppler frequency to be $f_D = \bar{f}_D + f_D'$ the lower limit is $f_D > 0.5\Delta f$, where Δf is the filter band width. This limit occurs when f_D is reduced to the point where the upper side band $f_o + f_D$ begins to pass through the band pass filter. Note that the lower limit of $\bar{f}_D$ depends on the level of turbulence because of the turbulence broadening contained in f_D'. The band pass filter also limits the band width of the turbulence such that f_D' must be less the filter band width. The readout system has 500 kHz and 1000 kHz band pass filters.

Now consider how turbulence can be measured. Since the radial Doppler frequency ω_D varies with the velocity, let

$$\omega_D = \bar{\omega}_D + \omega_D' \tag{4.11}$$

where ω_D' is the fluctuating component and $\bar{\omega}_D$ is the time average value. Substituting this into Equation (4.9) gives

$$E_4(t) = \frac{\overline{e(t)\ e(t-\tau)}}{8} \cos\left[(\omega_o - \bar{\omega}_D)\tau - \omega_D'\tau\right] \tag{4.12}$$

Expanding this yields

$$E_4(t) = \frac{\overline{e(t)\ e(t-\tau)}}{8} \left[\cos\ (\omega_o - \bar{\omega}_D)\tau \cos\ \omega_D'\tau + \sin\ (\omega_o - \bar{\omega}_D)\tau \sin\ \omega_D'\tau\right] \tag{4.13}$$

At null, $\cos(\omega_o - \bar{\omega}_D)\tau = 0$ and $\sin(\omega_o - \bar{\omega}_D)\tau = 1$;

therefore,

$$E_4(t) = \frac{\overline{e(t)\ e(t-\tau)}}{8} \sin \omega_D' \tag{4.14}$$

For small $\omega_D'\tau$

$$E_4(t) = \frac{\overline{e(t)\ e(t-\tau)}}{8} \tau\ \omega_D' \tag{4.15}$$

and since τ is constant $E_4(t)$ varies as ω_D'. The instantaneous voltage output at null is, therefore, proportional to the turbulent component of velocity u'. From Figure 4.7 the voltage $E_4(t)$ can be considered to be the voltage fluctuating about null as the frequency ω_D fluctuates. The constant of proportionality $\tau\ \overline{e(t)\ e(t-\ )}/8$ is the slope of the frequency-to-voltage curve in Figure 4.7. The slope is determined by observing the average output of the null meter ΔE for a selected frequency offset Δf.

4.3 SIGNAL PROCESSING

A variety of auxiliary equipment was used with the basic readout system as shown in Figure 4.8. A scope was used to monitor the output of the first amplifier in the readout system. This was very valuable as it aided in optical adjustments and provided a check on the magnitude and quality of the Doppler signal being processed.

The output signals were processed by using the amplifier, low-pass filter, null meter, true "rms" meter, signal correlator, and X-Y recorder shown in Figure 4.8. Model 3400 CALICO amplifiers with 10 kHz bandwidth and selectable fixed gains were used to amplify the

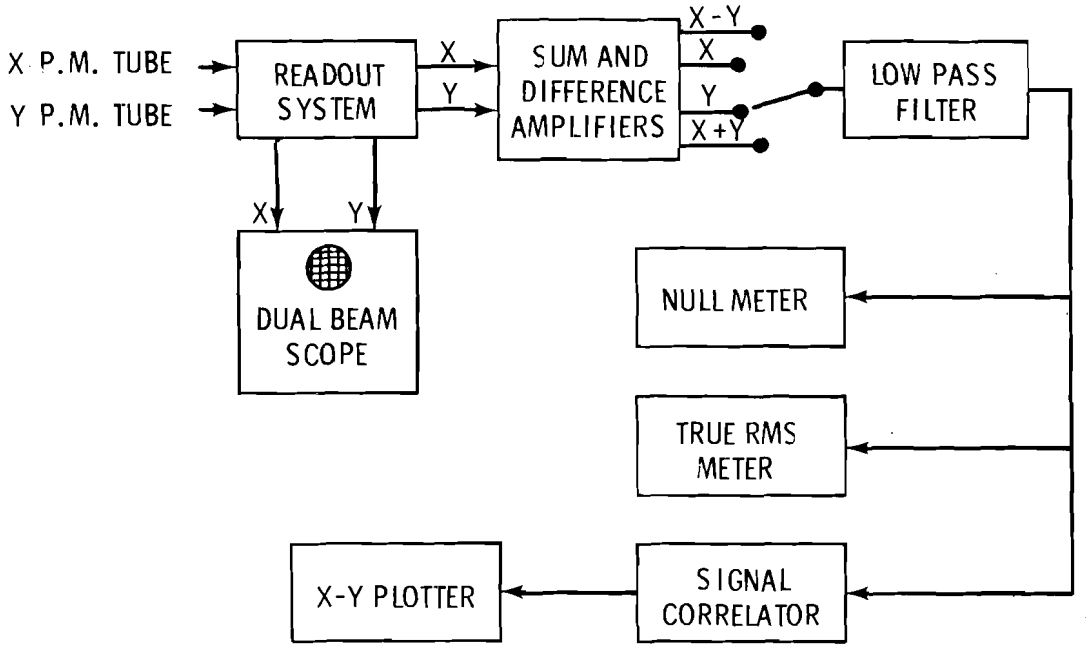

Figure 4.8. Auxiliary readout for velocity measurement.

signals. Following the initial amplification the signals were low-pass filtered by a Rockland Laboratory Model 1020F filter. A Model 419A Hewlett Packard differential voltmeter was used to detect null voltage for measuring average velocity and also for measuring the slope of the frequency-to-voltage detector. A Model 931AB, Fluke differential "true rms" volt meter was used to measure the rms voltage E'.

The autocorrelation function of the signal was computed "on-line" by using a Model 100 Princeton Applied Research Signal Correlator. This correlator computed the autocorrelation function

$$C(\tau) = \lim_{t\to\infty} \frac{1}{t} \int_0^t E(t')\, E(t' - t)\, dt' \qquad (4.16)$$

over a selected total delay range T. The correlator divided the total delay range into 100 increments $\Delta\tau$ = T/100 and simultaneously computed $C(\tau)$ for each of these increments. For a short total delay time where $\Delta\tau$ was small, $C(\Delta\tau) \simeq C(o)$ and

$$C(o) = \overline{E(t)^2} \qquad (4.17)$$

Thus the height of the correlation function at t = 0 was the mean square voltage. Since the correlator memory time constant was 20 seconds, letting the correlator accumulate data over a period of about 1 minute satisfied the condition of $t \to \infty$. The correlation functions were plotted on a Honeywell Model 520 X-Y recorder.

For two-component measurements the two output signals were processed simultaneously using the sum and difference amplifiers shown in Figure 4.9 where E_x and E_y represent the output of the X and Y readout channels, respectively. Each output was first amplified by a CALICO amplifier. The Hewlett Packard null meter was switched into either channel and the gain of one amplifier adjusted until each channel had the same sensitivity $\Delta E/\Delta f$. Since the vertical velocity component u and the horizontal component v were proportional to the sum and difference of E_x and E_y, respectively, two CALICO amplifiers were used to form sum and different circuits. The operation of these circuits were verified by putting identical time varying signals ($\sim$1 volt) into

the system and observing that their difference was zero (<1 mV noise) and their sum was twice the input. A switch was used to select the desired velocity component for processing.

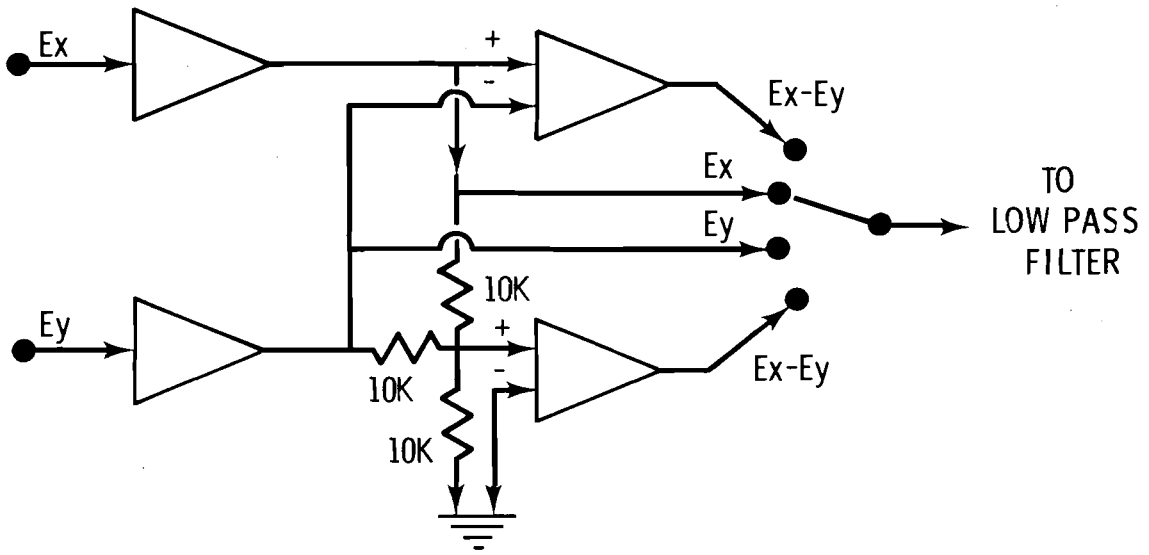

Figure 4.9. Sum and difference amplifier circuit.

4.4 METHOD OF DATA ACQUISITION

The flow loop was operated according to standard laboratory procedures. The loop had a very stable flow, pressure, and temperature control and did not require adjustment during data acquisition.

Once the loop was operating at the selected conditions the optical system was adjusted to give optimum Doppler signals as observed on the scope and by maximizing the frequency-to-voltage conversion slope

$\Delta E/\Delta f$. Milk was injected into the loop to provide sufficient scattering centers. For single-component measurements the optical adjustment procedure was reasonably fast and straightforward. For two-component measurement, however, a trial procedure was required to assure that the sample volumes for each optical channel were sufficiently close. This procedure was rather time consuming and tedious; however, with patience the two sample volumes could be adjusted to be about 0.010 inch of each other. This was verified by observing the loss of signal from each optical channel on a dual-beam oscilloscope as the sample volumes were traversed into the glass window at the side of the test section. This procedure was also used to determine the reference location for the z direction traverse. This procedure located the reference value for z to within about ±0.015 inch. The y direction was determined similarly but to within ±0.001 inch accuracy because of the smaller sample volume size in the y direction.

Data was taken sequentially along a selected traverse through or across the test section. The sample volume could be positioned to within 0.001 inch for each measurement point.

For each location the local oscillator was adjusted to obtain the null point. Then the rms meter, oscillator frequency and position location were recorded. Then the value of ΔE was recorded for a selected frequency offset Δf. After approximately one minute, the output of the correlator was plotted on the X-Y recorder for selected

data points. The same procedure was used for two component data except two readout channels were involved. Also the gain of one CALICO amplifier was adjusted to give identical values of $\Delta E/\Delta f$ for each channel. All data were recorded on computer coding forms for later punching to cards and automatic data processing.

For one-component velocity measurements the experimental data were reduced to average velocity by using Equation (4.2) or

$$\bar{u} = 11.96\ (f_o - 1) \tag{4.18}$$

where f_o is the oscillator frequency in MHz.

The fluctuating Doppler frequency was computed from

$$f'_{D_1} = E' \frac{\Delta f}{\Delta E} \tag{4.19}$$

and the local rms turbulence velocity was calculated from

$$\frac{u'}{\bar{u}} = \frac{E'}{\Delta E} \frac{\Delta f}{\bar{f}_D} \tag{4.20}$$

For two component measurements the axial component Doppler frequency was calculated from

$$f_{D_1} = \frac{\sqrt{2}}{2} (f_{D_x} + f_{D_y}) \tag{4.21}$$

The axial component fluctuating Doppler frequency was calculated from

$$\frac{u'}{\bar{u}} = \frac{\Delta f}{\Delta E} \frac{(E_x + E_y)'}{(\bar{f}_{D_x} + \bar{f}_{D_y})} \tag{4.22}$$

and for the transverse component

$$\frac{v'}{\bar{u}} = \frac{\Delta f}{\Delta E} \frac{(E_x - E_y)'}{(\bar{f}_{D_x} + \bar{f}_{D_y})} \tag{4.23}$$

Pressure drop data were taken for each of the flow channels over the Reynolds number range of interest in the experiments. Pressure drop was measured over one-foot increments between taps 3 and 4 and between taps 4 and 5. Pressure drop was measured with a manometer containing 2.95 specific gravity oil.

4.5 METHOD OF DATA REDUCTION

A digital computer program was written to reduce the recorded data. For each data point it was necessary to (1) shift the measurement location to a consistent set of coordinates and correct for refractive index; (2) convert the Doppler frequency to velocity; (3) convert the rms voltage to turbulence intensity; and, (4) estimate the Eulerian macroscale from the correlation function plots. A listing of the digital computer program used for these calculations is given in Appendix A.

The measurement locations corrections were made according to the equations

$$z = (z - z_o)\, C_n \tag{4.24}$$

and

$$y = y - y_o \tag{4.25}$$

The refractive index correction C_n was required for the z direction because of the change in direction of the light path at the glass water interface as shown in Figure 10. This correction was derived from Snell's law of refraction,

$$n_1 \sin \theta_1 = n_2 \sin \theta_2 \tag{4.26}$$

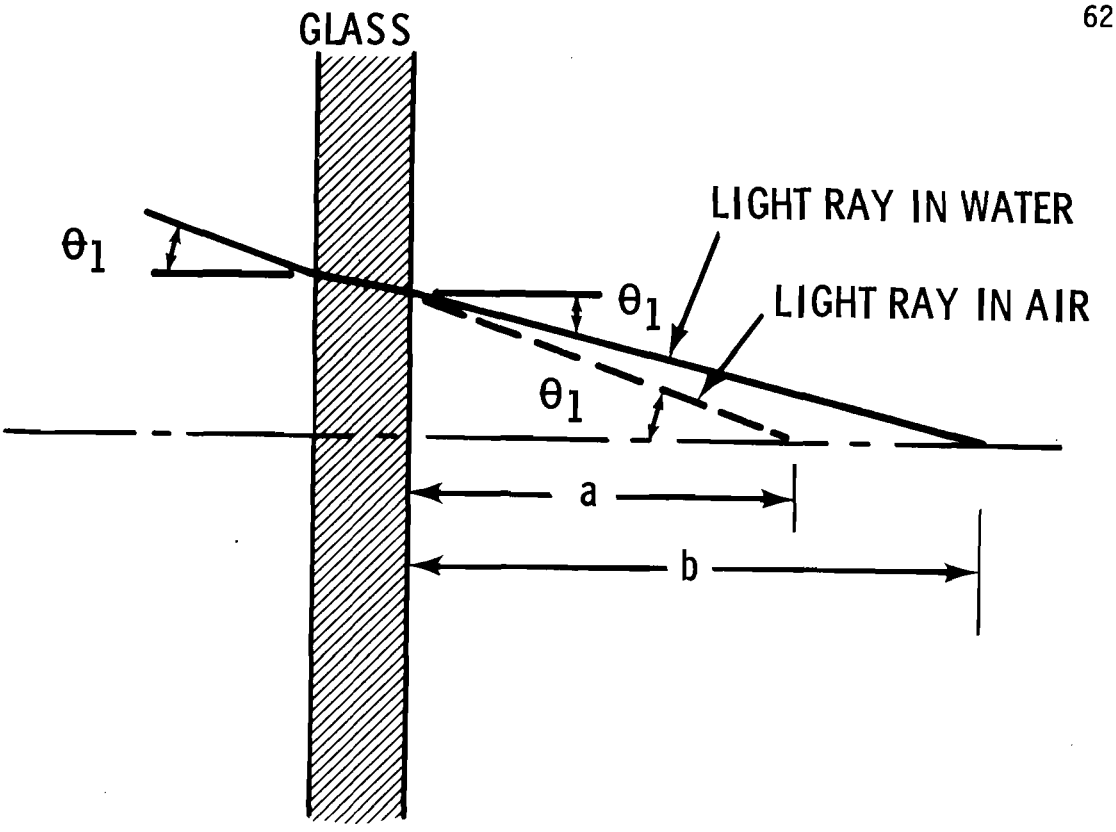

Figure 4.10. Refractive index correction for light ray path in water.

For air, $n_1 = 1.0$; therefore,

$$\theta_2 = \sin^{-1}\left(\frac{\sin\theta_1}{n_2}\right) \tag{4.27}$$

where n_2 is the index of refraction in water.

From Figure 4.10 the true position "b" and the indicated position "a" were related by

$$a \tan\theta_1 = b \tan\theta_2 \tag{4.28}$$

therefore

$$b = \frac{a \tan\theta_1}{\tan\left[\sin^{-1}\left(\frac{\sin\theta_1}{n_2}\right)\right]} \tag{4.29}$$

and

$$C_n = \frac{\tan \theta_1}{\tan \left[\sin^{-1}\left(\frac{\sin \theta_1}{n_2}\right)\right]} \tag{4.30}$$

Although this expression was used in data reduction, C_n reduced to just n if the small angle approximation ($\tan \theta = \theta = \sin \theta$) was used.

The calculation of velocity and turbulence intensity was a straight forward application of Equations 4.18 through 4.23. The shear velocity used to normalize the intensity data was calculated from the measured channel friction factors.

The calculation of the Eulerian macrotime scale in the direction of flow was determined by fitting the autocorrelation function to an equation of the form

$$R(\tau) = e^{\alpha_1 \tau} \cos \alpha_2 \tau \tag{4.31}$$

This equation allows for periodicity in the correlation function. From Equation (2.20) the macrotime scale is given by

$$T_E = \frac{\alpha_1}{\alpha_1^2 + \alpha_2^2} \tag{4.32}$$

and from Taylor's hypothesis the longitudinal macroscale is

$$\Lambda = \bar{u}\, T_E \tag{4.33}$$

The autocorrelation function data was fit to Equation (4.31) by using a "least-squares" curve fitting routine written by Howell (25). This routine was used in a "least-squares" and a "least-squares-distance" mode with identical results. Eleven equally spaced points

taken from the correlator plots and normalized to unity at $\tau = 0$ were used as input to the curve fitting routine. This curve fitting procedure provided a consistent method of quantifying the correlation function data from which it was possible to estimate the local macroscale and the frequency of flow pulsations.

A complete tabulation of the reduced data is presented in Appendix B.

5.0 EXPERIMENTAL RESULTS

Measurements of local velocity, turbulence intensity and Eulerian time-scale were obtained within selected regions of the flow channels shown in Figure 4.3. In summary, the results of the experiments indicate the following:

1. The axial ($u'/\bar{u}$) and lateral ($v'/\bar{u}$) components of turbulence intensity are highly nonuniform with relative minima near the center of subchannels and at the center of rod gaps. Maxima occur midway between the gap and subchannel center and near solid boundaries.
2. The lateral component of turbulence intensity ($v'/\bar{u}$) ranges from about 50% to 80% of the axial component ($u'/\bar{u}$) at $p/d = 1.25$.
3. The axial macroscale of turbulence as estimated by Taylor's hypothesis is on the order of 0.4 times the average channel hydraulic diameter.
4. Rod gap spacing significantly affects the intensity and scale. Reducing the spacing by a factor of two nearly doubles the scale in some regions and increases the turbulence intensity along the centerline through the rod-rod gaps.
5. The data indicate the presence of secondary flows; however, their direct measurement was not possible because their magnitude was less than the measurement accuracy of the instrumentation.

6. The flow structure within a symmetrically shaped gap between a pair of simple subchannels at p/d = 1.25 is not significantly affected by the shape of the adjacent subchannels. Increasing the degree of lateral freedom by adding more subchannels increases the intensity moderately. Flow structure in the gaps along the housing wall are moderately affected by the asymmetry of the gap.
7. Reynolds number generally has a weak affect on the velocity ($\bar{u}/U$), turbulence intensity ($u'/\bar{u}$), and Eulerian longitudinal macroscale (Λ/D) as estimated by using Taylor's hypothesis.

The following sections discuss this data in detail. The first section is concerned with the flow structure in the subchannels of flow channels A, B, and C. The second section is concerned with the flow in the rod gaps of all channels. The final section presents a brief presentation and correlation of the pressure drop data.

5.1 SUBCHANNEL FLOW STRUCTURE

The subchannel flow structure was investigated in Channel A which is shown in Figure 4.3. Velocity, turbulence intensity, and turbulence scale were measured in this channel to: (1) map the velocity and turbulence intensity distribution; (2) evaluate the effect of rod gap spacing; and (3) determine the effect of Reynolds number. Limited two-component data were also taken in a wall subchannel of Channel A to determine the magnitude of the lateral component of intensity.

Additional maps of velocity and intensity were taken in Channels B and C to determine how a more restrictive flow configuration affects the subchannel flow structure.

5.1.1 Maps of Velocity and Intensity

Figures 5.1 and 5.2 show maps of velocity and turbulence intensity distribution in the side, corner, and interior subchannels of Channel A. The velocity profiles are quite symmetrical and are similar in shape to the profiles predicted by Deissler and Taylor (11) except for the isovels (constant velocity lines) being farther from the rod surfaces in the open part of the subchannel. This is believed to be caused by secondary flows which are discussed later in more detail.

The axial component turbulence intensity ($u'/\bar{u}$) map in Figure 5.2 show some new and interesting information regarding turbulence flow structure in rod bundles. An interesting feature of these data are the relative minima of turbulence intensity in the subchannel centers and rod gap centers. The minimum values of 0.041 and 0.045 in the center and wall subchannels are both higher than 0.035 which is typical for fully developed pipe flow (36,37,46). The relative minima of 0.050 and 0.052 in the interior rod gaps are higher than the subchannel center values. Another interesting feature is the relative maximum[3] that occurs along the centerline between subchannel centers and the

---

[3]This is actually a "saddle point" because the intensity increases toward the wall.

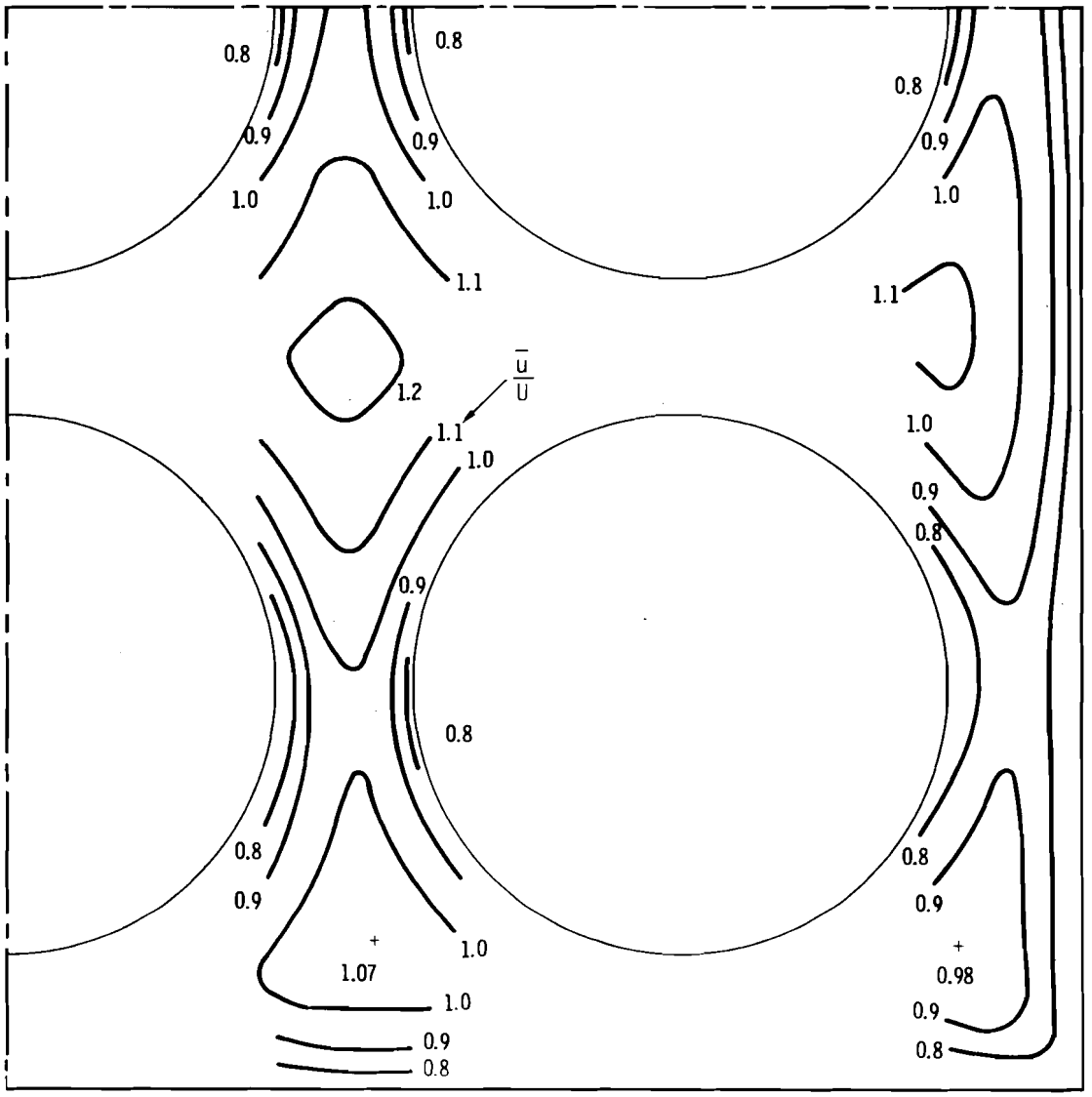

Figure 5.1. Axial component velocity ($\bar{u}/U$) map in Channel A, Re = 100,000 p/d = 1.25.

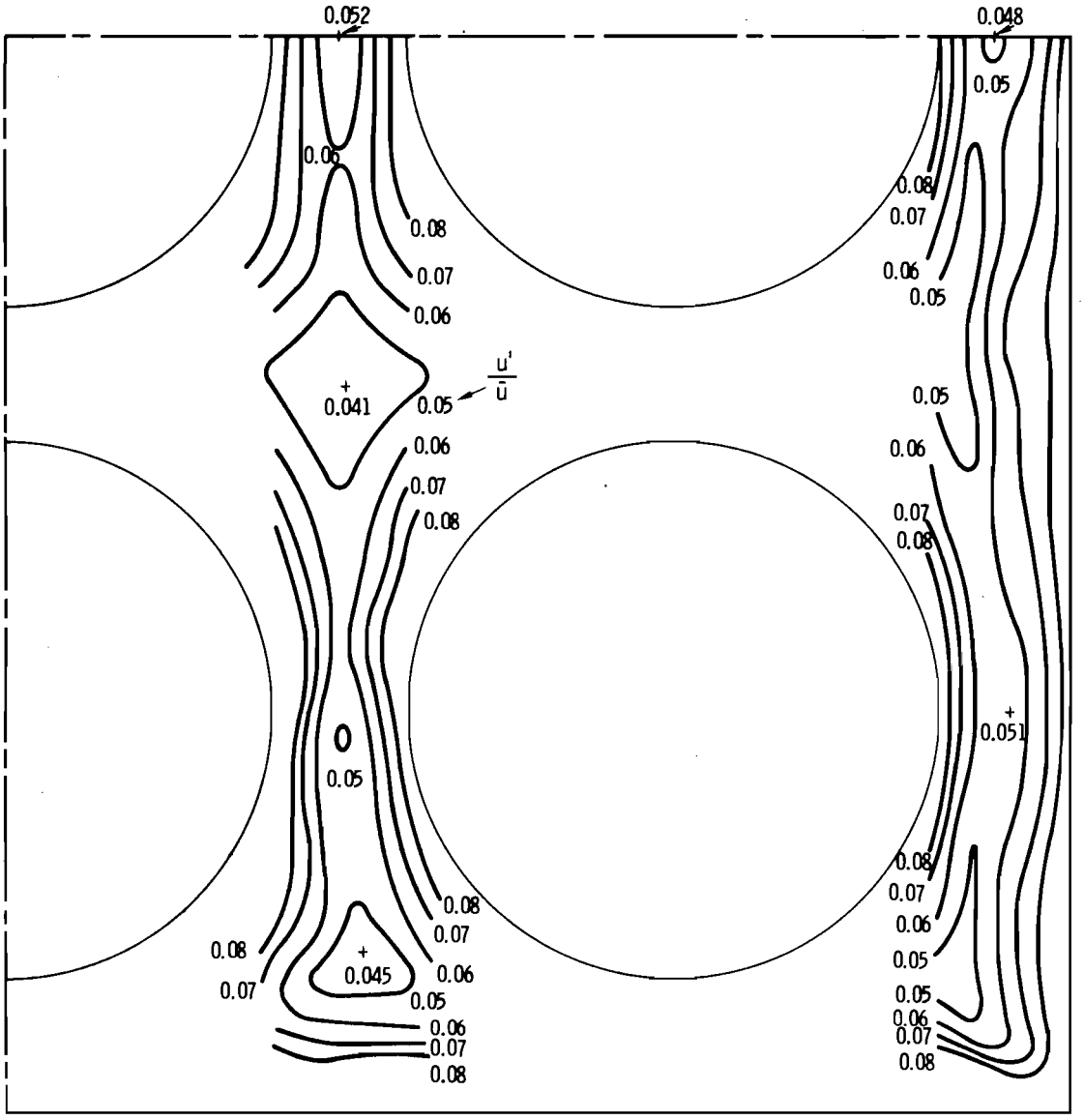

Figure 5.2. Axial component turbulent intensity (u'/U) map, Channel A, Re = 100,000, p/d = 1.25, 4 kHz cutoff.

rod gap. The corner and wall subchannel map show behavior similar to that found in the interior channel; however, it is modified by the presence of the flow housing wall. The relative minima and maxima are comparable to those in the interior.

Figures 5.3 and 5.4 show maps of turbulence intensity obtained in two component directions within a wall subchannel. The axial component intensity distribution is very similar to that shown in Figure 4.1; however, the values of intensity are about 10% lower. The reason for this difference is believed to be caused by the lower turbulence cutoff frequency (3.0 kHz) compared to the previous data (4.0 kHz). The lateral component of turbulence intensity is seen to be less than the axial component by about 40% near the gap and about 30% lower near the subchannel center. The lateral component near the wall is also lower by about 50%. The gradients of the lateral component are also seen to be smaller in the interior part of the subchannel and gap. It should be noted that the lateral component is in the cartesian coordinate y direction.

One of the most obvious features of the intensity map is the distortion of the intensity distribution. These are believed to be caused by secondary flows. Secondary flows are known to occur in the corner of square channels where a pair of secondary flow circuits move along the bisector of the corner angle toward the corner, along the channel wall and out into the main flow stream. These secondary flows also transport the properties of the flow such as the turbulence kinetic

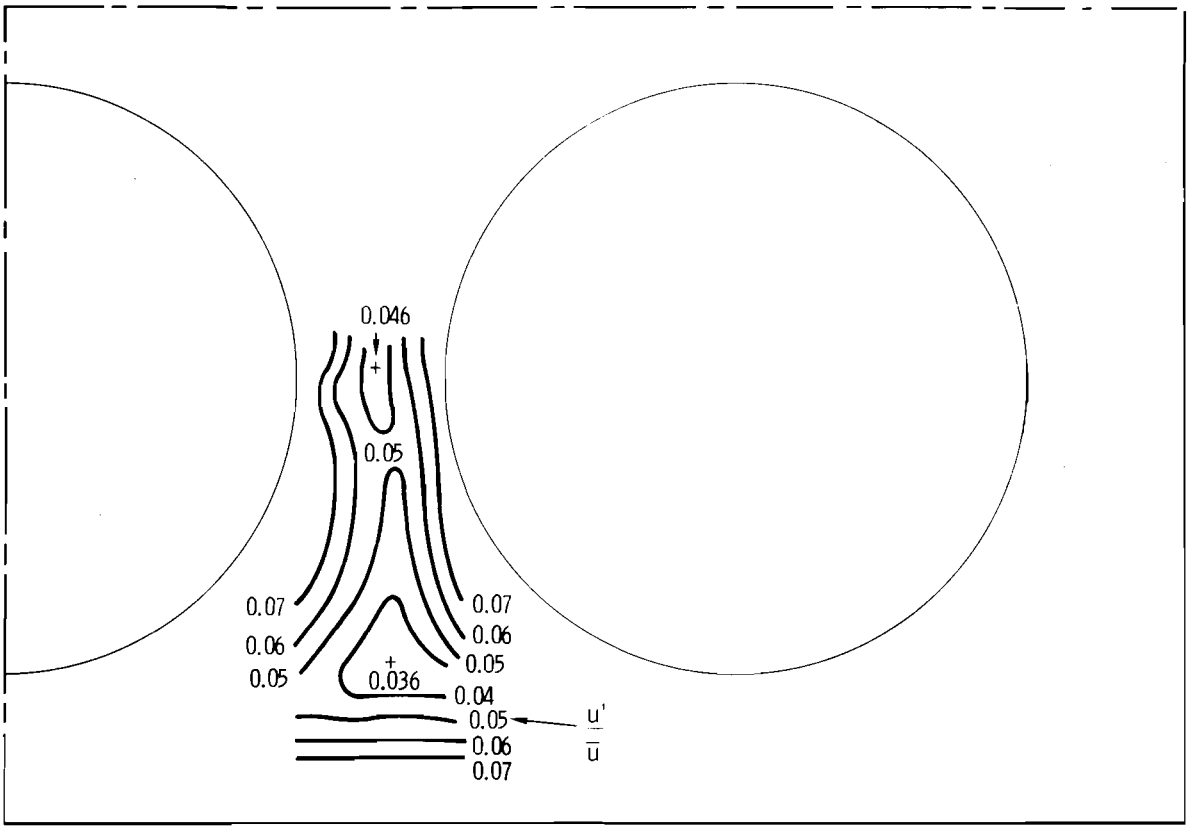

Figure 5.3. Axial component turbulence intensity (u'/U), Channel A, Re = 100,000, p/d = 1.25.

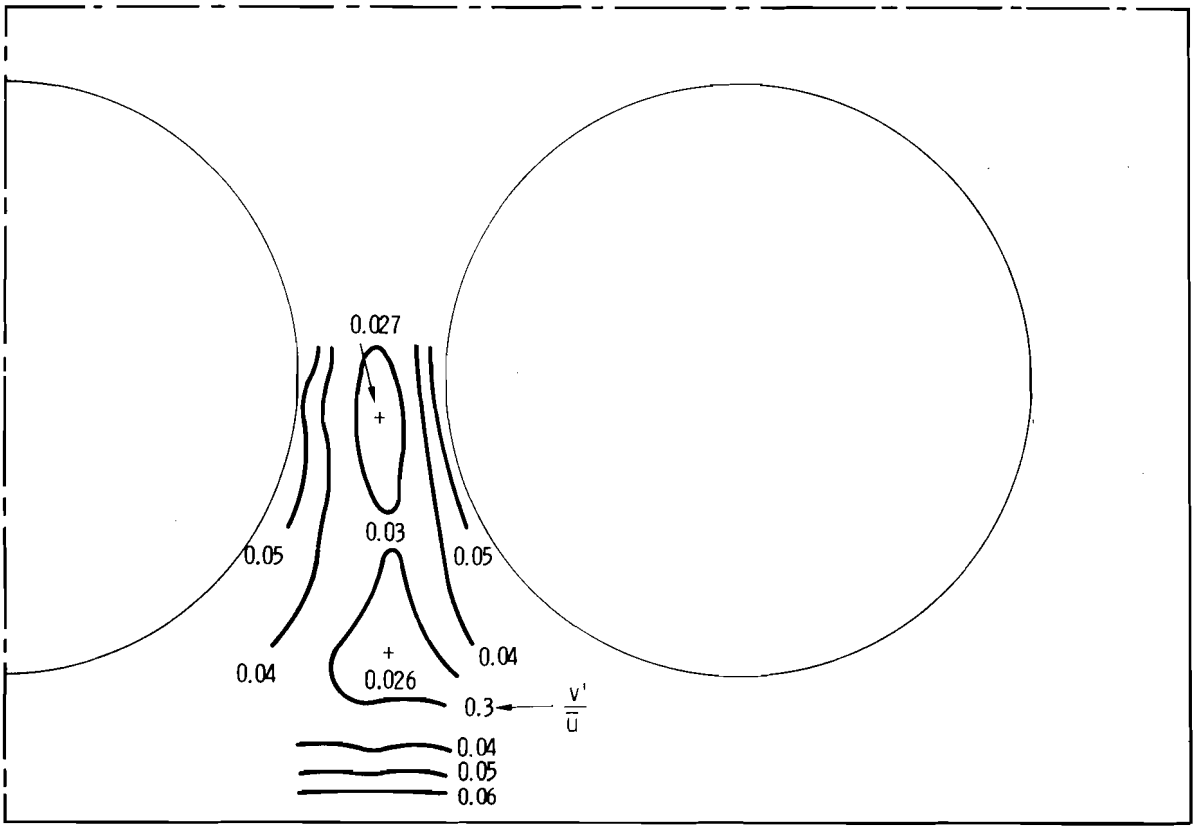

Figure 5.4. Transverse component turbulence intensity (u'/U), Channel A, Re = 100,000, p/d = 1.25.

energy. In the corner subchannel of Figure 5.2 a secondary flow moves toward the corner carrying lower intensity flow into the corner thus causing the intensity lines to "bulge" toward the corner. Likewise, the return path carries high-intensity wall-turbulence toward the open part of the channel, causing a "bulge" away from the wall.

Examination of Figure 5.2 indicates several other regions of secondary flow. Of particular importance are those that occur in regions between the rod gaps and subchannel centers. The secondary motion are not entirely consistent as indicated by the different intensity distortions in the various subchannels. It is interesting to note that the interior subchannels do not have the same shape intensity distributions and there is incomplete symmetry about these lines of symmetry normally associated with unit cell analyses. A more complete discussion of the secondary flow patterns is presented later.

Figures 5.5 and 5.6 show a plot of the velocity, intensity, and longitudinal scale along the centerline from the wall through a rod-rod gap to an interior subchannel and from the corner subchannel through a rod-wall gap to a wall subchannel. These plots are used in subsequent comparisons to show the effect of experimental parameters. The plot of axial turbulence intensity ($u'/\bar{u}$) for the interior channel shows the relative minima and maxima indicated by the previous intensity maps. An average value along the centerline of about 0.05 is somewhat higher than the value 0.035 that would be expected at the center of pipe flow. Figure 5.5 shows a rather uniform distribution of longitudinal

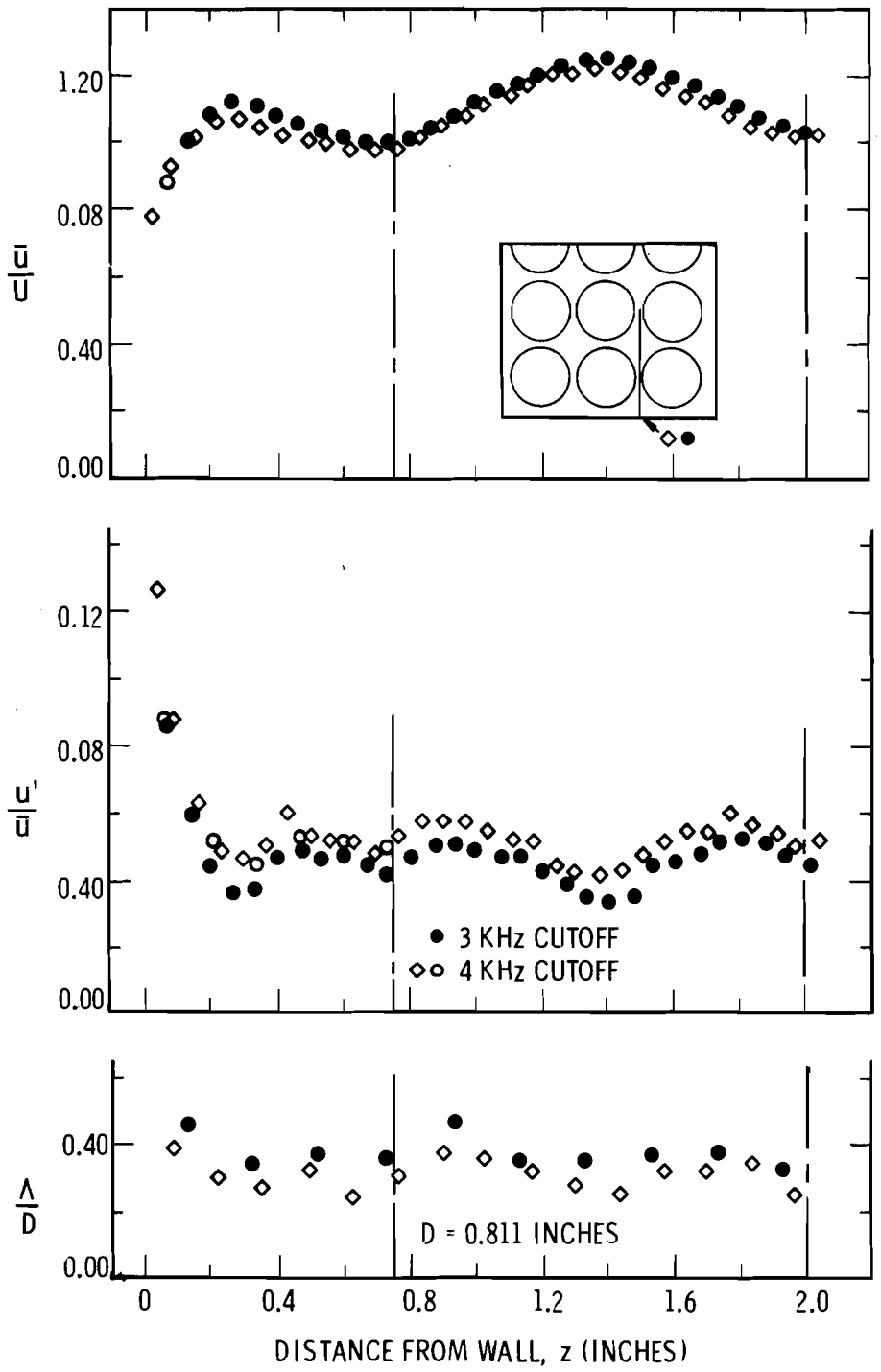

Figure 5.5. Centerline traverse from wall through interior subchannel, Re = 100,000, p/d = 1.25, y = 0.625 inches.

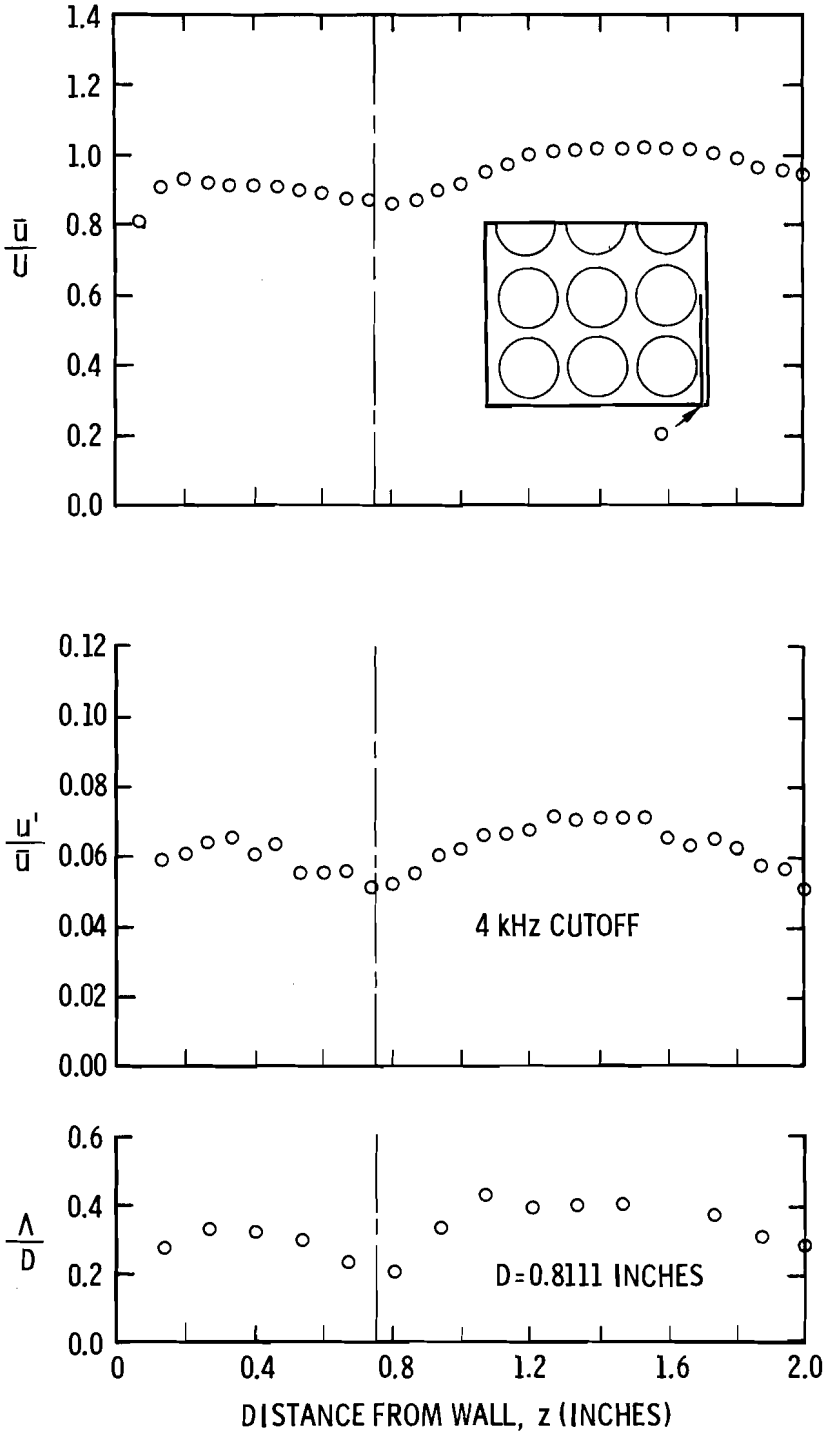

Figure 5.6. Centerline traverse from corner through wall subchannel, Re = 100,000, p/d = 1.25, y = 1.875 inches.

turbulence scale. There is no evidence of significantly smaller scale in the gaps and larger scale in the subchannel as has been postulated by other investigators (47). For an average value $\Lambda/D = 0.35$ and $D = 0.811$ inches, $\Lambda = 0.28$ inches. Figure 5.6 shows a more nonuniform distribution of scale along a line through the center of the rod-wall gaps. Although this is not a symmetric centerline traverse as in Figure 5.5 the scales are of comparable magnitude. The corner subchannel shows somewhat smaller scale as compared to wall and interior subchannels. This could be expected because of the smaller subchannel hydraulic diameter as compared to the bundle average value. The scale in the gap between the corner and wall subchannel is about one-half that in the side subchannel. The scale in the gap between the side-wall channels is only a little smaller than the scale in the wall subchannels. The general result for Channel A is that the scale is rather uniform with moderately reduced values in some rod gaps. The longitudinal scale is generally 0.3 to 0.4 times the hydraulic diameter.

5.1.2 Effect of Rod Gap Spacing

The effect of rod gap spacing on the velocity, intensity, and scale was investigated in Channel A by increasing the rod diameter from 1 inch to 1-1/8 inch. This decreased the center rod gap spacing from 1/4 to 1/8 inch and decreased the side wall gap spacing from 1/4 to 3/16 inch. The increased radius of curvature would be of little concern since the geometric parameter of interest is the pitch-to-diameter ratio.

Figures 5.7 and 5.8 show the effect of reducing the gap spacing at a Reynolds number of 100,000. The reduced gap spacing significantly increases the intensity and modifies the scale distribution, especially near the rod gap. As for the larger spacing, relative minima in intensity occur near the subchannel center and the center of the rod gap. The average intensity is about 60% higher along the interior channel centerline for the 1/8 inch gap spacing as compared to the 1/4 inch gap spacing. Most of this increase is due to significantly higher intensity on each side of the gap. The gap intensity is also higher but less than the adjacent peak values. Figure 5.7 also shows a significantly modified distribution of scale and a general increase of scale in the wall and interior subchannel at the reduced gap spacing. Maximum and minimum values of $\Lambda/D = 0.60$ and 0.25 correspond to values of $\Lambda = 0.57$ inches and 0.20 inches, respectively. This magnitude of scale as compared to the 1/8 gap spacing suggests elongated eddies in the axial direction. Because of the bounding surfaces of the rod gap the scale in the direction normal to the wall would probably be much smaller. In the other lateral direction, however, there is no reason for the scale to be so restrained. If the supposition of Ibragimov (26) is correct, the motion in the circumferential would be of large scale; however, it is not known what its relation would be with the longitudinal scale.

This distribution of scale is rather interesting because the largest scales are in the rod gap and at the subchannel centers. The

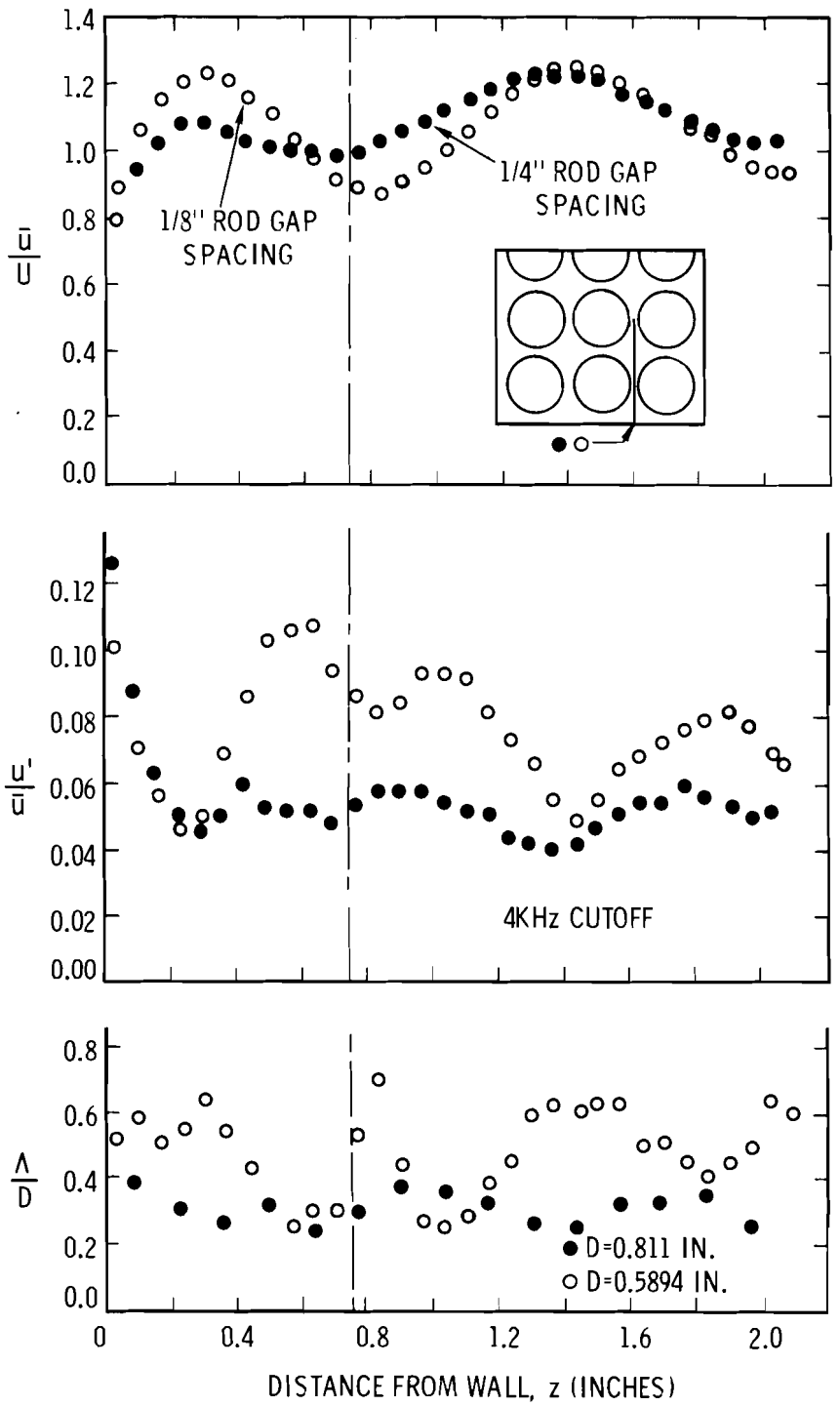

Figure 5.7. Effect of gap spacing, centerline traverse from wall through interior subchannel, Re = 100,000, y = 0.625 inches.

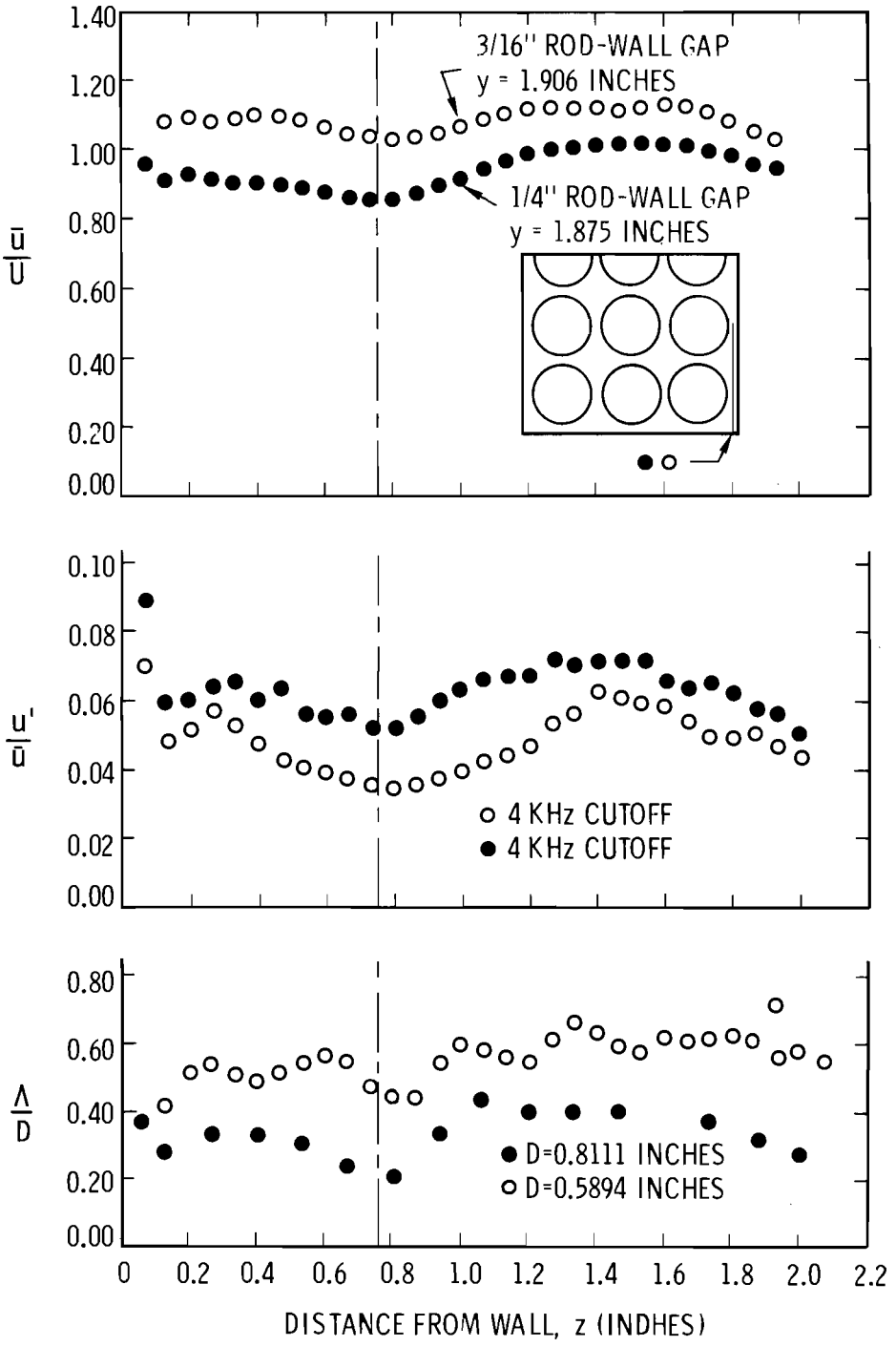

Figure 5.8. Effect of gap spacing, centerline traverse from corner through wall subchannel, Re = 100,000.

smaller scale turbulence is located between the gap and subchannel center. The correlation functions also show this to be a region of significant periodic flow pulsation; whereas, no significant flow pulsations are indicated in the data at the larger gap spacing.

The results for the corner and wall subchannels are quite different. The intensity data do not show an increase but a decrease for the reduced gap spacing (3/16 inch). This occurs mostly near the gap with a small reduction near the subchannel center. The longitudinal scale, however, shows nearly a factor of two increase for the reduced spacing. The scale is a little smaller in the gap as compared to the scale in the subchannel. Maximum and minimum values of $\Lambda/D = 0.78$ and 0.49 correspond to values of $\Lambda = 0.60$ inches and 0.30 inches, respectively, for the 3/16 inch wall gap spacing. These are a little smaller than the maximum and minimum values obtained at the interior. This is rather paradoxical because the interior channels and gaps are smaller.

The different behavior between interior and wall subchannels suggests a subchannel shape effect on intersubchannel mixing. Subsequent data show that different shape adjacent subchannels do not significantly affect the flow structure near the rod gap; however, all of those subchannels had symmetry about the centerline through the gap. The wall subchannels are different in that they do not have the same symmetry.

Figure 5.9 shows plots of the autocorrelation functions obtained at identical centerline locations in the interior channels for the two gap spacings. There are some interesting features in these plots.

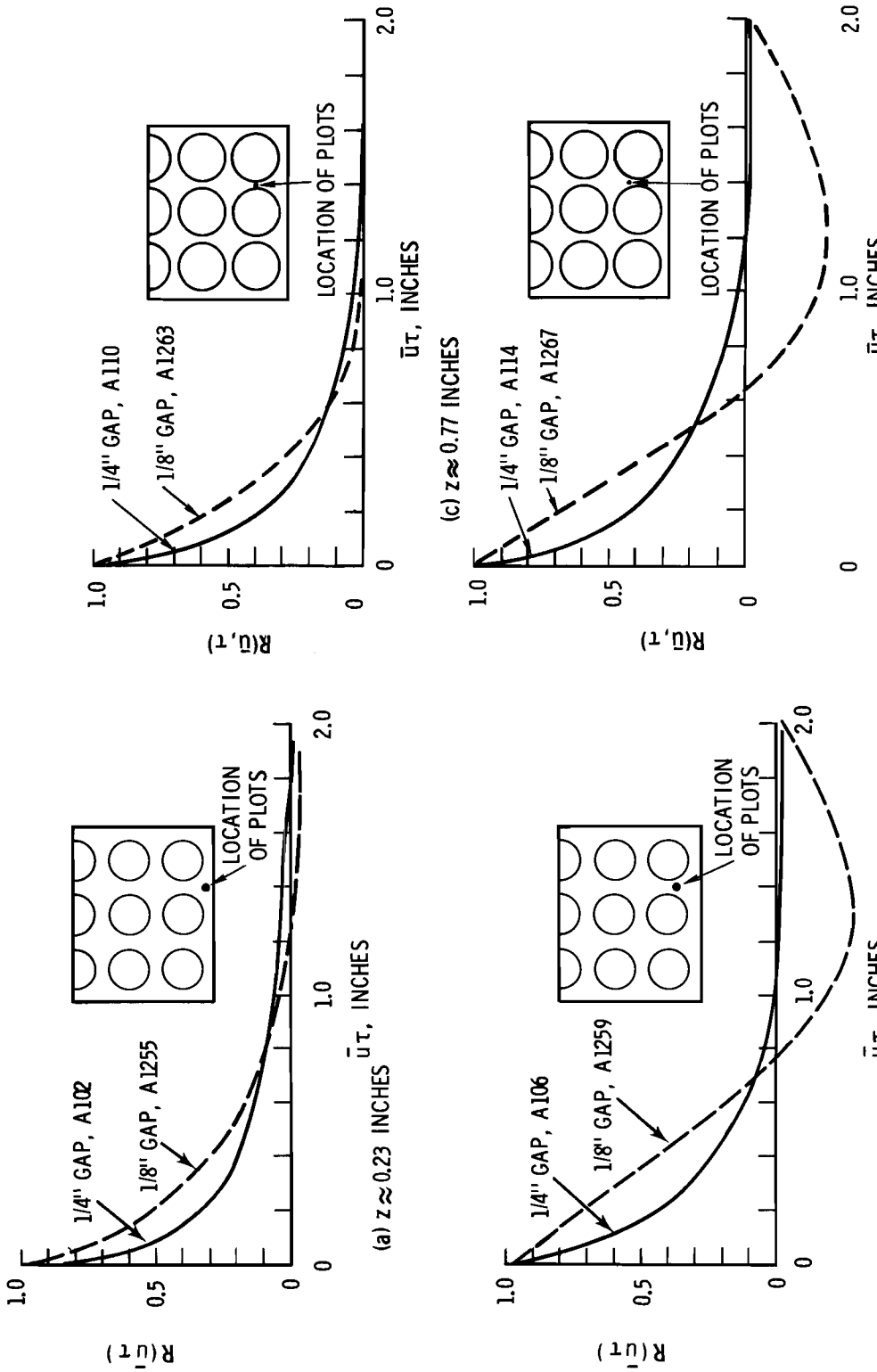

Figure 5.9. Autocorrelation functions along centerline from wall through interior subchannel, Re = 100,000.

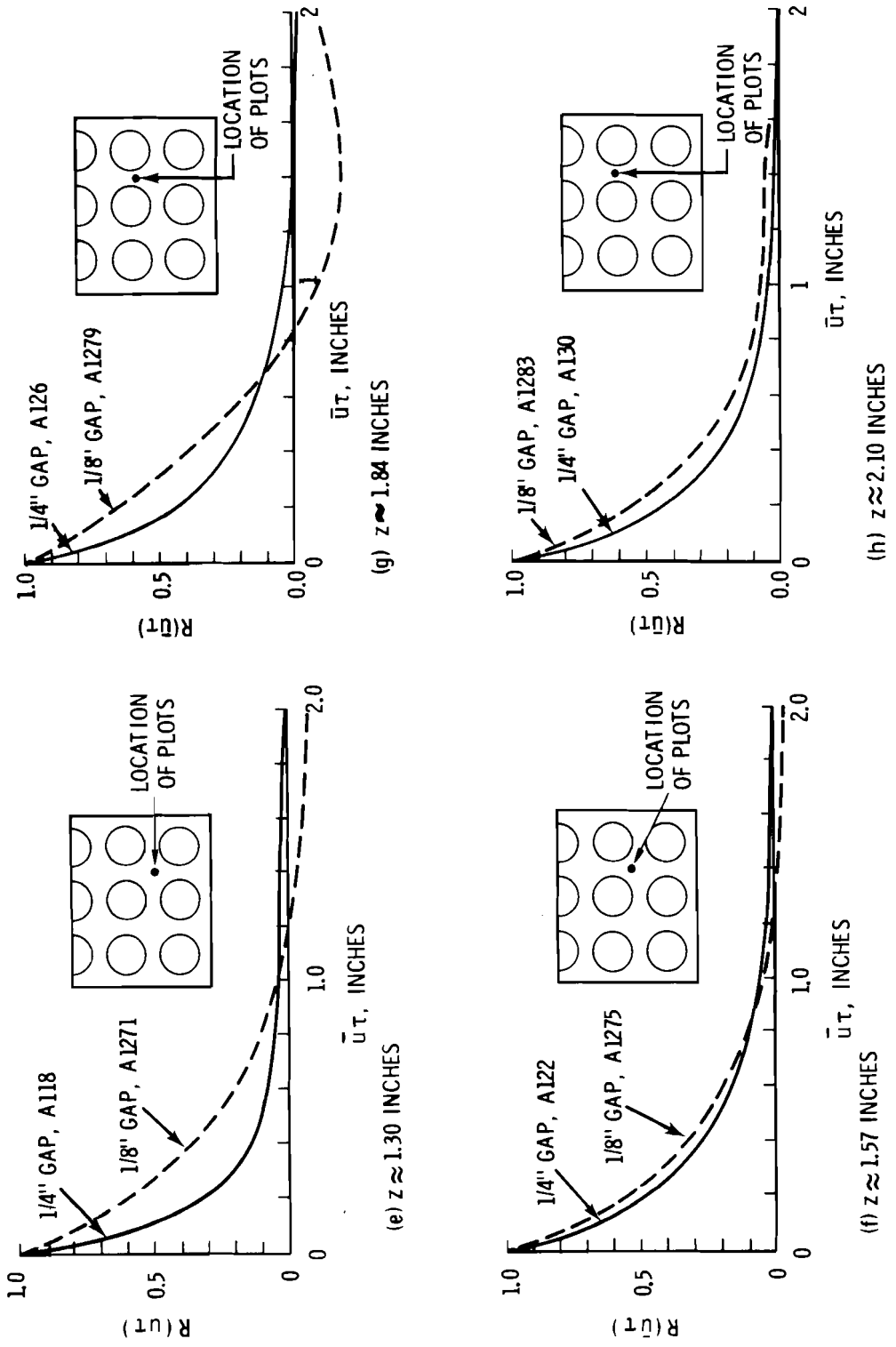

Figure 5.9. (contd)

Notice that the correlation functions for the larger gap spacing decrease faster which indicates smaller eddy size. The larger gap spacing correlation functions always have a nearly exponential decay which indicates a rather wide spectral distribution of turbulence but with energy dominance at low frequency. The correlation functions for the smaller gap spacing have a negative overshoot and periodicity which indicate a higher dominant frequency in the turbulence. This periodic behavior is limited to those regions between the subchannel center and gap center and only to the interior gaps at the 1/8 inch gap spacing. This periodic behavior was not found at any other locations or in any other of the flow channels considered in this study. The occurrence of this periodic motion in a region of expected secondary flow together with the large-scale and high-intensity suggests vigorous lateral turbulent flow near the rod gap. As shown by the nearly exponential decay of the autocorrelation in Figure 5.9, the periodic behavior does not exit (or is very weak) near the flow housing wall, in the rod gap, and at the subchannel center. This indicates that the periodic macroscopic flow process are limited to the region between the gap and subchannel center; however, these flow processes do affect the turbulent flow in the adjacent regions.

Figure 5.10 shows selected autocorrelation functions obtained in the corner and wall subchannels for the two gap spacings. These plots do not show significant periodic behavior as for those obtained at the interior part of the bundle.

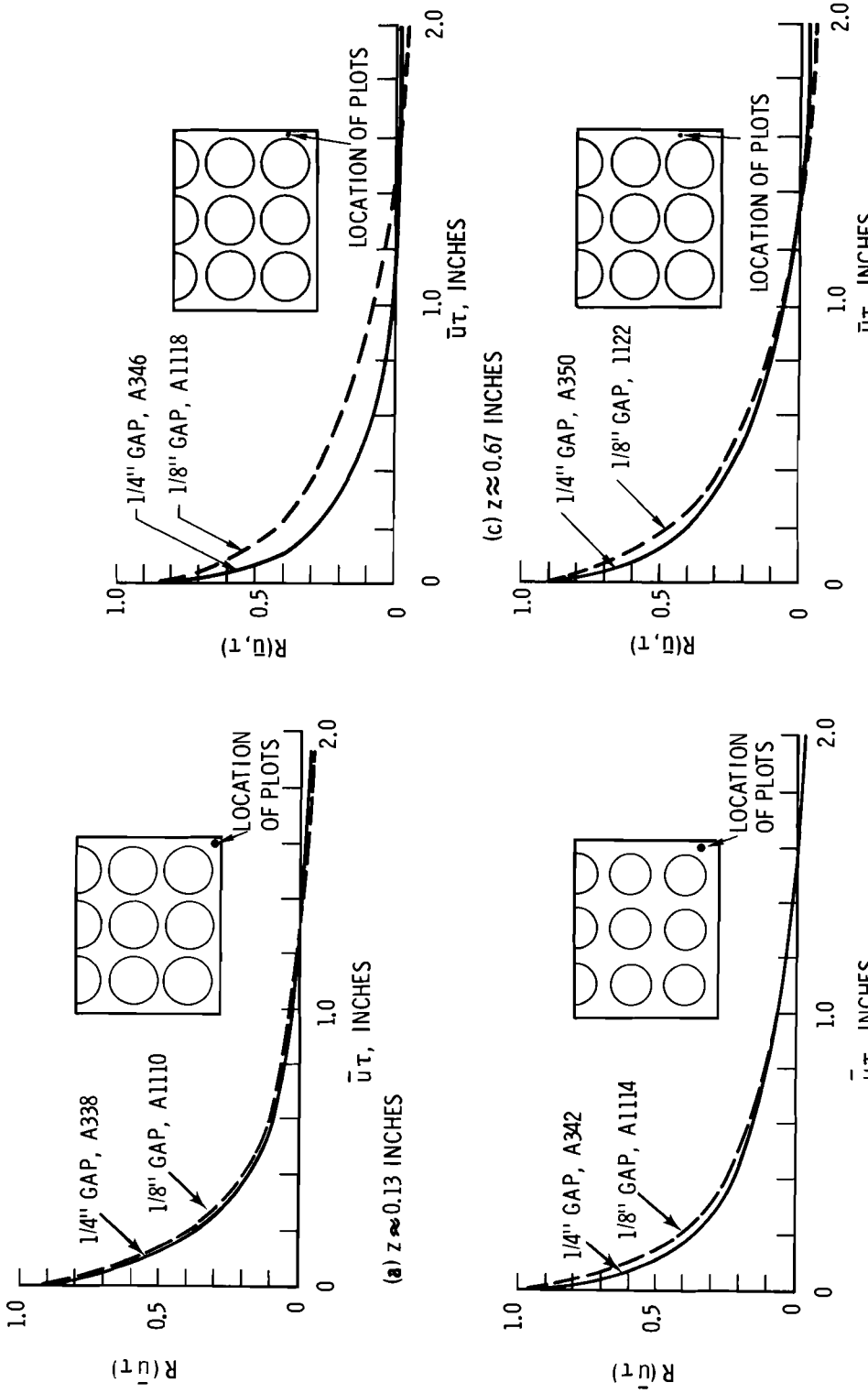

Figure 5.10. Autocorrelation function along centerline from corner through wall subchannel, Re = 100,000.

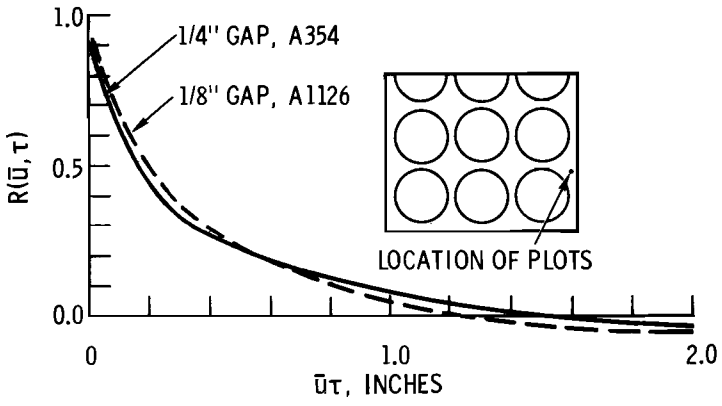

(e) $z \approx 1.21$ INCHES

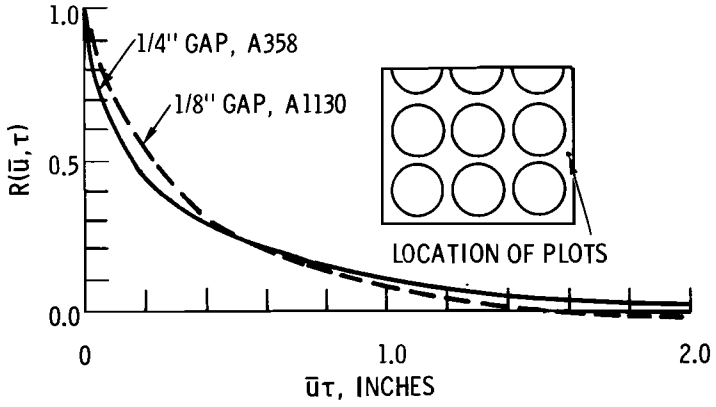

(f) $z \approx 1.48$ INCHES

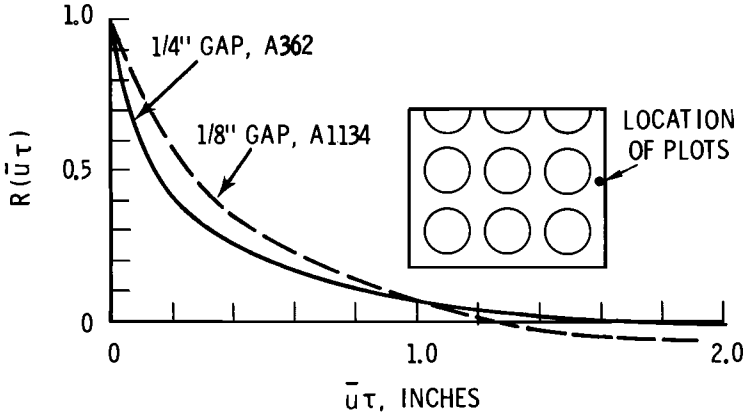

(g) $z \approx 1.75$ INCHES

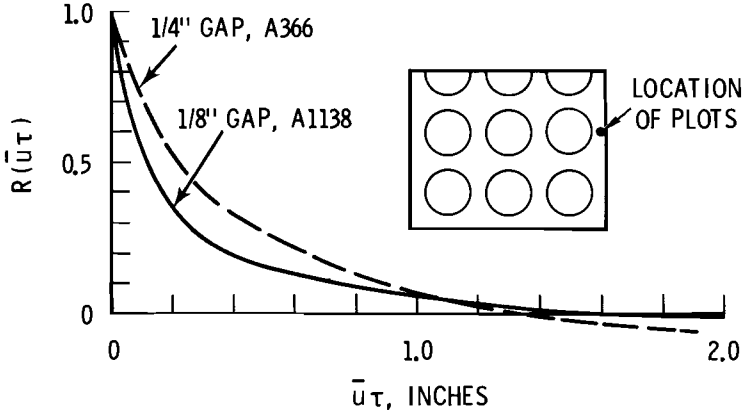

(h) $z \approx 2.01$ INCHES

Figure 5.10. (contd)

The observed effect of gap spacing on the interior subchannels is very significant as it is the first known measurement of turbulence parameters that can explain why intersubchannel mixing rates in rod bundles are weakly dependent upon gap spacing. These results show that the scale, periodicity and intensity increase as the lateral mixing area decreases. The implication is that, for sufficiently large gaps, a reduction in the gap spacing does not significantly reduce the lateral mixing process in rod bundles.

5.1.3 Effect of Reynolds Number

Figures 5.11 through 5.16 show profiles of velocity, intensity, and scale along centerlines through rod gaps for Reynolds numbers of 50,000, 100,000 and 200,000. The lower value was obtained by reducing the flow by a factor of two at a given temperature and the higher value was obtained by increasing temperature to decrease the kinematic viscosity by a factor of two. The data in Figures 5.11 and 5.12 show very little change with Reynolds number at the 1/4 inch gap spacing. The scale data seem to show some increase with increasing Reynolds number; however, the effect is not large considering the four-fold change in Reynolds number.

Figures 5.13 and 5.14 show similar data obtained for the 1/8 inch gap spacing. A more significant effect of Reynolds number seems to exist in this data; however, this effect is not believed to be real. An explanation for this apparent effect was found subsequent to data acquisition and reduction. Examination of the flow model showed that

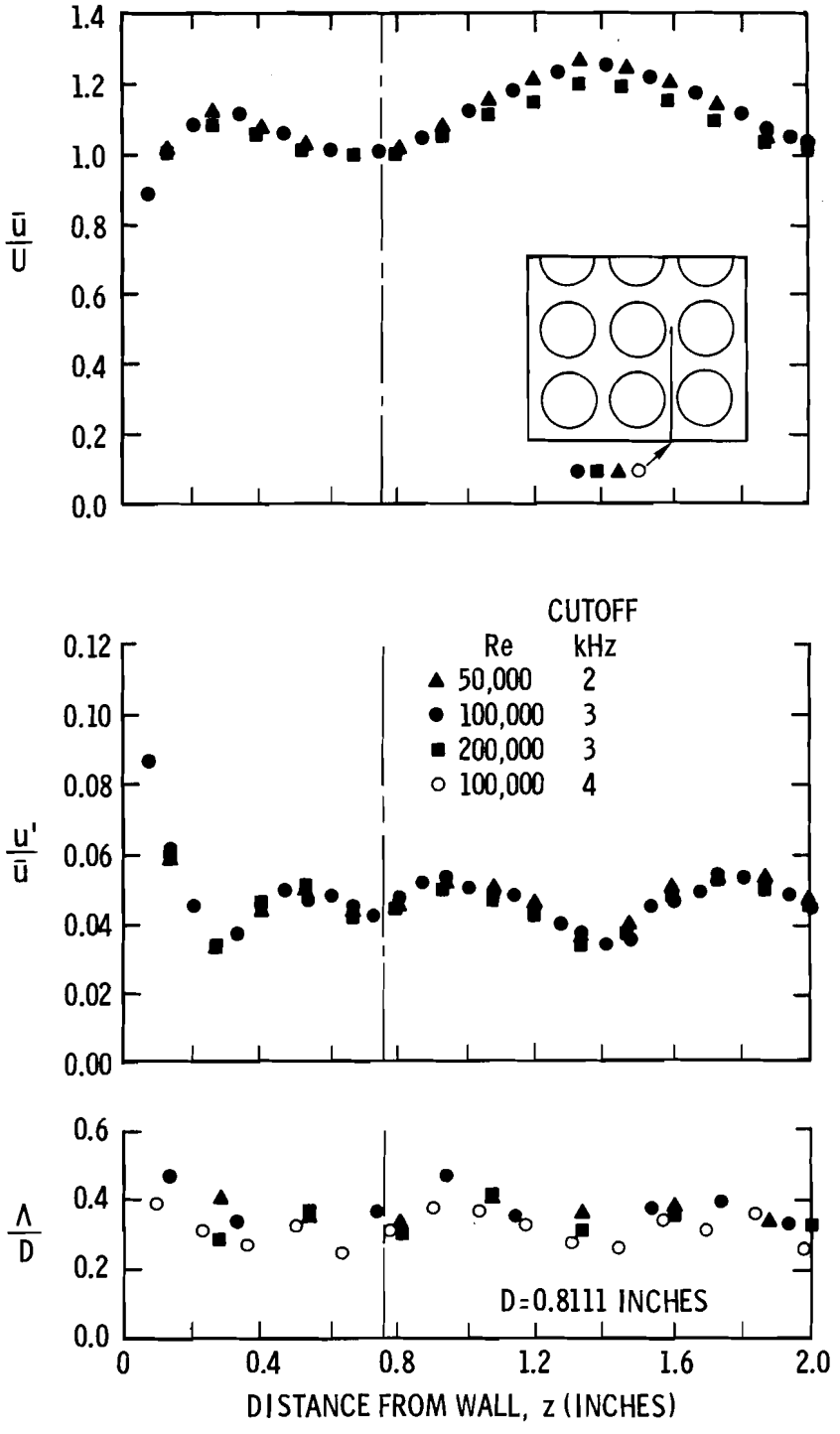

Figure 5.11. Effect of Reynolds number, centerline traverse from wall through interior subchannel, 1/4 inch rod-rod spacing, y = 0.625 inches.

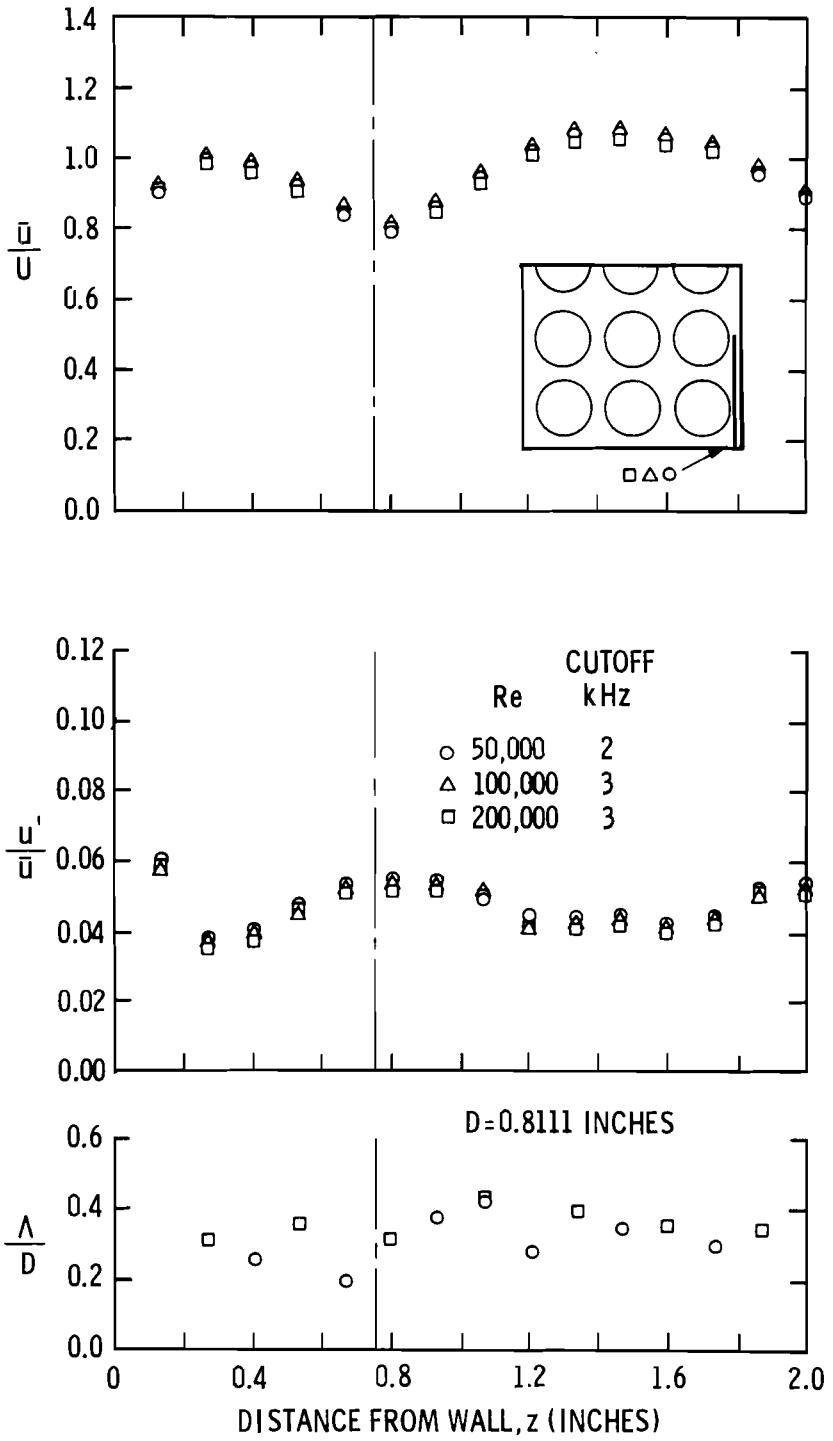

Figure 5.12. Effect of Reynolds number, traverse from corner through wall subchannel, 1/4 inch rod-wall spacing, y = 1.820 inches.

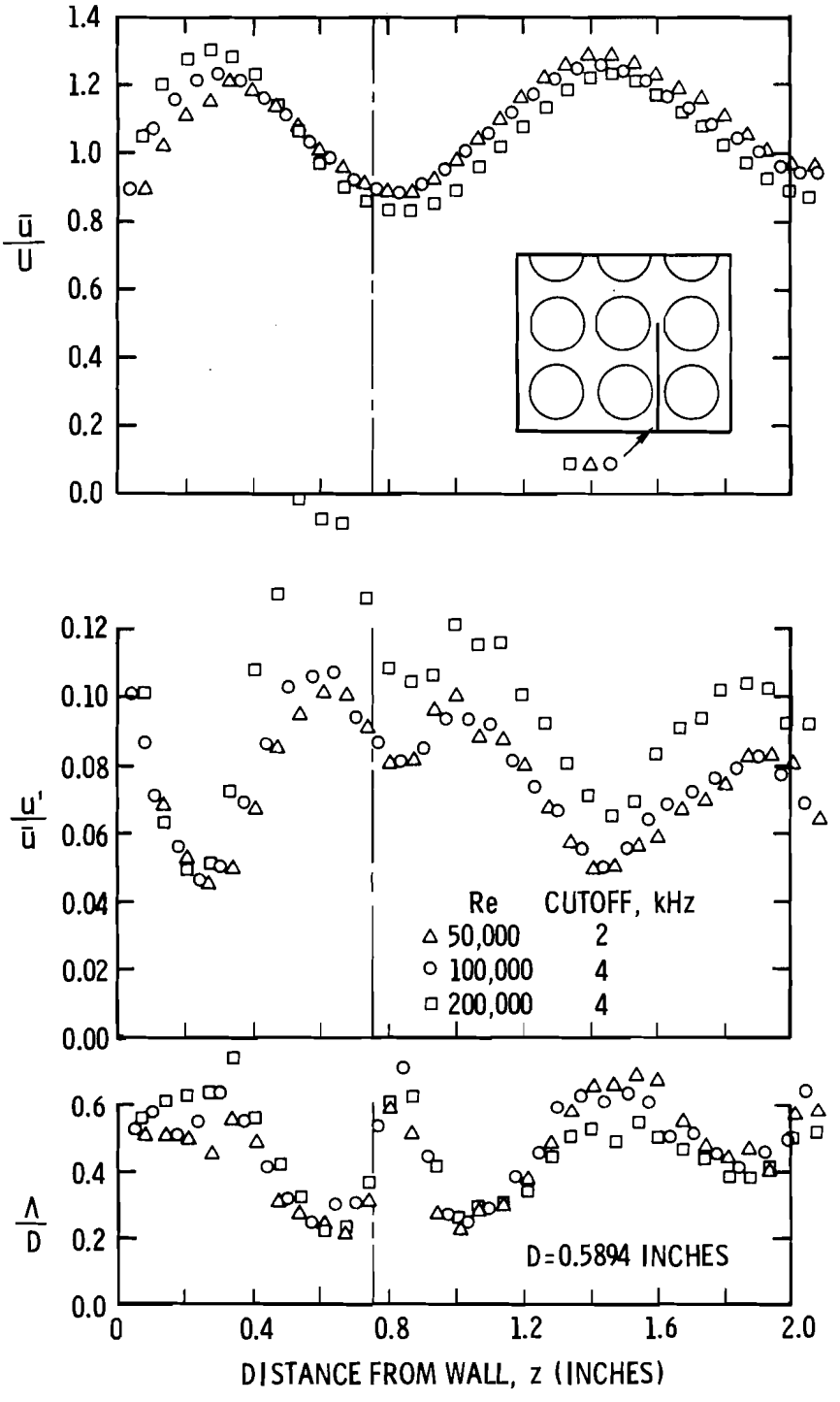

Figure 5.13. Effect of Reynolds number, centerline traverse from wall through interior subchannel, 1/8 inch rod-rod spacing, y = 0.625 inches.

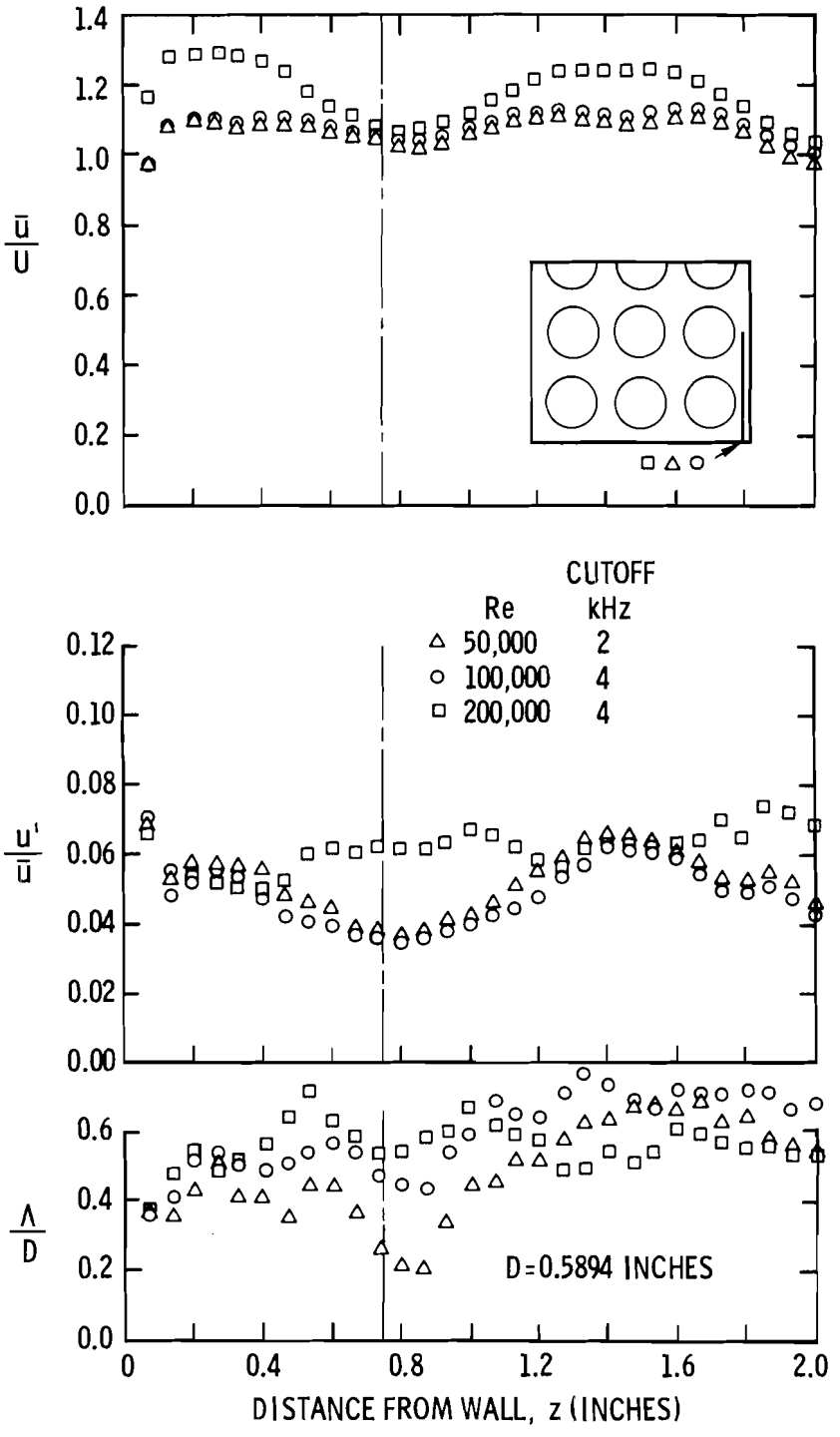

Figure 5.14. Effect of Reynolds number, centerline traverse from corner through wall subchannel, 3/16 inch rod-wall spacing, y = 1.906 inches.

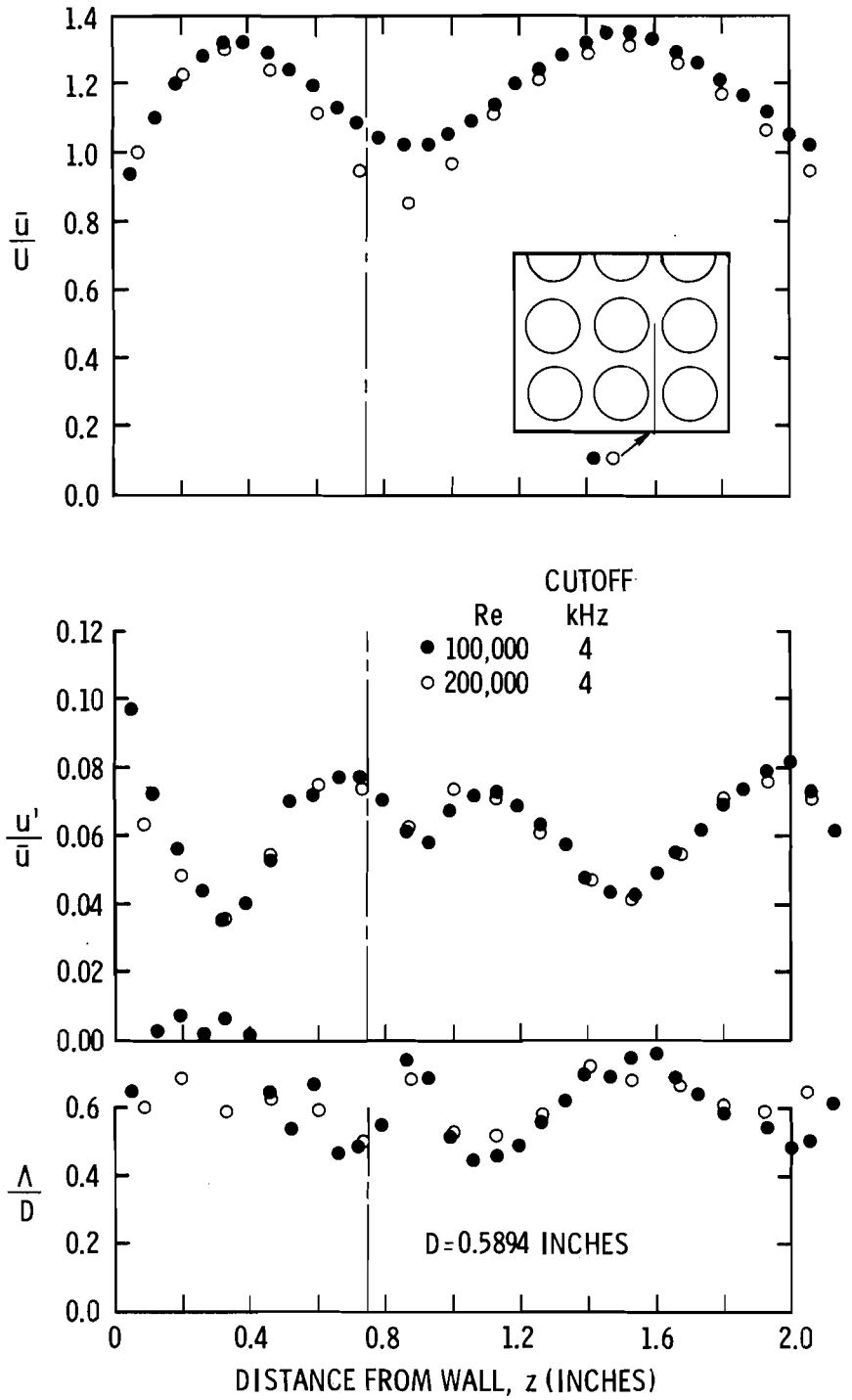

Figure 5.15. Rerun, effect of Reynolds number, centerline traverse from wall through interior subchannel, 1/8 inch rod-rod spacing, y = 0.625 inches.

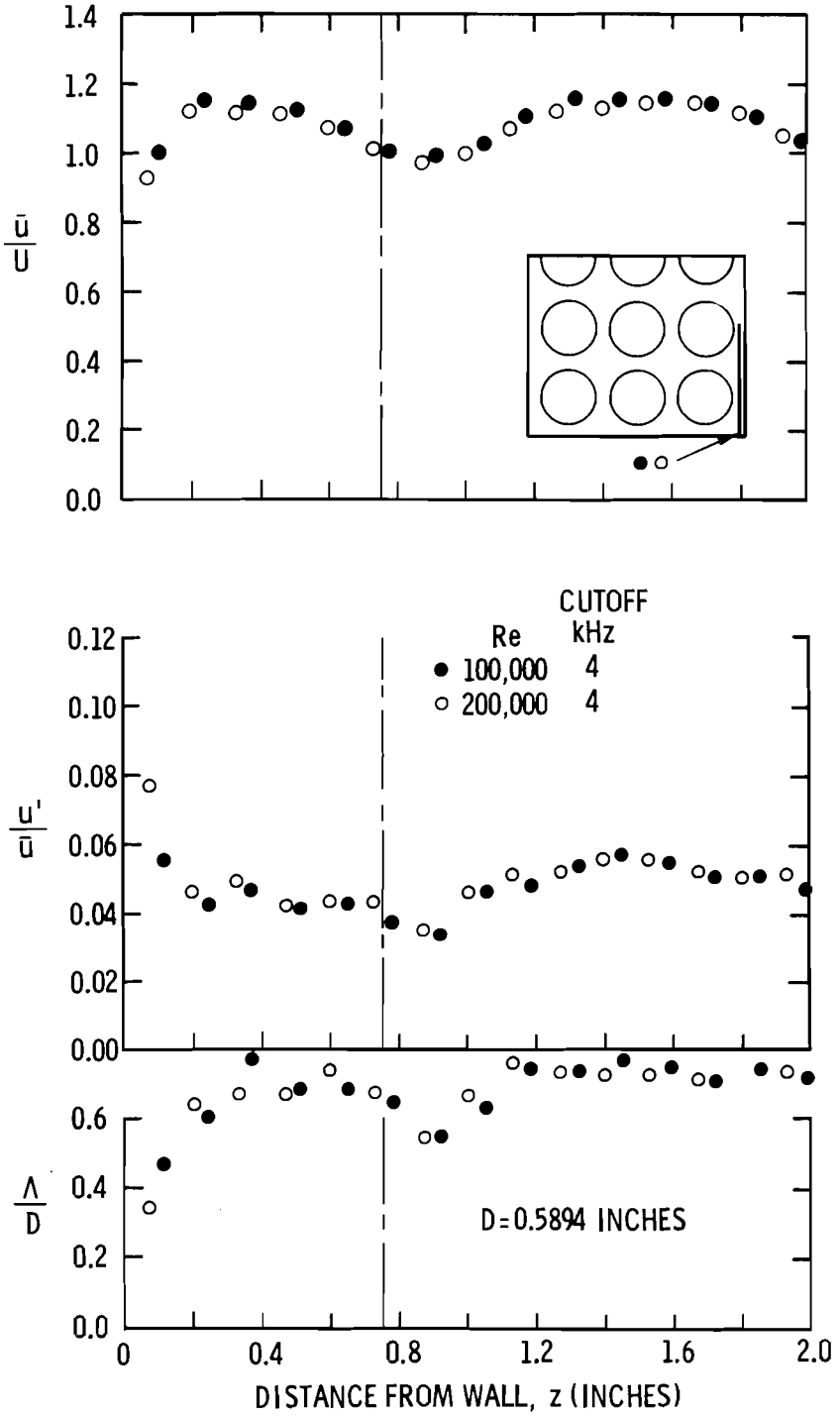

Figure 5.16. Rerun, effect of Reynolds number, centerline traverse from corner through wall subchannel, 3/16 inch rod-wall spacing, y = 1.906 inches.

it had been severely corroded beneath a paint coating that was put on the rods to minimize light reflections. The surface at the time of examination was similar to very rough sandpaper with patches of paint peeling off the rods. The bundle was reinstalled to check the pressure drop and was found to have a friction factor about 80% above that of a smooth tube. It was apparent that the previously described Reynolds number effect was affected by an increased roughness of the rods since the data were obtained in order of increasing Reynolds number over about a five day period after installing the bundle.

The bundle was disassembled, cleaned and reinstalled for some check runs to re-evaluate the effect of Reynolds number. The results in Figures 5.15 and 5.16 show that the Reynolds number effect is weak and that the data runs A1000 through A1491 probably experienced the effect of progressive roughening of the rods. The results in Figures 5.15 and 5.16 show moderate differences from the first set of data in Figures 5.13 and 5.14 obtained at Re = 50,000. In particular, the turbulence intensity is about 20% lower and the scale about 20% higher near the outer rod-rod gap. The reason for this is believed to be caused by slightly different rod spacings. Lateral traverses indicated a gap width of about 0.105 inch originally[4] and 0.125 inch for the rerun.

When the data in Figures 5.13 and 5.14 are viewed in light of increasing rod surface roughness (unknown magnitude) with Reynolds

---

[4]This gap width reduction was caused by a bowed rod which was straightened for the rerun. This was the only case where dimensions differed from the nominal tolerances of the flow model.

number, some rather interesting observations can be made. The velocity profile changes moderately with increasing Reynolds number. The velocity in the wall subchannel tends to increase and move toward the wall while the velocity in the gaps and interior subchannel tends to decrease and shift toward the interior. The turbulence intensity shows a definite increase with increasing Reynolds number especially for the change from 100,000 to 200,000. The largest changes are seen to occur near the outer rod-rod gap. The intensity distribution in the outer gap also shifts slightly toward the interior as does the velocity. The turbulence scale is not affected very much by increasing the Reynolds number. The only trend is a small increase in scale in the corner subchannel and a small decrease in the scale near the center of the interior subchannel. Figure 5.14 shows the results for the 3/16 inch rod-wall spacing. The velocity profile shows a significant increase in the open part of the subchannels in going from a Reynolds number of 100,000 to 200,000. The observed increase in the wall subchannel velocity is consistent with the shift shown previously in Figure 5.13. The intensity data show a sudden shift but it is limited to the gap region of both rod-wall gaps. An increase in scale occurs with increasing Reynolds number primarily near the corner rod-wall gap. Only small changes in scale occur at other regions in the wall subchannels.

The observed shift in the corner and wall region suggests a change in the turbulence flow pattern. Since flow transitions are known to occur in turbulent flows in the presence of secondary motions; and,

since secondary flow circuits exist as a finite number, a change in their number could cause shifts in velocity, intensity, and scale distributions. These changes could be caused by nonuniform changes in wall shear stress such as by roughened rods in the presence of a smooth housing wall.

Figures 5.17 through 5.19 present autocorrelation function plots at identical channel locations at the three Reynolds numbers considered. Figures 5.17 and 5.18 show very little effect of Reynolds number on the shape of the curves for the 1/4 and 1/8 inch gap spacing in Channel A. This is consistent with the weak Reynolds number effect found in the interior channels as previously shown in Figures 5.11 and 5.12. The data in Figure 5.19 indicates increasing scale with increasing Reynolds number in the corner rod-wall gap. The region near this gap is the only location where any meaningful increase in scale was observed with increasing Reynolds number.

5.1.4 Effect of Flow Model Size

It is desirable to use a simple rod bundle flow model for mixing studies; however, the model should not restrict or alter the basic flow processes being investigated. To investigate the effect of reduced flow model size and its effect on reduced lateral freedom, turbulence data were taken in Channels B and C shown in Figure 4.3. These contained side-by-side subchannels of different shapes that are often used in simple crossflow mixing studies.

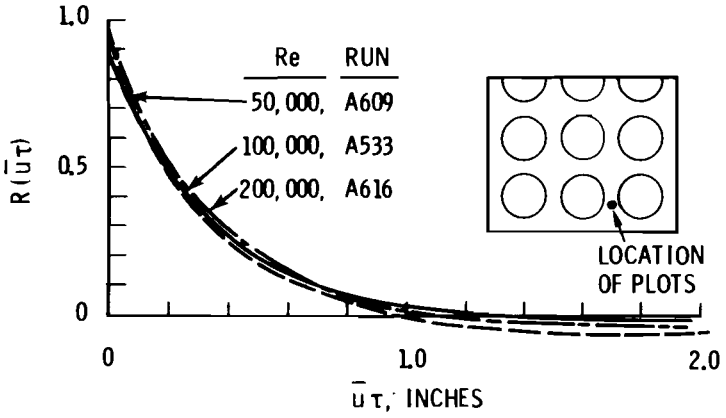

(a) WALL SUBCHANNEL, TOWARD GAP

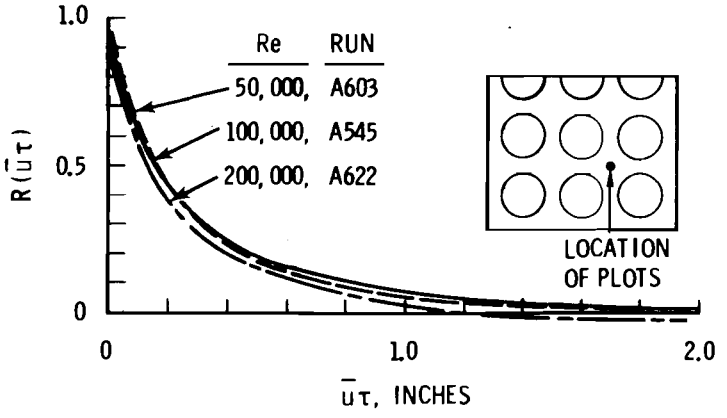

(b) INTERIOR SUBCHANNEL

Figure 5.17. Effect of Reynolds number on autocorrelation function, 1/2 inch gap spacing.

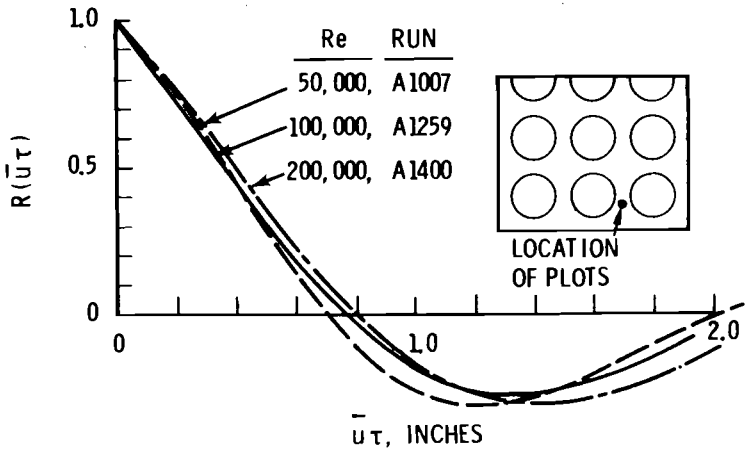

(a) WALL SUBCHANNEL, TOWARD GAP

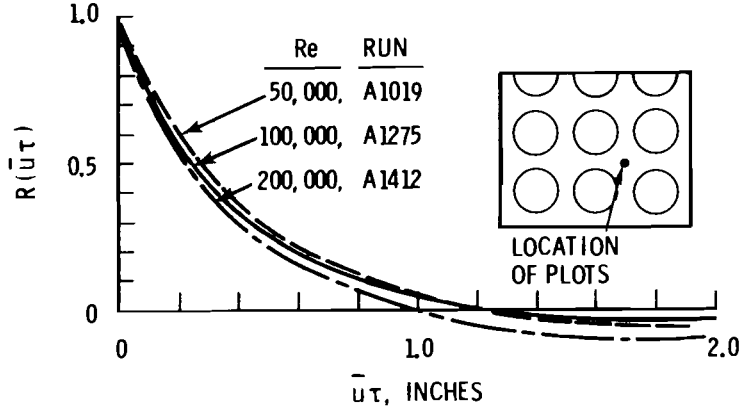

(b) INTERIOR SUBCHANNEL

Figure 5.18. Effect of Reynolds number on autocorrelation function, 1/8 inch gap spacing.

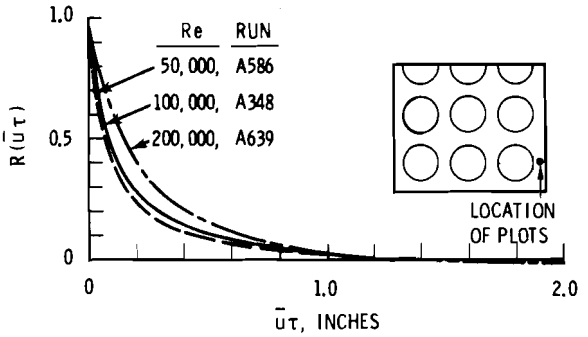

(a) CORNER ROD-WALL GAP, 1/4 INCH SPACING

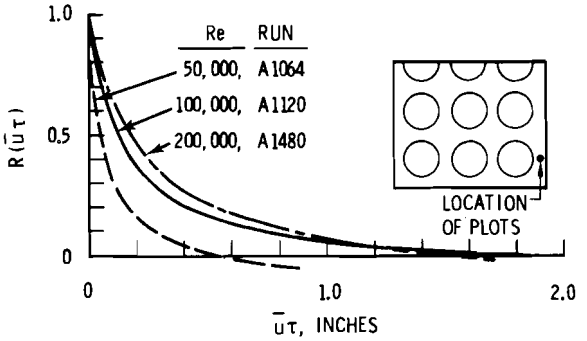

(b) CORNER ROD-WALL GAP, 3/16 INCH SPACING

Figure 5.19. Effect of Reynolds number on autocorrelation function in corner rod gap.

Figures 5.20 through 5.23 show the velocity and turbulence intensity maps in the interior and wall subchannels. The velocity and intensity profiles in the side and center subchannel are seen to be nearly identical for these two flow models. The only difference between Channel B and C is the flow channel shape on the left side of the centerline.

The distinguishing feature of the contour maps in Channels B and C is the secondary flow currents in the corners of the flow channels as indicated by the distortion of the lines of constant velocity

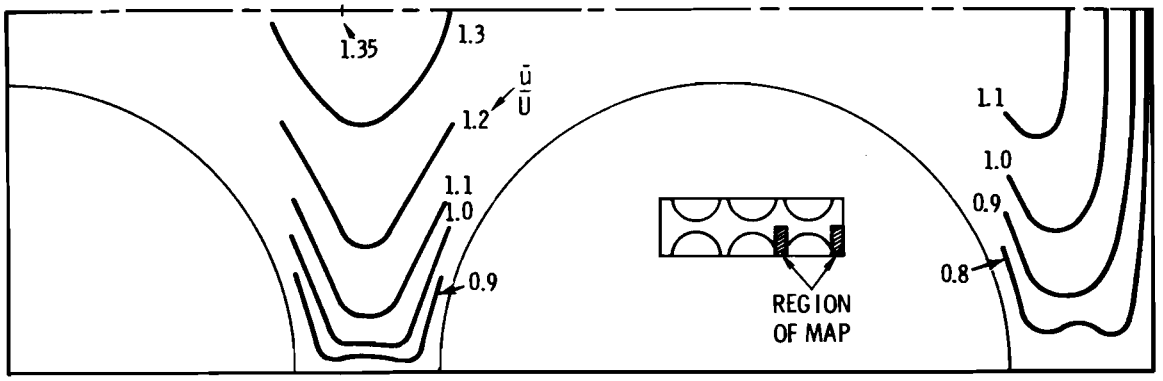

Figure 5.20. Velocity ($\bar{u}/U$) map in Channel B, Re = 100,000, p/d = 1.25.

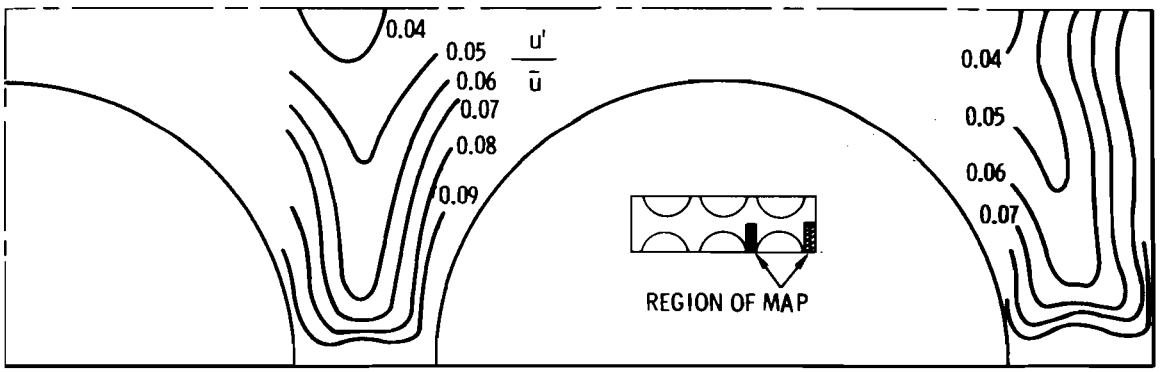

Figure 5.21. Axial component turbulence intensity ($u'/\bar{u}$) map in Channel B, Re = 100,000, p/d = 1.25.

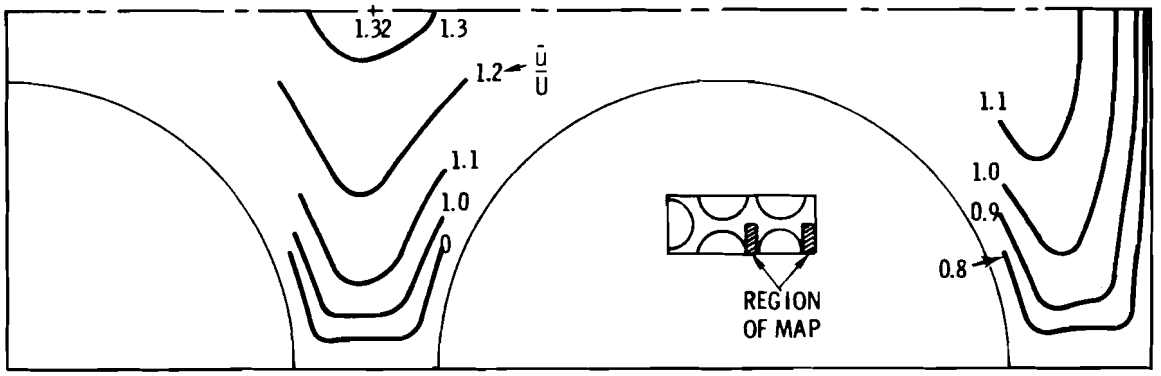

Figure 5.22. Velocity ($\bar{u}/U$) map in Channel C, Re = 100,000, p/d = 1.25.

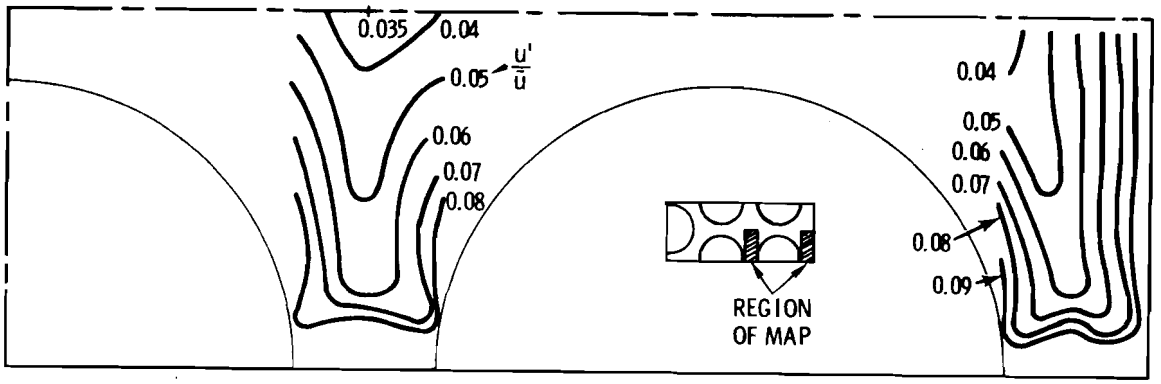

Figure 5.23. Axial component turbulence intensity ($u'/\bar{u}$) map in Channel C, Re = 100,000, p/d = 1.25.

and intensity. These distortions are very similar to those of Channel A shown in Figures 5.1 and 5.2. Except for the corners in Channels B and C, the shape of velocity and intensity profiles are nearly identical to those in Channel A; however, the values of intensity are about 20% lower. These lower values are believed to be real since the cutoff frequency for these channels was equal to or higher than for Channel A. The lower intensity could possibly be attributed to less lateral freedom in the flow channel.

Figure 5.24 shows data obtained along a centerline traverse in the interior subchannel of Channel B. The distributions of data are quite similar to the data for the interior subchannel of Channel A except for the channel extremities. The magnitude of turbulence intensity and scale compare well.

5.2 FLOW STRUCTURE IN ROD GAP

Since there has been considerable interest and speculation concerning turbulent flow structure in rod gaps of rod bundles, considerable experimental effort was directed toward investigating this region. The effects of subchannel shape, multiple degrees of lateral freedom and gap spacing were considered.

5.2.1 Effect of Subchannel Shape

Figures 5.25 and 5.26 present the velocity, intensity, and scale distribution along a traverse across the rod gaps of Channels D and E. Channel D has identical subchannels on each side of the gap whereas Channel E has different adjacent subchannels. The results in

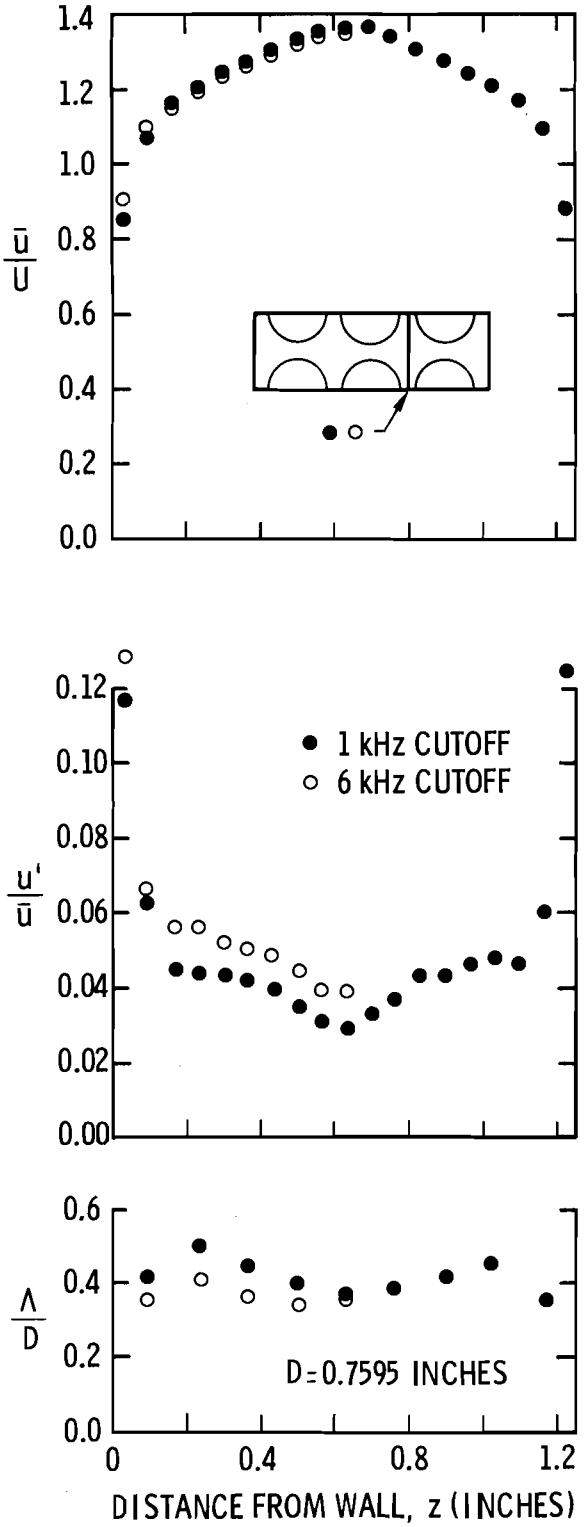

Figure 5.24. Centerline traverse through interior subchannel, Re = 100,000, y = 0.625 inches, 1/4 inch rod-rod spacing.

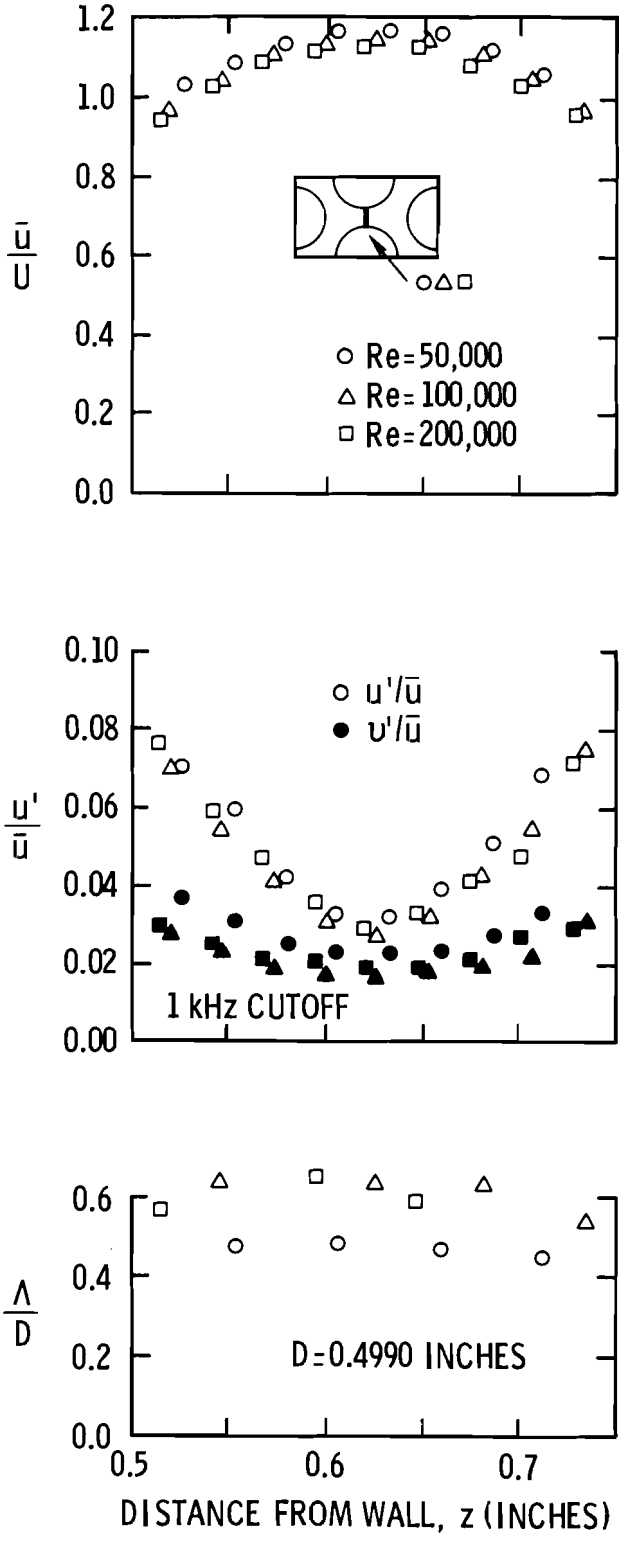

Figure 5.25. Velocity, intensity and scale in gap, Channel D.

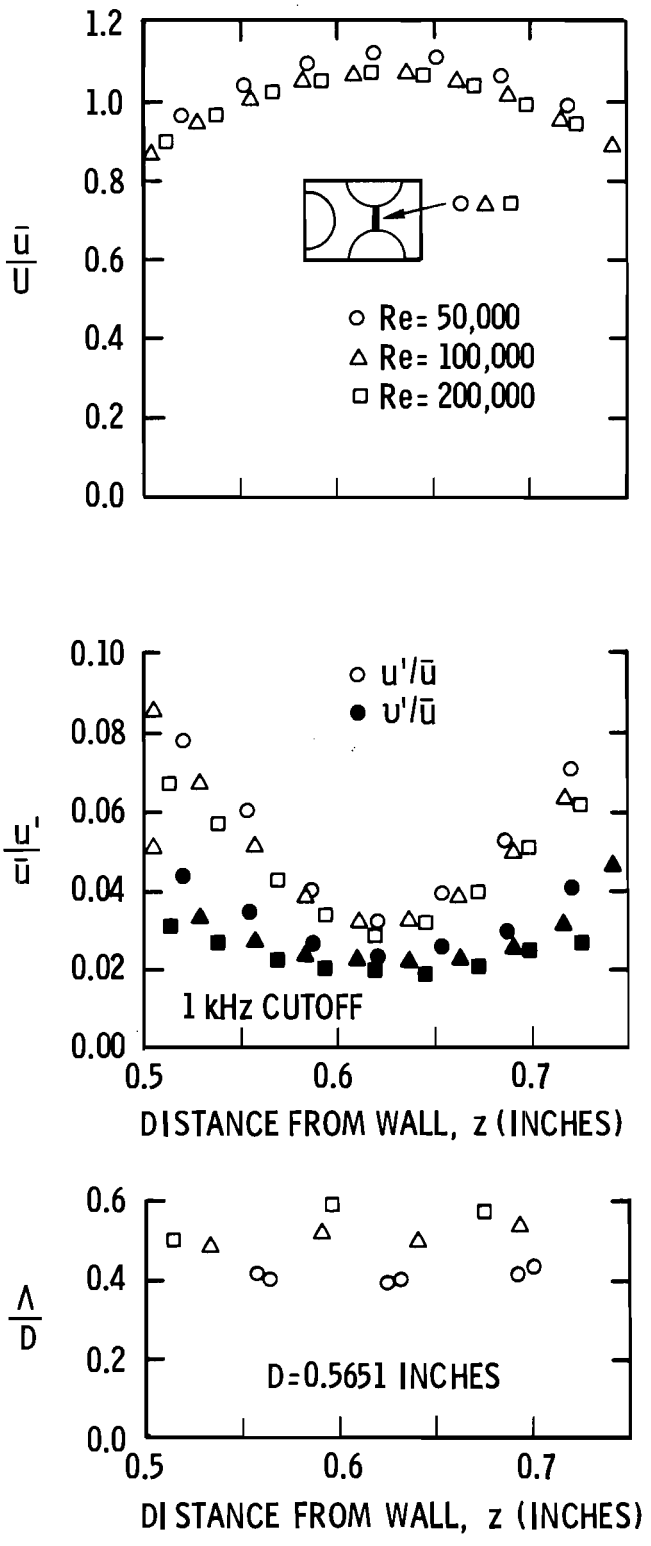

Figure 5.26. Velocity, intensity and scale in gap, Channel E.

Figures 5.25 and 5.26 are nearly identical for the two channels. They both show only a slight influence of Reynolds number. The slight decrease in the velocity profile with increasing Reynolds number is within experimental error so it is not conclusive. The turbulence intensity profiles show a slight decrease and flattening with increasing Reynolds number. The lateral component of intensity is seen to be about 50% to 70% of the axial component depending upon the location in the gap. The shapes and values of the intensity profiles are similar to those found for flow in round pipes (36,37,46).

All data obtained in Channels D and E were taken with a frequency cutoff of 1 kHz. Subsequent to taking these data, a higher frequency cutoff was adopted. The consequence of this lower cutoff is that the turbulence intensity data are too low, especially for the two higher Reynolds number as they were at the same velocity. It is estimated that the intensity should be increased by 10% to 15% for Re = 100,000 and 200,000. The scale should also be reduced for these two Reynolds numbers. A lower frequency cutoff would lower the value of the autocorrelation function at $\tau = 0$; therefore, it would decrease the slope in that region. This would give a larger value of T_E and therefore a larger value of Λ.

Comparison of Figure 5.25 and 5.26 shows a small change in the velocity profile magnitude. The velocity profiles are about 5% lower in the gap of Channel E as compared to Channel D. This is due to the lower velocity in the triangular shaped subchannel. The intensity data

are essentially identical for the two channels. The dimensionless scale Λ/D within the gap of Channel E is about 20% smaller than in Channel D. If average values of $\Lambda/D = 0.50$ and 0.42 are taken at a Reynolds number of 50,000 for Channels D and E, respectively, then the corresponding scales are 0.25 and 0.24 inches.

These results show that the turbulence intensity and scale are nearly identical for Channels D and E; therefore, the shape of the adjacent subchannels in this case has little effect on the flow structure in rod gaps. Furthermore, the results are not significantly affected by Reynolds number which is in agreement with the results presented previously.

5.2.2 Effect of Lateral Freedom

Channels D and E represent a very simple model of a rod bundle subchannel pair. It is natural to wonder if adding more subchannels would change the gap flow structure by allowing more lateral freedom. The data obtained in Channels B and C represent added side-by-side lateral freedom. The results are presented in Figures 5.27 and 5.28. A comparison of these data with the data in Channels D and E show that the added lateral freedom has only a small effect on the flow structure in the rod gap. The slightly higher turbulence intensity for the side gap as compared to the center gap in Channel B is due in part to the data being taken inadvertently 0.080 inches from the gap centerline. As for Channels D and E, there appears to be no affect of adjacent subchannel shape. A comparison of the scale indicates slightly larger

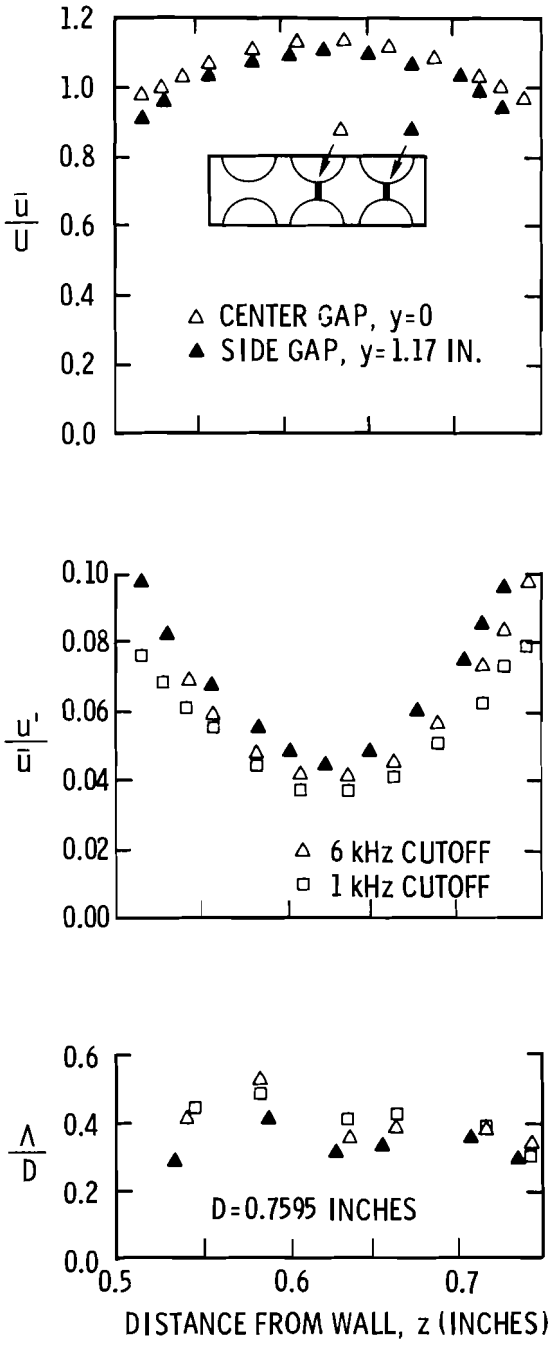

Figure 5.27. Velocity, intensity and scale in the gaps of Channel B, Re = 100,000.

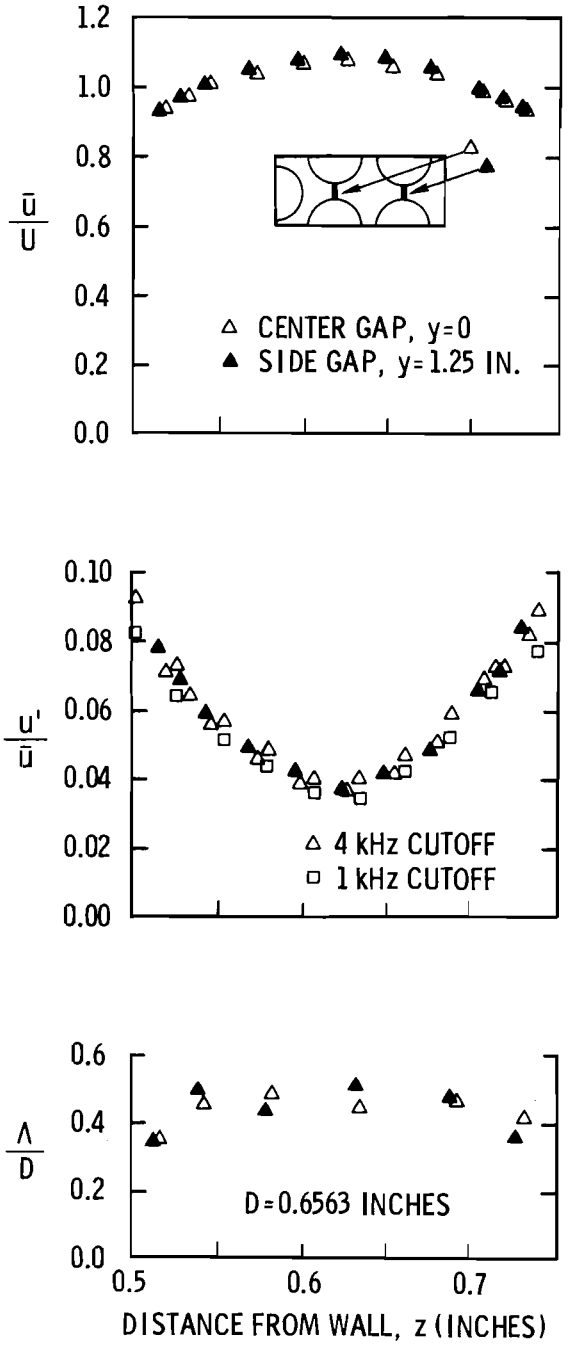

Figure 5.28. Velocity, intensity and scale in gaps of Channel C, Re = 100,000.

scale in the gaps of Channel C. However, if a mean values of Λ/D of 0.37 and 0.46 are taken for Channels B and C, then the corresponding scales are 0.28 and 0.30 inches, respectively. This turbulence scale is larger than the rod gap spacing and is also about 15% larger than the data from Channels D and E. This seems to indicate that the added lateral freedom causes larger scale turbulence in the gap region; however, the effect is small.

Since the data of Channels D and E were obtained with a frequency cutoff of 1 kHz, data were taken in Channels B and C to assess the importance of the cutoff frequency. The results of these measurements are presented in Figures 5.27 and 5.28. These data show about 10% increase in intensity and a corresponding decrease in scale for the higher cutoff frequency. At a cutoff of 1 kHz the intensity in Channels B and C are about 20% higher at the center of the gap than in Channels D and E. Toward the wall the results are nearly identical.

These results indicate that adding side-by-side lateral freedom has only a small effect on the turbulence intensity and scale in the rod gap. These results also agree with the insensitive subchannel shape effect found in Channels D and E.

Now consider the data taken in the gaps of Channel A. This channel allows even more degrees of lateral freedom than in Channels B, C, D, and E. The results for the rod gaps of Channel A are presented in Figures 5.29 through 5.32.

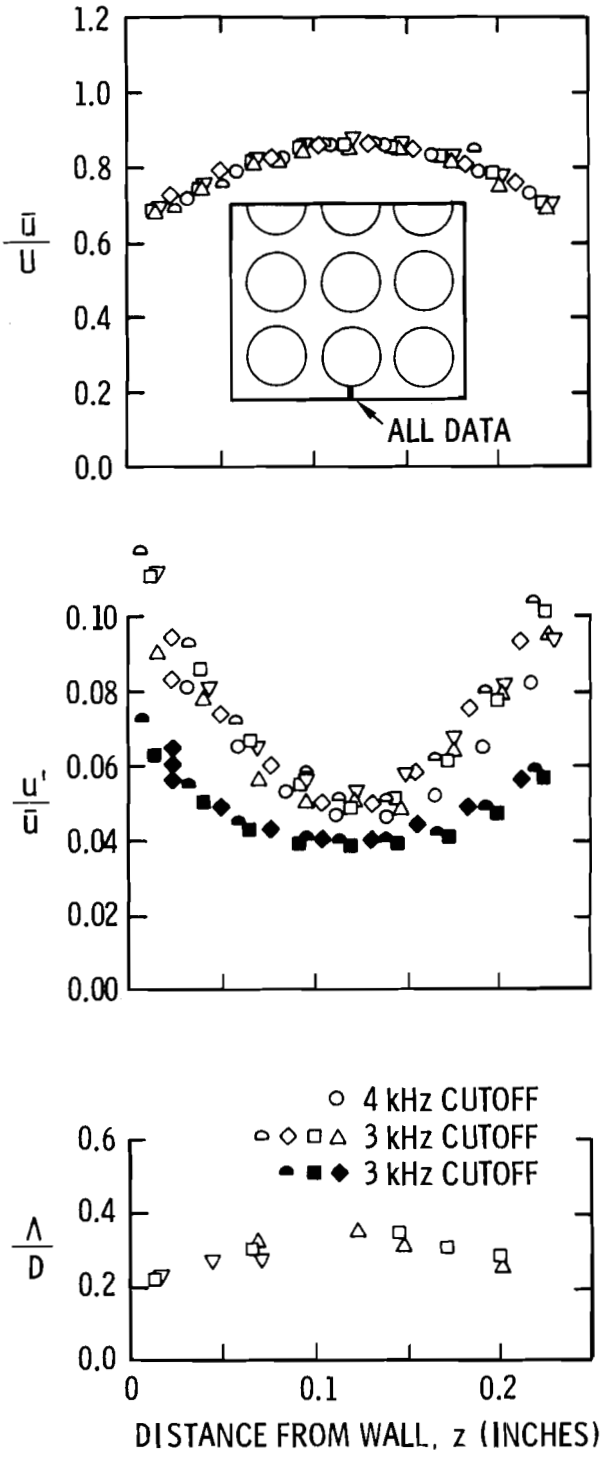

Figure 5.29. Velocity, intensity and scale in center wall gap, Channel A, Re = 100,000, y = 0.0 inches.

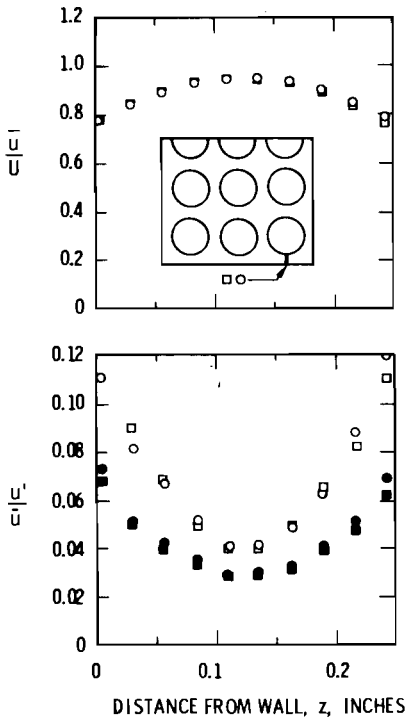

Figure 5.30. Velocity, intensity and scale in corner rod wall gap, Channel A, Re = 100,000, y = 1.250 inches.

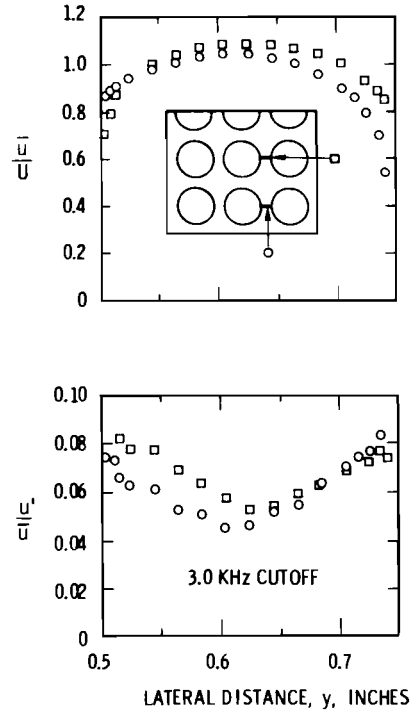

Figure 5.31. Velocity and intensity in interior gaps, Channel A, Re = 100,000.

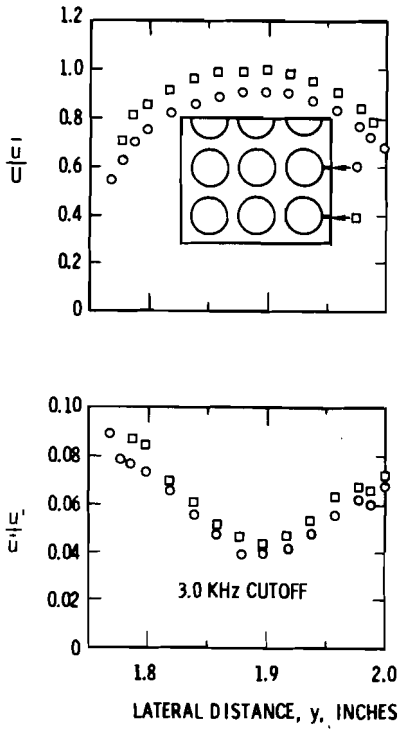

Figure 5.32. Velocity and intensity in rod-wall gaps, Channel A, 1/4 inch gap, Re = 100,000.

Figure 5.27 presents the results for both single- and two-component turbulence data obtained in the center rod-wall gap. The several sets of data obtained at this location show good reproducibility and minimal data scatter. A comparison with the previous data obtained in Channels B, C, D, and E shows that the turbulence intensity is definitely higher than in those channels. At the minimum point the axial component of intensity is about 0.050 as compared to 0.04 for Channels B and C and 0.03 for Channels D and E. The lateral component of intensity is also significantly higher. At its minimum point it has a value of 0.040 as compared to about 0.03 for Channels D and E. The

scale parameter Λ/D has a value of about 0.30 which corresponds to an actual scale of approximately 0.25 inches. This scale is comparable to the scale found in Channels B, C, D, and E.

The turbulence intensity for the other gaps of Channel A shown in Figures 5.30 through 5.32 also indicate higher intensity than observed in the simpler flow channels. A further comparison shows that there is an effect of rod gap location on the values of turbulence intensity in the gaps of Channel A. The corner rod-wall gaps have the lowest values of intensity. The next highest intensities are the center rod-wall gaps followed by the outer rod-rod gaps. The interior rod-rod gaps seem to have the highest turbulence intensity. Distortions of the velocity and intensity profiles in the rod gaps are believed to be caused by slight displacements of the rods and the presence of secondary flows.

In conclusion, these data indicate that allowing lateral freedom, as in an actual rod bundle, gives about 20% higher turbulence intensity than in simple channels with limited lateral freedom. The lateral component of turbulence intensity ranges from about 60% to 80% of the axial component. A small subchannel shape effect seems to appear with the added lateral freedom, especially in the rod gaps near the flow housing wall.

5.2.3 Effect of Rod Gap Spacing

The effect of reducing the gap spacing was investigated by increasing the rod diameter in Channel A from 1 inch to 1-1/8 inch. This produced a 1/8 inch rod-rod gap and a 2/16 inch rod-wall gap. The experimental results within these two gaps are shown in Figures 5.31 through 5.36.

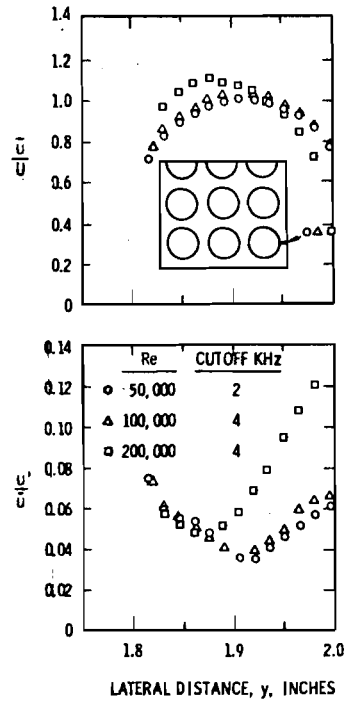

Figure 5.33. Velocity and intensity in corner rod-wall gap, Channel A, 3/16 inch gap.

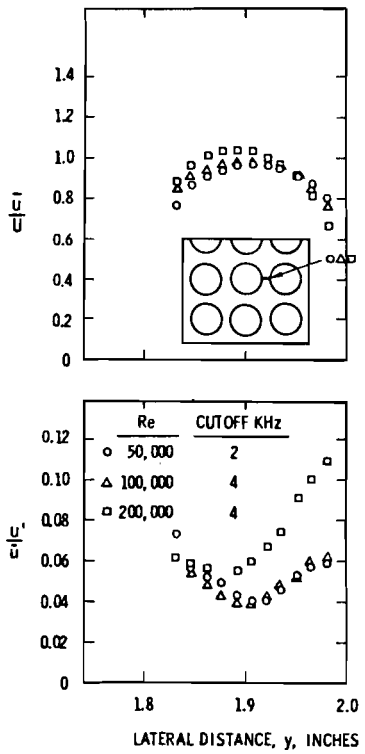

Figure 5.34. Velocity and intensity in center rod-wall gap, Channel A, 3/16 inch gap.

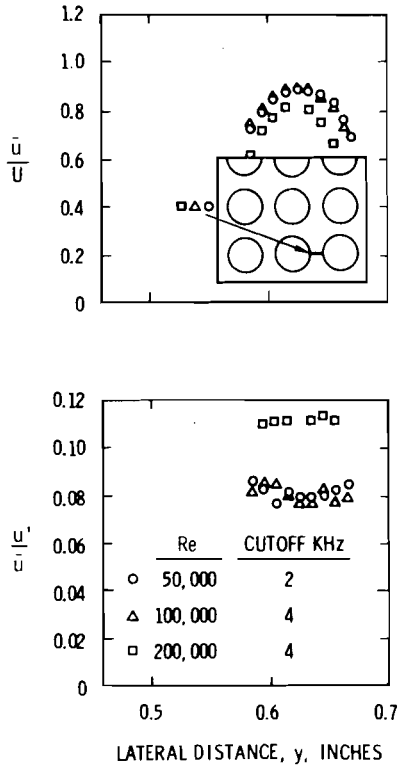

Figure 5.35. Velocity and intensity in interior gaps, Channel A, 1/8 inch gap.

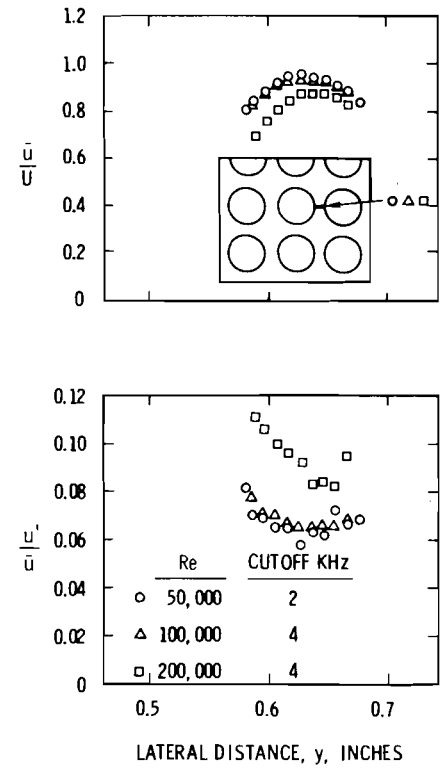

Figure 5.36. Velocity and intensity in interior gap, Channel A, 1/8 inch gap.

The data obtained in the 3/16 inch rod-wall gaps show turbulence intensities with distribution and magnitude, about the same as those obtained with a 1/4 inch rod-wall gap. Minimum values in both cases are typically 0.04. The exception to this is at Re = 200,000 for the 3/16 inch spacing where the distribution shifted and the magnitude of the minimum values increased by about 25%. This exception is believed to be caused by a change in secondary flow patterns and gradual roughening of the rods as mentioned earlier.

The rod-rod gaps show a significant increase in intensity and flattening of the intensity profile for the 1/8 inch gap as compared to the 1/4 inch gap. Similar behavior was found for both the interior and exterior rod-rod gaps; however, the exterior gap changes were more extreme. An increase of average intensity from about 0.055 to 0.08 occurred for the exterior gap and from about 0.06 to 0.07 occurred for the interior gap. The shift in distribution and an increase in intensity at Re = 200,000, is believed to be caused by a secondary flow pattern change as was mentioned earlier.

5.3 CHANNEL FRICTION FACTORS

Pressure drop was measured in all of the experimental flow models used for the turbulence measurements. A tabular list of the data are presented in Table B-2, Appendix B.

Figure 5.37 presents the pressure drop data as a plot of friction factor versus Reynolds number and compares it with the well known smooth tube friction factor correlation. The agreement is seen to be quite

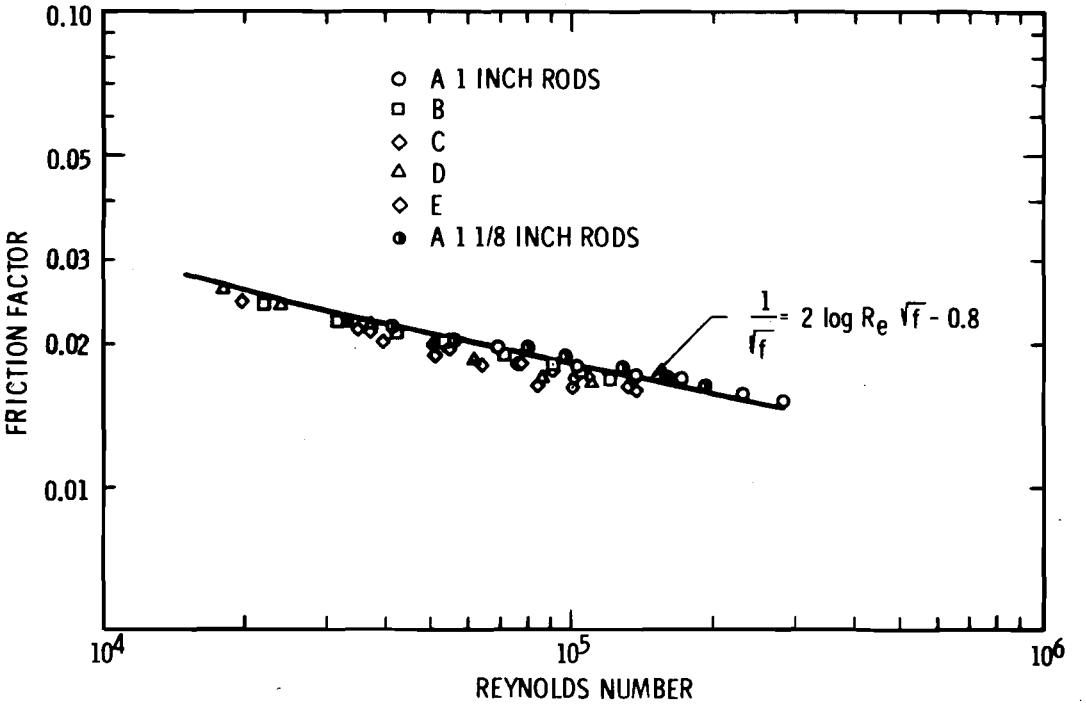

Figure 5.37. Friction factor data for experimental flow models.

good for all of the flow channels but with the data tending to fall lower. There appears to be a small decrease in friction factor for successively smaller flow channels and also a steepening of the slope. A least squares fit of the friction factor data was performed by assuming a correlation of the form

$$f = \alpha_1 \, Re^{\alpha_2}$$

where α_1 and α_2 are the correlation parameters. The results of the curve fit are presented in Table 5.1 together with the computed standard deviation.

TABLE 5.1. Friction Factor Curve Fit Parameters

Channel	α_1	α_2	σ
A 1 in. Diam Rods	0.1566	-0.1869	0.00024
A 1-1/8 in. Diam Rods	0.2112	-0.2110	0.00012
B	0.2182	-0.2196	0.00003
C	0.2008	-0.2142	0.00011
D	0.3746	-0.2725	0.00020
E	0.3431	-0.2678	0.00018

6.0 DISCUSSION OF RESULTS

The experimental results have shown that turbulent flow in rod bundles has complex turbulent motions and probably secondary flows. The following discussion presents several topics concerning the interpretation of the experimental data as it is related to turbulent flow in rod bundles. First, selected experimental results are compared with the rod bundle data of Kjellström (32,33) and with the round pipe data of Laufer (36,37). A discussion of secondary flows follows next in an attempt to estimate the probable secondary flow patterns in the rod bundles considered in this study. The next section presents a discussion of the correlation functions that were used to estimate the turbulence macroscale. Finally, the data are discussed in relationship to the crossflow mixing processes in rod bundles.

6.1 COMPARISON WITH OTHER EXPERIMENTAL DATA

The only rod bundle turbulence data known to exist is that of Kjellström (32,33). As discussed in Chapter 2.0 he performed experimental measurements of turbulence parameters for air flowing through an enlarged flow channel (10X). The flow channel modeled a triangular array subchannel surrounded by three adjacent subchannels as shown in Figure 6.1. His measurements were reported for the shaded region. Although the measurements of the present study cannot be compared directly because of flow channel differences, several interesting comparisons can be made.

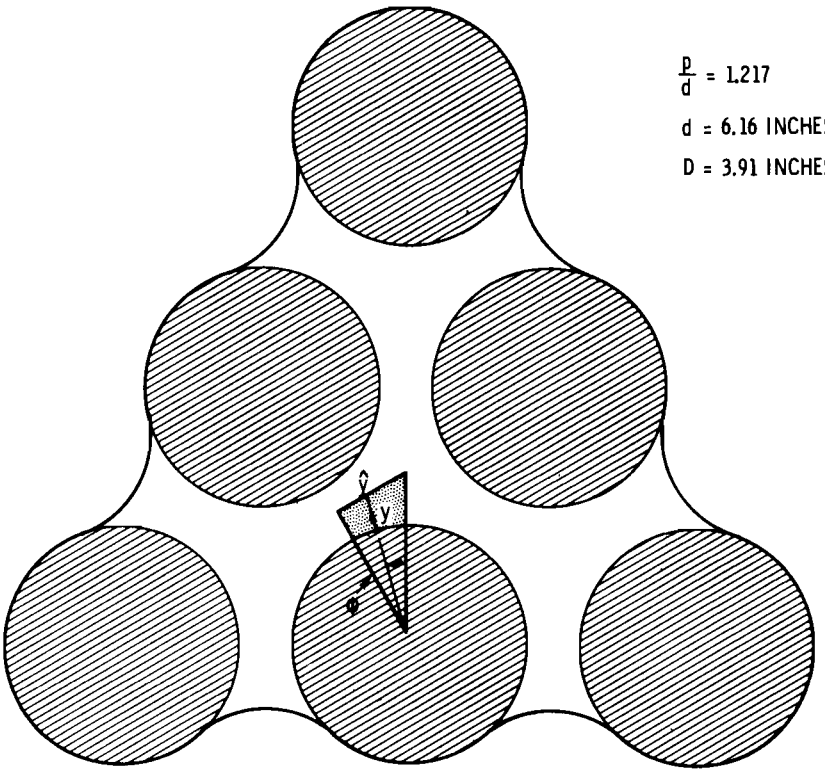

Figure 6.1. Experimental flow model and coordinate system used by Kjellström.

The data obtained for traverses across the rod gaps at the larger spacing (p/d = 1.25) provide a reasonable basis for comparison with his experiment at p/d = 1.217. Figures 6.2 through 6.7 compare the data of Kjellström and Laufer to the present data in terms of the turbulence intensity based on the shear velocity U* where it is calculated from the channel average velocity and the friction factor correlations for each flow channel.

Figure 6.2 compares the two-component turbulence intensity data obtained along a traverse through the gap in Channels D and E. Recalling that the data for Channels D and E are low by about 10% because

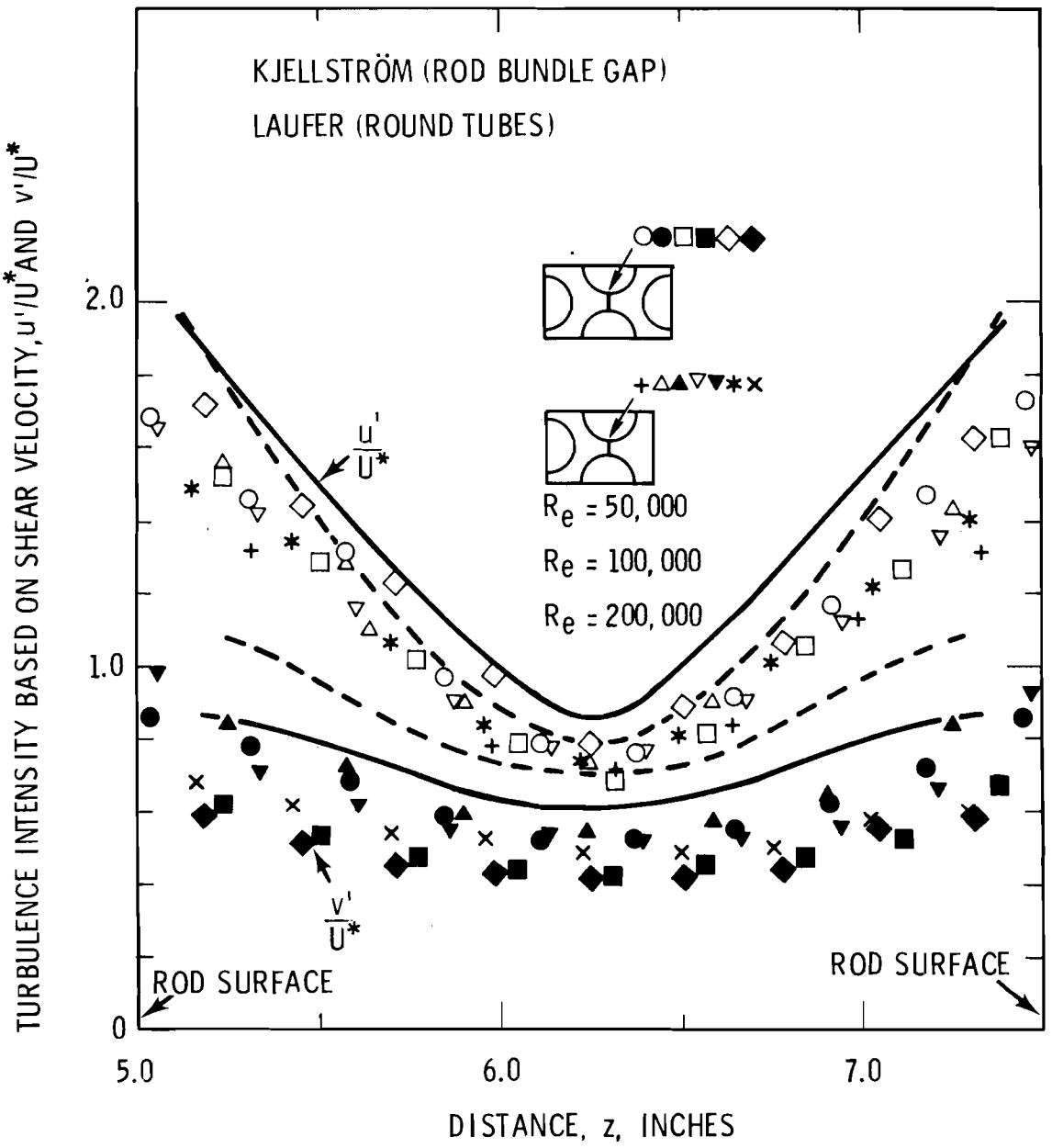

Figure 6.2. Comparison of the data in rod gap of Channels D and E with the data of Laufer and Kjellström.

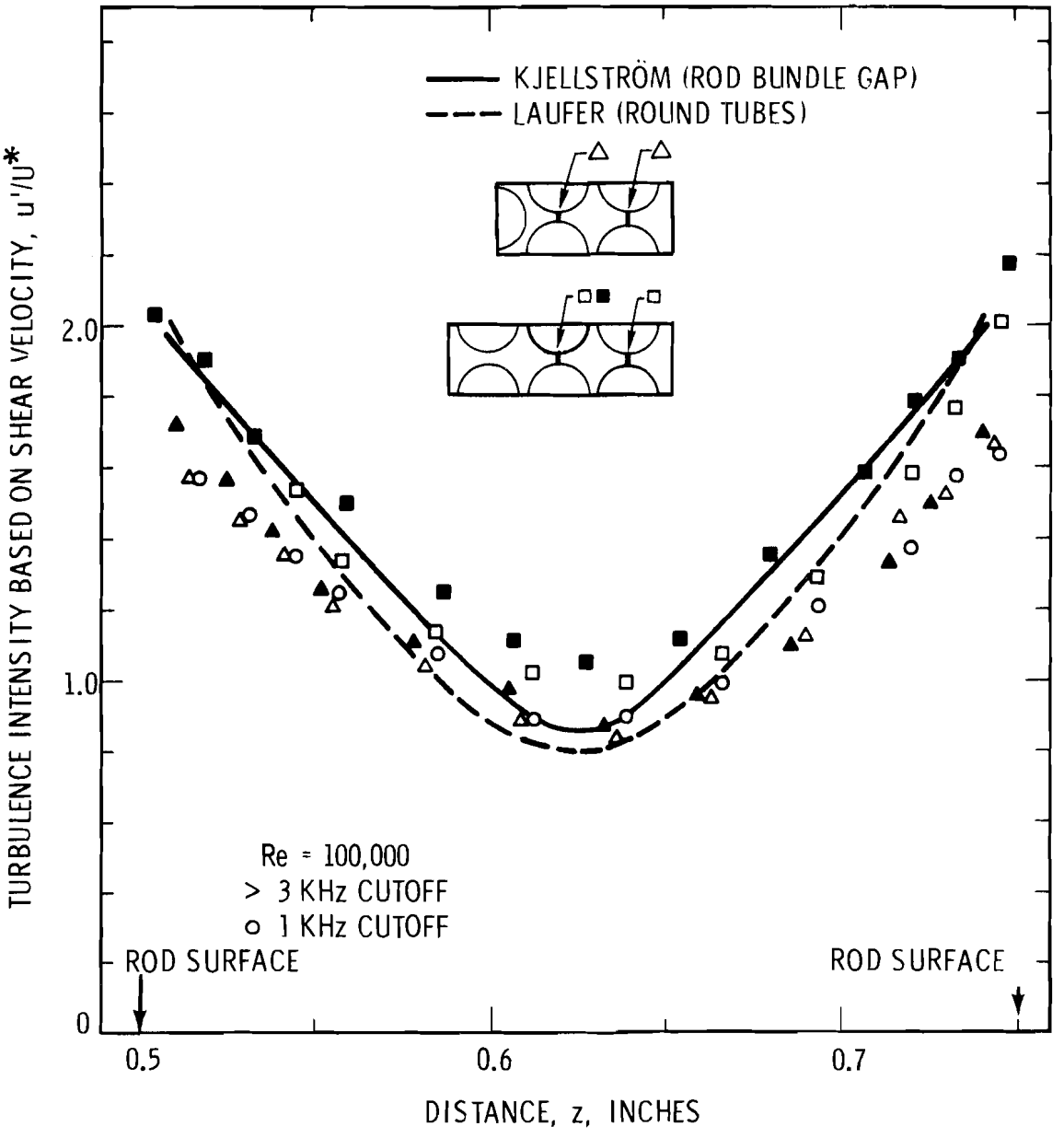

Figure 6.3. Comparison of the data in rod gap of Channels B and C with the data of Laufer and Kjellström.

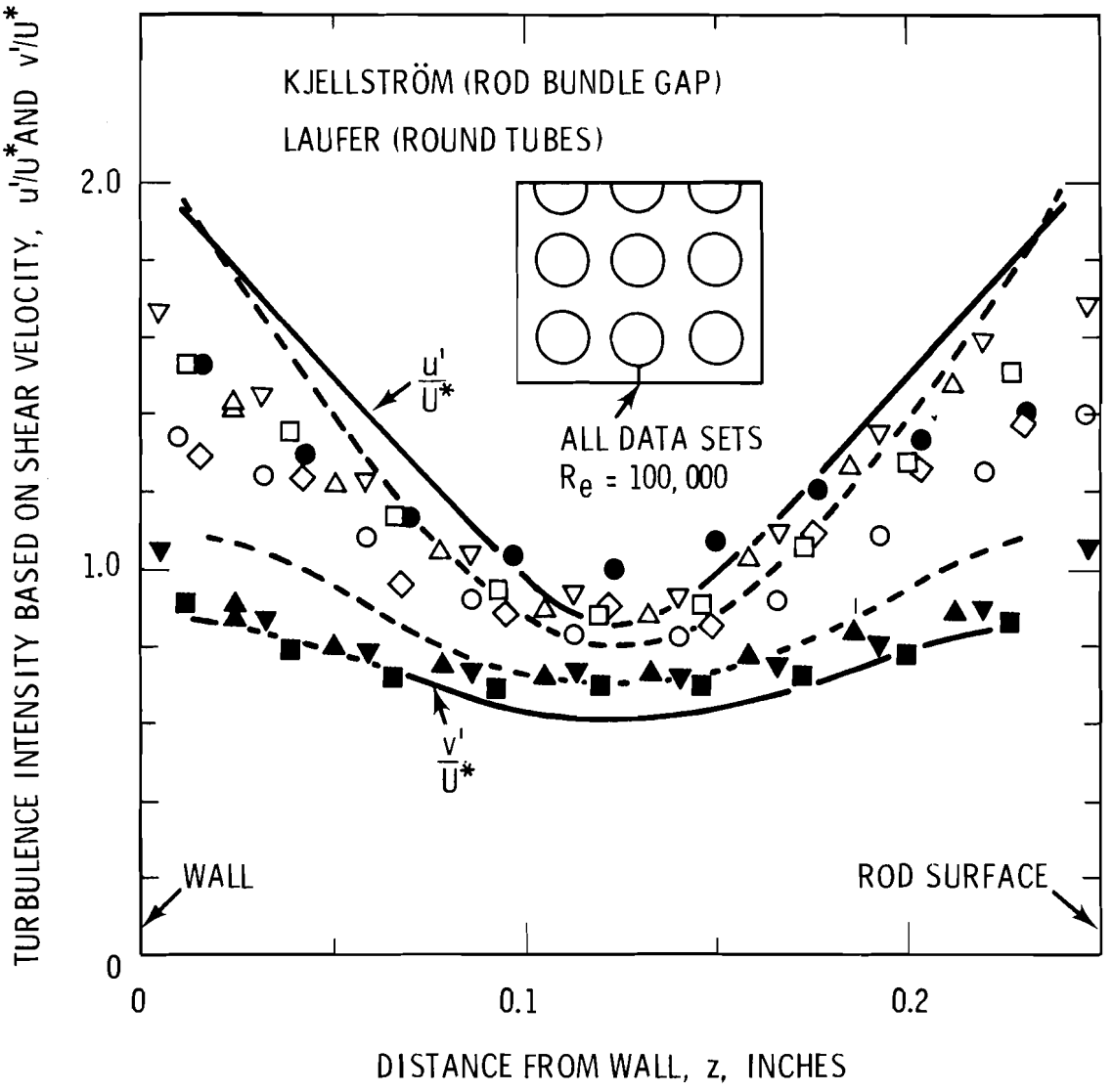

Figure 6.4. Comparison of data in rod gap of Channel A with the data of Laufer and Kjellström.

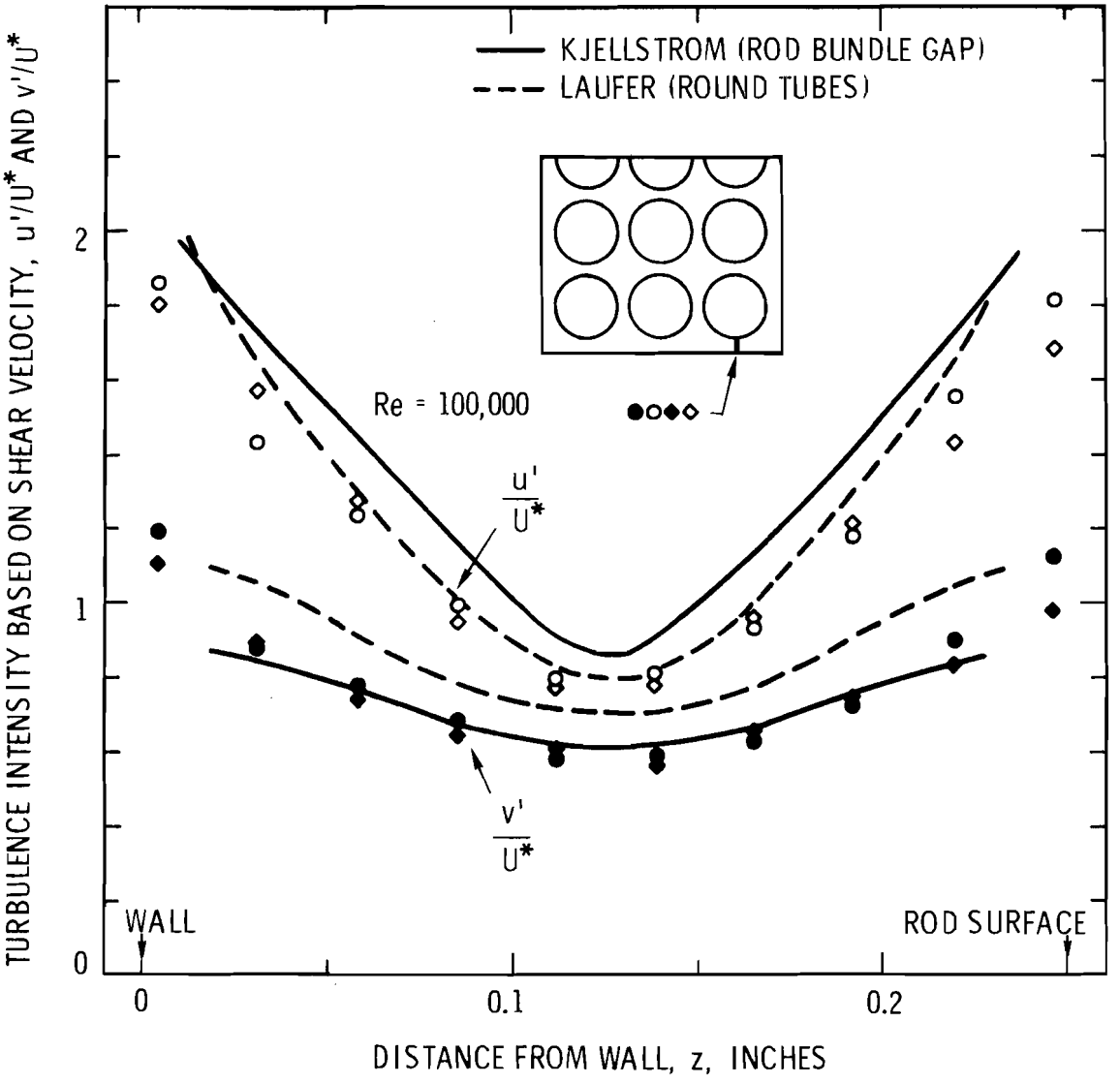

Figure 6.5. Comparison of Data in rod gap of Channel A with the data of Laufer and Kjellström

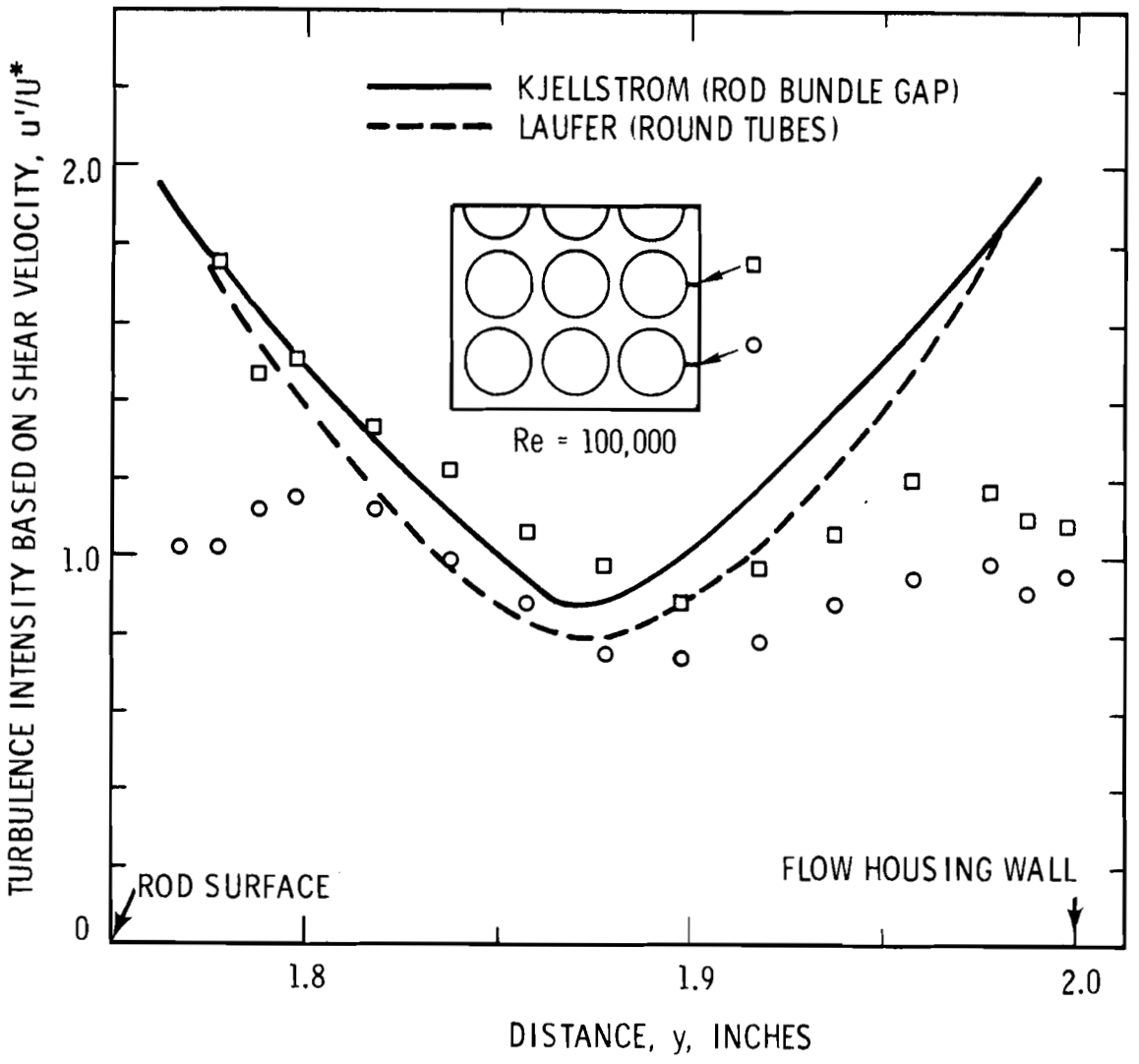

Figure 6.6. Comparison of data in rod gap of Channel A with the data of Laufer and Kjellström.

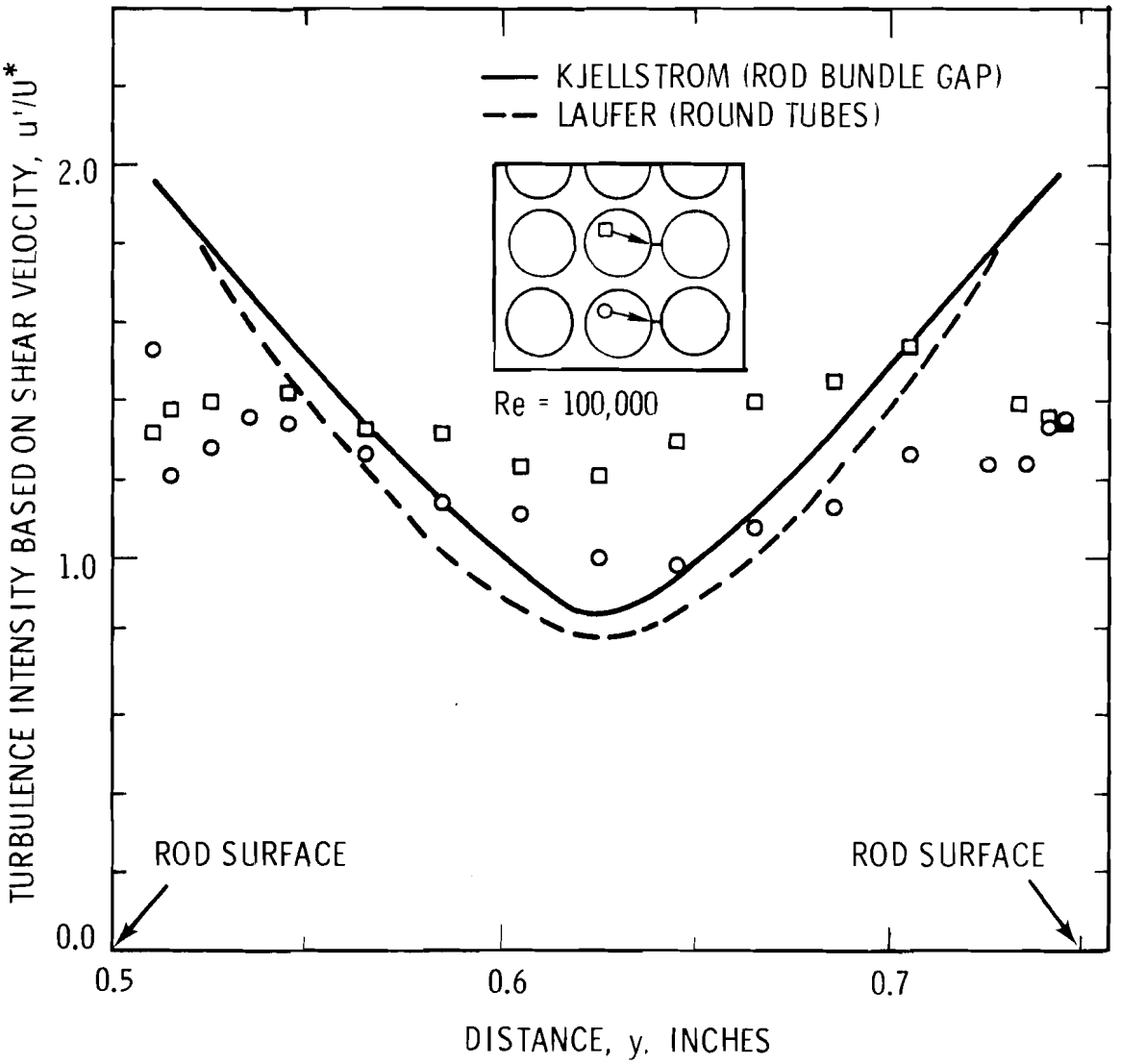

Figure 6.7. Comparison of data in rod gap of Channel A with the data of Laufer and Kjellström.

of the low cutoff frequency (1 kHz), an upward shift of that amount would give good agreement with Kjellström's data for both the lateral and axial components of intensity. The data also tend to confirm Kjellström's trend of lower lateral intensity than for round tubes. The generally higher values of intensity at Re = 50,000 are attributed to the flow conditions being more correctly matched with the cutoff frequency rather than a Reynolds number effect on the data. Figure 6.3 shows a similar comparison for the axial component turbulence intensity in the gaps of Channels B and C. As in Channels D and E the data show good agreement with the data of Kjellström. Data are also presented in Figure 6.3 to show the effect of cutoff frequency. The difference between the 6 kHz and 1 kHz cutoff is seen to be on the order of 10%. Comparing Figures 6.2 and 6.3 it could be concluded there is no effect of adjacent subchannel shape or flow model size on the turbulence intensity in the gap. The slight flow channel differences noted earlier appear to be eliminated by normalizing the intensity with the shear velocity.

Figures 6.4 and 6.5 present two-component data obtained in the rod-wall gaps of Channel A. Again the agreement is good; however, there is an indication of lower axial component intensity near the walls. Normalizing the intensity with the shear velocity also removes the apparent turbulence intensity increase with increased bundle size reported earlier when using the intensity based on local velocity. This is because Channel A has higher friction factors than the other channels; thus, giving higher shear velocity and lower intensity.

Figures 6.6 and 6.7 present turbulence intensity data obtained in the side rod-wall gaps and interior rod-rod gaps. These data show about the same average values as the data of Kjellström and Laufer; however, the distributions are significantly different. The intensity map (Figure 5.2) suggests that secondary flows could exist in, or near, these rod gaps. Secondary flows carrying turbulence from the wall or subchannel interior into the rod gap could produce the observed redistribution effects.

Comparison of the data in Figure 6.6 with the data in Figures 6.4 and 6.5 shows a dependence on the orientation of the wall. In Figure 6.6 the wall was parallel with the laser beam and was smooth over its entire length. The front wall, however, was normal to the laser beam and contained five window ports located every foot. Each window, or filler plug, was flush with the inner surface of the flow housing wall but very small slots approximately 0.010 inches wide and full width existed at the leading and trailing edge of each window port. These slots could have modified the boundary layer and secondary flow development along the wall so as to reduce the effect of secondary flows on the turbulence in the gaps.

Figures 6.8 and 6.9 present a comparison of the turbulence intensity in regions away from the rod gap at angles of ϕ = 18° and 30°. Although the comparison with the tricusp channel data of Kjellström is not entirely valid because of the different geometries involved, the trends are of interest. At both 18° and 30°, the values estimated

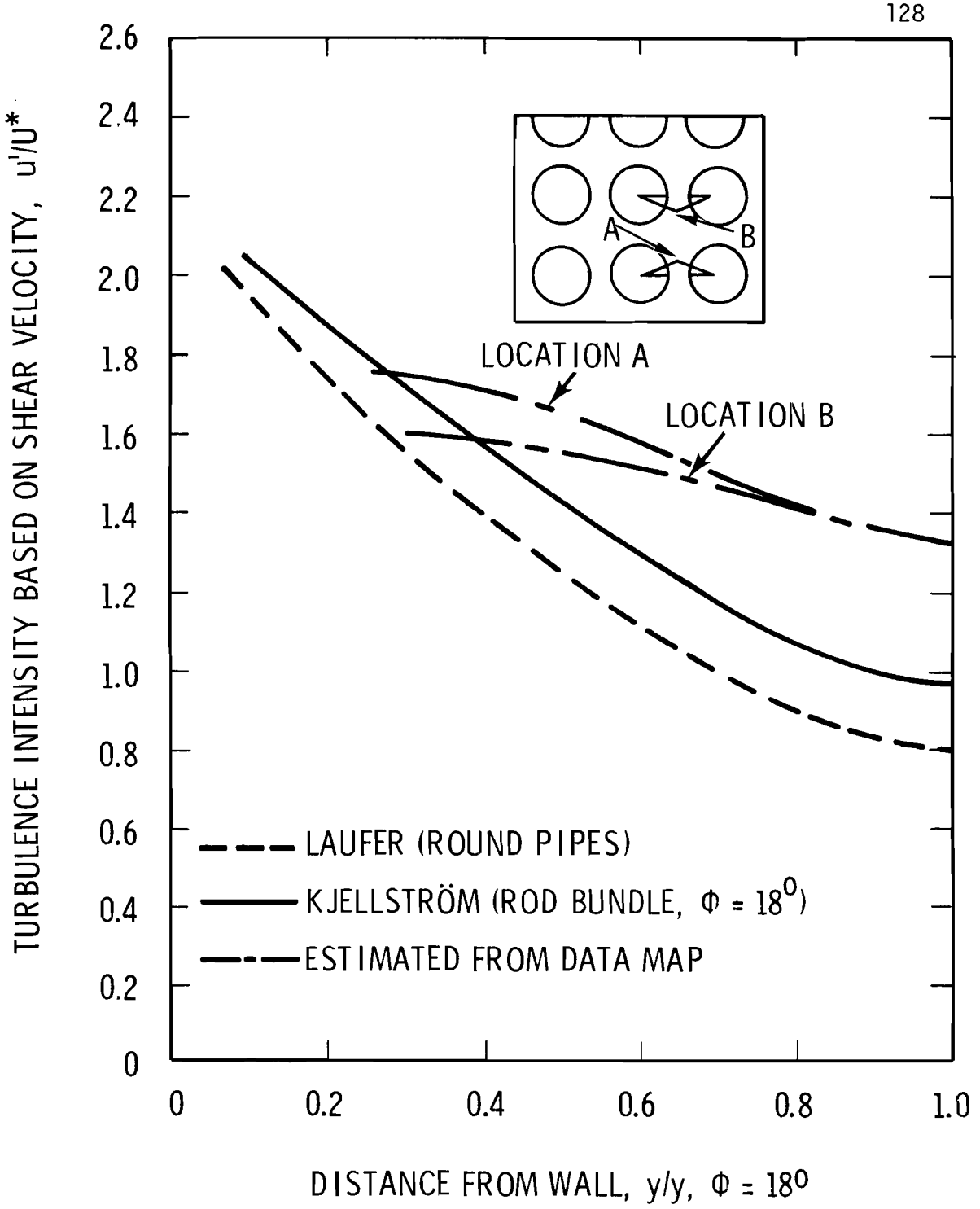

Figure 6.8. Comparison of data in Channel A with the data of Laufer and Kjellström.

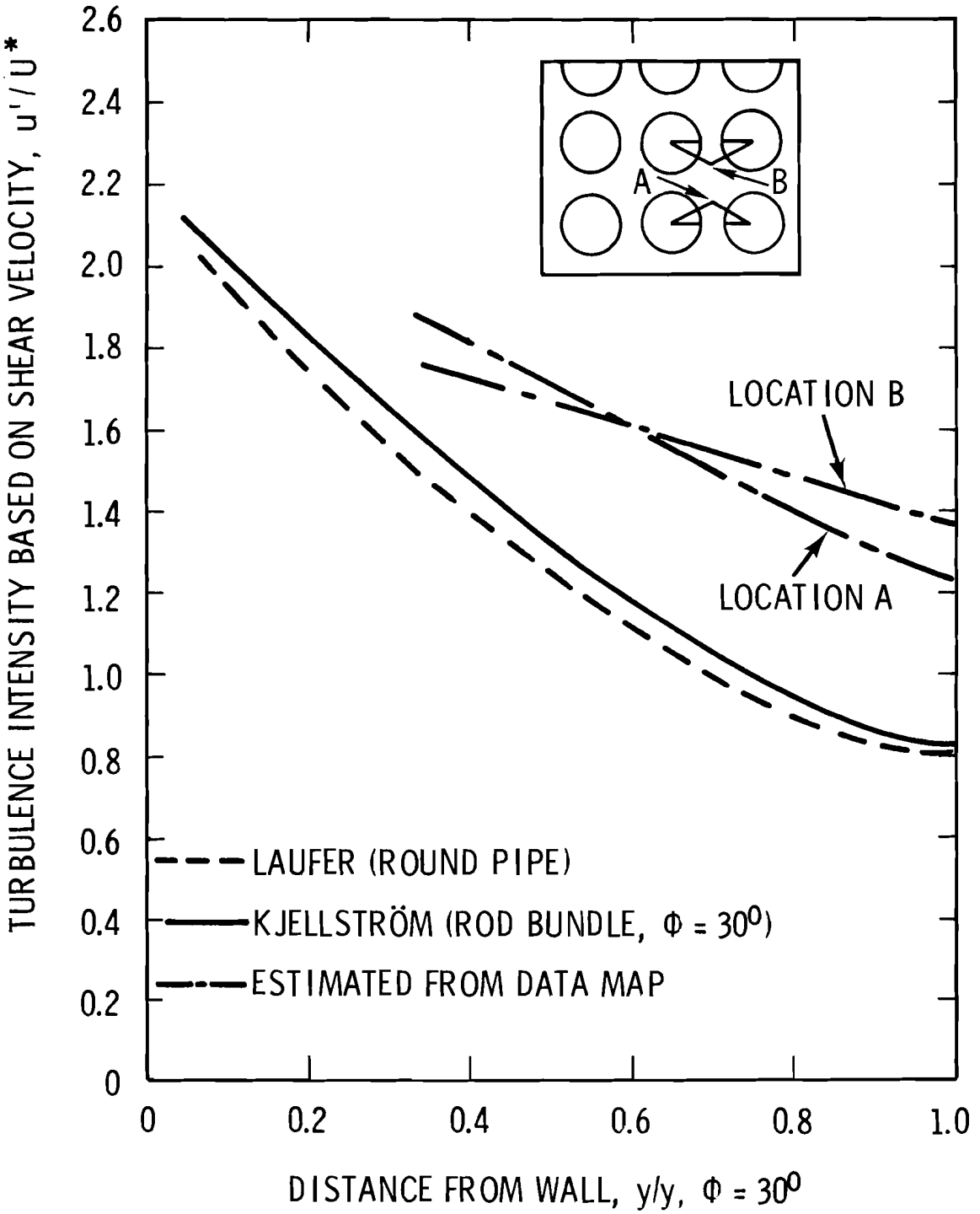

Figure 6.9. Comparison of data from Channel A with the data of Laufer and Kjellström.

from the experimental data fall above the data of Kjellström and Laufer and with a flatter distribution. Kjellström's data shows an increase at $\phi = 18°$ but no significant increase at $\phi = 30°$. It is interesting to note that this increase is about midway between the gap ($\phi = 0$) and subchannel center ($\phi = 30°$). The data from this study show the same trend but the angle is larger ($\phi = 45°$) to the subchannel center. The increase at the intermediate location is higher for the present experiment than for Kjellström's experiment. This result suggests a subchannel shape effect on the flow structure within a subchannel where a square-pitch array has higher turbulence intensity than in a triangular-pitch array. The reason could be attributed to a more rapid change in flow channel shape in the square-pitch array as compared to the triangular array.

Examination of the data for the smaller rod gap spacing in Figures 5.33 through 5.36 show turbulence intensity profiles that are of significantly different shape than those found at larger gap spacings. For the interior rod-rod gaps the intensity profiles are quite flat and with high values. The larger rod-wall gaps show lower intensity levels than in the interior but with significant distortion. These data can not be compared on a meaningful basis with Kjellström's turbulence data for rod bundles or with any other data.

Another comparison of the experimental data can be made with a commonly used method to determine velocity profiles in rod bundles. This method assumes the validity of some sort of universal velocity profile along normals from the rod surface to the line of maximum

velocity. If the wall shear stress can be determined the entire turbulent velocity profile can be calculated. One possibility is the Kármán-Prandtl velocity profile derived from circular tube data. For the region in the turbulent core the velocity is given by

$$\frac{\bar{u}}{U^*} = 2.5 \ln \frac{U^* y}{\nu} + 5.5 \qquad (6.1)$$

where U^* is the shear velocity based on the wall shear stress. For purposes of comparing the present velocity data to this equation, it is most convenient to normalize the velocity to the maximum velocity at $y = \hat{y}$; therefore,

$$\frac{\bar{u} - \hat{\bar{u}}}{U^*} = 2.5 \ln \frac{y}{\hat{y}} \quad . \qquad (6.2)$$

The value of $\hat{y}$ was taken to be one half the nominal gap spacing plus a 0.010 inch allowance for the window flat on each rod. The centerline was established from considerations of symmetry of the velocity field.

Figures 6.10 through 6.17 provide a comparison between the experimental data obtained in rod gaps and the above expression. The data generally fall below the universal profile, especially toward the wall. The typical values of $u^+ = \bar{u}/U^*$ are the range from about 15 to 22 where the lower values are toward the wall. Values of U^* approaching 15 for tubes are known to start dropping below the universal profile. Kjellström found that a slope of 2.23 agreed best with his experiments. This also agreed with the value determined by Eifler and Nijsing (13) in their studies. To make a more accurate comparison with the 2.23

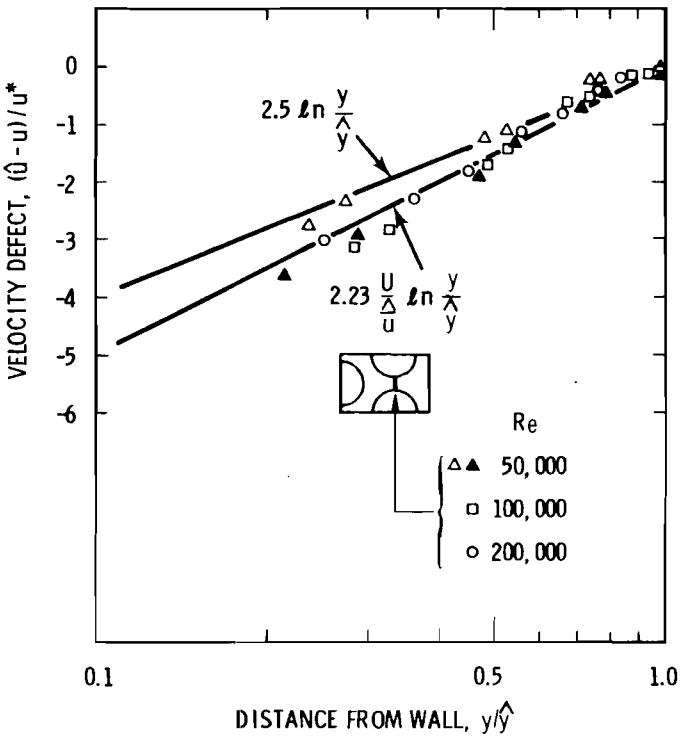

Figure 6.10. Velocity distribution in rod gap of Channel E, 1/4 inch spacing.

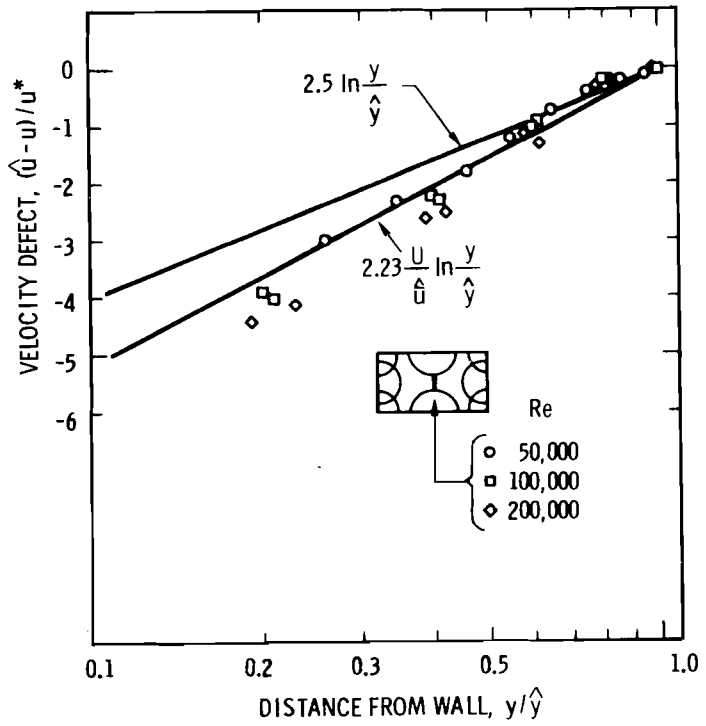

Figure 6.11. Velocity distribution in rod gap of Channel D, 1/4 inch spacing.

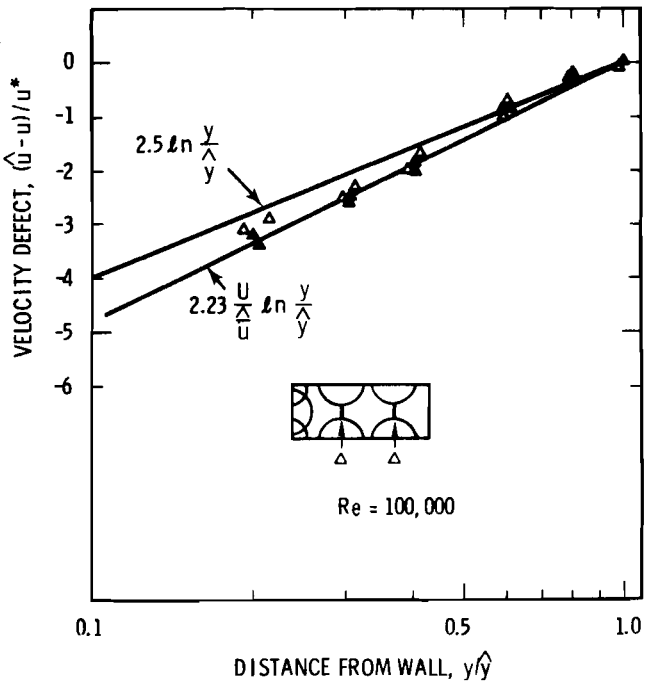

Figure 6.12. Velocity distribution in rod gaps of Channel C, 1/4 inch spacing.

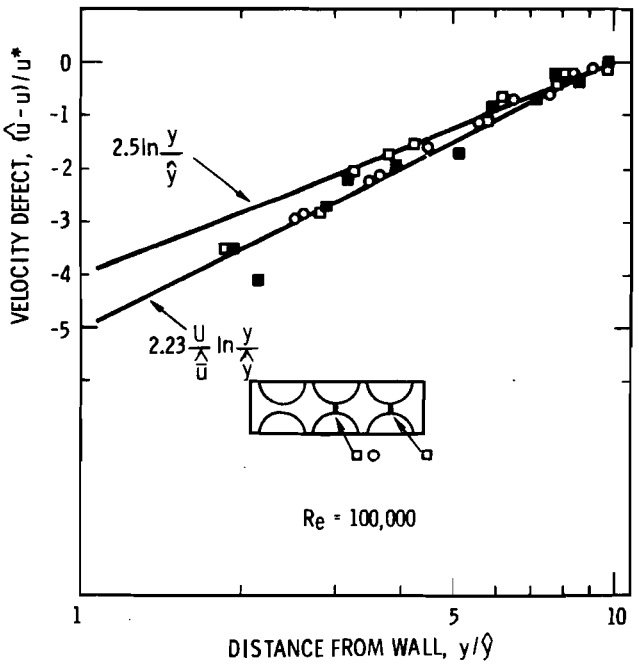

Figure 6.13. Velocity distribution in rod gaps of Channel B, 1/4 inch spacing.

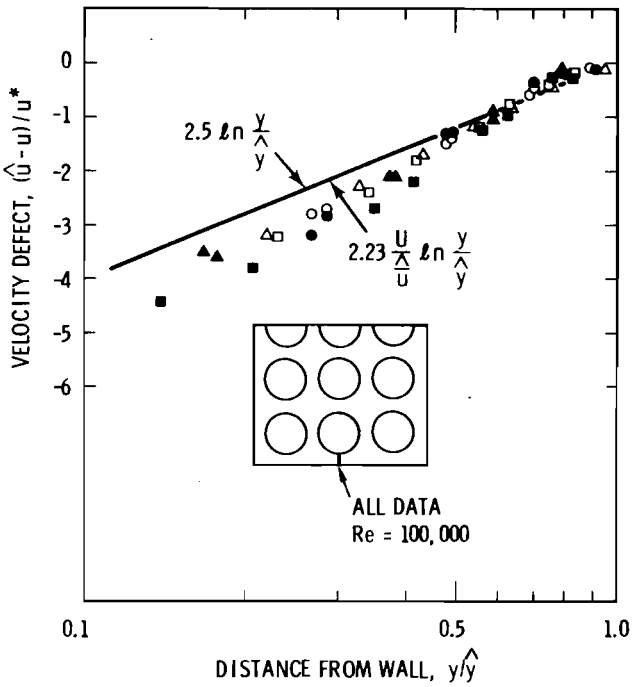

Figure 6.14. Velocity distribution in rod gaps of Channel A, 1/4 inch spacing.

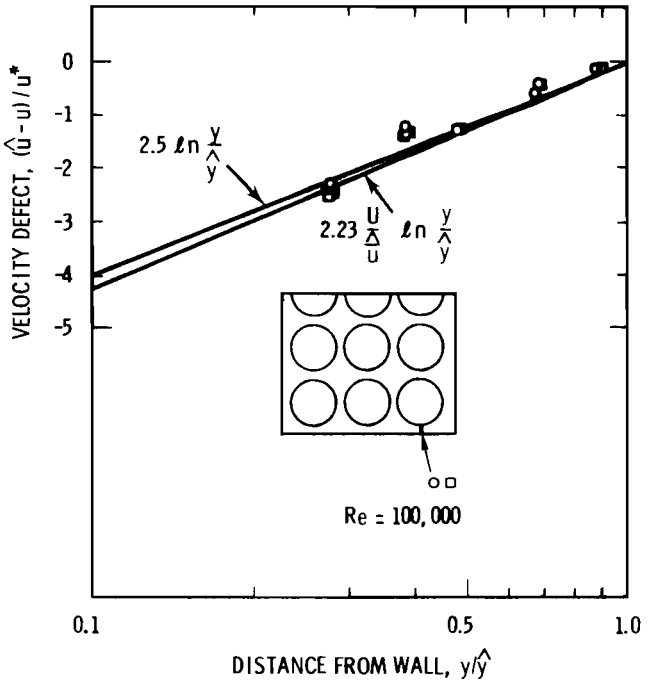

Figure 6.15. Velocity distribution in rod gaps of Channel A, 1/4 inch spacing.

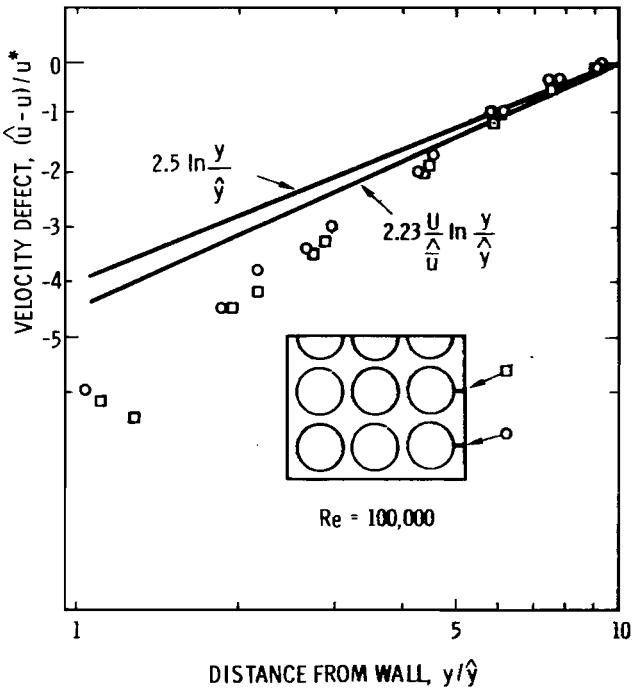

Figure 6.16. Velocity distribution in rod gaps of Channel A, 1/4 inch spacing.

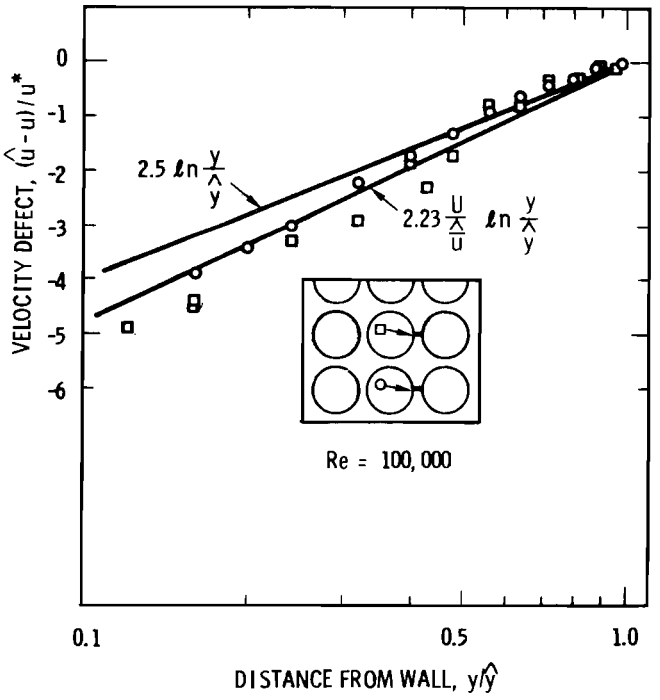

Figure 6.17. Velocity distribution in rod gaps of Channel A, 1/4 inch spacing.

factor, a local shear velocity, rather than a bundle average value, would be more correct. By assuming the shear stress is proportional to the square of the velocity $\hat{\bar{u}}$ along a normal to the rod surface equation can be written as

$$\frac{\bar{u} - \hat{\bar{u}}}{\hat{\bar{u}}^*} = 2.23 \frac{U}{\hat{\bar{u}}} \ln \frac{y}{\hat{y}} \tag{6.3}$$

Much of the experimental data in Figure 6.10 agree quite well with this equation but some data still fall lower toward the wall. The data also show a flatter profile near the centerline than given by the universal velocity profile. This can be seen by the bulge upward from about $\frac{y}{\hat{y}} = 0.7$ to 1.0. This same trend is also evident in the results of Kjellström. Round tube data (36,37) does not show the same trend.

6.2 SECONDARY FLOW PATTERNS

The driving forces for secondary flows can be found by considering the axial vector component of vorticity (41) given by the equation

$$\frac{D\xi}{Dt} = \nabla^2\xi + \xi \cancelto{0}{\frac{\partial u}{\partial x}} + \eta \cancelto{0}{\frac{\partial u}{\partial y}} + \xi \cancelto{0}{\frac{\partial u}{\partial z}} + \frac{\partial}{\partial x}\left(\frac{\partial \overline{uv'}}{\partial z} - \cancelto{0}{\frac{\partial \overline{uw'}}{\partial y}}\right)$$

$$+ \frac{\partial}{\partial y \partial z}\left(\overline{v^2} - \overline{w^2}\right) + \left(\frac{\partial^2}{\partial z^2} - \frac{\partial^2}{\partial y^2}\right) \overline{vw'} \tag{6.4}$$

where

$$\xi = \frac{\partial w}{\partial y} - \frac{\partial v}{\partial z} \tag{6.5}$$

$$\eta = \frac{\partial u}{\partial z} - \frac{\partial w}{\partial z} \tag{6.6}$$

$$\zeta = \frac{\partial v}{\partial x} - \frac{\partial u}{\partial y} \tag{6.7}$$

This equation can be derived by eliminating pressure from the two equations of motion normal to the x direction. For fully developed flow in straight channels some of the terms are zero[5] as indicated. The remaining terms are the substantial derivative of stream wise vorticity, the viscous diffusion and the Reynolds stress driving terms. If the Reynolds stresses have no variation in the z or y direction (homogeneous turbulence) secondary flows do not exist. Secondary flows also do not exist in inhomogeneous turbulence if there is proper symmetry to balance the turbulence stresses. Examples of this are flows between parallel plates or in circular channels where there is no lateral shear stress ($\overline{u'w'}$) and the normal stresses have no variation in either the z or y direction. In inhomogeneous turbulent flows, secondary flows occur where the second derivatives of the Reynolds stress are nonzero. In terms of geometry, non-uniform changes in flow channel boundaries will cause secondary flows and, the greater the rate of change of shape, the greater the secondary flow.

Perkins (41) has considered the features of this equation in considerable detail. He concludes that (41, p.723), "anisotropic wall turbulence in any boundary-layer situation is potentially a source of secondary currents whenever the flow is additionally inhomogeneous parallel to the bounding surfaces in the y,z plane". His experimental measurements show that the transverse direct stresses ($\overline{v^2} - \overline{w^2}$) are the most important terms responsible for the production of stream wise

---

[5] $\eta \frac{\partial u}{\partial y} + \xi \frac{\partial u}{\partial z} = \frac{\partial u}{\partial z} \frac{\partial v}{\partial x} - \frac{\partial u}{\partial y} \frac{\partial w}{\partial x}$

vorticity. The transverse shear stresses are much less important. The difference between $\overline{v'^2}$ and $\overline{w'^2}$ is strongest in the vicinity of the wall. If v' is the component normal to the wall, it is damped by the proximity of the wall. In the same region the w' component is relatively unaffected. This ceases to be true on approaching the wall because both v' and w' are rapidly damped by fluid viscosity.

A physical description for the secondary flow driving force attributed to Prandtl and reported by Perkins (41, p.722), "is that velocity fluctuations tangential to the isovel (line of constant velocity) exceed those perpendicular to the isovel so that centrifugal acceleration is induced in regions of isovel curvature, propelling the fluid outward. Secondary currents, he concluded, must therefore be established in the direction of the isovel distortions and be supported by the anisotropy of the turbulent direct stresses. All subsequent secondary flow measurements in fully developed (axially-homogeneous) straight noncircular duct flows have substantiated this qualitative argument."

Gessner and Jones (19,20,21) have investigated secondary flows in rectangular channels for Reynolds numbers ranging from 50,000 to 300,000. They found typical secondary flow velocities on the order of 1% of the axial velocity and that this fraction tended to decrease for increasing Reynolds number with the largest change near the wall.

Brundrett and Baines (9) found the basic secondary flow pattern to be independent of Reynolds number but, with increasing values of Reynolds number, the flows penetrated the corners and approached the

walls. The corner bisectors were found to separate independent secondary flow circulation zones. Measurements of turbulence kinetic energy showed a significant penetration of low turbulence energy toward the corner along the bisector and high turbulence energy carried out from the wall away from the corner. The pattern was very similar to the corner distortion of turbulence intensity shown in Figure 6.18.

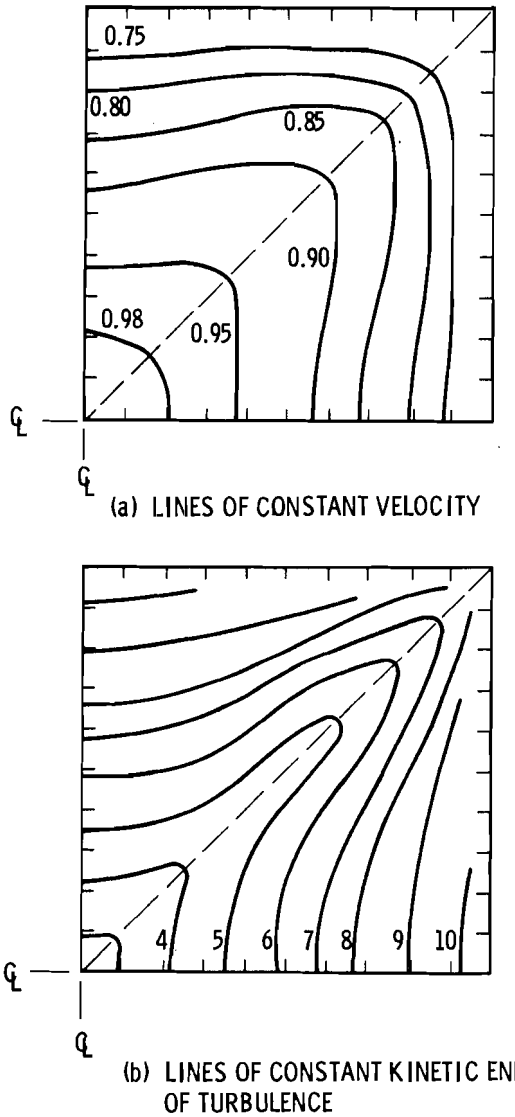

Figure 6.18. Examples of velocity and kinetic energy of turbulence distributions for square channels.

Brundrett and Baines also discuss secondary flows in nonrectangular ducts and in particular polygons. From symmetry of the Reynolds stress tensor about lines connecting the center to the mid-points of the sides and to the corners they concluded (9, p.391), "there must be twice as many sectors as sides and that the circulation be of opposite sense in adjoining sectors". Also, (9, p.391) "as the number of sides is increased, the longitudinal vortices must be smaller in magnitude and more concentrated in the neighborhood of the corners. Thus, there must be a critical Reynolds number for each polygon below which Ω (vorticity) is zero everywhere since the zone of production will be within the "inner-law" flow regime, a regime which does not appear to be associated with vorticity production." There is strong evidence to indicate that corner symmetry applies to all polygons such that the turbulence correlation $(w'^2 - v'^2)$ which is responsible for vorticity production is zero on the corner bisector. As a consequence, each corner polygon will have two circulations which are separated by the corner bisector and which direct fluid into the corner and therefore are of opposite rotation.

Although the direct measurement of secondary flows was not possible in the present study the distortions in the maps of the axial turbulence intensity provide some insight concerning secondary flow circuits in bundles. Prior to doing this however, consider the distortions of velocity and intensity observed in rectangular channels with known secondary flow patterns. Figure 6.18 shows the lines of constant

velocity and constant turbulence kinetic energy in a square duct as reported by Brundrett and Baines (9). The secondary flows are known to move toward the corner, out along the wall and then back toward the center of the duct. The turbulence kinetic energy is seen to be more distorted by the secondary flow than is the axial velocity field. The distortions show the transport of lower kinetic energy turbulence from the center of the duct toward the corner along the corner bisector and higher kinetic energy turbulence from the wall near mid-span toward the center of the duct. Since the axial turbulence intensity is one of the components of the turbulence kinetic energy, it would have similar distortions in the presence of secondary flows.

Based upon the previous reasoning and the distortions of the turbulence intensity and velocity maps of Figures 5.20 through 5.24, Figure 6.19 was prepared as an estimate of the secondary flow patterns in Channels B and C. The secondary flows appear to be quite strong in the corner regions as indicated by the velocity and intensity distortions in Figures 5.21 and 5.23. The interior subchannel appears to have a single secondary flow circuit, except for the corner, along lines of symmetry. This circuit moves toward the gap, then toward the wall, out along the rod surface and then back toward the subchannel center. The wall subchannel appears to contain a similar secondary flow circuit -- the strongest one being in the corner. Although the other indicated secondary flow circuits are larger they do not have the strength of those in the corner. It is not entirely clear whether the secondary

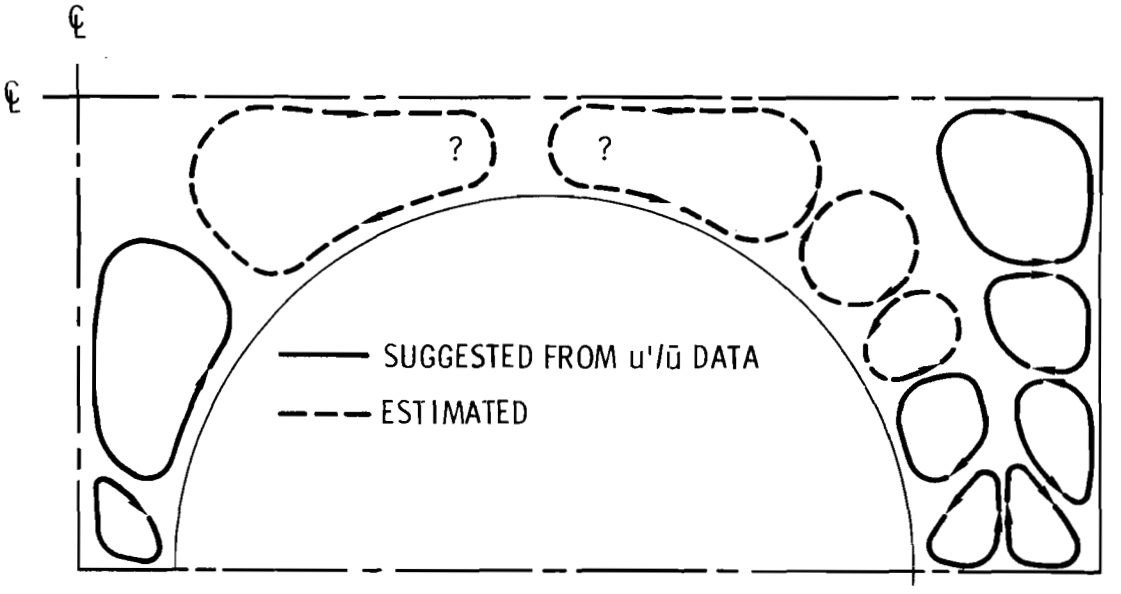

Figure 6.19. Estimated secondary flow circuits in Channels B and C, Re = 100,000.

flow circuits along the wall consists of three pair of circuits . The inflections in the u'/u distributions shown in Figures 5.21 and 5.23 suggest that there are three pair of circuits. Since the entire flow field could not be mapped, the dashed secondary flow circuits are provided only as an estimate.

Figure 6.20 presents an estimate of the secondary flow map for Channel A based upon the velocity and intensity maps shown in Figures 5.1 and 5.2. The interior rod-rod gap appears to have a pair of symmetric flow circuits moving along the centerline toward the rod gap and back along the rod surface and out toward the central part of the subchannel. The rod-rod gap between the wall and interior subchannel

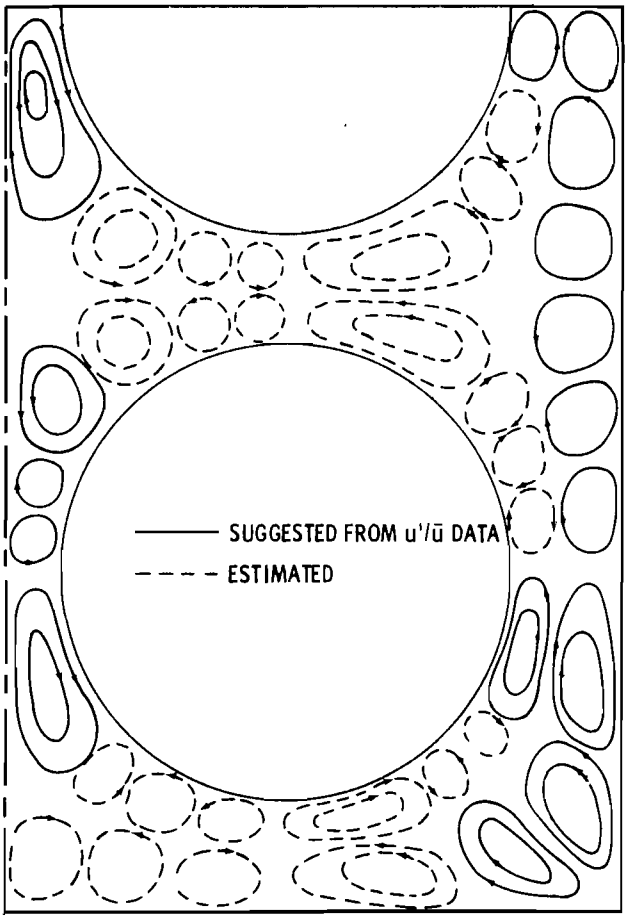

Figure 6.20. Estimated secondary flow circuits in Channel A, Re = 100,000.

appears to be more complex where two pair of symmetric secondary flows appear to be involved. One moves toward the gap along the center line, then toward the rod, along the rod and out toward the center of the subchannel. The other smaller flow circuit appears to be limited to the gap region and rotates in the opposite direction. Such an additional pair does not appear to exist for the interior rod-rod gap. The secondary flow in the corner subchannel is largely dominated by

the square corner of the flow housing. The flow circuit moves toward the corner, along the channel wall and out into the subchannel much as a secondary flow would move in a rectangular channel. The distortions toward the gap suggest two symmetric secondary flows moving as those near the interior rod gaps. It is not clear, whether or not, another flow circuit exists near the rod, next to the diagonal from the rod to the corner. The wall subchannel secondary flow circuits appear to be very complex and uncertain in some regions because of only slight intensity distortions, presumably due to smaller velocities. Secondary flow circuits as in the interior region are presumed to occur in the wall subchannel as in the wall subchannel of Channel B. The multiple distortions suggest that there are three pair of circuits along the wall between the rod gap and subchannel center; however, it is conceivable that this could be just a pair of circuits.

The distortions of turbulence intensity in the side-wall subchannels was different than for the wall subchannels adjacent to the viewing windows. The reason for this difference is not known for sure but it could have had something to do with the periodic interruption of the boundary layer at each window. There were 5 window ports with two full-width slots approximately 0.010 inches wide and 2 inches apart at each window. Although the windows were flush with the inside the boundary layer would be interrupted by the slots and, therefore, have a different development than in the smooth side-wall subchannels. The different boundary layer development could also be responsible for the intensity asymmetry observed in the corner subchannel.

Most of the experimental data expressed as dimensionless ratios were weakly affected by Reynolds number. In all cases the lower of the three Reynolds numbers for this research was obtained by reducing flow at constant temperature and the higher value by holding flow but increasing the temperature. The only apparent exception to the weak Reynolds number dependence was found for the reduced gap spacing. As explained earlier this apparent effect is believed to be caused by a gradual roughening of the flow model which may have also changed the secondary flow pattern. Recirculating flows are known to change their flow patterns with increasing Reynolds number. Classic examples are the development of Kaman vortex streets in the wake of obstacles placed in a flow stream. Figure 6.20 shows the estimated secondary flow pattern for the larger rod spacing in bundle A. It is conceivable that, with the proper conditions, the corner flow circuit could become dominant and shift the secondary flow pattern. Inspection of the data in Figures 5.13, 5.14, 5.33, and 5.34 show two distinctive trends: 1) shift of the velocity peak and minimum intensity away from the wall and toward the rod in the rod-wall gaps; and, 2) shift of the velocity peak and minimum intensity toward the wall in both the corner and wall subchannels. Based on these observations the secondary flow pattern is believed to have been similar to that in Figure 6.20 for a Reynolds number of 50,000 and 100,000 but to have shifted to the pattern shown in Figure 6.21 at a Reynolds number of 200,000. The basic change is believed to be large scale recirculation zones as compared to smaller

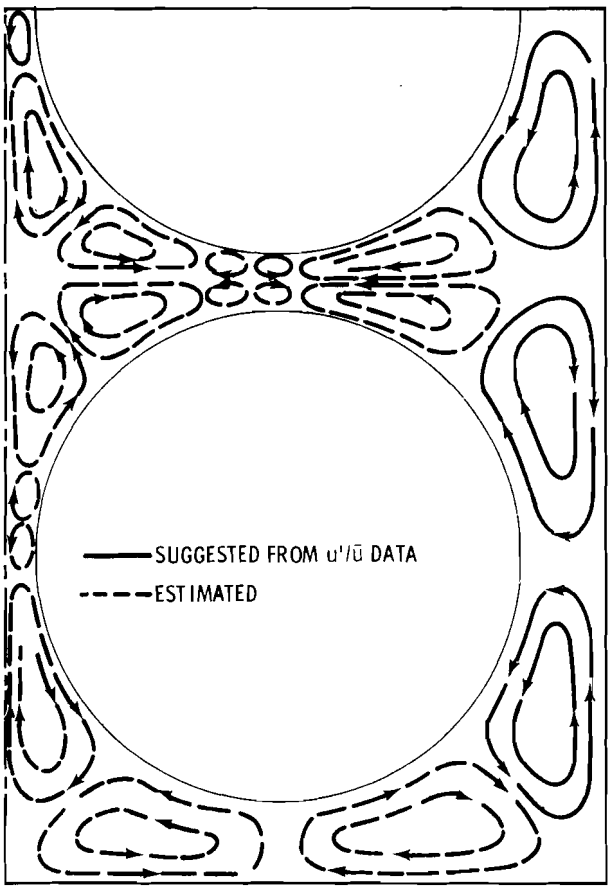

Figure 6.21. Estimated secondary flow circuits in Channel A Re = 200,000, reduced gap spacing.

ones at lower Reynolds number and at larger gap spacing. The flow patterns agree quite well with observed data shift. The maximum velocity in the rod-wall gaps are shifted toward the rod with a corresponding shift in turbulence intensity. A similar but opposite shift occurs in the corner and wall subchannel. The result is a significantly asymmetric distribution of velocity and intensity in the rod-wall gaps. The interior gaps possess symmetry which indicates that the postulated secondary flow pattern shift did not reach beyond the wall subchannels.

The postulated shift in secondary flow pattern indicated by these results pose some interesting points of conjecture regarding some of the inconsistencies observed in rod bundle mixing experiments. There have been notable differences reported between so-called "simple channel" and "bundle" experiments. Rogers and Rosehart (47) has proposed a mixing correlation for each type. For the simple channel, significantly different results have been found between investigators (48). These differences have been attributed to such things as experimental error, pressure bias, heated experiment versus tracer experiment and model configuration. The role of secondary flows found in this study indicate that secondary flow patterns of various models could significantly affect the results of crossflow mixing experiments. The secondary flow pattern differences could be caused by the shape and the relative roughness of the surfaces of the flow channel.

6.3 MACROSCALE AND CORRELATION FUNCTIONS

The estimate for the longitudinal macroscale Λ was obtained by using Taylor's hypothesis which is discussed in Chapter 2. To use this approach it is necessary to obtain an estimate for the Eulerian macrotime scale. This is defined formally by Equation (2.20) where the autocorrelation function is integrated from zero to infinity. Unfortunately, it is not possible to perform such an integration when a complete correlation function does not exist or where the correlation function oscillates about the horizontal axis. Since the correlation functions

in this study were limited to a finite time delay and some functions had oscillatory behavior, it was necessary to devise a way to quantify the essential features of the function and obtain an estimate of the macrotime scale. The approach chosen was to fit the correlation function plot to the function of the form (6).

$$R_E(\tau) = e^{\alpha_1 \tau} \cos \alpha_2 \tau \tag{6.8}$$

This is a convenient but approximate way to quantify the correlation function yet preserve its essential features, namely, the decay and any periodicity. A presentation of all correlation function plots would be cumbersome and unwieldly.

It is well known that the Fourier cosine transform of the autocorrelation function gives the power spectrum of turbulence energy. The power spectrum defines the distribution of energy as a function of frequency; therefore, the sum of energy contained in all frequencies must equal the total turbulence energy. Following the notation of Hinze (23, p.54) for the one dimensional spectrum in the axial direction, this can be stated mathematically as

$$\overline{u'^2} = \int_0^\infty E(n)dn \quad . \tag{6.9}$$

The relationship between the power spectrum and the autocorrelation function is given by the cosine transform

$$E(n) = 4\,\overline{u'^2} \int_0^\infty R_E(\tau) \cos 2\pi n\tau \, d\tau \tag{6.10}$$

and the inverse transform is defined as

$$R(\tau) = \frac{1}{\overline{u'^2}} \int_0^\infty E(n) \cos 2\pi n \tau dn \qquad (6.11)$$

By using the correlation function given by Equation (6.8), the Fourier cosine transform can be shown to be

$$E(n) = 2\overline{u'^2} \left[\frac{\alpha_1}{\alpha_1^2 + (\alpha_2+2\pi n)^2} + \frac{\alpha_1}{\alpha_1^2 + (\alpha_2-2\pi n)^2} \right] \qquad (6.12)$$

If $\alpha_2 \to 0$ the correlation function given by Equation (6.8) has only an exponential decay and the power spectrum has a monotonic decay with increasing frequency n. If α_2 is nonzero, the correlation function exhibits periodic behavior with an exponential decay and the power spectrum has a peak at a frequency corresponding to the dominant frequency of correlation function. Periodic behavior shown by the correlation function, therefore, indicates a dominant frequency in the power spectrum. The relative importance of the periodic component can be judged rather quickly by just inspecting the correlation function.

Most of the measured correlation functions in this study had nearly an exponential decay with little or no evidence of dominant periodic behavior; however, some of the correlation functions obtained in certain regions of Channel A at the smaller rod gap spacing did show definite periodic behavior. These were limited to the region between the subchannel center and rod gap where there was also evidence of secondary flows.

The estimate of longitudinal scale was made by first fitting the correlation with Equation (6.8) and then performing the integration of Equation (2.20) to obtain T_E. The validity of this approach depends upon the ability of the function to fit the correlation plot which in turn affects the coefficients α_1 and α_2. The importance of the coefficients can be evaluated by considering the macrotime scale which is defined by Equations (2.20) and (6.10) as

$$T_E = -\frac{1}{\alpha_1}\left[\frac{1}{1+\left(\frac{\alpha_2}{\alpha_1}\right)^2}\right] \tag{6.13}$$

For no significant periodic motion compared to the time of decay ($\alpha_2 << \alpha_1$) the time scale is just $T_E = -1/\alpha_1$ and the value of α_2 has little if any effect on the estimate of T_E. If α_2 is of the same magnitude of α_1 then the value of T_E becomes less than the value given by α_1 and the value of α_2 has importance.

Figure 5.9 shows correlation functions obtained along the interior subchannel centerline of Channel A at a Reynolds number of 100,000 for the 1/4 and 1/8 inch gap spacings. Note the definite change in the correlation function with distance from the wall and on through the gap into the interior subchannel. Near the wall, subchannel center and in the rod gap the correlation function is nearly exponential. Here the macroscale estimate depends primarily on the exponential decay. In the region between the gap and subchannel center the correlation function at the 0.125 inch gap spacing clearly shows periodic behavior. Here the macroscale estimate also depends on the frequency of the function.

Figures 6.22 and 6.23 show plots of the frequency distribution along the centerline through the rod gaps of Channel A at the 1/8 inch gap spacing. They clearly show the regions of dominant periodic motion between the rod gap and subchannel center. A comparison of the data listed in Appendix B shows that most data at the 1/4 inch gap spacing did not exhibit this dominant periodicity.

It can be concluded that the reduction of rod gap spacing leads to more dominant periodic flow pulsations in the regions adjacent to the rod gap. This, together with secondary flows, increased turbulence intensity and increased macroscale suggest an enhancement of crossflow mixing processes.

6.4 IMPLICATIONS REGARDING CROSSFLOW MIXING

A simplified crossflow mixing model commonly used in the subchannel analysis of rod bundles was discussed in Chapter 2. The crossflow mixing was given by Equation (2.38) as

$$\frac{w'}{GD} = \left(\frac{\varepsilon}{UD}\right)\left(\frac{s}{\Delta y}\right) \quad . \tag{6.14}$$

The ratio $s/\Delta y$ was shown to present some conflicting views regarding the role of geometry on the crossflow mixing processes.

In the present study, experimental data has been obtained that indicates geometry effects cannot be solely accounted for by the $s/\Delta y$ parameter. Present data suggests significant variations of ε/UD also occur with changes in geometry and that additional macroscopic flow processes contribute to ε/UD in regions adjacent to the rod gaps.

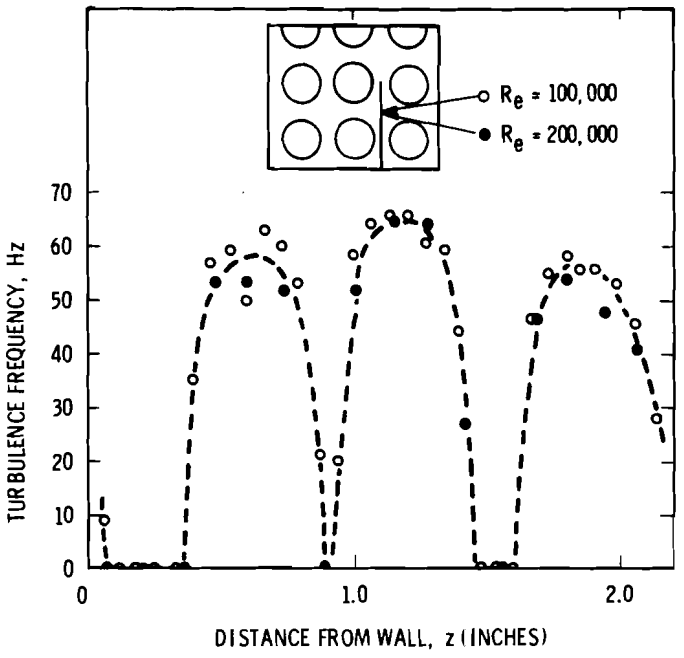

Figure 6.22. Dominant turbulence frequency along a centerline traverse from the wall through an interior subchannel, 1/8 inch gap spacing.

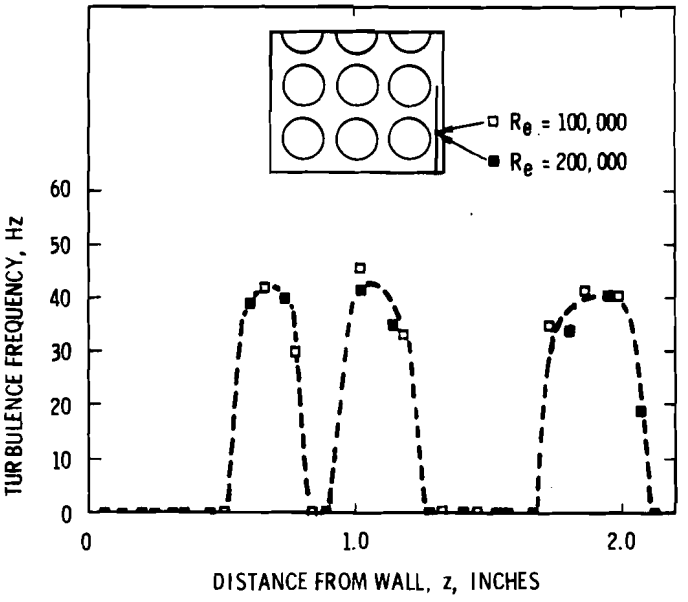

Figure 6.23. Dominant turbulence frequency along a centerline from the wall through a corner and wall subchannel, 3/16 inch rod-wall gap spacing.

Referring to Equation (2.15) the eddy diffusion coefficient could be expressed as the ratios

$$\frac{\varepsilon}{UD} = \left(\frac{u'}{\bar{u}}\right)\left(\frac{\bar{u}}{U}\right)\left(\frac{\Lambda}{D}\right)\left(\frac{\Lambda_L}{\Lambda}\right)\left(\frac{v'}{u'}\right) \qquad (6.15)$$

The first three parameters are those measured in this study. The last two are the ratios required to convert from an Eulerian to a Lagrangian representation of lateral scalar transport. As discussed in Chapter 2, not much is known about this conversion even for very simple channels. It would be necessary to perform a scalar mixing experiment together with turbulence measurements to obtain estimates of their values. For homogeneous turbulence the value of v' would be of the same magnitude as the lateral component of turbulence velocity. Based on the measurements in this study the ratio v'/u' would be less than unity and would probably have values in the range from about 0.5 to 0.8. The Lagrangian lateral macroscale could be expected to be of the same order of magnitude as the Eulerian lateral macroscale of turbulence which would probably be less than the longitudinal macroscale measured in this study. The ratio (Λ_L/Λ) would probably be less than unity but with uncertain value. An estimate for ε/UD would therefore be

$$\frac{\varepsilon}{UD} \propto \left(\frac{u'}{\bar{u}}\right)\left(\frac{\bar{u}}{U}\right)\left(\frac{\Lambda}{D}\right) \qquad (6.16)$$

where the constant of proportionality would be less than unity and with uncertain functional variation with geometry and flow conditions.

The present data is not complete enough to determine channel average values for the above parameters; however, from the centerline traverses some estimates can be prepared to give an indication of how the parameters change with geometry. The summary estimates in Table 6.1 are taken from the figures in Chapter 5 pertaining to Channel A. The data show an increase in $(u'/U)(\Lambda/D)$ that varies inversely with the gap spacing. The change is primarily due to an increase in macroscale with a decrease in gap spacing. This macroscale increase is rather interesting because the scale in round pipes would vary directly with pipe diameter. The present data indicates that scale cannot be estimated just from channel geometry alone by using methods such as those proposed by Buleev (10). The flow structure within the subchannels of rod bundles has an important influence on the scale of turbulence.

TABLE 6.1. Representative Average Estimates of Turbulence Parameters Along Traverse Centerlines, Channel A

	$\frac{u'}{U}$	$\frac{\Lambda}{D}$	$\frac{s}{\Delta y}$	$(\frac{u'}{U})(\frac{\Lambda}{D})$	$\frac{u'}{U}\frac{\Lambda}{D}\frac{s}{\Delta y}$
Interior Subchannels:					
1/4 in. gap spacing	0.050	0.35	0.20	0.018	0.0035
1/8 in. gap spacing	0.060	0.60	0.15	0.036	0.0036
Wall Subchannels:					
1/4 in. gap spacing	0.060	0.35	0.20	0.021	0.0042
3/16 in. gap spacing	0.050	0.70	0.15	0.035	0.0052
Corner Subchannels:					
1/4 in. gap spacing	0.055	0.30	0.22	0.017	0.0037
3/16 in. gap spacing	0.045	0.60	0.17	0.027	0.0046

The macroscale estimates presented here are for the longitudinal direction. It is probable that the scale is smaller in the lateral directions. While the scale may be restricted in size in the direction normal to the wall, the scale in the direction parallel to the wall may not be so restricted. The present data suggests that the lateral freedom of the open array allows rather large scale turbulence to move through the gap with relative ease. As discussed in Chapter 2, this is consistent with the ideas of Ibragimov, et al. (26), involving the motion of large scale eddies being felt most strongly along the perimeter of a channel with a sharply varying cross sectional shape, such as a rod bundle. This ease of movement through the gap could not exist for very small gap spacing because the turbulent motion would be "damped" by the laminar boundary layer. Galbraith (14) found a significant reduction in crossflow mixing when his rod gap was reduced from 0.028 inches to 0.011 inches when using 1 inch diameter rods.

The changes of $(u'/U)(\Lambda/D)$ shown in Table 6.1 are nearly inversely proportional to gap spacing and taken together with the ratio $s/\Delta y$ yield a value for w'/GD that is relatively constant. This result together with the weak effect of Reynolds number on the turbulence parameters is consistent with the predicted trends of present crossflow mixing correlations. This is a significant result because it helps to explain why crossflow mixing in bundles is weakly dependent on rod spacing over a rather wide range of sufficiently large spacings.

The direct measurement of the turbulence parameters related to the crossflow mixing processes provides additional insight concerning the physical processes of crossflow mixing. The experimental data of this study indicate that the regions adjacent to the rod gaps have flow processes that are both diffusive and convective; whereas, the subchannel center and rod gaps are more nearly diffusive. The data also indicate that the eddy diffusion estimates could not be predicted from pipe data alone. The eddy diffusion in bundles seems to be augmented by macroscopic flow processes. This result supports the earlier contentions of Rowe (54), Skinner, et al. (58), and Ibragimov (26) that macroscopic flow processes in addition to eddy diffusion must be responsible for lateral mixing in rod bundles. It does not support the contention of Rogers and Rosehart (47) that the Lagrangian macroscale is nearly proportional to the gap spacing.

Hinze (23, p.288) has suggested an equation of the form

$$\overline{v'\gamma'} = \varepsilon_\gamma \frac{\partial \bar{\Gamma}}{\partial y} + \overline{V'\gamma'} \tag{6.17}$$

to account for scalar transport in the presence of macroscopic flows and eddy diffusion. The same equation has been suggested by Ibragimov (26) for bundles. From the discussion of classical mixing length theory presented in Chapter 2, $\overline{V'\gamma'}$ can be expressed as

$$\overline{V'\gamma'} = \overline{V'L} \frac{\partial \bar{\Gamma}}{\partial y} ; \tag{6.18}$$

therefore

$$\overline{v'\gamma'} = (\varepsilon_\gamma + \overline{V'L}) \frac{\partial \bar{\Gamma}}{\partial y} \quad . \tag{6.19}$$

The macroscopic part of the scalar transport is seen to add to diffusive term by using mixing length theory. The total could also be thought of as an eddy diffusion coefficient but it would not necessarily correspond to an eddy diffusion coefficient for simple channels. Equation (6.19) contains the effects of flow channel geometry through the geometric effect on intensity and scale.

7.0 ACCURACY OF EXPERIMENTAL DATA

This chapter discusses the accuracy of the experimental data as affected by the inherent limitations of the LDV measurement technique, the design capability of the measuring instrument, and the accuracy to which the instrument can be read. These are discussed as they are related to the location of the data point and the measurement of the mean velocity, turbulence intensity and turbulence scale.

The accuracy of the experimental results are estimated by using the method of compounding errors presented by Wilson (64). In this method, a computed experimental result is assumed to have a known functional form given by

$$y = F(x_1, x_2, \text{-- }, x_n). \tag{7.1}$$

Small variations dx_i in x_i alter y by the amount

$$dy = \sum_{i=1}^{n} \frac{\partial F}{\partial X_i} \, dx_i \tag{7.2}$$

The square of the error is

$$(dy)^2 = \sum_{i,j} \frac{\partial F}{\partial x_i} \frac{\partial F}{\partial x_j} \, dx_i \, dx_j \tag{7.3}$$

If the components dx_1, dx_2, --- , dx_n are independently distributed and symmetrical with respect to positive and negative values as they are in the following discussion, then the product $dx_i \, dx_j$ $(i \neq j)$ vanishes so that

$$\overline{(dy)^2} = \sum_{i=1}^{n} \left(\frac{\partial F}{\partial x_i}\right)^2 \overline{dx_i^2} \tag{7.4}$$

This may also be written in terms of the variance as

$$\sigma^2 = \sum_{i=1}^{n} \left(\frac{\partial F}{\partial x_i}\right)^2 \sigma_i^2 \qquad (7.5)$$

7.1 SAMPLE VOLUME SIZE AND LOCATION

The measurement point, or more properly called the sample volume, is estimated to have cylindrical shape of approximately 0.026 inches long by about 0.0034 inches in diameter. Its location within the flow channel is estimated to be known within ±0.019 inches in traverses parallel to the laser beam and ±0.006 inches in traverses perpendicular to the laser beam. The basis for this estimate is summarized in Table 7.1.

TABLE 7.1. Summary of Accuracy Estimate for Sample Volume Size and Location

	Along Beam	Normal to Beam
Sample Volume Size	0.026	0.0034 in.
Components affecting location:		
1. Flow channel dimensions	±0.006 in.	±0.006 in.
2. Traverse position	±0.001 in.	±0.001 in.
3. Uncertainty due to sample volume size	±0.013 in.	±0.0017 in.
Total	±0.019 in.	±0.006 in.

The sample volume location is calculated from the equations

$$z = (z_r - z_o) * C_n \qquad (7.6)$$

$$y = (y_r - y_o) \qquad (7.7)$$

By using Equation (7.5) the variances are

$$\sigma_z^2 = (C_n)^2 \sigma_{z_r}^2 + (Cn)^2 \sigma_{z_o}^2 + (z_r - z_o)^2 \sigma_{c_n}^2 \qquad (7.8)$$

$$\sigma_y^2 = \sigma_{y_r}^2 + \sigma_{y_o}^2 \qquad (7.9)$$

The variance of the index of refraction correction is assumed to be negligibly small since the refractive index is used as a fixed property of the fluid and for small angles $C_n \simeq n$. The variance is then just the sum of variances involved in the reading and the reference values except for the z direction which must be increased by the square of refractive index.

The sample volume size was estimated by using the equation

$$d = 2\sigma = \frac{2}{\pi} \frac{\lambda f}{D} \qquad (7.10)$$

where σ is the standard deviation of intensity, D is the beam diameter at the $1/e^2$ intensity points of a Gaussian laser beam at the lens and f is the focal length of the focusing lens. For H_e-N_e laser with $\lambda = 0.6328$ μm, f = 237 mm, D = 1.1 mm the value of d was 0.087 mm or 0.0034 inch. The receiving optics had focal lengths and aperature diameter that were no more limiting than the focusing optics; therefore, the sample volume was estimated to have the focused beam diameter and length corresponding to the diameter viewed at the 10° scattering angle, times the factor 1.33 to account for elongation due to the refractive index. This gives an estimated length of 0.026 inch.

Several factors influenced the position of the measurement point within the flow channel. Since the dimensions were referenced to the flow channel, its fabrication tolerance were considered. The flow channel was fabricated with a general tolerance of ±0.002 inches for all decimal dimensions unless otherwise noted. Those tolerances governing the size of the flow channel were the thickness of the flow housing (±0.0025 inches), distance between the restraining shoulders at the "O-ring" seal (±0.0025 inches) and location of the rod inserts (±0.005 inches). By taking the square root of the sum of the variances, the overall tolerance for flow channel dimension was estimated to be ±0.006 inches. This tolerance was consistent with check measurements made on the flow channel during the experiments. The only exception to this occurred for the experimental runs A1000 through A1491 where rod straightness was not within tolerance. One of the rod gaps was believed to be closer to 0.105 inches rather than the nominal 0.125 inches. The rods were straightened and were within tolerance for the rerun designated by runs A1492 through A1574.

The traverse position of the measurement point was located to within ±0.001 inch as read on the digital position display of the instrument.

The uncertainty due to sample volume size was related to the loss of the Doppler signal at the channel boundaries. The values shown represent the uncertainty due to the estimated size of the sample volume. Uncertainties of this magnitude occurred when locating the edge of the flow channel. By using the previous estimates the variances are

$$\sigma_z^2 = (1.33)^2\ (0.006)^2 + (0.001)^2 + (0.013)^2 = (0.019)^2 \qquad (7.11)$$

and

$$\sigma_y^2 = (0.006)^2 + (0.001)^2 + (0.0017)^2 = (0.006)^2 \qquad (7.12)$$

For those data known to have symmetry about a given location, slight position corrections were made to the data along the z axis after the data were plotted. In all cases the correction was less than the ±0.019 inch uncertainty in the z direction. The corrected data have less than the ±0.019 inch uncertainty. It should also be realized that less uncertainty exists between data points of a common set because of the high precision (±0.001 inch) of the traversing system.

7.2 MEAN VELOCITY

The mean velocity measurement was estimated to be accurate to within ±3.2%. This estimate was composed of the several factors shown in Table 7.2.

TABLE 7.2. Summary of Accuracy Estimate for Mean Velocity

Components Affecting Mean Velocity	Estimated Accuracy, %
Scattering Angle	±1.5
Doppler Frequency Measurement	±2.8
Total	±3.2

The mean velocity is computed from the equation

$$\bar{u} = \frac{\lambda}{u \sin\theta}\,\bar{f}_D \qquad (7.13)$$

The variance on $\bar{u}$ is

$$\sigma_u^2 = \left(\frac{\lambda}{n \sin \theta}\right)^2 \sigma_{f_D}^2 + \left(\frac{\lambda}{n \sin \theta}\right)^2 \left(\frac{f_D}{\tan \theta}\right)^2 \sigma_\theta^2 \qquad (7.14)$$

In terms of a fraction this can be written as

$$\frac{\sigma_u^2}{\bar{u}^2} = \frac{\sigma_{f_D}^2}{\bar{f}_D^2} + \frac{\sigma_\theta^2}{\tan^2 \theta} \qquad (7.15)$$

A 10° scattering angle was built into the receiving optics; however, measurement of this angle during the experiments indicated variations of about ±0.15° or ±1.5%. Most of this was due to small changes in scattering angle that occurred during optical alignment adjustments.

Doppler frequency measurement consisted of several factors including reading of the frequency meter and null meter. The frequency meter could be read to 1 kHz; however, the certainty for any point was about ±2 kHz. The null meter could be read to within ±10 mV, where recorded values were typically 500 mV. For most data, a 500 mV offset corresponded typically to 100 kHz offset giving 5 mV/kHz. Reading the null meter to ±10 mV (±2%) was consistent with the readability of the frequency meter. For Doppler frequencies typically of 2000 kHz, read to within 2 kHz, the null meter was the limiting element in reading the Doppler frequency. The ability of the readout system to measure standard signals of known frequency was checked with an independent frequency meter. Agreement in the range of interest was always within 10 kHz. With noisy Doppler signals, larger variation in the form of an

offset was noted. A value of ±40 kHz was selected as a representative range of uncertainty. For Doppler frequencies of about 2000 kHz this corresponded to a ±2.0% uncertainty. The total due to Doppler uncertainty (±2.0%), frequency meter (±0.1%) and null meter ±2% was about ±2.8%. The total variance was estimated to be

$$\frac{\sigma^2_u}{\bar{u}^2} = \left((0.02)^2 + (0.001)^2 + (0.02)^2\right) + (0.015)^2 = (0.032)^2 \quad (7.16)$$

In addition to the above uncertainties there are some other considerations.

Equation (7.13) is an approximation to Equation (4.1) and is valid for small scattering angles. At 10° the error introduced by this approximation is less than 0.5%. In reality this error is one sided and is therefore a bias.

The effect of velocity gradient on the measured velocity is small for most measurements, especially those near the interior of the channel. An approximate equation for estimating uncertainty due to velocity gradient is

$$\frac{\Delta\omega}{\omega} = \frac{2\sigma_{max}}{u}\frac{\Delta u}{\Delta x} \quad (7.17)$$

Taking values of $2\sigma/u = 0.026/20$ and $\Delta u/\Delta x = 1/0.1$ the uncertainty is of the order 1.3%. For larger gradients this would, of course, be larger. This estimated uncertainty is believed to be considerably larger than that resolved by a mean frequency detecting device. This uncertainty is actually a shift of the Doppler frequency.

For any given data set, the accuracy was better than the stated total. The uncertainties due to scattering angle and third velocity component, and noise would be small. The primary uncertainty would be due to the reading accuracy (2.0%).

7.3 TURBULENCE INTENSITY

The turbulence intensity measurement was estimated to be accurate to within about ±5.1%. This larger uncertainty as compared to mean velocity was due to the uncertainty of additional factors required to obtain the turbulence velocity as summarized in Table 7.3.

TABLE 7.3. Summary of Accuracy Estimate for Turbulence Intensity

Components Affecting Turbulence Intensity:	Accuracy, %
Linearity of $\Delta f/\Delta E$	±2.0
Frequency Offset, Δf	±1.4
Null Offset, ΔE	±2.0
"rms" voltage, E'	±2.0
System Noise	±1.2
Doppler Broadening	±2.5
Total	±5.1

The turbulence intensity was calculated from the equation

$$\frac{u'}{\bar{u}} = \frac{E'}{\Delta E}\frac{\Delta f}{\bar{f}_D} \qquad (7.18)$$

The variance on the intensity is

$$\sigma_I^2 = \left(\frac{E'}{\Delta E \bar{f}_D}\right)^2 \sigma^2_{\Delta_f} + \left(\frac{\Delta f}{\Delta E \bar{f}_D}\right)^2 \sigma^2_{E'} + \left(\frac{E'\Delta F}{\Delta E \bar{f}_D}\right)^2 \frac{\sigma^2 f_D}{f_D^2} + \left(\frac{E'\Delta f}{\Delta F \bar{f}_D}\right)^2 \frac{\sigma^2 \Delta E}{\Delta E^2} \qquad (7.19)$$

where I is taken to be the ratio $u'/\bar{u}$. As a fraction, this is

$$\frac{\sigma_I^2}{I^2} = \frac{\sigma_{\Delta f}^2}{\Delta f^2} + \frac{\sigma_{E'}^2}{E'^2} + \frac{\sigma_{f_D}^2}{f_D^2} + \frac{\sigma_{\Delta E}^2}{\Delta E^2} \quad . \tag{7.20}$$

Effects of system noise and linearity of the $\Delta E/\Delta f$ slope should also be added to this.

The measurement of the fluctuating Doppler frequency consisted of several components. The frequency-to-voltage conversion slope $\Delta f/\Delta E$ was estimated to be linear to within ±2% based on check measurements of linearity during the experiments. The frequency offset accuracy was estimated at ±1.4% based upon reading the frequency meter to within 1 kHz at null and at offset position for a typical offset of 100 kHz. For the 100 kHz offset, the voltage offset was usually greater than 500 mV. By reading the null meter to within ±10 mV the accuracy of ΔE was estimated to be within ±2%. This had to be considered twice, however, because null meter had to be read at null and the offset point. The rms voltmeter reading was typically about 500 mV. It could be read to within ±10 mV which gave an uncertainty of ±2.0%. The rms meter also was used to measure the system noise without a Doppler signal. All checks indicated less than 5 mV noise for both the single- and two-component data processing. This gave a noise estimate compared to E' of about ±1.2%.

The work of George and Lumley (16,17,18) was used to help define the contribution of the Doppler ambiquity. According to George and Lumley, broadening causes a nearly constant noise base level on the

power density spectrum as shown in Figure 3.2. If this is true, then a plot of turbulence energy should show a linear increase in turbulence energy with increasing cutoff frequency of the low-pass filters. Several sets of data were taken to check their theory and to select an appropriate cutoff frequency. An example of such data in Figure 7.1 shows an approximately linear increase with frequency. These represent a worse case since most all other data did not show as much variation with cutoff frequency in the higher frequency range. The results show that, depending upon the relative importance of broadening, about 10% increase in turbulence energy occurs beyond the break point at about 4 kHz. By cutting off at a frequency of 4 kHz in this case, the effect of broadening due to higher frequency can be reduced. For most data a frequency cutoff in the range of 3 to 6 kHz was used. Since a definitive correction procedure does not exist, a ±2.5% uncertainty was applied to the intensity data for uncertainty in the proper cutoff frequency. This corresponds to a cutoff frequency uncertainty of about ±1.5 kHz in the linear range. Figure 7.2 shows a turbulence intensity plot through the center gap of Channel C for three cutoff frequencies. The data show about 15% increase between 1 kHz and 4 kHz cutoff frequencies but less than about 5% increase between 4 kHz and 10 kHz. All data in Channels D and E were taken at a cutoff frequency of 1 kHz and therefore low. Based upon the data of Figure 7.2 they would be about 15% low. From the above estimates the total estimated variance for the turbulence intensity is

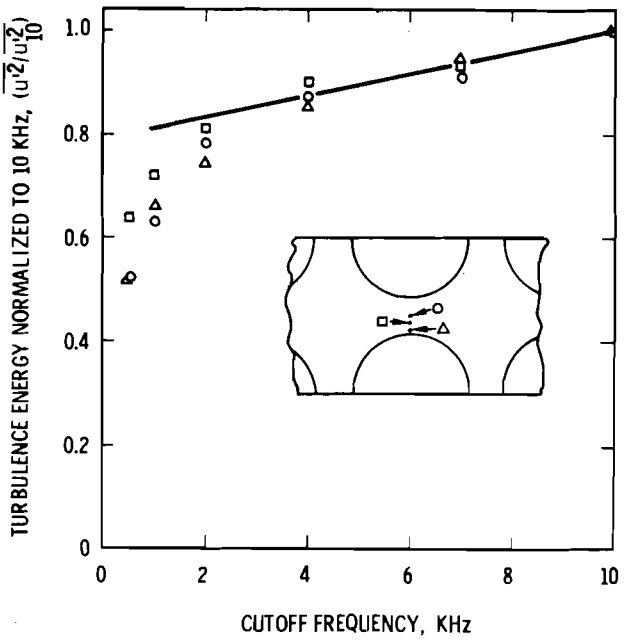

Figure 7.1. Turbulence energy versus low pass filter cutoff frequency in center gap of Channel C.

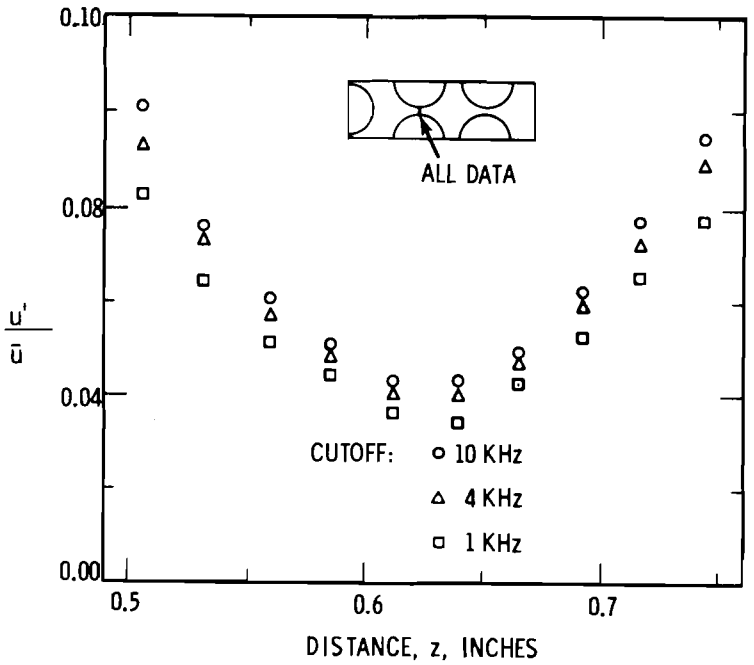

Figure 7.2. Turbulence intensity distribution in center gap of Channel C at selected cutoff frequencies, Re = 100,000.

$$\frac{\sigma_I^2}{I^2} = (0.02)^2 + (014)^2 + (2(0.02)^2 + (0.02)^2 + (0.012)^2 + (0.025)^2$$

$$= (0.051)^2 \qquad (7.21)$$

7.4 TURBULENCE SCALE

The Eulerian time macroscale estimates were obtained by fitting an exponentially decaying cosine function through the autocorrelation plots obtained from the x-y recorder. By accepting this functional form approximation and Taylor's hypothesis, it is possible to estimate the accuracy of the turbulence scale data. The total estimated uncertainty of ±8.3% consisted of the factors shown in Table 7.4.

TABLE 7.4. Summary of Uncertainties for Macroscale Estimate

Components Affecting Macroscale	Accuracy (%)
Mean Velocity	±3.2
Time Macroscale:	
Reading Plot	±5.0
Correlation Fit	±5.0
Plotter Accuracy	±2.0
Correlation Function	±2.0
Total	±8.3

The estimated macroscale was calculated from the equation

$$\Lambda = \bar{u}\, T_E \qquad (7.22)$$

where

$$T_E = -\alpha_1/(\alpha_1^2 + \alpha_2^2) \qquad (7.23)$$

and where α_1 and α_2 are the parameters used to fit the correlation function to the form

$$R(\tau) = \exp(\alpha_1\tau) \cos(\alpha_2\tau) \tag{7.24}$$

By using Equation (7.5), the variance of Λ on a fractional basis is

$$\frac{\sigma^2_\Lambda}{\Lambda^2} = \frac{\sigma^2_u}{\bar{u}^2} + \frac{\sigma^2_{T_E}}{T_E^2} \tag{7.25}$$

The variance due to recording, plotting and reading the correlation plot should also be added to these.

For most cases where the correlation function is nearly an exponential decay, $\alpha_1 > \alpha_2$; therefore, as an approximation

$$T_E \simeq -\frac{1}{\alpha_1} \tag{7.26}$$

or

$$\frac{dT_E}{T_E} = \frac{d\alpha_1}{\alpha_1} \tag{7.27}$$

From Equation (7.16) for small α_2

$$\frac{dR}{R} = \tau d\alpha \tag{7.28}$$

If τ is taken to be $1/\alpha_1$; then, an estimate for the variance on T_E is approximately

$$\frac{\sigma^2_{T_E}}{T_E^2} \simeq \frac{\sigma^2_R}{R^2} \tag{7.29}$$

Each correlation plot was divided into eleven equally spaced points for input to a least squares curve fitting routine. Each coordinate value was read from the plot to within ±1 on a scale of typically 20 giving a reading accuracy of about 5%.

The correlation function was fit with an exponential function by using a least-squares curve fitting routine (25). The calculated standard deviation for the fit was usually calculated to be less than 5%. The value of the standard deviation of the curve fit can be obtained from the data tabulation in Appendix B. Since all plotter data were normalized, absolute scale accuracy was not required. The plotter linearity and accuracy for this range was estimated to be about 2%. The correlator specifications stated an accuracy of better than 2%.

The above variance estimates give a total variance of

$$\frac{\sigma_\Lambda^2}{\Lambda^2} = (0.032)^2 + (0.05)^2 + (0.05)^2 + (0.02)^2 + (0.02)^2 = (0.083)^2 \tag{7.30}$$

7.5 REPRODUCIBILITY

Several sets of data were taken to verify repeatability of both the single-and two-component data. The data of Figure 5.29 show the results of 5 different sets of data taken in both the single- and two-component configuration. The velocity, intensity and scale data show uncertainties that are of the magnitudes previously described.

Figure 7.3 shows a comparison of axial component data taken in the rod gap of Channel E for both the one- and two-component configurations. The excellent agreement here verifies the method of resolving the two-component data.

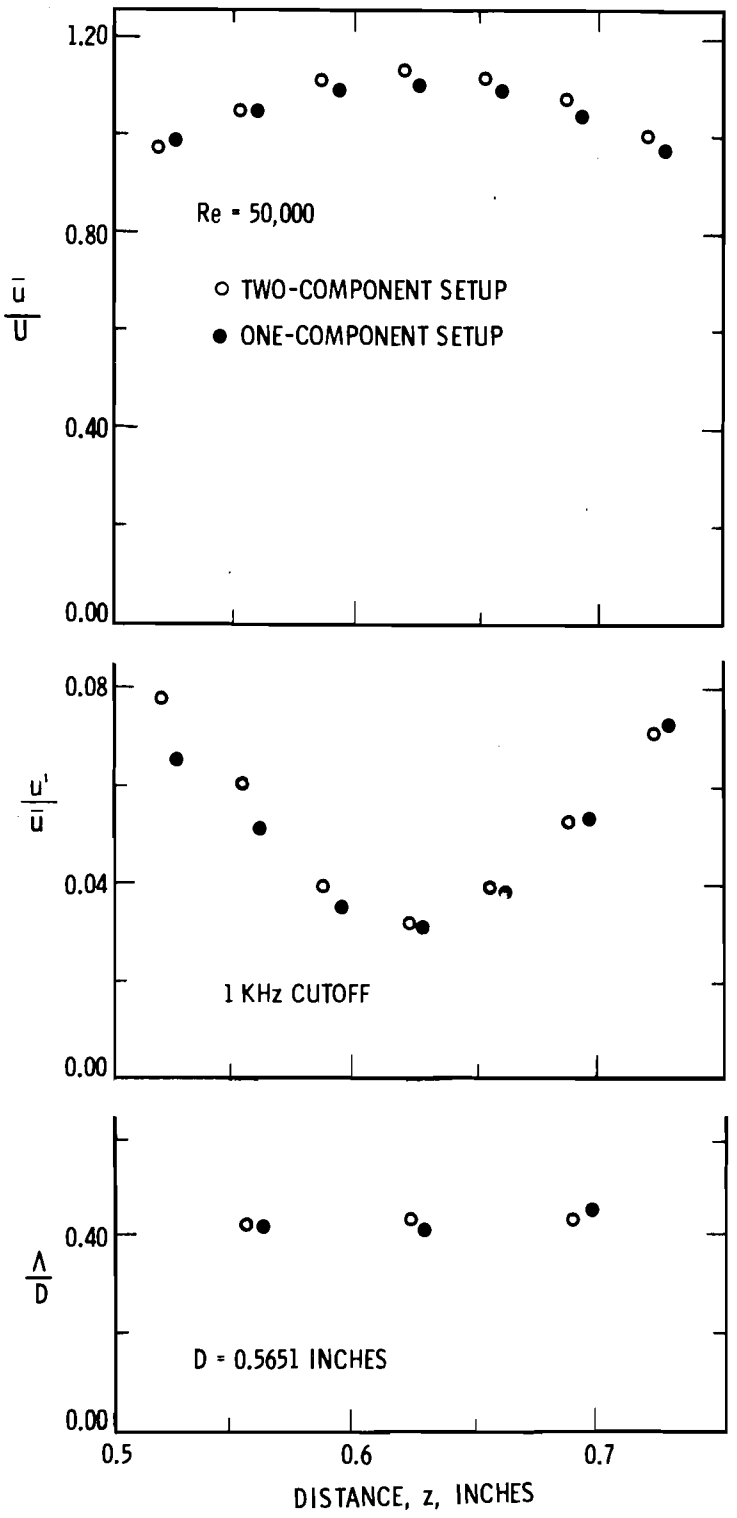

Figure 7.3. Comparison of data obtained in one- and two-component configuration, Channel E, Re = 50,000.

8.0 CONCLUSIONS AND RECOMMENDATIONS

The present experimental study has provided new and useful information regarding the turbulent flow through rod bundles. This has been accomplished by measuring the velocity, turbulence intensity and Eulerian autocorrelation functions locally within several flow channels by using a laser-Doppler velocimeter (LDV). The LDV proved to be a very valuable and useful tool for this study. The small size and the ease of locating the sample volume within the channel made the experimental study possible.

The experimental program has shown that rod gap spacing has significant influence on the turbulent flow structure in rod bundles in a way that cannot be deduced from round pipes. While the velocity profiles are in reasonable agreement with universal profiles in pipes, the turbulence intensity and macroscale are larger than for pipe flows of the same hydraulic diameter. A fundamental source of the difference seems to be related to the secondary flow patterns caused by the non-uniformly shaped channels in rod bundles.

The following conclusions can be made regarding the experimental results:

1. The dimensionless parameters $\bar{u}/U$, $u'/\bar{u}$ and Λ/D are weakly dependent on Reynolds number,
2. The shape of subchannels adjacent to a rod gap does not significantly affect the velocity and turbulence parameter distribution in the gap.

3. Reducing the rod gap spacing increases the intensity and the longitudinal macroscale.
4. The turbulence generally has a frequency ranging up to a few kHz with the energy content greatest at very low frequency; however, reducing the rod gap spacing causes a shift toward a higher dominant frequency between the subchannel center and rod gap.
5. Adding more lateral freedom to a flow model does not significantly modify the velocity and turbulence parameter distribution within a rod gap.
6. The lateral component of turbulence intensity ($v'/\bar{u}$) varies depending upon location but ranges from about 50% to 80% of the axial component intensity ($u'/\bar{u}$).
7. The turbulence intensities show highly nonuniform distributions with relative minima at the subchannel center and in the rod gap.
8. The axial Eulerian macroscale as estimated by Taylor's hypothesis is on the order of 0.4 times the hydraulic diameter for $p/d = 1.25$.
9. The experimental results for velocity and turbulence intensity are in general agreement with the results of Kjellström.
10. Distortions of turbulence intensity maps show the existence of secondary flows; however, their magnitude is believed to be less than 1% of the axial velocity.
11. The region between the rod gap and subchannel center appears to have periodic macroscopic flow processes that increase in scale, intensity, and frequency as the rod spacing is reduced.

12. The crossflow mixing parameter w'/GD as estimated by the product $(u'/u)(\Lambda/D)(s/\Delta y)$ changes only moderately with a change in rod gap spacing. This is the first known measurement of turbulence parameters that can explain the weak influence of rod gap spacing on rod bundle intersubchannel mixing.

Several recommendations are offered as a result of this study:

1. An experimental study of longitudinal spatial correlation functions in rod bundles would provide useful information to assess the accuracy of using Taylor's hypothesis. This could be done with a dual channel and a multiple beam LDV system.
2. To provide more quantitative data on local eddy diffusion coefficients, more information is needed on the relationships between Lagrangian and Eulerian turbulence parameters. A combined experiment involving scalar mixing in the same flow channels where Eulerian turbulence parameters are measured would be very valuable to assess the relationship between these two important parameters.
3. Additional experimental data over a wider range of gap spacings should be obtained to provide a more complete description of the important effect of gap spacing on the turbulent flow processes.
4. The effect of surface roughness should be investigated in more detail since significantly enhanced turbulence intensity and periodic flow pulsations were indicated in the presence of roughness.

9.0 NOMENCLATURE

A	Flow area
C_n	Refractive index correction to traverse dimension z
$C(\tau)$	Autocorrelation function
d	Diameter of laser beam at focal point
d	Rod diameter
D	Hydraulic diameter (4A/Pw)
D	Diameter at $1/e^2$ intensity points of a Gaussian distributed laser beam at the lens
D_γ	Molecular diffusion coefficient
$e(t)$	Fluctuating voltage amplitude
E'	"Rms" fluctuating voltage
$E(n)$	Turbulence energy spectrum
$E(t)$	Electronic signal voltage
f	Focal length
f	Darcy friction factor
f_D	Doppler frequency
f'_D	Fluctuating component of Doppler frequency
f_o	Oscillator frequency
$f(x)$	Eulerian longitudinal spatial correlation function
G	Mass flux, ρu
i	Photo tube current
k'	Turbulence kinetic energy
$\bar{K}$	Scattering vector
ℓ	Lateral turbulence scale

L	Mixing length
n	Frequency
n	Refractive index
$n(t)$	Noise contribution to electronic signal voltage
p	Rod pitch
P	Pressure
P_w	Wetted perimeter
r	Radial distance
$\bar{r}_o$	Reference unit vector
$\bar{r}_s$	Scattering unit vector
Re	Reynolds number (GD/μ)
$R_E(\tau)$	Eulerian correlation function
$R_L(\tau)$	Lagrangian correlation function
$R_E(\delta,\tau)$	Eulerian space-time correlation function
s	Rod gap spacing
t	Time
T	Averaging time
T_E	Eulerian time macroscale
T_L	Lagrangian time macroscale
$\hat{u}$	Velocity along line of maximum velocity
U	Channel average velocity
u^*	Shear velocity based on u
u, v, w	Instantaneous velocity components in the x, y, z direction

u', v', w'	Fluctuating velocity components in the x, y, z direction
$\bar{u}$, $\bar{v}$, $\bar{w}$	Mean velocity component in the x, y, z direction
$\overline{u'v}$, $\overline{v'w}$, $\overline{w'u'}$	Turbulent shear stress components
$\overline{u'^2}$, $\overline{v'^2}$, $\overline{w'^2}$	Principle turbulent stress components
$\overline{u'V'}$	Macroscopic shear stress component
ν	Kinematic viscosity (μ/ρ)
$\bar{V}$	Velocity vector
ω	Radial frequency
ω'_D	Fluctuating component of radial Doppler frequency
$\bar{\omega}_D$	Average radial Doppler frequency
ω_D	Radial Doppler frequency
w'	Turbulent crossflow per unit length
ω_o	Radial oscillator frequency
x, y, z	Cartesian coordinates
y	Distance from wall
$\hat{y}$	Distance from wall to line of maximum velocity
Υ	Correlation parameter of Ingesson, et al.
y_o, z_o	Reference coordinates for (y, z)
$\overline{y^2(t)}$	Mean square diffusion distance
α_1,α_2	Function fit parameters
γ	Fluctuating component of scalar
Γ	Scalar quantity
$\bar{\Gamma}$	Average value of scalar quantity

ΔE	Voltage offset
Δf	Frequency offset
Δy	Centroid or "mixing" distance between subchannels
δ	Space-time correlation parameter
ε	Eddy diffusivity
ξ,η,ζ	Vorticity components in x, y, z direction
θ	Scattering angle
λ	Wavelength of light
λ	Turbulence microscale
λ_o	"in-vacro" wavelength of laser light (λ_o = 6328Å, H_e-N_e)
Λ	Eulerian longitudinal space macroscale as estimated by Taylor's hypothesis
Λ_f	Eulerian longitudinal space macroscale
Λ_L	Lagrangian space macroscale
μ	Absolute viscosity
ρ	Density
σ	Sample volume standard deviation of intensity distribution
σ	Standard deviation
τ	Time delay
τ_w	Wall shear stress
ϕ	Angular coordinate

10. BIBLIOGRAPHY

1. Baldwin, Lionel V. and Thomas J. Walsh. Turbulent diffusion in the core of fully developed pipe flow. A.I.Ch.E. Journal 7:53-61. 1961.

2. Bobkov, V. P., S. P. Beschastnov, Yu. I. Gribanov, M. Kh. Ibragimov, and P. K. Karpov. Statistical investigation of the temperature field during turbulent flow of water in a pipe. High Temperature 8:760-765. 1970.

3. Bobkov, V. P. and M. Kh. Ibragimov. Application of the uniform diffusion model to the calculation of the tangential stresses and velocity field in a turbulent fluid flow. High Temperature 8:305-310. 1970.

4. Bobkov, V. P., M. Kh. Ibragimov, E. V. Nomofilov and V. I. Subbotin. The three-dimensional correction coefficients and the transverse scales of the temperature perturbation in turbulent flow of mercury in a round tube. High Temperature 4:367-374. 1966.

5. Bobkov, V. P., M. Kh. Ibragimov, and G. I. Sabelev. The calculation of the coefficient of turbulent heat diffusion channels of noncircular cross section. High Temperature 6:645-651. 1968.

6. Bobkov, V. P., M. Kh. Ibragimov, and V. I. Subbotin. Time characteristics and temperature pulsation spectrum for the turbulent flow of liquid in a pipe. High Temperature 6:93-99. 1968.

7. Bobkov, V. P., M. Kh. Ibragimov, and V. I. Subbotin. Calculating the coefficient of turbulent heat transfer for liquid flowing in a tube. Soviet Atomic Energy 24:545-550. 1968.

8. Bowring, R. W. HAMBO: A computer program for the subchannel analysis of the hydraulic and burnout characteristics of rod clusters. 1968. 60 p. (Atomic Energy Establishment. AEEW-R-582).

9. Brundrett, E. and W. D. Baines. The production and diffusion of vorticity in duct flow. Journal of Fluid Mechanics 19:375:392. 1964.

10. Buleev, N. I. Theoretical model of the mechanism of turbulent exchange in fluid flows. 1963. (United Kingdom Atomic Energy Authority. AERE-Trans 957).

11. Deissler, Robert G. and Maynard F. Taylor. Analysis of axial turbulent flow and heat transfer through banks of rods or tubes. 1956. (Reactor Heat Transfer Conference of 1956. TID-7529, Pt.1 Bk 2, pp. 416-461).

12. Edwards, Robert V., et al. Spectral analysis of the signal from the laser-Doppler flowmeter: Time Independent Systems. Journal of Applied Physics 42:837-850. 1971.

13. Eifler, W. and R. Nijsing. Fundamental studies of fluid flow and heat transfer in fuel element geometries. 1965. (Euratom, EUR 2193C).

14. Galbraith, Kirk P. Single phase turbulent mixing between adjacent channels in rod bundles. Ph.D. Thesis. Corvallis, Oregon, Oregon State University, June, 1971. 171 numb. leaves.

15. Galbraith, K. P. and J. G. Knudsen. Turbulent mixing between adjacent channels for single phase flow in a rod bundle. American Institute of Chemical Engineers, Preprint 19. 1971.

16. George, W. K. An analysis of the laser-Doppler velocimeter and its application to the measurement of turbulence. Ph.D. Thesis. Baltimore, Maryland, The Johns Hopkins University, 1971.

17. George, W. K. and J. L. Lumley. Limitations on the measurement of turbulence using a laser-Doppler velocimeter. Proceedings, Electro-Optical Conference. New York, New York. 1970.

18. George, W. K. and J. L. Lumley. Limitations on the measurement of turbulence using a laser-Doppler velocimeter. January, 1971. (ASCE National Water Resources Meeting. Phoenix, Arizona. Preprint number 1345.)

19. Gessner, F. B. A method of measuring Reynolds stresses with a constant-current, hot-wire anemometer. American Society of Mechanical Engineers, ASME Paper 64-WA/FE-34. 1964.

20. Gessner, F. B. and J. B. Jones. A preliminary study of turbulence characteristics of flow along a corner. Journal of Basic Engineering 83:657-662. 1961.

21. Gessner, F. B. and J. B. Jones. On some aspects of fully developed turbulent flow in rectangular channels. Journal of Fluid Mechanics 23:689-713. 1965.

22. Hetsroni, G., J. Leon, and M. Hakim. Cross flow and mixing of water between semiopen channels. Nuclear Science and Engineering 34:189-193. 1968.

23. Hinze, J. O. Turbulence. New York, McGraw-Hill, 1959. 586 p.

24. Hinze, J. O. Secondary currents in wall turbulence. Boundary layers and turbulence. Physics of Fluids Supplement 10:S122-S125.

25. Howell, John Q. A least-square-distance curve-fitting technique. July 1971. 22p. (National Aeronautics and Space Administration. NASA TN D-6374).

26. Ibragimov, M. Kh., I. A. Isupov, L. L. Kobzar and V. I. Subbotin. Calculation of the tangential stresses at the wall in a channel and the velocity distribution in a turbulent flow of liquid. Atomic Energy 21:731-739. 1966.

27. Ibragimov, M. Kh., G. I. Sabelev, V. I. Sidorov and V. I. Subbotin. Spatial structure of temperature perturbations in the nonisothermal turbulent flow of a liquid in a square channel. High Temperature 6:441-446. 1968.

28. Ibragimov, M. Kh., G. I. Sabelev, V. I. Sidorov and V. I. Subbotin. Space-time characteristics of temperature pulsations during turbulent liquid flow in a square channel. High Temperature 6:1020-1024. 1968.

29. Ingesson, Lars and Stellan Hedberg. Heat transfer between subchannels in a rod bundle. Heat Transfer 1970 3:FC7.11, 12 p. 1970.

30. Ingesson, L. and B. Kjellström. On gas mixing in rod bundles. International Journal of Heat and Mass Transfer 13:429-431. 1970.

31. Kashcheev, V. M. and E. V. Nomofilov. Turbulence scale in channels formed by closely packed rods. International Journal of Heat and Mass Transfer 11:267-277. 1968.

32. Kjellström, B. Studies of turbulent flow parallel to a rod bundle of triangular array. 1971. (AB Atomenergi, Studsvik, 611 01 Nyköping, Sweden. STU 68-263/u210).

33. Kjellström, B. Transport processes in turbulent channel flow. 1972. (AB Atomenergi, Studsvik, 611 01 Nyköping, Sweden, STU project 70-409/u340 [final report]. AE-RL-1344).

34. Kolmogoroff, A. N. Izv. Akad. Nauk SSSR Ser. Fiz. 6:56. 1942. [Imperial College Mech. Eng. Dept. Rept. ON/6 (1968)].

35. Lading, L. Differential Doppler heterodyning technique. Applied Optics 10:1943-1949. 1971.

36. Laufer, J. Investigation of turbulent flow in a two-dimensional channel. 1951. (National Advisory Committee for Aeronautics. NACA Rep. No. 1053).

37. Laufer, John. The structure of turbulence in fully developed pipe flow. 1953. 53 p. (National Advisory Committee for Aeronautics. NACA-TN-2954).

38. Lumley, J. L., W. K. George and Y. Kobiashi. The influence of ambiguity and noise on the measurement of turbulent spectra by Doppler scattering. Proceedings, Symposium, Turbulent Measurement in Liquids. Rolla, Missouri. 1969.

39. Mathews, Larry K. and James H. Rust. Laser-Doppler velocimeter - performance in open and confined flow. Personal communication. November, 1971.

40. Ng, K. H. and D. B. Spalding. Turbulence model for boundary layers near walls. Physics of Fluids 15:20-30. 1972.

41. Perkins, H. J. The formation of streamwise vorticity in turbulent flow. Journal of Fluid Mechanics 44:721-740. 1970.

42. Pike, E. R., D. A. Jackson, P. J. Bourke and D. I. Page. Measurement of turbulent velocities from the Doppler shift in scattered laser light. Journal of Scientific Instruments 1:727-730. 1968.

43. Prandtl, L. Z. Angew. Math. Mech. 5:136. 1925.

44. Prandtl, L. Uber ein neues Formelsystem fur die ausgebildete turbulenz. Nachr. Akad. der Wissenschaften zer Goettingen. Math. Physik. Klasse 1945. (pg 6-19 reprinted in Ludwig Prandtl Gesamelte Abhandlungen Berlin 1961, 874-887.)

45. Rapier, A. C. Turbulent mixing in a fluid flowing in a passage of constant cross section. 1967. [United Kingdom Atomic Energy Authority, Reactor Development Laboratory, Windscale, Great Britain. TGR Report 1417 (W).]

46. Rehme, K. Untersuchungen der turbulenz - und schubspannungsverteilung an einem kreisrohr mit einem Hitzdraht-Anemometer. 1972. (Gesellschaft für Kernfarschung mbH., Karlsruhe. KFK-1642).

47. Rogers, J. T. and R. G. Rosehart. Mixing by turbulent interchange in fuel bundles, correlations and inferences. ASME paper no. 72-HT-53, 13 p. 1972.

48. Rogers, J. T. and N. E. Todreas. Coolant interchannel mixing in reactor fuel rod bundles, single-phase coolants. Heat Transfer in Rod Bundles. pp 1-56. American Society of Mechanical Engineers. 1968.

49. Rotta, J. C. Z Physik. 131:51. 1951.

50. Rowe, D. S. and C. W. Angle. Experimental study of mixing between rod-bundle fuel-element flow channels during boiling. Transactions of the American Nuclear Society 10:655. 1967.

51. Rowe, D. S. and C. W. Angle. Cross-flow mixing between parallel flow channels during boiling. Part II. Measurement of flow and enthalpy in two parallel channels. 1967. 55 p. (Battelle Memorial Institute. Pacific Northwest Laboratories. BNWL-371-PTII).

52. Rowe, D. S. and C. W. Angle. Cross-flow mixing between parallel flow channels during boiling. Part III. Effect of spacers on mixing between channels. 1968. 69 p. (Battelle Memorial Institute. Pacific Northwest Laboratories. BNWL-371-PTIII).

53. Rowe, D. S. A thermal-hydraulic subchannel analysis for rod bundle nuclear fuel elements. Heat Transfer 1970 3:FC 7.11. 1970.

54. Rowe, D. S. A mechanism for turbulent mixing between rod bundle subchannels. Transactions of the American Nuclear Society, 12:805. 1969.

55. Rowe, D. S. COBRA-II: A digital computer program for thermal-hydraulic subchannel analysis of rod bundle nuclear fuel elements. 1970. 60 p. (Battelle Memorial Institute. Pacific Northwest Laboratories. BNWL-1229).

56. Rowe, D. S. Cross-flow mixing between parallel flow channels during boiling. Part I. COBRA-computer program for coolant boiling in rod arrays. 1967. 87 p. (Battelle Memorial Institute. Pacific Northwest Laboratories. BNWL-371-PT1)

57. Schlichting, Hermann. Boundary layer theory. 6th ed. New York, McGraw-Hill, 1968.

58. Skinner, J. R., A. R. Freeman and H. G. Lyall. Gas mixing in rod clusters. International Journal of Heat and Mass Transfer 12:265-278. 1969.

59. Subbotin, V. I., M. Kh. Ibragimov and E. V. Nomofilov. Statistical study of turbulent temperature pulsations in a liquid stream. High Temperature 2:59-64. 1964.

60. Subbotin, V. I., P. A. Ushakov, Yu. D. Levchenko, and A. M. Aleksandrov. Velocity fields in turbulent flow past rod bundles. Heat Transfer - Soviet Research 3:9-35. 1971.

61. Taylor, G. I. Statistical theory of turbulence. Proceedings of the Royal Society of London, Series A 151:4210478. 1935.

62. Van Der Ross, T. and M. Bogaardt. Mass and heat exchange between adjacent channels on liquid-cooled rod bundles. Nuclear Engineering and Design 12:259-268. 1970.

63. Welty, James R., Charles E. Wicks and Robert E. Wilson. Fundamentals of momentum, Heat and Mass Transfer. John Wiley and Sons, New York. 1969.

64. Wilson, E. Bright, Jr. An introduction to Scientific Research (1952). McGraw Hill, New York) pg 272.

65. Yeh, Y. and H. Z. Cummins. Localized fluid flow measurements with a H_e-N_e laser spectrometer. Applied Physics Litters 4:176-178. 1964.

APPENDIX A

DATA REDUCTION COMPUTER PROGRAM

APPENDIX A

DATA REDUCTION COMPUTER PROGRAM

```
      DIMENSION  FO(2), ERMS(2), DELTAF(2), DELTAE(2), BAND(2), LPF(2),
     1 U(2), UP(2), FO(2), FP(2)
      DIMENSION  COMENT(11)
      DIMENSION C(11), TAU(11)
      DIMENSION AL(9), X(11)
      DIMENSION TITLE(16)
      DIMENSION F(20), FMT(20)
      REAL LPF
      DATA         (F(I),I=1,19)/     4H(A7,,5HF9.0,,5HF7.3,,5HF7.3,,
     1 5HF6.1,,5HF6.2,,5HF6.1,,5HF6.3,,5HF6.2,,
     2 5HF6.3,,5HF6.2,,5HF6.2,,5HF6.2,,5HF6.0,,
     3 5HF6.3,,3HI4),3HA6,,3HA5,,3HA4)/
      DATA NBLANK,BLANK,BLANK5/4H    -,5H     -,4H    -/
      DATA (N(I),I=1,11)/11*1./
    1 FORMAT(A6,I4,2F5.3,F5.0,11A5)
    2 FORMAT (A6,F4.0,F5.0,2F5.3,2(4F5.3,F2.0,F3.0),F5.3)
    3 FORMAT( '  HYDRAULIC DIAMETER, D ='F5.3,' INCHES.',
     1'     AVERAGE VELOCITY, U ='F5.1,' FT/SEC,  U ='F5.3,' FT/SEC.'/
     1      ' * QUESTIONABLE DATA POINT.' ,
     3'     - NO DATA POINT.')
    5 FORMAT(4E5.2)
    6 FORMAT(6X,F4.0,12F5.2)
    8 FORMAT (16A5)
    9 FORMAT('1           TABLE B-1 (CONT.). TABULATION OF EXPERIMENTAL D
     1ATA.'//1X,16A5//
     2'   RUN   REYNOLDS     Z       Y      U     U/U    U/U    U/U    U/U    V/
     3U    V/U CUTOFF       CURVE FIT'/
     4'           NUMBER     IN.     IN.  FT/SEC
     5          KHZ    /D  F(HZ)          ')
      AVISC(T) = 0.0583*10.**(446./(207.6+T))
      RHO(T) = 62.76-0.5376*(T/100.)-0.365*(T/100.)**2-.0173*(T/100.)**3
      VISC(T) = AVISC(T)/RHO(T)/3600.
      RINDEX(T) = 1.3370 - 0.000174*(T-32.)*5./9.
      AA1 = 7.110
      AA2 = 5.545
      AB  = 2.644
      AC  = 1.890
      AD  = 1.137
      AE  = 1.113
      PI = 3.14159
   10 READ 1,    RUN,NRUNS, XO,YO,PSI,COMENT
      IF(NRUNS .LT.1) STOP
      READ 6, TITLE
      PRINT 9, TITLE
      READ 5, A, DHYD, XCORR, YCORR
      XO = XO - XCORR
      YDUMY = YO
C  INTERCHANGE NEXT 2 CARDS FOR Y TRAVERSE OPTION
      YO = YDUMY - YCORR
      YO = YDUMY + YCORR
C  YO=YDUMY-YCORR IS THE OPTION FOR RUNS A1000 - A1491 ONLY.
C
      COSINE = COS(PSI*PI/180.)
      SINE   = SIN(PSI*PI/180.)
      LINE = 0
      DO 100 K=1,1000
      LINE = LINE + 1
      IF(LINE.LE.40) GO TO 11
      PRINT  3, DHYD, UAVG, USTAR
      PRINT 9, TITLE
      LINE = 1
   11 READ 2,  RUN, TEMP, FLOW, X, Y, (FO(I),ERMS(I),DELTAF(I),
     1  DELTAE(I),BAND(I), LPF(I),I=1,2), E1E2
      IF(TEMP.LT.1.) PRINT 3, DHYD, UAVG, USTAR
      IF(TEMP.LT.1.) GO TO 10
```

```
      READ 6, T, DIVISN, C
   12 IF(FO(1) .GT. 0.) GO TO 15
      FO(1) = FO(2)
      FO(2) = 0.
      ERMS(1) = ERMS(2)
      ERMS(2) =0.
      DELTAF(1) = DELTAF(2)
      DELTAF(2) = 0.
      DELTAE(1) = DELTAE(2)
      DELTAE(2) =0.
      BAND(1) = BAND(2)
      BAND(2) = 0.
      LPF(1) = LPF(2)
      LPF(2) = 0.
   15 THETA = .17453
      CN = SIN(THETA)/RINDEX(TEMP)
      CN = ASIN(CN)
      CN = TAN(THETA)/TAN(CN)
      X = (X-XO)*CN
      YDUMY = Y - YO
C  INTERCHANGE NEXT 2 CARDS FOR Y TRAVERSE OPTION
      Y =  YDUMY
      Y = -YDUMY
C  Y=YDUMY IS THE OPTION FOR RUNS A1000 - A1491 ONLY.
C
      DO 18 I=1,16
   18 FMT(I) = F(I)
      DO 20 I=1,2
      FD(I) = FO(I)-1.
      IF(FD(I).LT.0.) FD(I) = 0.
      U(I) = 11.96*FD(I)
      FP(I) = DELTAF(I)/DELTAE(I)*ERMS(I)
      UP(I) = 11.96*FP(I)
   20 CONTINUE
   25 U1U2  =  DELTAF(1)*DELTAF(2)/DELTAE(1)/DELTAE(2)
     I *E1E2*11.96**2
      V1   = U(1)*COSINE - U(2)*SINE
      V2   = U(1)*SINE + U(2)*COSINE
      VP1 = UP(1)
      IF(PSI.NE.0.) VP1 = VP1/1.414
      V1V2 = U1U2
      TURB1 = VP1/V1
      VP2 = UP(2)
      IF(PSI.NE.0.) VP2 = VP2/1.414
      TURB2 = VP2/V1
      IF(V1.LE.0.) GO TO 40
      CMAX = C(1)
      IF(CMAX.LE..01) GO TO 40
      DELTAT = T/DIVISN
      DO 30 I=1,11
      C(I) = C(I)/CMAX
   30 TAU(I) = DELTAT*FLOAT(I-1)
      AL(1) =(C(2)-C(1))/DELTAT
      AL(2) =-0.6*AL(1)
      M = 2
      LSO = 1
      LSO = 2
      ERR = 1.E-5
      NTRIES = 150
      CALL LSO(TAU,C,M,I,AL,M,ERR,RMS,LSO,NTRIES)
      AL(1) = AL(1)*1000.
      AL(2) = AL(2)*1000.
      TE =-1./AL(1)*(1./(1.+(AL(2)/AL(1))**2))
      SCALE = V1*TE*12.
      DSCALE = SCALE/DHYD
      FREQ = AL(2)/2./PI
      GO TO 45
```

```
 40 DSCALE = BLANKS
    FMT(13) = F(18)
    FREQ = BLANK
    FMT(14) = F(17)
    RMS = BLANK
    FMT(15) = F(17)
 45 UAVG = FLOW/A/7.48/60.*144.
    RE = UAVG*DHYD/VISC(TEMP)/12.
    UD = V1/UAVG
    FF = 1.
    IF(ABS(A-AA1).LT.,001) FF=.1566/RE**.1869
    IF(ABS(A-AA2).LT.,001) FF=.2112/RE**.2110
    IF(ABS(A-AB ).LT.,001) FF=.2182/RE**.2196
    IF(ABS(A-AC ).LT.,001) FF=.2004/RE**.2142
    IF(ABS(A-AD ).LT.,001) FF=.3746/RE**.2725
    IF(ABS(A-AE ).LT.,001) FF=.3431/RE**.2678
    USTAR = SQRT(FF/8.)*UAVG
    US = V1/USTAR
    UPS1 = VP1/USTAR
    UPS2 = VP2/USTAR
    IF(V1.GT.0.) GO TO 49
    V1 = BLANK
    FMT(5) = F(17)
    UD = BLANK
    FMT(6) = F(17)
    US = BLANK
    FMT(7) = F(17)
    LPF(1) = BLANK
    FMT(12) = F(17)
 49 IF(TURB1.GT.0.) GO TO 50
    TURB1 = BLANK
    FMT(8) = F(17)
    UPS1 = BLANK
    FMT(9) = F(17)
    LPF(1) = BLANK
    FMT(12) = F(17)
 50 IF(TURB2.GT.0.) GO TO 60
    TURB2 = BLANK
    FMT(10) = F(17)
    UPS2 = BLANK
    FMT(11) = F(17)
 60 IF(Y.LE.1.E-5) Y = 0.
    WRITE(6,FMT) RUN,RE,X,Y,V1,UD,US,TURB1,UPS1,TURB2,UPS2,LPF(1),
   1 DSCALE,FREQ,RMS
100 CONTINUE
    GO TO 10
    END
```

```
      SUBROUTINE LSD(X,Y,W,N,AL,M,ERR,RMS,LSO,NTRIES)
C
C  THIS IS A LEAST SQUARE DISTANCE CURVE FITTING SUBROUTINE.
C  IT HAS BUILT IN THE SUCESSIVE TANGENT LINE SCHEME TO FIND THE
C    DISTANCE FROM A DATA POINT TO THE CURVE.
C  IT CALLS DECOMP AND SOLVE TO SOLVE THE LINEAR SIMULTANEOUS EQUATION
C    AZ=B IN M UNKNOWNS.
C  IT CALLS FUNC TO OBTAIN INFORMATION ABOUT THE FUNCTION BEING FITTED.
C     LSO OPTION ADDED BY D.S. KOKE.
C      IF LSO=1, THE LEAST SQUARES DISTANCE TECHNIQUE IS USED.
C      IF LSO=2, THE CONVENTIONAL LEAST SQUARES TECHNIQUE IS USED.
      PARAMETER ND=11
      PARAMETER NP=4
      DIMENSION X(ND),Y(ND),W(ND),AL(NP),D(NP,ND)
      DIMENSION DIS(ND),X1(ND),W2(ND),ID(3),Y1(ND),DX(ND)
      COMMON /BUL/ A(NP,NP),Z(NP),B(NP),IPS(NP)
C
C  IF IPRINT=0,  THERE IS NO PRINTED OUTPUT FROM THIS SUBROUTINE.
      IPRINT=2
      IPRINT=0
      TRMS=1.E10
      ID(1)= 6HCONVER
      ID(2)= 6HVERGED
      ID(3) = 6H
      DO 2 I=1,N
    2 DX(I)=0.
C
C   START ITERATION
      DO 100 ITER=1,NTRIES
C
      GO TO (5,35),LSO
C     LEAST SQUARES DISTANCE OPTION
C  FIND CLOSEST POINTS ON CURVE
    5 DO 30 I=1,N
      W2(I)=W(I)
C  FIND CLOSEST POINT GIVEN AN INDIVIDUAL DATA POINT
      DO 10 K=1,50
      IF(ABS(W(I)).LT.1.E-9)GO TO 20
      XT=X(I)+DX(I)
      CALL FUNC(XT,Y1,I,AL,XDER,D)
      DY=Y(I)-Y1(I)
      DXT=(-DX(I)+DY*XDER)/(1.+XDER**2)
C
C  THE NEXT 3 CARDS PREVENT OVERSHOOT BY DECREASING THE INCREMENT.
C    THIS GIVES INCREASED STABILITY AT THE EXPENCE OF INCREASED
C    CONVERGENCE TIME.
      TT=2.
      IF(ABS(DX(I)).GT.1.E-4)TT=ABS(DXT/DX(I))
      DX(I)=DX(I)+DXT/(1.+TT*.5)
      T=ABS(DY)+ABS(DX(I))
      IF(ABS(DXT).LT.ABS(1.E-4*DX(I)).OR.T.LT.1.E-8)GO TO 20
   10 CONTINUE
      PRINT 1005
 1005 FORMAT(' SHORTEST DISTANCE NOT FOUND')
      W2(I)=0.
   20 CONTINUE
C
C  CLOSEST POINT FOUND,  NOW FIND DISTANCE
      X1(I)=X(I)+DX(I)
      DIS(I)=SQRT(DX(I)**2+DY**2)
      IF(DIS(I).LT.1.E-8)DIS(I)=1.E-8
   30 CONTINUE
      GO TO 39
C
C     LEAST SQUARES OPTION
   35 DO 38 I=1,N
      W2(I) = W(I)
```

```
      XT = X(I)
      CALL FUNC(XT,YI,I,AL,XDER,D)
      DY = Y(I)-YI(I)
      XI(I) = X(I)
      DIS(I) = ABS(DY)
      IF(DIS(I).LT.1.E-8) DIS(I) = 1.E-8
   38 CONTINUE
C  COMPLETE SET OF CLOSEST POINTS AND DISTANCES FOUND
C  NOW FIND A NEW SET OF PARAMETERS
   39 DDM=0.
      WT=0.
      DO 40 I=1,N
      DDM=DDM+DIS(I)*DIS(I)*W2(I)
   40 WT=WT+W2(I)
      RMS=SQRT(DDM/WT)
      IF(IPRINT.GE.1)PRINT 1001,RMS,(AL(I),I=1,M)
 1001 FORMAT(' RMS='G15.7/' PARAMETERS='5G15.7,(12X,5G15.7))
   44 IF(ABS(TRMS-RMS).LT.ERR*RMS)GO TO 110
      TRMS=RMS
      CALL FUNC(XI,YI,N,AL,XDER,D)
      DO 45 K=1,M
      DO 45 I=1,N
   45 D(K,I)=(Y(I)-YI(I))*D(K,I)/DIS(I)
      DO 60 K=1,M
      DO 50 J=K,M
      A(K,J)=0.
      DO 47 I=1,N
   47 A(K,J)=A(K,J)+D(K,I)*D(J,I)*W2(I)
   50 A(J,K)=A(K,J)
      B(K)=0.
      DO 60 I=1,N
   60 B(K)=B(K)+D(K,I)*DIS(I)*W2(I)
C  THE NEXT 6 CARDS ARE DERIVED FROM A DAMPING TECHNIQUE THAT INCREASES
C    STABILITY AS MENTIONED IN THE DESCRIPTION.  IT WILL INCREASE
C    CONVERGENCE TIME TO SOME EXTENT.
      T=0.
      DO 65 I=1,M
   65 T=T+B(I)**2
      WW=.5*DDM/T
      DO 67 I=1,M
   67 A(I,I)=A(I,I)+.5/WW
C
C  THE FOLLOWING SUBROUTINE CALL SOLVES THE LINEAR SIMULTANEOUS
C    EQUATION GIVEN BY AZ=B WITH M UNKNOWNS.
      CALL DECOMP(M,IERROR)
      CALL SOLVE(M)
      IF(IERROR.GT.1) IPRINT = 2
      DO 70 I=1,M
      IF(ABS(Z(I)).GT..5*ABS(AL(I))) Z(I) = .5*ABS(AL(I))*ABS(Z(I))/Z(I)
   70 AL(I)=AL(I)+Z(I)
  100 CONTINUE
      IPRINT = 1
      ID(1)= 6HNOT CO
      ID(2) = 6HNVERGE
      ID(3) = 6HD
  110 CONTINUE
      IF(IPRINT.GE.1)PRINT 1004,ID,RMS,ERR,ITER
 1004 FORMAT(/' SUBROUTINE LSD    '3A6       /' RMS='E15.7/' CONVERGENCE C
     *RITERION='E15.7/' ITERATION COUNT='I3/)
      IF(IPRINT .GE.1) PRINT 1006, AL
      IF(IPRINT .GE.1) PRINT 1006, B
 1006 FORMAT (1GE10.5)
      IF(IPRINT.GE.1)PRINT 1000,(X(I),Y(I),YI(I),DIS(I),W(I),I=1,N)
 1000 FORMAT(' X,Y,YI,DIS,W='/(5G15.7))
      RETURN
      END
```

```
      SUBROUTINE DECOMP (NN,IERROR)
C  SIMULTANEOUS LINEAR EQUATION SOLVER, REF - G. FORSYTHE AND C.B. MOLER,
C  COMPUTER SOLUTION OF LINEAR ALGEBRAIC SYSTEMS, PRENTICE-HALL(1967).
      PARAMETER MG=4
      COMMON /BUL/ UL(MG,MG), X(MG), B(MG), IPS(MG)
      DIMENSION SCALES(MG)
      N = NN
C
C     INITIALIZE IPS, UL AND SCALES
      NOUT = 6
      N = N
      DO 5 I = 1,N
         IPS(I) = I
         ROWNRM = 0.0
      N = N
         DO 2 J = 1,N
            IF(ROWNRM-ABS(UL(I,J))) 1,2,2
    1       ROWNRM = ABS(UL(I,J))
    2    CONTINUE
         IF (ROWNRM) 3,4,3
    3    SCALES(I) = 1.0/ROWNRM
         GO TO 5
    4    WRITE (NOUT,111)
  111 FORMAT(54HOMATRIX WITH ZERO ROW IN DECOMPOSE.
         IERROR = 12
      GO TO 100
    5 CONTINUE
C
C     GAUSSIAN ELIMINATION WITH PARTIAL PIVOTING
      NM1 = N-1
      DO 17  K = 1,NM1
         BIG = 0.0
         DO 11 I = K,N
            IP = IPS(I)
            SIZE = ABS(UL(IP,K))*SCALES(IP)
            IF (SIZE-BIG) 11,11,10
   10          BIG = SIZE
               IDXPIV = I
   11    CONTINUE
         IF (BIG) 13,18,13
   13    IF (IDXPIV-K) 14,15,14
   14       J = IPS(K)
            IPS(K) = IPS(IDXPIV)
            IPS(IDXPIV) = J
   15    KP = IPS(K)
         PIVOT = UL(KP,K)
         KP1 = K+1
         DO 16 I = KP1,N
            IP = IPS(I)
            EM = -UL(IP,K)/PIVOT
            UL(IP,K) = -EM
            IF (EM) 20,16,20
   20          DO 21 J = KP1,N
   21             UL(IP,J) = UL(IP,J) + EM*UL(KP,J)
   16    CONTINUE
   17 CONTINUE
      KP = IPS(N)
      IF (UL(KP,N)) 19,18,19
   18 PRINT 112
  100 PRINT 113, ((UL(K,L),L=1,NN),K=1,NN)
  113 FORMAT(7E14.8)
  112 FORMAT(54HOSINGULAR MATRIX IN DECOMPOSE.  ZERO DIVIDE IN SOLVE.  )
      IERROR = 12
   19 RETURN
      END
```

```
      SUBROUTINE SOLVE(NN)
      PARAMETER MG=4
      COMMON /BUL/ UL(MG,MG), X(MG), B(MG), IPS(MG)
      N = NN
      NP1 = N+1
C
      IP = IPS(1)
      X(1) = B(IP)
      DO 2 I = 2,N
         IP = IPS(I)
         IM1 = I-1
         SUM = 0.0
         DO 1 J = 1,IM1
    1       SUM = SUM + UL(IP,J)*X(J)
    2 X(I) = B(IP) - SUM
C
      IP = IPS(N)
      X(N) = X(N)/UL(IP,N)
      DO 4 IBACK = 2,N
      I = NP1-IBACK
C        I GOES (N-1),...,1
         IP = IPS(I)
         IP1 = I+1
         SUM = 0.0
         DO 3 J = IP1,N
    3       SUM = SUM + UL(IP,J)*X(J)
    4 X(I) = (X(I)-SUM)/UL(IP,I)
      RETURN
      END
```

```
      SUBROUTINE FUNC(X,Y ,N,AL,XDER,DER)
C
      PARAMETER ND=11
      PARAMETER NP=4
      DIMENSION X(ND),Y(ND),DER(NP,ND),AL(NP)
      AL(2) = ABS(AL(2))
      IF(N.NE.1)GO TO 50
C
C  IF N=1, CALCULATE THE FUNCTION AND ITS X-DERIVATIVE AT X(I).
      X1 = X(1)
      Y(1) = EXP(AL(1)*X1)*COS(AL(2)*X1)
      XDER = AL(1)*Y(1) - AL(2)*EXP(AL(1)*X1)*SIN(AL(2)*X1)
      RETURN
C  IF N NOT = 1, CALCULATE THE FUNCTION AND DERIVATIVES WITH RESPECT
C    TO ALL PARAMETERS AT POINTS X(I),I=1,N.
   50 DO 100 I=1,N
      X1 = X(I)
      Y(I) = EXP(AL(1)*X1)*COS(AL(2)*X1)
      DER(1,I) = X1*Y(I)
      DER(2,I) = -X1*EXP(AL(1)*X1)*SIN(AL(2)*X1)
  100 CONTINUE
      RETURN
      END
```

APPENDIX B

TABULATION OF REDUCED DATA

APPENDIX B

TABULATION OF REDUCED DATA

TABLE B-1 TABULATION OF EXPERIMENTAL DATA.

CHANNEL A: WALL AND INTERIOR CHANNEL MAPS 1/4 INCH GAP SPACING.

RUN	REYNOLDS NUMBER	X IN.	Y IN.	$\bar{U}$ FT/SEC	$\bar{U}/U$	$\bar{U}/U^*$	$\sqrt{\bar{U}}$	$\sqrt{\bar{U}}/U^*$	$\sqrt{\bar{U}}/U$	V/U* CUTOFF KHZ	A/D	CURVE FIT F(HZ)	σ
A-1	99729.	.127	.745	12.2	.76	16.4	.126	2.06	-	-	4.00	.30	0.	.042
A-2	99729.	.094	.745	13.6	.84	19.7	.080	1.69	-	-	4.00	-	-	-
A-3	99729.	.101	.745	13.8	1.02	21.3	.081	1.30	-	-	4.00	.30	0.	.036
A-4	99729.	.223	.745	14.3	1.05	22.1	.052	1.15	-	-	4.00	-	-	-
A-5	99729.	.295	.745	14.4	1.05	22.1	.051	1.13	-	-	4.00	.26	0.	.045
A-6	99729.	.362	.745	15.9	1.03	21.5	.041	1.31	-	-	4.00	-	-	-
A-7	99729.	.431	.745	15.4	.99	20.7	.036	1.37	-	-	4.00	.30	0.	.024
A-8	99729.	.497	.745	14.6	.95	2020	.070	1.41	-	-	4.00	-	-	-
A-9	99729.	.564	.745	13.9	.90	18.8	.080	1.51	-	-	4.00	.26	0.	.042
A-10	99729.	.631	.745	13.1	.84	17.6	.032	1.45	-	-	4.00	-	-	-
A-11	99729.	.698	.745	12.4	.80	16.7	.086	1.44	-	-	4.00	.21	0.	.033
A-12	99729.	.765	.745	12.2	.78	16.4	.092	1.61	-	-	4.00	-	-	-
A-13	99729.	.832	.745	12.6	.83	17.3	.087	1.51	-	-	4.00	.29	0.	.036
A-14	99729.	.899	.745	13.9	.90	18.8	.091	1.72	-	-	4.00	-	-	-
A-15	99729.	.967	.745	15.0	.96	20.2	.087	1.75	-	-	4.00	.42	0.	.023
A-16	99729.	1.034	.745	15.9	1.02	21.5	.035	1.82	-	-	4.00	-	-	-
A-17	99729.	1.101	.745	16.6	1.07	22.4	.077	1.73	-	-	4.00	.39	0.	.030
A-18	99729.	1.166	.745	17.2	1.11	23.2	.070	1.61	-	-	4.00	-	-	-
A-19	99729.	1.235	.745	17.6	1.15	24.1	.060	1.46	-	-	4.00	.38	0.	.033
A-20	99729.	1.302	.745	18.4	1.18	24.8	.052	1.30	-	-	4.00	-	-	-
A-21	99729.	1.369	.745	18.6	1.20	25.1	.048	1.19	-	-	4.00	.30	0.	.023
A-22	99729.	1.436	.745	18.4	1.18	24.8	.051	1.26	-	-	4.00	-	-	-
A-23	99729.	1.503	.745	17.9	1.16	24.2	.058	1.41	-	-	4.00	.36	0.	.031
A-24	99729.	1.571	.745	17.3	1.11	23.3	.071	1.65	-	-	4.00	-	-	-
A-25	99729.	1.638	.745	16.8	1.06	22.6	.073	1.58	-	-	4.00	.42	0.	.029
A-26	99729.	1.705	.745	15.9	1.02	21.5	.085	1.82	-	-	4.00	-	-	-
A-27	99729.	1.772	.745	15.0	.97	20.3	.088	1.78	-	-	4.00	.39	0.	.033
A-28	99729.	1.839	.745	13.8	.89	18.7	.097	1.82	-	-	4.00	-	-	-
A-29	99729.	1.906	.745	12.5	.81	16.9	.088	1.49	-	-	4.00	.29	0.	.036
A-30	99729.	1.973	.745	11.1	.72	15.0	.098	1.46	-	-	4.00	-	-	-
A-31	99729.	2.040	.745	10.9	.70	14.7	.101	1.49	-	-	4.00	.25	0.	.026
A-32	99729.	2.108	.745	12.4	.80	16.7	.091	1.51	-	-	4.00	-	-	-
A-33	99729.	2.175	.745	13.8	.89	18.6	.089	1.65	-	-	4.00	.37	0.	.031
A-34	99729.	2.242	.745	14.8	.96	20.0	.090	1.80	-	-	4.00	-	-	-
A-35	99729.	2.309	.745	15.5	1.00	21.0	.083	1.74	-	-	4.00	.40	0.	.028
A-36	99729.	2.376	.745	16.2	1.04	21.8	.077	1.68	-	-	4.00	-	-	-
A-37	99729.	2.443	.745	17.0	1.09	22.9	.075	1.71	-	-	4.00	.38	0.	.036
A-38	99729.	2.510	.745	17.7	1.14	23.9	.061	1.46	-	-	4.00	-	-	-
A-39	99729.	2.577	.745	18.2	1.17	24.5	.056	1.37	-	-	4.00	.33	0.	.021
A-40	99729.	2.644	.745	18.2	1.17	24.6	.056	1.37	-	-	4.00	-	-	-
A-41	99729.	2.712	.745	17.9	1.15	24.2	.060	1.45	-	-	4.00	.36	0.	.022
A-42	99729.	2.779	.745	17.2	1.11	23.3	.071	1.64	-	-	4.00	-	-	-
A-43	99729.	2.846	.745	16.5	1.06	22.3	.081	1.80	-	-	4.00	.40	0.	.028
A-44	99729.	2.913	.745	15.8	1.02	21.3	.086	1.82	-	-	4.00	-	-	-
A-45	99729.	2.980	.745	15.0	.97	20.3	.086	1.75	-	-	4.00	.40	0.	.030
A-46	99729.	3.047	.745	14.1	.91	19.0	.095	1.80	-	-	4.00	-	-	-
A-47	99729.	3.114	.745	13.0	.83	17.5	.092	1.61	-	-	4.00	.24	0.	.029
A-48	99729.	3.181	.745	11.5	.74	15.5	.096	1.49	-	-	4.00	-	-	-
A-49	99729.	3.249	.745	9.4	.60	12.7	.155	1.97	-	-	4.00	-	-	-
A-50	99729.	3.249	.685	11.0	.71	14.9	.136	2.02	-	-	4.00	-	-	-
A-51	99729.	3.181	.685	13.9	.90	18.8	.084	1.58	-	-	4.00	-	-	-
A-52	99729.	3.114	.685	15.3	.98	20.6	.074	1.52	-	-	4.00	-	-	-
A-53	99729.	3.047	.685	15.8	1.02	21.4	.078	1.67	-	-	4.00	-	-	-
A-54	99729.	2.980	.685	16.3	1.05	22.0	.080	1.77	-	-	4.00	-	-	-
A-55	99729.	2.913	.685	16.8	1.08	22.6	.074	1.67	-	-	4.00	-	-	-
A-56	99729.	2.846	.685	17.4	1.12	23.4	.065	1.53	-	-	4.00	-	-	-
A-57	99729.	2.779	.685	17.9	1.15	24.1	.061	1.47	-	-	4.00	-	-	-
A-58	99729.	2.712	.685	18.4	1.18	24.8	.057	1.41	-	-	4.00	-	-	-
A-59	99729.	2.644	.685	18.7	1.20	25.2	.050	1.26	-	-	4.00	-	-	-
A-60	99729.	2.577	.685	18.6	1.20	25.1	.050	1.26	-	-	4.00	-	-	-
A-61	99729.	2.510	.685	18.3	1.18	24.7	.054	1.33	-	-	4.00	-	-	-
A-62	99729.	2.443	.685	17.6	1.13	23.7	.065	1.55	-	-	4.00	-	-	-
A-63	99729.	2.376	.685	17.1	1.10	23.1	.064	1.52	-	-	4.00	-	-	-
A-64	99729.	2.309	.685	16.6	1.07	22.4	.073	1.69	-	-	4.00	-	-	-
A-65	99729.	2.242	.685	16.3	1.05	22.0	.075	1.65	-	-	4.00	-	-	-
A-66	99729.	2.175	.685	16.0	1.03	21.6	.069	1.49	-	-	4.00	-	-	-
A-67	99729.	2.108	.685	15.6	1.00	21.1	.065	1.37	-	-	4.00	-	-	-
A-68	99729.	2.040	.685	15.1	.98	20.4	.067	1.37	-	-	4.00	-	-	-
A-69	99729.	1.973	.685	15.1	.97	20.3	.067	1.37	-	-	4.00	-	-	-
A-70	99729.	1.906	.685	15.3	.98	20.6	.068	1.40	-	-	4.00	-	-	-
A-71	99729.	1.839	.685	15.8	1.02	21.3	.069	1.46	-	-	4.00	-	-	-
A-72	99729.	1.772	.685	16.4	1.06	22.1	.072	1.58	-	-	4.00	-	-	-
A-73	99729.	1.705	.685	17.0	1.09	22.9	.067	1.52	-	-	4.00	-	-	-
A-74	99729.	1.638	.685	17.5	1.12	23.6	.062	1.46	-	-	4.00	-	-	-
A-75	99729.	1.571	.685	17.9	1.15	24.2	.060	1.46	-	-	4.00	-	-	-
A-76	99729.	1.503	.685	18.3	1.18	24.7	.059	1.45	-	-	4.00	-	-	-
A-77	99729.	1.436	.685	18.7	1.20	25.2	.047	1.18	-	-	4.00	-	-	-
A-78	99729.	1.369	.685	19.0	1.22	25.6	.041	1.09	-	-	4.00	-	-	-
A-79	99729.	1.302	.685	18.7	1.21	25.3	.049	1.23	-	-	4.00	-	-	-
A-80	99729.	1.235	.685	18.4	1.19	24.9	.051	1.26	-	-	4.00	-	-	-

HYDRAULIC DIAMETER= D = .611 INCHES. AVERAGE VELOCITY, U = 15.5 FT/SEC. U* = .741 FT/SEC.

* QUESTIONABLE DATA POINT. - NO DATA POINT.

TABLE B-1 (CONT.). TABULATION OF EXPERIMENTAL DATA.

CHANNEL A: BALL AND EXTENSION CHANNEL MAP: 1/4 INCH GAP SPACING.

RUN	REYNOLDS NUMBER	Z IN.	Y IN.	U FT/SEC	U/U	U/U*	V/U	U/U*	V/U	V/U*	CUTOFF KHZ	A/D	CURVE FIT (KHZ)	σ
A-81	99729.	1.101	.625	17.9	1.16	24.2	.059	1.43	-	-	4.00	-	-	-
A-82	99729.	1.101	.625	17.5	1.13	23.6	.061	1.44	-	-	4.00	-	-	-
A-83	99729.	1.034	.625	17.0	1.10	22.9	.062	1.43	-	-	4.00	-	-	-
A-84	99729.	.967	.625	16.5	1.06	22.2	.068	1.52	-	-	4.00	-	-	-
A-85	99729.	.899	.625	15.9	1.03	21.5	.000	1.46	-	-	4.00	-	-	-
A-86	99729.	.832	.625	15.2	.98	20.6	.071	1.46	-	-	4.00	-	-	-
A-87	99729.	.765	.625	14.9	.96	20.1	.066	1.36	-	-	4.00	-	-	-
A-88	99729.	.698	.625	14.8	.95	20.0	.061	1.21	-	-	4.00	-	-	-
A-89	99729.	.631	.625	14.9	.96	20.1	.060	1.20	-	-	4.00	-	-	-
A-90	99729.	.564	.625	15.2	.98	20.6	.059	1.21	-	-	4.00	-	-	-
A-91	99729.	.497	.625	15.7	1.01	21.1	.056	1.19	-	-	4.00	-	-	-
A-92	99729.	.430	.625	16.1	1.04	21.7	.053	1.15	-	-	4.00	-	-	-
A-93	99729.	.362	.625	16.4	1.06	22.1	.052	1.15	-	-	4.00	-	-	-
A-94	99729.	.295	.625	16.7	1.07	22.5	.045	1.01	-	-	4.00	-	-	-
A-95	99729.	.228	.625	16.5	1.06	22.3	.051	1.13	-	-	4.00	-	-	-
A-96	99729.	.161	.625	15.9	1.02	21.4	.061	1.31	-	-	4.00	-	-	-
A-97	99729.	.094	.625	14.6	.94	19.7	.089	1.75	-	-	4.00	-	-	-
A-98	99729.	.027	.625	12.3	.79	16.5	.117	1.99	-	-	4.00	-	-	-
A-99	99729.	.027	.625	12.1	.78	16.3	.127	2.06	-	-	4.00	-	-	-
A-100	99729.	.094	.625	14.5	.93	19.5	.086	1.66	-	-	4.00	.38	0.	.034
A-101	99729.	.161	.625	15.8	1.02	21.3	.063	1.35	-	-	4.00	-	-	-
A-102	99729.	.228	.625	16.5	1.06	22.2	.049	1.10	-	-	4.00	.30	0.	.043
A-103	99729.	.295	.625	16.5	1.06	22.3	.046	1.04	-	-	4.00	-	-	-
A-104	99729.	.362	.625	16.3	1.05	21.9	.050	1.11	-	-	4.00	.26	0.	.037
A-105	99729.	.430	.625	15.9	1.02	21.5	.060	1.29	-	-	4.00	-	-	-
A-106	99729.	.497	.625	15.7	1.01	21.2	.053	1.12	-	-	4.00	.32	0.	.027
A-107	99729.	.564	.625	15.5	1.00	20.9	.052	1.09	-	-	4.00	-	-	-
A-108	99729.	.631	.625	15.3	.98	20.6	.052	1.07	-	-	4.00	.24	0.	.030
A-109	99729.	.698	.625	15.3	.98	20.6	.048	.98	-	-	4.00	-	-	-
A-110	99729.	.765	.625	15.4	.99	20.7	.054	1.12	-	-	4.00	.30	0.	.038
A-111	99729.	.832	.625	15.8	1.02	21.4	.058	1.23	-	-	4.00	-	-	-
A-112	99729.	.899	.625	16.3	1.05	22.0	.058	1.29	-	-	4.00	.37	0.	.028
A-113	99729.	.967	.625	16.6	1.08	22.7	.058	1.32	-	-	4.00	-	-	-
A-114	99729.	1.034	.625	17.3	1.12	23.4	.055	1.28	-	-	4.00	.35	0.	.026
A-115	99729.	1.101	.625	17.7	1.14	23.9	.053	1.27	-	-	4.00	-	-	-
A-116	99729.	1.168	.625	18.2	1.17	24.5	.052	1.29	-	-	4.00	.32	0.	.018
A-117	99729.	1.235	.625	18.6	1.20	25.2	.049	1.10	-	-	4.00	-	-	-
A-118	99729.	1.302	.625	18.9	1.21	25.5	.043	1.11	-	-	4.00	.26	0.	.031
A-119	99729.	1.369	.625	18.9	1.22	25.6	.041	1.05	-	-	4.00	-	-	-
A-120	99729.	1.436	.625	18.8	1.21	25.4	.043	1.09	-	-	4.00	.25	0.	.023
A-121	99729.	1.503	.625	18.5	1.19	25.0	.047	1.18	-	-	4.00	-	-	-
A-122	99729.	1.571	.625	18.1	1.17	24.5	.052	1.27	-	-	4.00	.31	51.	.025
A-123	99729.	1.638	.625	17.8	1.14	24.0	.055	1.32	-	-	4.00	-	-	-
A-124	99729.	1.705	.625	17.4	1.12	23.4	.055	1.29	-	-	4.00	.32	0.	.015
A-125	99729.	1.772	.625	16.9	1.09	22.8	.061	1.40	-	-	4.00	-	-	-
A-126	99729.	1.839	.625	16.4	1.06	22.2	.057	1.26	-	-	4.00	.36	0.	.024
A-127	99729.	1.906	.625	16.1	1.03	21.7	.054	1.17	-	-	4.00	-	-	-
A-128	99729.	1.973	.625	15.9	1.02	21.4	.051	1.10	-	-	4.00	.25	0.	.027
A-129	99729.	2.040	.625	16.0	1.03	21.6	.052	1.11	-	-	4.00	-	-	-
A-130	99729.	2.108	.625	16.2	1.05	21.9	.054	1.22	-	-	4.00	.32	0.	.026
A-131	99729.	2.175	.625	16.7	1.07	22.5	.057	1.29	-	-	4.00	-	-	-
A-132	99729.	2.242	.625	17.1	1.10	23.0	.055	1.26	-	-	4.00	.36	36.	.018
A-133	99729.	2.309	.625	17.4	1.12	23.4	.057	1.34	-	-	4.00	-	-	-
A-134	99729.	2.376	.625	17.7	1.14	23.9	.061	1.46	-	-	4.00	.30	0.	.020
A-135	99729.	2.443	.625	18.2	1.17	24.5	.055	1.35	-	-	4.00	-	-	-
A-136	99729.	2.510	.625	18.6	1.20	25.1	.049	1.23	-	-	4.00	.32	0.	.022
A-137	99729.	2.577	.625	18.9	1.22	25.5	.042	1.07	-	-	4.00	-	-	-
A-138	99729.	2.644	.625	18.9	1.22	25.6	.042	1.09	-	-	4.00	.32	0.	.021
A-139	99729.	2.712	.625	18.7	1.20	25.2	.047	1.17	-	-	4.00	-	-	-
A-140	99729.	2.779	.625	18.3	1.18	24.7	.054	1.34	-	-	4.00	.32	0.	.019
A-141	99729.	2.846	.625	17.9	1.15	24.1	.058	1.39	-	-	4.00	-	-	-
A-142	99729.	2.913	.625	17.4	1.12	23.5	.060	1.41	-	-	4.00	.31	0.	.025
A-143	99729.	2.980	.625	17.0	1.09	22.9	.062	1.41	-	-	4.00	-	-	-
A-144	99729.	3.047	.625	16.5	1.06	22.2	.062	1.38	-	-	4.00	.33	0.	.034
A-145	99729.	3.114	.625	15.8	1.02	21.3	.061	1.30	-	-	4.00	-	-	-
A-146	99729.	3.181	.625	14.1	.91	19.1	.089	1.71	-	-	4.00	.23	0.	.035
A-147	99729.	3.249	.625	11.0	.71	14.9	.137	2.09	-	-	4.00	-	-	-
A-148	99729.	3.249	.565	11.2	.72	15.1	.126	1.91	-	-	4.00	-	-	-
A-149	99729.	3.181	.565	13.8	.89	18.6	.082	1.53	-	-	4.00	-	-	-
A-150	99729.	3.114	.565	14.9	.96	20.1	.080	1.61	-	-	4.00	.26	0.	.034
A-151	99729.	3.047	.565	15.9	1.02	21.4	.077	1.64	-	-	4.00	-	-	-
A-152	99729.	2.980	.565	16.7	1.08	22.6	.070	1.58	-	-	4.00	.34	0.	.005
A-153	99729.	2.913	.565	17.4	1.12	23.5	.064	1.51	-	-	4.00	-	-	-
A-154	99729.	2.846	.565	17.9	1.15	24.2	.059	1.44	-	-	4.00	.32	0.	.014
A-155	99729.	2.779	.565	18.3	1.18	24.7	.056	1.39	-	-	4.00	-	-	-
A-156	99729.	2.712	.565	18.7	1.21	25.3	.049	1.23	-	-	4.00	.30	0.	.023
A-157	99729.	2.644	.565	19.0	1.22	25.6	.044	1.14	-	-	4.00	-	-	-
A-158	99729.	2.577	.565	19.0	1.22	25.6	.042	1.07	-	-	4.00	.25	0.	.021
A-159	99729.	2.510	.565	18.7	1.20	25.2	.046	1.17	-	-	4.00	-	-	-
A-160	99729.	2.443	.565	18.3	1.18	24.7	.051	1.26	-	-	4.00	.29	0.	.011

HYDRAULIC DIAMETER, D = .811 INCHES. AVERAGE VELOCITY, U = 15.5 FT/SEC. U^* = .741 FT/SEC.

* QUESTIONABLE DATA POINT. - NO DATA POINT.

TABLE D-1 (CONT.). TABULATION OF EXPERIMENTAL DATA.

CHANNEL A, WALL AND INTERIOR CHANNEL MAPS, 1/4 INCH GAP SPACING.

RUN	KEYHOLDS NUMBER	Z IN.	Y IN.	$\bar{U}$ FT/SEC	$\bar{U}/U$	$\bar{U}/U^*$	$u'/\bar{U}$	u'/U^*	$v'/\bar{U}$	v'/U^*	CUTOFF KHZ	A/D	CURVE F(HZ)	FIT σ
A-161	99729.	2.376	.565	17.8	1.15	24.0	.057	1.37	-	-	4.00	-	-	-
A-162	99729.	2.309	.565	17.4	1.12	23.5	.057	1.35	-	-	4.00	.34	18.	.011
A-163	99729.	2.242	.565	16.8	1.08	22.7	.062	1.40	-	-	4.00	-	-	-
A-164	99729.	2.175	.565	16.2	1.04	21.8	.064	1.40	-	-	4.00	.43	0.	.020
A-165	99729.	2.108	.565	15.5	1.00	20.9	.067	1.40	-	-	4.00	-	-	-
A-166	99729.	2.040	.565	15.1	.97	20.4	.066	1.35	-	-	4.00	.28	0.	.023
A-167	99729.	1.973	.565	15.0	.97	20.3	.067	1.37	-	-	4.00	-	-	-
A-168	99729.	1.906	.565	15.4	.99	20.8	.066	1.37	-	-	4.00	.34	0.	.033
A-169	99729.	1.839	.565	15.9	1.03	21.5	.068	1.46	-	-	4.00	-	-	-
A-170	99729.	1.772	.565	16.6	1.07	22.5	.069	1.43	-	-	4.00	.40	0.	.025
A-171	99729.	1.705	.565	17.1	1.10	23.1	.066	1.52	-	-	4.00	-	-	-
A-172	99729.	1.638	.565	17.5	1.13	23.7	.063	1.49	-	-	4.00	.37	0.	.019
A-173	99729.	1.571	.565	17.9	1.15	24.1	.059	1.42	-	-	4.00	-	-	-
A-174	99729.	1.503	.565	18.3	1.18	24.6	.055	1.36	-	-	4.00	.27	0.	.026
A-175	99729.	1.436	.565	18.7	1.20	25.2	.048	1.21	-	-	4.00	-	-	-
A-176	99729.	1.369	.565	18.8	1.21	25.4	.044	1.11	-	-	4.00	.29	0.	.029
A-177	99729.	1.302	.565	18.7	1.21	25.3	.046	1.17	-	-	4.00	-	-	-
A-178	99729.	1.235	.565	18.4	1.19	24.8	.051	1.27	-	-	4.00	.27	0.	.025
A-179	99729.	1.168	.565	17.9	1.15	24.2	.059	1.42	-	-	4.00	-	-	-
A-180	99729.	1.101	.565	17.4	1.12	23.4	.062	1.46	-	-	4.00	.38	0.	.028
A-181	99729.	1.034	.565	16.8	1.08	22.7	.067	1.52	-	-	4.00	-	-	-
A-182	99729.	.967	.565	16.2	1.05	21.9	.071	1.55	-	-	4.00	.37	0.	.030
A-183	99729.	.899	.565	15.4	.99	20.8	.076	1.58	-	-	4.00	-	-	-
A-184	99729.	.832	.565	14.8	.95	20.0	.076	1.51	-	-	4.00	.35	0.	.035
A-185	99729.	.765	.565	14.3	.92	19.3	.075	1.45	-	-	4.00	-	-	-
A-186	99729.	.698	.565	14.2	.91	19.2	.068	1.30	-	-	4.00	.28	0.	.032
A-187	99729.	.631	.565	14.4	.93	19.4	.065	1.27	-	-	4.00	-	-	-
A-188	99729.	.564	.565	14.7	.95	19.9	.069	1.38	-	-	4.00	.33	0.	.034
A-189	99729.	.497	.565	14.9	.96	20.2	.071	1.42	-	-	4.00	-	-	-
A-190	99729.	.430	.565	15.2	.98	20.6	.072	1.48	-	-	4.00	.34	0.	.034
A-191	99729.	.362	.565	15.7	1.01	21.2	.063	1.33	-	-	4.00	-	-	-
A-192	99729.	.295	.565	16.1	1.04	21.7	.060	1.30	-	-	4.00	.25	0.	.035
A-193	99729.	.228	.565	16.2	1.04	21.9	.051	1.12	-	-	4.00	-	-	-
A-194	99729.	.161	.565	15.6	1.01	21.1	.065	1.38	-	-	4.00	.32	0.	.034
A-195	99729.	.094	.565	14.4	.93	19.4	.081	1.58	-	-	4.00	-	-	-
A-196	99729.	.027	.565	12.0	.77	16.2	.116	1.88	-	-	4.00	.25	0.	.028
A-197	99729.	.027	.505	11.8	.76	15.9	.120	1.90	-	-	4.00	-	-	-
A-198	99729.	.094	.505	14.1	.91	19.0	.091	1.73	-	-	4.00	.38	0.	.055
A-199	99729.	.161	.505	15.3	.99	20.7	.070	1.44	-	-	4.00	-	-	-
A-200	99729.	.228	.505	15.7	1.01	21.2	.062	1.31	-	-	4.00	.27	0.	.043
A-201	99729.	.295	.505	15.5	1.00	20.9	.069	1.45	-	-	4.00	-	-	-
A-202	99729.	.362	.505	14.8	.95	20.0	.081	1.61	-	-	4.00	.28	0.	.038
A-203	99729.	.430	.505	14.1	.91	19.0	.087	1.65	-	-	4.00	-	-	-
A-204	99729.	.497	.505	13.4	.86	18.1	.087	1.58	-	-	4.00	.33	0.	.046
A-205	99729.	.564	.505	12.5	.80	16.9	.094	1.58	-	-	4.00	-	-	-
A-206	99729.	.631	.505	11.0	.71	14.9	.103	1.53	-	-	4.00	.21	0.	.038
A-207	99729.	.698	.505	8.4	.54	11.3	.189	2.13	-	-	4.00	-	-	-
A-208	99729.	.765	.505	-	-	-	-	-	-	-	-	-	-	-
A-209	99729.	.832	.505	10.6	.68	14.4	.127	1.82	-	-	4.00	-	-	-
A-210	99729.	.899	.505	12.8	.83	17.3	.106	1.83	-	-	4.00	.30	0.	.039
A-211	99729.	.967	.505	14.5	.94	19.7	.066	1.68	-	-	4.00	-	-	-
A-212	99729.	1.034	.505	15.6	1.00	21.0	.086	1.80	-	-	4.00	-	-	-
A-213	99729.	1.101	.505	16.3	1.05	22.1	.081	1.80	-	-	4.00	-	-	-
A-214	99729.	1.168	.505	17.1	1.10	23.1	.068	1.58	-	-	4.00	-	-	-
A-215	99729.	1.236	.505	17.8	1.15	24.0	.061	1.47	-	-	4.00	-	-	-
A-216	99729.	1.302	.505	18.3	1.18	24.7	.051	1.26	-	-	4.00	.30	0.	.022
A-217	99729.	1.369	.505	18.4	1.19	24.9	.048	1.20	-	-	4.00	-	-	-
A-218	99729.	1.436	.505	18.2	1.17	24.6	.050	1.23	-	-	4.00	-	-	-
A-219	99729.	1.503	.505	17.6	1.14	23.8	.060	1.44	-	-	4.00	-	-	-
A-220	99729.	1.571	.505	17.1	1.10	23.1	.077	1.76	-	-	4.00	.40	0.	.040
A-221	99729.	1.638	.505	16.7	1.08	22.6	.072	1.61	-	-	4.00	-	-	-
A-222	99729.	1.705	.505	16.1	1.04	21.8	.076	1.65	-	-	4.00	-	-	-
A-223	99729.	1.772	.505	15.3	.99	20.6	.080	1.65	-	-	4.00	-	-	-
A-224	99729.	1.839	.505	14.1	.91	19.1	.083	1.58	-	-	4.00	-	-	-
A-225	99729.	1.906	.505	12.6	.82	17.3	.084	1.49	-	-	4.00	-	-	-
A-226	99729.	1.973	.505	11.8	.76	15.9	.090	1.43	-	-	4.00	-	-	-
A-227	99729.	2.040	.505	11.7	.76	15.8	.086	1.36	-	-	4.00	-	-	-
A-228	99729.	2.108	.505	12.7	.82	17.2	.088	1.51	-	-	4.00	-	-	-
A-229	99729.	2.175	.505	14.1	.91	19.1	.089	1.69	-	-	4.00	-	-	-
A-230	99729.	2.242	.505	15.4	.99	20.8	.087	1.81	-	-	4.00	-	-	-
A-231	99729.	2.309	.505	16.5	1.06	22.2	.071	1.58	-	-	4.00	-	-	-
A-232	99729.	2.376	.505	17.1	1.10	23.1	.067	1.54	-	-	4.00	-	-	-
A-233	99729.	2.443	.505	17.7	1.14	23.9	.058	1.39	-	-	4.00	-	-	-
A-234	99729.	2.510	.505	18.2	1.17	24.6	.054	1.32	-	-	4.00	-	-	-
A-235	99729.	2.577	.505	18.6	1.20	25.1	.044	1.10	-	-	4.00	-	-	-
A-236	99729.	2.644	.505	18.4	1.19	24.9	.050	1.24	-	-	4.00	-	-	-
A-237	99729.	2.712	.505	18.1	1.17	24.5	.055	1.36	-	-	4.00	-	-	-
A-238	99729.	2.777	.505	17.6	1.13	23.7	.063	1.50	-	-	4.00	-	-	-
A-239	99729.	2.846	.505	16.9	1.09	22.9	.065	1.50	-	-	4.00	-	-	-
A-240	99729.	2.913	.505	16.1	1.04	21.7	.078	1.70	-	-	4.00	-	-	-

HYDRAULIC DIAMETER, D = .811 INCHES. AVERAGE VELOCITY, U = 15.5 FT/SEC. U^* = .741 FT/SEC.

* QUESTIONABLE DATA POINT. - NO DATA POINT.

TABLE B-1 (CONT.). TABULATION OF EXPERIMENTAL DATA.

CHANNEL A, WALL AND INTERIOR CHANNEL MAP, 1/4 INCH GAP SPACING.

RUN	REYNOLDS NUMBER	Z IN.	Y IN.	$\bar{U}$ FT/SEC	$\bar{U}/U$	$\bar{U}/U^*$	$u/\bar{U}$	u/U^*	$v/\bar{U}$	v/U^*	CUTOFF KHZ	A/D	CURVE FIT F(HZ)	CURVE FIT σ
A-241	99729.	2.930	.505	15.2	.98	21.5	.097	1.99	-	-	9.00	-	-	-
A-242	99729.	3.047	.505	13.7	.88	19.5	.116	2.14	-	-	9.00	-	-	-
A-243	99729.	3.114	.505	11.9	.77	16.1	.125	1.69	-	-	9.00	-	-	-
A-244	99729.	3.181	.505	9.7	.63	13.1	.126	1.66	-	-	9.00	-	-	-
A-245	99729.	3.249	.505	-	-	-	-	-	-	-	-	-	-	-
A-246	99729.	.295	.505	15.5	1.00	21.0	.066	1.38	-	-	7.00	-	-	-
A-247	99729.	.295	.505	15.5	1.00	21.0	.062	1.30	-	-	9.00	-	-	-
A-248	99729.	.295	.505	15.5	1.00	21.0	.059	1.24	-	-	2.00	-	-	-
A-249	99729.	.295	.505	15.5	1.00	21.0	.053	1.10	-	-	1.00	-	-	-
A-250	99729.	.295	.505	15.5	1.00	21.0	.050	1.05	-	-	.50	-	-	-
A-251	99729.	.295	.565	16.1	1.04	21.8	.043	.94	-	-	.50	-	-	-
A-252	99729.	.295	.565	16.1	1.04	21.8	.044	.97	-	-	1.00	-	-	-
A-253	99729.	.295	.565	16.1	1.04	21.8	.047	1.03	-	-	2.00	-	-	-
A-254	99729.	.295	.565	16.1	1.04	21.8	.051	1.12	-	-	9.50	-	-	-
A-255	99729.	.295	.565	16.1	1.04	21.8	.053	1.16	-	-	7.00	-	-	-
A-256	99729.	.295	.565	16.1	1.04	21.8	.055	1.20	-	-	10.00	-	-	-
A-257	99729.	.295	.625	16.5	1.07	22.9	.049	1.11	-	-	10.00	-	-	-
A-258	99729.	.295	.625	16.6	1.07	22.9	.048	1.08	-	-	7.00	-	-	-
A-259	99729.	.295	.625	16.6	1.07	22.9	.047	1.05	-	-	9.00	-	-	-
A-260	99729.	.295	.625	16.6	1.07	22.9	.041	.93	-	-	2.00	-	-	-
A-261	99729.	.295	.625	16.6	1.07	22.9	.038	.85	-	-	1.00	-	-	-
A-262	99729.	.295	.625	16.6	1.07	22.9	.033	.75	-	-	.50	-	-	-
A-263	99729.	.295	.685	16.7	1.08	22.6	.032	.72	-	-	.50	-	-	-
A-264	99729.	.295	.685	16.7	1.08	22.6	.034	.78	-	-	1.00	-	-	-
A-265	99729.	.295	.685	16.7	1.08	22.6	.038	.87	-	-	2.00	-	-	-
A-266	99729.	.295	.685	16.7	1.08	22.6	.042	.95	-	-	9.00	-	-	-
A-267	99729.	.295	.685	16.7	1.08	22.6	.044	1.00	-	-	7.00	-	-	-
A-268	99729.	.295	.685	16.7	1.08	22.6	.046	1.04	-	-	10.00	-	-	-
A-269	99729.	.295	.745	16.5	1.06	22.2	.051	1.12	-	-	10.00	-	-	-
A-270	99729.	.295	.745	16.5	1.06	22.2	.049	1.10	-	-	7.00	-	-	-
A-271	99729.	.295	.745	16.5	1.06	22.2	.047	1.04	-	-	9.00	-	-	-
A-272	99729.	.295	.745	16.5	1.06	22.2	.043	.95	-	-	2.00	-	-	-
A-273	99729.	.295	.745	16.5	1.06	22.2	.038	.85	-	-	1.00	-	-	-
A-274	99729.	.295	.745	16.5	1.06	22.2	.035	.78	-	-	.50	-	-	-

CHANNEL A, CORNER AND WALL CHANNEL MAP, 1/4 INCH GAP SPACING.

RUN	REYNOLDS NUMBER	Z IN.	Y IN.	$\bar{U}$ FT/SEC	$\bar{U}/U$	$\bar{U}/U^*$	$u/\bar{U}$	u/U^*	$v/\bar{U}$	v/U^*	CUTOFF KHZ	A/D	CURVE FIT F(HZ)	CURVE FIT σ
A-275	99729.	.067	1.755	12.2	.78	16.4	.104	1.71	-	-	9.00	-	-	-
A-276	99729.	.134	1.755	14.0	.90	18.9	.079	1.40	-	-	9.00	.37	0.	.063
A-277	99729.	.201	1.755	15.0	.97	20.2	.051	1.04	-	-	9.00	-	-	-
A-278	99729.	.268	1.755	15.3	.98	20.6	.047	.96	-	-	9.00	.25	0.	.045
A-279	99729.	.336	1.755	14.9	.96	20.1	.053	1.07	-	-	9.00	-	-	-
A-280	99729.	.403	1.755	14.4	.93	19.4	.064	1.23	-	-	9.00	.29	0.	.061
A-281	99729.	.470	1.755	13.7	.88	18.5	.067	1.24	-	-	9.00	-	-	-
A-282	99729.	.537	1.755	12.8	.83	17.3	.076	1.31	-	-	9.00	.27	0.	.037
A-283	99729.	.604	1.755	11.5	.74	15.6	.081	1.26	-	-	9.00	-	-	-
A-284	99729.	.671	1.755	9.9	.64	13.4	.088	1.18	-	-	9.00	.19	0.	.044
A-285	99729.	.738	1.755	-	-	-	-	-	-	-	-	-	-	-
A-286	99729.	.805	1.755	-	-	-	-	-	-	-	-	-	-	-
A-287	99729.	.873	1.755	10.1	.65	13.6	.092	1.25	-	-	9.00	-	-	-
A-288	99729.	.940	1.755	11.8	.76	16.0	.080	1.27	-	-	9.00	.27	0.	.042
A-289	99729.	1.007	1.755	13.3	.86	18.0	.074	1.33	-	-	9.00	-	-	-
A-290	99729.	1.074	1.755	14.5	.94	19.6	.068	1.33	-	-	9.00	.37	0.	.037
A-291	99729.	1.141	1.755	15.5	1.00	20.9	.059	1.23	-	-	9.00	-	-	-
A-292	99729.	1.208	1.755	16.2	1.04	21.8	.056	1.22	-	-	9.00	.31	0.	.037
A-293	99729.	1.275	1.755	16.8	1.08	22.6	.051	1.14	-	-	9.00	-	-	-
A-294	99729.	1.342	1.755	17.1	1.10	23.1	.049	1.02	-	-	9.00	.28	0.	.035
A-295	99729.	1.409	1.755	17.4	1.12	23.5	.043	1.01	-	-	9.00	-	-	-
A-296	99729.	1.477	1.755	17.3	1.12	23.4	.043	1.01	-	-	9.00	.27	0.	.042
A-297	99729.	1.544	1.755	17.1	1.10	23.1	.046	1.07	-	-	9.00	-	-	-
A-298	99729.	1.611	1.755	16.6	1.07	22.4	.056	1.26	-	-	9.00	.33	0.	.043
A-299	99729.	1.678	1.755	16.1	1.03	21.7	.059	1.27	-	-	9.00	-	-	-
A-300	99729.	1.745	1.755	15.3	.99	20.7	.062	1.29	-	-	9.00	.30	0.	.038
A-301	99729.	1.812	1.755	14.4	.93	19.4	.072	1.39	-	-	9.00	-	-	-
A-302	99729.	1.879	1.755	13.2	.85	17.8	.087	1.55	-	-	9.00	.30	0.	.033
A-303	99729.	1.946	1.755	12.2	.78	16.4	.076	1.25	-	-	9.00	-	-	-
A-304	99729.	2.014	1.755	11.6	.75	15.6	.077	1.20	-	-	9.00	.22	0.	.030
A-305	99729.	2.081	1.755	11.0	.74	15.9	.077	1.23	-	-	9.00	-	-	-
A-306	99729.	2.081	1.815	14.4	.93	19.4	.054	1.04	-	-	9.00	.24	0.	.030
A-307	99729.	2.014	1.815	14.4	.93	19.5	.057	1.10	-	-	9.00	-	-	-
A-308	99729.	1.946	1.815	14.7	.95	19.9	.057	1.13	-	-	9.00	.28	0.	.049
A-309	99729.	1.879	1.815	15.2	.98	20.6	.054	1.11	-	-	9.00	-	-	-
A-310	99729.	1.812	1.815	15.7	1.01	21.2	.050	1.07	-	-	9.00	.32	0.	.028
A-311	99729.	1.745	1.815	16.2	1.04	21.9	.047	1.02	-	-	9.00	-	-	-
A-312	99729.	1.678	1.815	16.5	1.06	22.2	.049	1.09	-	-	9.00	.32	0.	.047
A-313	99729.	1.611	1.815	16.7	1.08	22.6	.049	1.11	-	-	9.00	-	-	-
A-314	99729.	1.544	1.815	16.9	1.09	22.7	.052	1.18	-	-	9.00	-	-	-

HYDRAULIC DIAMETER, D = .811 INCHES. AVERAGE VELOCITY, U = 15.5 FT/SEC, U^* = .741 FT/SEC.
* QUESTIONABLE DATA POINT. - NO DATA POINT.

TABLE B-1 (CONT.). TABULATION OF EXPERIMENTAL DATA.

CHANNEL A, CORNER AND WALL CHANNEL MAP, 1/4 INCH GAP SPACING.

RUN	REYNOLDS NUMBER	Z IN.	Y IN.	$\bar{U}$ FT/SEC	$\bar{U}/U$	$\bar{U}/U^*$	$v'/\bar{U}$	v'/U^*	v'/U^* CUTOFF KHZ	N/D	CURVE FIT F(NZ)	CURVE FIT σ
A-315	99729.	1.477	1.815	16.9	1.09	22.9	.051	1.17	-	-	4.00	-	-	-
A-316	99729.	1.409	1.815	16.9	1.09	22.7	.055	1.26	-	-	4.00	.34	0.	.056
A-317	99729.	1.342	1.815	16.8	1.08	22.7	.051	1.15	-	-	4.00	-	-	-
A-318	99729.	1.275	1.815	16.6	1.07	22.4	.050	1.11	-	-	4.00	.31	0.	.039
A-319	99729.	1.208	1.815	16.3	1.05	22.0	.050	1.09	-	-	4.00	-	-	-
A-320	99729.	1.141	1.815	15.6	1.02	21.3	.052	1.11	-	-	4.00	.36	0.	.037
A-321	99729.	1.074	1.815	15.3	.98	20.6	.056	1.16	-	-	4.00	-	-	-
A-322	99729.	1.007	1.815	14.6	.94	19.7	.056	1.09	-	-	4.00	.39	0.	.044
A-323	99729.	.940	1.815	13.8	.89	18.7	.059	1.10	-	-	4.00	-	-	-
A-324	99729.	.873	1.815	13.2	.85	17.8	.059	1.05	-	-	4.00	.23	0.	.043
A-325	99729.	.805	1.815	12.8	.82	17.3	.058	1.00	-	-	4.00	-	-	-
A-326	99729.	.738	1.815	12.8	.82	17.2	.063	1.09	-	-	4.00	.21	0.	.037
A-327	99729.	.671	1.815	13.1	.84	17.7	.059	1.05	-	-	4.00	-	-	-
A-328	99729.	.604	1.815	13.7	.88	18.4	.053	.97	-	-	4.00	.26	0.	.044
A-329	99729.	.537	1.815	14.2	.91	19.1	.053	1.02	-	-	4.00	-	-	-
A-330	99729.	.470	1.815	14.6	.94	19.7	.048	.95	-	-	4.00	.28	0.	.047
A-331	99729.	.403	1.815	14.9	.96	20.1	.049	.98	-	-	4.00	-	-	-
A-332	99729.	.336	1.815	15.1	.97	20.3	.049	1.01	-	-	4.00	.29	0.	.062
A-333	99729.	.268	1.815	15.2	.98	20.6	.047	.96	-	-	4.00	-	-	-
A-334	99729.	.201	1.815	15.1	.97	20.3	.048	.98	-	-	4.00	.28	0.	.031
A-335	99729.	.134	1.815	14.4	.93	19.4	.060	1.16	-	-	4.00	-	-	-
A-336	99729.	.067	1.815	12.4	.80	16.7	.104	1.73	-	-	4.00	.41	0.	.029
A-337	99729.	.067	1.875	12.5	.81	16.9	.088	1.50	-	-	4.00	-	-	-
A-338	99729.	.134	1.875	14.1	.91	19.1	.059	1.12	-	-	4.00	.27	0.	.024
A-339	99729.	.201	1.875	14.4	.93	19.5	.060	1.17	-	-	4.00	-	-	-
A-340	99729.	.268	1.875	14.3	.92	19.3	.064	1.23	-	-	4.00	.32	0.	.044
A-341	99729.	.336	1.875	14.2	.91	19.1	.065	1.25	-	-	4.00	-	-	-
A-342	99729.	.403	1.875	14.2	.91	19.1	.060	1.15	-	-	4.00	.31	0.	.044
A-343	99729.	.470	1.875	14.0	.90	19.0	.063	1.20	-	-	4.00	-	-	-
A-344	99729.	.537	1.875	13.9	.90	18.8	.055	1.04	-	-	4.00	.29	0.	.042
A-345	99729.	.604	1.875	13.7	.89	18.5	.055	1.02	-	-	4.00	-	-	-
A-346	99729.	.671	1.875	13.5	.87	18.3	.055	1.01	-	-	4.00	.22	0.	.038
A-347	99729.	.738	1.875	13.5	.87	18.2	.051	.93	-	-	4.00	-	-	-
A-348	99729.	.805	1.875	13.4	.87	18.1	.052	.94	-	-	4.00	.20	0.	.046
A-349	99729.	.873	1.875	13.6	.88	18.4	.055	1.01	-	-	4.00	-	-	-
A-350	99729.	.940	1.875	13.9	.90	18.8	.060	1.13	-	-	4.00	.33	0.	.044
A-351	99729.	1.007	1.875	14.3	.92	19.3	.062	1.19	-	-	4.00	-	-	-
A-352	99729.	1.074	1.875	14.7	.95	19.9	.066	1.30	-	-	4.00	.42	0.	.044
A-353	99729.	1.141	1.875	15.1	.97	20.4	.066	1.34	-	-	4.00	-	-	-
A-354	99729.	1.208	1.875	15.4	.99	20.7	.067	1.39	-	-	4.00	.38	0.	.043
A-355	101044.	1.275	1.875	15.6	1.01	21.1	.071	1.49	-	-	4.00	-	-	-
A-356	101044.	1.342	1.875	15.7	1.01	21.3	.070	1.49	-	-	4.00	.39	0.	.041
A-357	101044.	1.409	1.875	15.8	1.02	21.4	.071	1.52	-	-	4.00	-	-	-
A-358	101044.	1.476	1.875	15.8	1.02	21.4	.071	1.52	-	-	4.00	.39	0.	.055
A-359	101044.	1.544	1.875	15.8	1.02	21.4	.071	1.52	-	-	4.00	-	-	-
A-360	101044.	1.611	1.875	15.8	1.02	21.4	.065	1.39	-	-	4.00	-	-	-
A-361	101044.	1.678	1.875	15.8	1.02	21.3	.063	1.35	-	-	4.00	-	-	-
A-362	101044.	1.745	1.875	15.6	1.01	21.1	.065	1.37	-	-	4.00	.36	0.	.042
A-363	101044.	1.812	1.875	15.4	.99	20.8	.062	1.29	-	-	4.00	-	-	-
A-364	101044.	1.879	1.875	15.2	.98	20.5	.057	1.18	-	-	4.00	.30	0.	.041
A-365	101044.	1.946	1.875	14.9	.96	20.2	.056	1.13	-	-	4.00	-	-	-
A-366	101044.	2.013	1.875	14.8	.95	20.0	.050	1.01	-	-	4.00	.28	0.	.043
A-367	101044.	2.081	1.875	14.8	.95	19.9	.046	.92	-	-	4.00	-	-	-
A-368	101044.	2.081	1.925	13.9	.90	18.8	.058	1.09	-	-	4.00	.29	0.	.042
A-369	101044.	1.946	1.925	14.1	.91	19.1	.062	1.19	-	-	4.00	.32	0.	.058
A-370	101044.	1.812	1.925	14.5	.93	19.6	.064	1.26	-	-	4.00	.42	0.	.045
A-371	101044.	1.678	1.925	14.6	.95	20.0	.070	1.40	-	-	4.00	.41	0.	.042
A-372	101044.	1.544	1.925	14.9	.96	20.1	.070	1.40	-	-	4.00	.38	0.	.049
A-373	101044.	1.409	1.925	14.7	.95	19.9	.074	1.48	-	-	4.00	.44	0.	.036
A-374	101044.	1.275	1.925	14.6	.94	19.7	.073	1.44	-	-	4.00	.44	0.	.051
A-375	101044.	1.141	1.925	14.1	.91	19.0	.073	1.39	-	-	4.00	.43	0.	.049
A-376	101044.	1.007	1.925	13.5	.87	18.2	.067	1.22	-	-	4.00	.38	0.	.041
A-377	101044.	.872	1.925	12.9	.83	17.5	.064	1.11	-	-	4.00	.28	0.	.035
A-378	101044.	.738	1.925	12.8	.82	17.2	.062	1.07	-	-	4.00	.22	0.	.038
A-379	101044.	.604	1.925	13.0	.83	17.5	.065	1.14	-	-	4.00	.28	0.	.050
A-380	101044.	.470	1.925	13.1	.84	17.7	.071	1.26	-	-	4.00	.34	0.	.051
A-381	101044.	.336	1.925	13.1	.84	17.7	.078	1.38	-	-	4.00	.41	0.	.040
A-382	101044.	.268	1.925	13.1	.84	17.7	.076	1.35	-	-	4.00	-	-	-
A-383	101044.	.201	1.925	13.2	.85	17.8	.073	1.29	-	-	4.00	.29	0.	.037
A-384	101044.	.134	1.925	13.2	.85	17.8	.069	1.22	-	-	4.00	-	-	-
A-385	101044.	.067	1.925	12.4	.80	16.7	.074	1.24	-	-	4.00	.21	0.	.045
A-386	101044.	.067	1.965	10.3	.67	14.0	.104	1.45	-	-	4.00	-	-	-
A-387	101044.	.134	1.965	11.2	.72	15.2	.088	1.34	-	-	4.00	.22	0.	.027
A-388	101044.	.201	1.965	11.5	.74	15.6	.085	1.32	-	-	4.00	-	-	-
A-389	101044.	.268	1.965	11.5	.74	15.6	.086	1.34	-	-	4.00	.30	0.	.033
A-390	101044.	.336	1.965	11.5	.74	15.6	.086	1.35	-	-	4.00	-	-	-
A-391	101044.	.470	1.965	11.5	.74	15.6	.083	1.30	-	-	4.00	-	-	-
A-392	101044.	.604	1.965	11.4	.73	15.4	.077	1.19	-	-	4.00	.26	0.	.043
A-393	101044.	.738	1.965	11.3	.72	15.2	.072	1.10	-	-	4.00	.24	0.	.037
A-394	101044.	.872	1.965	11.4	.74	15.5	.073	1.12	-	-	4.00	.29	0.	.021

HYDRAULIC DIAMETER, D = 3.811 INCHES. AVERAGE VELOCITY, U = 15.5 FT/SEC. U^* = .740 FT/SEC.

* QUESTIONABLE DATA POINT. - NO DATA POINT.

TABLE A-1 (CONT.). TABULATION OF EXPERIMENTAL DATA.

CHANNEL A, CONVEX AND WALL CHANNEL MAP, 1/4 INCH GAP SPACING.

RUN	REYNOLDS NUMBER	Z IN.	Y IN.	$\bar{U}$ FT/SEC	$\bar{U}/U_0$	$\bar{U}/U^*$	$v'/\bar{U}$	$u'/\bar{U}$	v'/U^*	u'/U^*	CUTOFF KHZ	A/D	CURVE FIT F(HZ)	CURVE FIT σ
A-395	1013944.	1.007	1.965	11.9	.76	16.0	.080	1.28	-	-	4.00	.36	0.	.042
A-396	1013944.	1.141	1.965	12.4	.80	16.8	.084	1.41	-	-	4.00	.40	0.	.029
A-397	1013944.	1.275	1.965	12.9	.83	17.5	.082	1.44	-	-	4.00	-	-	-
A-398	1013944.	1.409	1.965	13.0	.84	17.6	.084	1.47	-	-	4.00	.36	0.	.034
A-399	1013944.	1.544	1.965	13.2	.85	17.8	.087	1.55	-	-	4.00	-	-	-
A-400	1013944.	1.678	1.965	13.1	.84	17.7	.077	1.37	-	-	4.00	.39	0.	.035
A-401	1013944.	1.812	1.965	12.8	.82	17.3	.076	1.35	-	-	4.00	-	-	-
A-402	1013944.	1.946	1.965	12.5	.81	16.9	.079	1.26	-	-	4.00	.31	0.	.028
A-403	1013944.	2.081	1.965	12.3	.79	16.6	.070	1.16	-	-	4.00	-	-	-
A-404	1013944.	1.678	1.965	13.1	.84	17.7	.080	1.41	-	-	4.00	-	-	-
A-405	1013944.	1.678	1.925	14.6	.95	20.0	.070	1.39	-	-	4.00	-	-	-
A-406	1013944.	1.678	1.875	15.9	1.02	21.5	.058	1.26	-	-	4.00	-	-	-
A-407	1013944.	1.678	1.815	16.6	1.07	22.5	.046	1.04	-	-	4.00	-	-	-
A-408	1013944.	1.678	1.755	16.2	1.04	21.9	.055	1.20	-	-	4.00	-	-	-
A-409	1013944.	1.678	1.755	16.2	1.04	21.9	.057	1.25	-	-	10.00	-	-	-
A-410	1013944.	1.678	1.755	16.2	1.04	21.9	.056	1.24	-	-	7.00	-	-	-
A-411	1013944.	1.678	1.755	16.2	1.04	21.9	.052	1.13	-	-	2.00	-	-	-
A-412	1013944.	1.678	1.755	16.2	1.04	21.9	.050	1.09	-	-	1.00	-	-	-
A-413	1013944.	1.678	1.755	16.2	1.04	21.9	.045	.99	-	-	.50	-	-	-
A-414	1013944.	1.678	1.755	16.2	1.04	21.9	.040	.88	-	-	.20	-	-	-

CHANNEL A, WALL AND INTERIOR CHANNEL MAP (CHECK RUN), 1/4 INCH GAP SPACING.

RUN	REYNOLDS NUMBER	Z IN.	Y IN.	$\bar{U}$ FT/SEC	$\bar{U}/U_0$	$\bar{U}/U^*$	$u'/\bar{U}$	u'/U^*	$v'/\bar{U}$	v'/U^*	CUTOFF KHZ	A/D	CURVE FIT F(HZ)	CURVE FIT σ
A-415	1013944.	.067	.505	13.9	.90	18.8	.091	1.70	-	-	4.00	-	-	-
A-416	1013944.	.201	.505	16.3	1.05	22.1	.064	1.20	-	-	4.00	-	-	-
A-417	1013944.	.336	.505	15.9	1.02	21.5	.061	1.31	-	-	4.00	-	-	-
A-418	1013944.	.470	.505	14.4	.92	19.4	.082	1.59	-	-	4.00	-	-	-
A-419	1013944.	.604	.505	12.3	.79	16.6	.089	1.48	-	-	4.00	-	-	-
A-420	1013944.	.738	.565	14.6	.94	19.7	.066	1.31	-	-	4.00	-	-	-
A-421	1013944.	.604	.565	14.9	.96	20.2	.068	1.37	-	-	4.00	-	-	-
A-422	1013944.	.470	.565	15.6	1.01	21.1	.068	1.43	-	-	4.00	-	-	-
A-423	1013944.	.336	.565	16.6	1.07	22.4	.055	1.24	-	-	4.00	-	-	-
A-424	1013944.	.201	.565	16.6	1.07	22.5	.052	1.17	-	-	4.00	-	-	-
A-425	1013944.	.067	.565	14.0	.90	18.9	.088	1.67	-	-	4.00	-	-	-
A-426	1013944.	.067	.625	14.1	.91	19.1	.087	1.67	-	-	4.00	-	-	-
A-427	1013944.	.201	.625	16.8	1.08	22.6	.052	1.19	-	-	4.00	-	-	-
A-428	1013944.	.336	.625	17.2	1.10	23.2	.049	1.03	-	-	4.00	-	-	-
A-429	1013944.	.470	.625	16.4	1.06	22.2	.053	1.18	-	-	4.00	-	-	-
A-430	1013944.	.604	.625	15.8	1.02	21.4	.052	1.12	-	-	4.00	-	-	-
A-431	1013944.	.736	.625	15.7	1.01	21.2	.050	1.06	-	-	4.00	-	-	-
A-432	1013944.	.738	.685	15.1	.97	20.4	.062	1.27	-	-	4.00	-	-	-
A-433	1013944.	.604	.685	15.5	1.00	21.0	.057	1.20	-	-	4.00	-	-	-
A-434	1013944.	.470	.685	16.3	1.05	22.1	.054	1.19	-	-	4.00	-	-	-
A-435	1013944.	.336	.685	17.1	1.10	23.1	.048	1.10	-	-	4.00	-	-	-
A-436	1013944.	.201	.685	16.7	1.08	22.6	.054	1.22	-	-	4.00	-	-	-
A-437	1013944.	.067	.685	14.1	.91	19.0	.096	1.83	-	-	4.00	-	-	-
A-438	1013944.	.067	.745	14.2	.91	19.2	.084	1.62	-	-	4.00	-	-	-
A-439	1013944.	.201	.745	16.8	1.08	22.6	.058	1.13	-	-	4.00	-	-	-
A-440	1013944.	.336	.745	16.8	1.08	22.6	.052	1.17	-	-	4.00	-	-	-
A-441	1013944.	.470	.745	15.6	1.00	21.0	.066	1.40	-	-	4.00	-	-	-
A-442	1013944.	.604	.745	14.0	.90	18.9	.082	1.54	-	-	4.00	-	-	-
A-443	1013944.	.738	.745	12.6	.81	17.0	.076	1.30	-	-	4.00	-	-	-
A-444	1013944.	.067	.745	13.9	.90	18.8	.093	1.75	-	-	10.00	-	-	-
A-445	1013944.	.134	.745	15.9	1.02	21.5	.069	1.37	-	-	10.00	-	-	-
A-446	1013944.	.201	.745	17.0	1.09	23.0	.045	1.04	-	-	10.00	-	-	-
A-447	1013944.	.201	.745	17.0	1.09	23.0	.045	1.04	-	-	4.00	-	-	-
A-448	1013944.	.268	.745	17.3	1.11	23.4	.036	.84	-	-	4.00	-	-	-
A-449	1013944.	.403	.745	16.4	1.06	22.2	.052	1.15	-	-	4.00	-	-	-
A-450	1013944.	.537	.745	15.2	.98	20.5	.060	1.24	-	-	4.00	-	-	-
A-451	1013944.	.671	.745	13.1	.84	17.7	.068	1.21	-	-	4.00	-	-	-
A-452	1013944.	.805	.745	12.4	.80	16.8	.071	1.20	-	-	4.00	-	-	-
A-453	1013944.	.940	.745	14.7	.95	19.9	.074	1.48	-	-	4.00	-	-	-
A-454	1013944.	.940	.685	15.6	1.07	22.4	.057	1.29	-	-	4.00	-	-	-
A-455	1013944.	.805	.685	15.4	.99	20.8	.056	1.16	-	-	4.00	-	-	-
A-456	1013944.	.671	.685	15.3	.99	20.7	.051	1.06	-	-	4.00	-	-	-
A-457	1013944.	.537	.685	16.1	1.04	21.8	.048	1.05	-	-	4.00	-	-	-
A-458	1013944.	.403	.685	17.0	1.09	22.9	.042	.97	-	-	4.00	-	-	-
A-459	1013944.	.268	.685	17.6	1.13	23.6	.033	.78	-	-	4.00	-	-	-
A-460	1013944.	.201	.685	17.1	1.10	23.1	.044	1.01	-	-	4.00	-	-	-
A-461	1013944.	.134	.685	15.9	1.03	21.5	.065	1.40	-	-	4.00	-	-	-
A-462	1013944.	.067	.685	14.1	.91	19.0	.090	1.71	-	-	4.00	-	-	-
A-463	1013944.	.067	.625	14.0	.90	18.9	.087	1.65	-	-	4.00	-	-	-
A-464	1013944.	.134	.625	15.9	1.03	21.5	.062	1.34	-	-	4.00	.42	0.	.043
A-465	1013944.	.201	.625	17.0	1.09	22.9	.046	1.06	-	-	4.00	-	-	-
A-466	1013944.	.268	.625	17.4	1.12	23.5	.036	.84	-	-	4.00	-	-	-
A-467	1013944.	.403	.625	16.6	1.08	22.7	.048	1.10	-	-	4.00	.35	24.	.039
A-468	1013944.	.537	.625	16.2	1.04	21.8	.052	1.13	-	-	4.00	.35	38.	.037
A-469	1013944.	.671	.625	15.8	1.02	21.3	.042	.89	-	-	4.00	.36	0.	.023

HYDRAULIC DIAMETER, D = .811 INCHES. AVERAGE VELOCITY, U = 15.5 FT/SEC. U^* = .740 FT/SEC.
? QUESTIONABLE DATA POINT. - NO DATA POINT.

TABLE B-1 (CONT.). TABULATION OF EXPERIMENTAL DATA.

CHANNEL A, WALL AND INTERIOR CHANNEL MAP (CHECK RUN), 1/4 INCH GAP SPACING.

RUN	REYNOLDS NUMBER	Z IN.	Y IN.	$\bar{U}$ FT/SEC	$\bar{U}/U$	$\bar{U}/U^*$	$u'/\bar{U}$	u'/U^*	$v'/\bar{U}$	v'/U^*	CUTOFF KHZ	Λ/D	CURVE F(HZ)	FIT σ
A-470	101044.	.805	.625	10.3	1.33	21.6	.047	1.02	-	-	9.00	-	-	-
A-471	101044.	.805	.565	13.3	.97	20.3	.061	1.25	-	-	9.00	-	-	-
A-472	101044.	.671	.565	14.9	.96	20.1	.058	1.16	-	-	9.00	-	-	-
A-473	101044.	.537	.565	15.4	.99	20.8	.067	1.39	-	-	9.00	-	-	-
A-474	101044.	.403	.565	16.2	1.04	21.9	.059	1.28	-	-	9.00	-	-	-
A-475	101044.	.268	.565	17.1	1.10	23.1	.042	.96	-	-	9.00	-	-	-
A-476	101044.	.201	.565	16.6	1.08	22.7	.046	1.03	-	-	9.00	-	-	-
A-477	101044.	.134	.565	15.9	1.02	21.5	.060	1.30	-	-	9.00	-	-	-
A-478	101044.	.134	.505	15.7	1.01	21.2	.063	1.34	-	-	9.00	-	-	-
A-479	101044.	.201	.505	16.5	1.07	22.4	.047	1.05	-	-	9.00	-	-	-
A-480	101044.	.268	.505	16.6	1.07	22.4	.050	1.11	-	-	9.00	-	-	-
A-481	101044.	.403	.505	15.2	.98	20.6	.072	1.48	-	-	9.00	-	-	-
A-482	101044.	.537	.505	13.7	.88	18.5	.083	1.54	-	-	9.00	-	-	-
A-483	101044.	.671	.505	11.2	.72	15.1	.079	1.20	-	-	9.00	-	-	-
A-484	101044.	.805	.505	10.1	.65	13.6	.097	1.33	-	-	9.00	-	-	-
A-485	101044.	.671	.625	15.8	1.02	21.3	.043	.92	-	-	10.00	-	-	-
A-486	101044.	.671	.625	15.8	1.02	21.3	.043	.91	-	-	7.00	-	-	-
A-487	101044.	.671	.625	15.8	1.02	21.3	.042	.89	-	-	4.00	-	-	-
A-488	101044.	.671	.625	15.8	1.02	21.3	.040	.86	-	-	2.00	-	-	-
A-490	101044.	.671	.625	15.8	1.02	21.3	.038	.82	-	-	1.00	-	-	-
A-491	101044.	.671	.625	15.8	1.02	21.3	.037	.78	-	-	.50	-	-	-
A-492	101044.	.671	.625	15.8	1.02	21.3	.034	.72	-	-	.30	-	-	-
A-493	101044.	.671	.625	15.8	1.02	21.3	.031	.66	-	-	.20	-	-	-
A-494	101044.	.671	.625	15.8	1.02	21.3	.026	.56	-	-	.10	-	-	-
A-495	101044.	.671	.625	15.8	1.02	21.3	.020	.43	-	-	.05	-	-	-
A-496	101044.	.671	.625	15.8	1.02	21.3	.015	.32	-	-	.03	-	-	-
A-497	101044.	.671	.625	15.8	1.02	21.3	.009	.20	-	-	.01	-	-	-

CHANNEL A, CENTER WALL GAP TRAVERSE, 1/4 INCH GAP SPACING.

RUN	REYNOLDS NUMBER	Z IN.	Y IN.	$\bar{U}$ FT/SEC	$\bar{U}/U$	$\bar{U}/U^*$	$u'/\bar{U}$	u'/U^*	$v'/\bar{U}$	v'/U^*	CUTOFF KHZ	Λ/D	CURVE F(HZ)	FIT σ
A-498	101044.	.005	.000	10.3	.66	13.9	.097	1.35	-	-	9.00	-	-	-
A-499	101044.	.032	.000	11.3	.73	15.2	.081	1.24	-	-	9.00	-	-	-
A-500	101044.	.059	.000	12.2	.79	16.5	.065	1.08	-	-	9.00	-	-	-
A-501	101044.	.086	.000	12.9	.83	17.5	.053	.92	-	-	9.00	-	-	-
A-502	101044.	.113	.000	13.3	.86	18.0	.047	.84	-	-	9.00	-	-	-
A-503	101044.	.140	.000	13.3	.86	18.0	.046	.82	-	-	9.00	-	-	-
A-504	101044.	.166	.000	13.0	.84	17.5	.052	.92	-	-	9.00	-	-	-
A-505	101044.	.193	.000	12.3	.79	16.6	.065	1.08	-	-	9.00	-	-	-
A-506	101044.	.220	.000	11.3	.73	15.3	.082	1.26	-	-	9.00	-	-	-
A-507	101044.	.247	.000	10.2	.66	13.8	.102	1.40	-	-	9.00	-	-	-

CHANNEL A, WALL AND INTERIOR CHANNEL CENTERLINE TRAVERSE, 1/4 INCH GAP SPACING.

RUN	REYNOLDS NUMBER	Z IN.	Y IN.	$\bar{U}$ FT/SEC	$\bar{U}/U$	$\bar{U}/U^*$	$u'/\bar{U}$	u'/U^*	$v'/\bar{U}$	v'/U^*	CUTOFF KHZ	Λ/D	CURVE F(HZ)	FIT σ
A-526	99729.	.067	.625	13.7	.68	18.5	.086	1.59	-	-	3.00	-	-	-
A-527	99729.	.134	.625	15.7	1.01	21.2	.060	1.26	-	-	3.00	.96	0.	.030
A-528	99729.	.201	.625	16.8	1.08	22.6	.045	1.01	-	-	3.00	-	-	-
A-529	99729.	.268	.625	17.2	1.11	23.2	.036	.83	-	-	3.00	-	-	-
A-530	99729.	.336	.625	17.2	1.11	23.2	.037	.85	-	-	3.00	.33	0.	.025
A-531	99729.	.403	.625	16.8	1.08	22.6	.047	1.06	-	-	3.00	-	-	-
A-532	99729.	.470	.625	16.4	1.06	22.1	.049	1.08	-	-	3.00	-	-	-
A-533	99729.	.537	.625	16.2	1.04	21.8	.046	1.01	-	-	3.00	.36	0.	.013
A-534	99729.	.604	.625	15.8	1.02	21.3	.047	1.00	-	-	3.00	-	-	-
A-535	99729.	.671	.625	15.6	1.01	21.1	.044	.94	-	-	3.00	-	-	-
A-536	99729.	.738	.625	15.6	1.01	21.1	.042	.88	-	-	3.00	.36	0.	.016
A-537	99729.	.805	.625	15.6	1.02	21.4	.047	1.00	-	-	3.00	-	-	-
A-538	99729.	.873	.625	16.3	1.05	22.0	.051	1.11	-	-	3.00	-	-	-
A-539	99729.	.940	.625	16.8	1.08	22.7	.051	1.16	-	-	3.00	.47	30.	.015
A-540	99729.	1.007	.625	17.4	1.12	23.5	.049	1.14	-	-	3.00	-	-	-
A-541	99729.	1.074	.625	17.9	1.15	24.1	.047	1.14	-	-	3.00	-	-	-
A-542	99729.	1.141	.625	18.3	1.18	24.7	.047	1.16	-	-	3.00	.36	0.	.012
A-543	99729.	1.208	.625	18.7	1.21	25.3	.043	1.08	-	-	3.00	-	-	-
A-544	99729.	1.275	.625	19.1	1.23	25.8	.039	1.01	-	-	3.00	-	-	-
A-545	99729.	1.342	.625	19.4	1.25	26.2	.035	.91	-	-	3.00	.34	0.	.031
A-546	99729.	1.409	.625	19.5	1.26	26.3	.033	.86	-	-	3.00	-	-	-
A-547	99729.	1.477	.625	19.3	1.25	26.1	.035	.92	-	-	3.00	-	-	-
A-548	99729.	1.544	.625	19.0	1.22	25.6	.044	1.12	-	-	3.00	.36	0.	.016
A-549	99729.	1.611	.625	18.6	1.20	25.1	.045	1.14	-	-	3.00	-	-	-
A-550	99729.	1.678	.625	18.2	1.17	24.5	.048	1.19	-	-	3.00	-	-	-
A-560	99729.	1.745	.625	17.7	1.14	23.9	.051	1.23	-	-	3.00	.38	43.	.015
A-561	99729.	1.812	.625	17.2	1.11	23.3	.052	1.21	-	-	3.00	-	-	-
A-562	99729.	1.879	.625	16.7	1.08	22.6	.051	1.16	-	-	3.00	-	-	-
A-563	99729.	1.946	.625	16.3	1.05	22.0	.047	1.04	-	-	3.00	.33	0.	.013
A-564	99729.	2.014	.625	16.0	1.03	21.6	.044	.95	-	-	3.00	-	-	-
A-565	99729.	2.081	.625	16.1	1.04	21.8	.045	.97	-	-	3.00	-	-	-

HYDRAULIC DIAMETER, D = .811 INCHES. AVERAGE VELOCITY, U = 15.5 FT/SEC, U^* = .741 FT/SEC.
* QUESTIONABLE DATA POINT. - NO DATA POINT.

TABLE B-1 (CONT.). TABULATION OF EXPERIMENTAL DATA.

CHANNEL A, CORNER AND WALL CHANNEL TRAVERSE, 1/4 INCH GAP SPACING.

RUN	REYNOLDS NUMBER	Z IN.	Y IN.	$\bar{U}$ FT/SEC	$\bar{U}/U$	$\bar{U}/U^*$	$u'/\bar{U}$	u'/U^*	$v'/\bar{U}$	v'/U^*	CUTOFF KHZ	Δ/D	CURVE FIT F(HZ)	σ
A-566	101044.	2.013	1.820	14.2	.92	19.2	.051	.97	-	-	3.00	-	-	-
A-567	101044.	1.879	1.820	13.1	.97	20.4	.049	1.00	-	-	3.00	-	-	-
A-568	101044.	1.745	1.820	16.2	1.04	21.9	.042	.92	-	-	3.00	-	-	-
A-569	101044.	1.611	1.820	16.0	1.08	22.7	.042	.95	-	-	3.00	-	-	-
A-570	101044.	1.476	1.820	17.3	1.10	23.0	.044	1.01	-	-	3.00	-	-	-
A-571	101044.	1.342	1.820	16.8	1.08	22.7	.043	.97	-	-	3.00	-	-	-
A-572	101044.	1.208	1.820	16.2	1.04	21.9	.041	.89	-	-	3.00	-	-	-
A-573	101044.	1.074	1.820	14.9	.96	20.2	.051	1.03	-	-	3.00	-	-	-
A-574	101044.	.940	1.820	13.5	.87	18.2	.052	.95	-	-	3.00	-	-	-
A-575	101044.	.805	1.820	12.6	.81	17.1	.054	.93	-	-	3.00	-	-	-
A-576	101044.	.671	1.820	13.3	.86	17.9	.053	.96	-	-	3.00	-	-	-
A-577	101044.	.537	1.820	14.4	.93	19.5	.044	.87	-	-	3.00	-	-	-
A-578	101044.	.403	1.820	15.3	.98	20.6	.037	.77	-	-	3.00	-	-	-
A-579	101044.	.268	1.820	15.6	1.00	21.1	.036	.76	-	-	3.00	-	-	-
A-580	101044.	.134	1.820	14.3	.92	19.3	.058	1.13	-	-	3.00	-	-	-
A-581	50522.	.134	1.820	7.0	.90	17.7	.062	1.09	-	-	2.00	-	-	-
A-582	50522.	.268	1.820	7.7	.99	19.5	.038	.75	-	-	2.00	-	-	-
A-583	50522.	.403	1.820	7.5	.97	19.1	.040	.76	-	-	2.00	.25	0.	.038
A-584	50522.	.537	1.820	7.1	.92	18.0	.046	.82	-	-	2.00	-	-	-
A-585	50522.	.671	1.820	6.5	.84	16.4	.053	.88	-	-	2.00	-	-	-
A-586	50522.	.805	1.820	6.2	.79	15.6	.055	.85	-	-	2.00	.19	0.	.046
A-587	50522.	.940	1.820	6.6	.86	16.8	.055	.93	-	-	2.00	-	-	-
A-588	50522.	1.074	1.820	7.4	.96	18.8	.049	.92	-	-	2.00	.36	8.	.042
A-589	50522.	1.208	1.820	8.1	1.04	20.4	.045	.92	-	-	2.00	-	-	-
A-590	50522.	1.342	1.820	8.4	1.08	21.3	.043	.92	-	-	2.00	.27	0.	.039
A-591	50522.	1.476	1.820	8.5	1.09	21.5	.044	.95	-	-	2.00	-	-	-
A-592	50522.	1.611	1.820	8.4	1.08	21.2	.042	.90	-	-	2.00	.34	0.	.032
A-593	50522.	1.745	1.820	8.0	1.04	20.4	.043	.88	-	-	2.00	-	-	-
A-594	50522.	1.879	1.820	7.4	.96	18.8	.052	.97	-	-	2.00	.29	0.	.032
A-595	50522.	2.013	1.820	6.9	.89	17.6	.055	.96	-	-	2.00	-	-	-
A-596	50522.	2.148	1.820	6.9	.89	17.6	.050	.88	-	-	2.00	.23	0.	.037

CHANNEL A, WALL AND INTERIOR CHANNEL CENTERLINE TRAVERSE, 1/4 INCH GAP SPACING.

RUN	REYNOLDS NUMBER	Z IN.	Y IN.	$\bar{U}$ FT/SEC	$\bar{U}/U$	$\bar{U}/U^*$	$u'/\bar{U}$	u'/U^*	$v'/\bar{U}$	v'/U^*	CUTOFF KHZ	Δ/D	CURVE FIT F(HZ)	σ
A-597	50522.	2.148	.625	8.2	1.06	20.8	.050	1.04	-	-	2.00	.34	8.	.011
A-598	50522.	2.013	.625	8.0	1.02	20.1	.046	.92	-	-	2.00	-	-	-
A-599	50522.	1.879	.625	8.3	1.07	21.0	.054	1.14	-	-	2.00	.32	26.	.047
A-600	50522.	1.745	.625	8.9	1.14	22.4	.053	1.18	-	-	2.00	-	-	-
A-601	50522.	1.611	.625	9.4	1.20	23.7	.049	1.16	-	-	2.00	.37	30.	.020
A-602	50522.	1.476	.625	9.8	1.26	24.7	.040	1.00	-	-	2.00	-	-	-
A-603	50522.	1.342	.625	9.8	1.27	24.9	.035	.86	-	-	2.00	.36	0.	.027
A-604	50522.	1.208	.625	9.5	1.22	24.0	.046	1.10	-	-	2.00	-	-	-
A-605	50522.	1.074	.625	9.0	1.16	22.8	.050	1.15	-	-	2.00	.40	2.	.027
A-606	50522.	.940	.625	8.4	1.09	21.4	.053	1.13	-	-	2.00	-	-	-
A-607	50522.	.805	.625	7.9	1.02	20.0	.045	.91	-	-	2.00	.33	0.	.026
A-608	50522.	.671	.625	7.7	1.00	19.6	.043	.85	-	-	2.00	-	-	-
A-609	50522.	.537	.625	8.0	1.03	20.2	.050	1.02	-	-	2.00	.33	23.	.041
A-610	50522.	.403	.625	8.4	1.08	21.2	.049	.99	-	-	2.00	-	-	-
A-611	50522.	.268	.625	8.6	1.11	21.9	.033	.73	-	-	2.00	.40	0.	.029
A-612	50522.	.134	.625	7.9	1.02	20.1	.058	1.17	-	-	2.00	-	-	-
A-613	203451.	.134	.625	15.4	.99	22.2	.059	1.31	-	-	3.00	-	-	-
A-614	203451.	.267	.625	16.8	1.08	24.2	.039	.82	-	-	3.00	.28	0.	.029
A-615	203451.	.401	.625	16.4	1.06	23.7	.046	1.09	-	-	3.00	-	-	-
A-616	203451.	.534	.625	15.8	1.02	22.7	.051	1.15	-	-	3.00	.37	37.	.018
A-617	203451.	.668	.625	15.5	1.00	22.3	.041	.92	-	-	3.00	-	-	-
A-618	203451.	.801	.625	15.5	1.00	22.3	.043	.97	-	-	3.00	.30	0.	.027
A-619	203451.	.935	.625	16.3	1.05	23.5	.049	1.15	-	-	3.00	-	-	-
A-620	203451.	1.069	.625	17.2	1.11	24.8	.046	1.15	-	-	3.00	.40	5.	.016
A-621	203451.	1.202	.625	18.0	1.16	26.0	.042	1.10	-	-	3.00	-	-	-
A-622	203451.	1.336	.625	18.6	1.20	26.9	.033	.88	-	-	3.00	.30	0.	.029
A-623	203451.	1.469	.625	18.5	1.19	26.7	.037	.99	-	-	3.00	-	-	-
A-624	203451.	1.603	.625	17.8	1.15	25.7	.047	1.22	-	-	3.00	.35	55.	.012
A-625	203451.	1.736	.625	17.0	1.10	24.5	.051	1.24	-	-	3.00	-	-	-
A-626	203451.	1.870	.625	16.1	1.04	23.3	.049	1.15	-	-	3.00	-	-	-
A-627	203451.	2.003	.625	15.7	1.01	22.7	.045	1.03	-	-	3.00	.31	0.	.036
A-628	203451.	2.137	.625	16.3	1.05	23.5	.050	1.18	-	-	3.00	-	-	-

HYDRAULIC DIAMETER, D = .611 INCHES. AVERAGE VELOCITY, U = 15.5 FT/SEC, U^* = .693 FT/SEC.
* QUESTIONABLE DATA POINT. - NO DATA POINT.

TABLE F-1 (CONT.). TABULATION OF EXPERIMENTAL DATA.

CHANNEL A, CORNER AND WALL CHANNEL TRAVERSE, 1/4 INCH GAP SPACING.

RUN	REYNOLDS NUMBER	Z IN.	Y IN.	$\bar{U}$ FT/SEC	$\bar{U}/U^*$	$\bar{U}/U^*$	$u'/\bar{U}$	u'/U^*	$v'/\bar{U}$	v'/U^*	CUTOFF KHZ	Δ/D	CURVE FIT F(HZ)	σ
A-629	203451.	2.137	1.422	14.2	.92	20.5	.046	.94	-	-	3.00	.33	0.	.037
A-630	203451.	2.033	1.822	14.3	.92	20.7	.050	1.04	-	-	3.00	-	-	-
A-631	203451.	1.837	1.422	13.0	.84	21.6	.051	1.10	-	-	3.00	.34	0.	.030
A-632	203451.	1.736	1.422	13.9	1.02	23.0	.042	.97	-	-	3.00	-	-	-
A-633	203451.	1.603	1.822	13.4	1.06	23.7	.040	.94	-	-	3.00	.35	0.	.030
A-634	203451.	1.469	1.822	13.5	1.06	23.8	.042	1.00	-	-	3.00	-	-	-
A-635	203451.	1.336	1.822	13.2	1.05	23.4	.041	.96	-	-	3.00	.39	0.	.036
A-636	203451.	1.202	1.822	13.6	1.01	22.5	.041	.93	-	-	3.00	-	-	-
A-637	203451.	1.069	1.822	14.5	.93	20.9	.050	1.05	-	-	3.00	.41	12.	.030
A-638	203451.	.935	1.822	13.2	.85	19.1	.052	1.00	-	-	3.00	-	-	-
A-639	203451.	.801	1.822	12.6	.81	18.1	.051	.93	-	-	3.00	.31	0.	.025
A-640	203451.	.668	1.822	13.2	.85	19.0	.051	.96	-	-	3.00	-	-	-
A-641	203451.	.534	1.822	14.1	.91	20.4	.046	.93	-	-	3.00	.36	0.	.042
A-642	203451.	.401	1.822	14.9	.96	21.5	.037	.80	-	-	3.00	-	-	-
A-643	203451.	.267	1.822	15.2	.98	22.0	.035	.76	-	-	3.00	.30	0.	.052
A-644	203451.	.134	1.822	13.9	.90	20.1	.059	1.18	-	-	3.00	-	-	-
A-645	203451.	.935	1.822	13.3	.85	19.1	.054	1.03	-	-	10.00	-	-	-
A-646	203451.	.935	1.822	13.3	.85	19.1	.054	1.03	-	-	6.00	-	-	-
A-647	203451.	.935	1.822	13.3	.85	19.1	.052	1.00	-	-	4.00	-	-	-
A-648	203451.	.935	1.822	13.3	.85	19.1	.052	1.00	-	-	3.00	-	-	-
A-649	203451.	.935	1.822	13.3	.85	19.1	.051	.98	-	-	2.00	-	-	-
A-650	203451.	.935	1.822	13.3	.85	19.1	.049	.93	-	-	1.00	-	-	-
A-651	203451.	.935	1.822	13.3	.85	19.1	.047	.90	-	-	.50	-	-	-

CHANNEL A, CENTER WALL GAP TRAVERSE, 1/4 INCH GAP SPACING.

RUN	REYNOLDS NUMBER	Z IN.	Y IN.	$\bar{U}$ FT/SEC	$\bar{U}/U^*$	$\bar{U}/U^*$	$u'/\bar{U}$	u'/U^*	$v'/\bar{U}$	v'/U^*	CUTOFF KHZ	Δ/D	CURVE FIT F(HZ)	σ
A-652	101044.	.015	.000	10.6	.68	14.3	.090	1.29	-	-	3.00	-	-	-
A-653	101044.	.015	.000	10.6	.68	14.3	.099	1.41	-	-	10.00	-	-	-
A-654	101044.	.015	.000	10.6	.68	14.3	.096	1.37	-	-	7.00	-	-	-
A-655	101044.	.015	.000	10.6	.68	14.3	.093	1.33	-	-	5.00	-	-	-
A-656	101044.	.015	.000	10.6	.68	14.3	.089	1.27	-	-	2.00	-	-	-
A-657	101044.	.015	.000	10.6	.68	14.3	.083	1.19	-	-	1.00	-	-	-
A-658	101044.	.042	.000	11.7	.76	15.9	.071	1.12	-	-	1.00	-	-	-
A-659	101044.	.042	.000	11.7	.76	15.9	.078	1.23	-	-	3.00	-	-	-
A-660	101044.	.068	.000	12.6	.81	17.1	.056	.96	-	-	3.00	.31	0.	.031
A-661	101044.	.068	.000	12.6	.81	17.1	.055	.93	-	-	1.00	-	-	-
A-662	101044.	.095	.000	13.1	.85	17.7	.047	.84	-	-	1.00	-	-	-
A-663	101044.	.095	.000	13.1	.85	17.7	.049	.87	-	-	2.00	-	-	-
A-664	101044.	.095	.000	13.1	.85	17.7	.050	.89	-	-	3.00	-	-	-
A-665	101044.	.095	.000	13.1	.85	17.7	.051	.90	-	-	5.00	-	-	-
A-666	101044.	.095	.000	13.1	.85	17.7	.052	.92	-	-	7.00	-	-	-
A-667	101044.	.095	.000	13.1	.85	17.7	.053	.93	-	-	10.00	-	-	-
A-668	101044.	.122	.000	13.3	.86	17.9	.050	.91	-	-	3.00	.34	0.	.035
A-669	101044.	.122	.000	13.3	.86	17.9	.046	.82	-	-	1.00	-	-	-
A-670	101044.	.149	.000	13.2	.85	17.8	.044	.78	-	-	1.00	-	-	-
A-671	101044.	.149	.000	13.2	.85	17.8	.048	.85	-	-	3.00	.30	0.	.029
A-672	101044.	.176	.000	12.5	.81	16.9	.064	1.09	-	-	3.00	-	-	-
A-673	101044.	.176	.000	12.5	.81	16.9	.061	1.03	-	-	1.00	-	-	-
A-674	101044.	.203	.000	11.7	.75	15.8	.080	1.26	-	-	3.00	.25	0.	.025
A-675	101044.	.203	.000	11.7	.75	15.8	.074	1.16	-	-	1.00	-	-	-
A-676	101044.	.230	.000	10.7	.69	14.4	.085	1.23	-	-	1.00	-	-	-
A-677	101044.	.230	.000	10.7	.69	14.4	.095	1.37	-	-	3.00	-	-	-
A-678*	101044.	.256	.000	9.6	.62	12.9	.114	1.47	-	-	3.00	.19	0.	.026
A-679*	101044.	.270	.000	8.8	.57	11.9	.179	2.13	-	-	3.00	.19	0.	.039
A-680	101044.	.012	.000	10.8	.70	14.6	.105	1.54	.063	.91	3.00	.21	0.	.029
A-681	101044.	.039	.000	11.7	.75	15.8	.086	1.36	.050	.79	3.00	-	-	-
A-682	101044.	.066	.000	12.6	.81	17.0	.067	1.14	.043	.72	3.00	.28	0.	.039
A-683	101044.	.093	.000	13.2	.85	17.8	.054	.96	.039	.69	3.00	-	-	-
A-684	101044.	.119	.000	13.4	.86	18.1	.049	.88	.039	.70	3.00	-	-	-
A-685	101044.	.119	.000	13.4	.86	18.1	.051	.91	.040	.72	10.00	-	-	-
A-686	101044.	.119	.000	13.4	.86	18.1	.050	.90	.040	.72	7.00	-	-	-
A-687	101044.	.119	.000	13.4	.86	18.1	.049	.88	.040	.71	5.00	-	-	-
A-688	101044.	.119	.000	13.4	.86	18.1	.047	.86	.038	.69	2.00	-	-	-
A-689	101044.	.119	.000	13.4	.86	18.1	.046	.84	.035	.63	1.00	-	-	-
A-690	101044.	.119	.000	13.4	.86	18.1	.044	.80	.033	.59	.50	-	-	-
A-691	101044.	.146	.000	13.3	.85	17.9	.051	.91	.039	.70	3.00	.33	0.	.031
A-692	101044.	.173	.000	12.8	.83	17.4	.061	1.06	.041	.72	3.00	.29	0.	.033
A-693	101044.	.200	.000	12.1	.79	16.4	.078	1.28	.047	.78	3.00	.27	0.	.029
A-694	101044.	.227	.000	11.1	.71	15.0	.101	1.52	.057	.86	3.00	-	-	-

HYDRAULIC DIAMETER, D = .811 INCHES. AVERAGE VELOCITY, U = 15.5 FT/SEC. U^* = .790 FT/SEC.
* QUESTIONABLE DATA POINT. - NO DATA POINT.

TABLE B-1 (CONT.). TABULATION OF EXPERIMENTAL DATA.

CHANNEL A, CENTER WALL GAP TRAVERSE, 1/4 INCH GAP SPACING.

RUN	REYNOLDS NUMBER	Z IN.	Y IN.	$\bar{U}$ FT/SEC	$\bar{U}/U$	$\bar{U}/U^*$	$u/\bar{U}$	u/U^*	$v/\bar{U}$	v/U^*	CUTOFF KHZ	A/D	CURVE FIT F(HZ)	σ
A-695	101044.	.212	.000	11.4	.76	15.9	.093	1.49	.056	.89	3.00	-	-	-
A-696	101044.	.185	.000	12.6	.81	17.0	.075	1.27	.049	.84	3.00	-	-	-
A-697	101044.	.156	.000	13.2	.85	17.8	.068	1.14	.044	.78	3.00	-	-	-
A-698	101044.	.132	.000	13.4	.87	18.2	.049	.86	.040	.73	3.00	-	-	-
A-699	101044.	.105	.000	13.4	.86	18.0	.050	.90	.040	.73	3.00	-	-	-
A-700	101044.	.078	.000	12.9	.83	17.5	.060	1.05	.043	.75	3.00	-	-	-
A-701	101044.	.051	.000	12.2	.79	16.5	.074	1.22	.049	.81	3.00	-	-	-
A-702	101044.	.024	.000	11.1	.72	15.1	.094	1.41	.060	.91	3.00	-	-	-
A-703*	101044.	.024	.030	11.3	.73	15.3	.083	1.28	.045	.99	3.00	-	-	-
A-704	101044.	.024	.100	11.3	.73	15.3	.093	1.43	.057	.87	3.00	-	-	-

CHANNEL A, WALL CHANNEL MAP, 1/4 INCH GAP SPACING.

RUN	REYNOLDS NUMBER	Z IN.	Y IN.	$\bar{U}$ FT/SEC	$\bar{U}/U$	$\bar{U}/U^*$	$u/\bar{U}$	u/U^*	$v/\bar{U}$	v/U^*	CUTOFF KHZ	A/D	CURVE FIT F(HZ)	σ
A-705	99729.	.090	.745	13.7	.88	18.5	.106	1.96	.066	1.22	3.00	-	-	-
A-706	99729.	.107	.745	15.9	1.02	21.5	.073	1.50	.043	.93	3.00	-	-	-
A-707	99729.	.175	.745	17.0	1.09	22.9	.050	1.14	.033	.77	3.00	-	-	-
A-708	99729.	.242	.745	17.4	1.12	23.5	.033	.78	.027	.64	3.00	-	-	-
A-709	99729.	.309	.745	17.1	1.10	23.1	.049	1.12	.033	.76	3.00	-	-	-
A-710	99729.	.376	.745	16.7	1.07	22.5	.056	1.30	.037	.83	3.00	-	-	-
A-711	99729.	.443	.745	16.1	1.04	21.8	.066	1.49	.041	.90	3.00	-	-	-
A-712	99729.	.510	.745	15.6	1.00	21.0	.068	1.53	.042	.88	3.00	-	-	-
A-713	99729.	.577	.745	14.8	.95	20.0	.073	1.65	.045	.90	3.00	-	-	-
A-714	99729.	.644	.745	13.9	.90	18.8	.080	1.80	.053	.99	3.00	-	-	-
A-715	99729.	.711	.745	13.3	.86	17.9	.077	1.38	.059	1.05	3.00	-	-	-
A-716	99729.	.779	.745	13.2	.85	17.8	.080	1.43	.061	1.09	3.00	-	-	-
A-717	99729.	.846	.745	13.8	.89	18.6	.067	1.29	.052	.96	3.00	-	-	-
A-718	99729.	.846	.685	14.1	1.03	21.7	.064	1.39	.036	.79	3.00	-	-	-
A-719	99729.	.779	.685	15.6	1.01	21.1	.060	1.26	.037	.77	3.00	-	-	-
A-720	99729.	.711	.685	15.5	1.00	20.9	.054	1.12	.033	.70	3.00	-	-	-
A-721	99729.	.644	.685	15.7	1.01	21.2	.052	1.11	.033	.69	3.00	-	-	-
A-722	99729.	.577	.685	16.0	1.03	21.6	.050	1.09	.032	.68	3.00	-	-	-
A-723	99729.	.443	.685	16.8	1.08	22.7	.049	1.11	.031	.70	3.00	-	-	-
A-724	99729.	.309	.685	17.5	1.13	23.7	.037	.89	.027	.65	3.00	-	-	-
A-725	99729.	.242	.685	17.5	1.13	23.7	.036	.85	.026	.66	3.00	-	-	-
A-726	99729.	.175	.685	16.9	1.09	22.8	.051	1.16	.033	.76	3.00	-	-	-
A-727	99729.	.107	.685	15.6	1.00	21.0	.077	1.61	.047	.98	3.00	-	-	-
A-728	99729.	.040	.685	13.2	.85	17.8	.109	1.98	.069	1.23	3.00	-	-	-
A-729	99729.	.107	.625	15.7	1.01	21.1	.070	1.48	.045	.94	3.00	-	-	-
A-730	99729.	.175	.625	16.9	1.09	22.8	.051	1.16	.033	.76	3.00	-	-	-
A-731	99729.	.242	.625	17.5	1.13	23.6	.036	.85	.027	.65	3.00	-	-	-
A-732	99729.	.309	.625	17.5	1.13	23.7	.037	.88	.026	.62	3.00	-	-	-
A-733	99729.	.376	.625	17.2	1.11	23.2	.046	1.07	.030	.69	3.00	-	-	-
A-734	99729.	.510	.625	16.5	1.06	22.2	.053	1.18	.031	.70	3.00	-	-	-
A-735	99729.	.644	.625	16.1	1.04	21.7	.043	.92	.027	.59	3.00	-	-	-
A-736	99729.	.711	.625	16.0	1.03	21.6	.039	.84	.027	.58	3.00	-	-	-
A-737	99729.	.779	.625	16.2	1.04	21.9	.046	1.01	.029	.63	3.00	-	-	-
A-738	99729.	.779	.565	15.2	.98	20.5	.065	1.33	.036	.74	3.00	-	-	-
A-739	99729.	.711	.565	15.0	.96	20.2	.060	1.22	.036	.72	3.00	-	-	-
A-740	99729.	.644	.565	15.1	.97	20.4	.062	1.27	.036	.73	3.00	-	-	-
A-741	99729.	.510	.565	15.7	1.01	21.2	.067	1.43	.036	.77	3.00	-	-	-
A-742	99729.	.376	.565	16.7	1.07	22.5	.056	1.26	.034	.76	3.00	-	-	-
A-743	99729.	.309	.565	17.1	1.10	23.1	.047	1.09	.030	.70	3.00	-	-	-
A-744	99729.	.242	.565	17.3	1.11	23.3	.041	.96	.030	.70	3.00	-	-	-
A-745	99729.	.175	.565	16.7	1.08	22.6	.051	1.16	.034	.77	3.00	-	-	-
A-746	99729.	.107	.565	15.5	1.00	20.9	.073	1.53	.046	.97	3.00	-	-	-
A-747	99729.	.107	.509	15.4	.99	20.8	.070	1.45	.045	.93	3.00	-	-	-
A-748	99729.	.175	.509	16.6	1.07	22.3	.051	1.14	.034	.77	3.00	-	-	-
A-749	99729.	.242	.509	16.9	1.09	22.8	.046	1.09	.032	.73	3.00	-	-	-
A-750	99729.	.309	.509	16.5	1.07	22.3	.059	1.31	.035	.79	3.00	-	-	-
A-751	99729.	.376	.509	15.8	1.02	21.3	.070	1.50	.040	.85	3.00	-	-	-
A-752	99729.	.510	.509	14.3	.92	19.2	.083	1.59	.044	.86	3.00	-	-	-
A-753	99729.	.644	.509	12.1	.78	16.4	.085	1.40	.049	.80	3.00	-	-	-
A-754	99729.	.577	.509	13.4	.86	18.1	.090	1.63	.049	.89	3.00	-	-	-
A-755	99729.	.711	.509	10.7	.69	14.4	.078	1.12	.047	.68	3.00	-	-	-
A-756	99729.	.779	.509	10.6	.68	14.3	.088	1.26	.060	.86	3.00	-	-	-

HYDRAULIC DIAMETER, D = .811 INCHES. AVERAGE VELOCITY, U = 15.5 FT/SEC, U^* = .791 FT/SEC.
* QUESTIONABLE DATA POINT. - NO DATA POINT.

TABLE B-1 (CONT.). TABULATION OF EXPERIMENTAL DATA.

CHANNEL A, CORNER GAP TRAVERSE, 1/4 INCH GAP SPACING.

RUN	REYNOLDS NUMBER	Z IN.	Y IN.	$\bar{U}$ FT/SEC	$\bar{U}/U$	$\bar{U}/U^*$	$u/\bar{U}$	u/U^*	$v/\bar{U}$	v/U^*	CUTOFF KHZ	Δ/D	CURVE FIT F(HZ)	σ
A-757	101044.	.304	1.250	12.1	.78	16.4	.119	1.87	.073	1.20	3.00	-	-	-
A-758	101044.	.331	1.250	13.1	.84	17.7	.081	1.43	.050	.89	3.00	-	-	-
A-759	101044.	.356	1.250	13.6	.89	18.7	.067	1.24	.042	.79	3.00	-	-	-
A-760	101044.	.385	1.250	14.4	.93	19.5	.051	1.00	.035	.69	3.00	-	-	-
A-761	101044.	.411	1.250	14.8	.95	20.0	.040	.81	.030	.61	3.00	-	-	-
A-762	101044.	.438	1.250	14.8	.95	20.0	.041	.82	.030	.61	3.00	-	-	-
A-763	101044.	.465	1.250	14.6	.94	19.7	.048	.94	.033	.69	3.00	-	-	-
A-764	101044.	.492	1.250	14.0	.90	19.0	.063	1.19	.039	.74	3.00	-	-	-
A-765	101044.	.519	1.250	13.2	.85	17.8	.088	1.56	.051	.91	3.00	-	-	-
A-766	101044.	.546	1.250	12.2	.78	16.5	.117	1.93	.069	1.14	3.00	-	-	-
A-767	101044.	.546	1.250	11.9	.77	16.1	.106	1.70	.062	.99	3.00	-	-	-
A-768	101044.	.519	1.250	13.0	.84	17.6	.082	1.44	.048	.84	3.00	-	-	-
A-769	101044.	.492	1.250	13.9	.90	18.8	.065	1.23	.040	.75	3.00	-	-	-
A-770	101044.	.465	1.250	14.6	.94	19.7	.049	.96	.032	.69	3.00	-	-	-
A-771	101044.	.438	1.250	14.8	.96	20.0	.039	.79	.029	.58	3.00	-	-	-
A-772	101044.	.411	1.250	14.8	.95	20.0	.040	.81	.029	.59	3.00	-	-	-
A-773	101044.	.385	1.250	14.5	.93	19.6	.049	.96	.033	.69	3.00	-	-	-
A-774	101044.	.358	1.250	13.9	.90	18.8	.068	1.27	.039	.74	3.00	-	-	-
A-775	101044.	.331	1.250	13.0	.84	17.6	.090	1.58	.051	.90	3.00	-	-	-
A-776	101044.	.304	1.250	12.1	.78	16.3	.111	1.82	.068	1.11	3.00	-	-	-
A-777	101044.	.331	1.250	13.0	.84	17.6	-	-	-	-	-	-	-	-
A-778	101044.	.358	1.250	14.0	.90	18.9	-	-	-	-	-	-	-	-
A-779	101044.	.385	1.250	14.5	.94	19.6	-	-	-	-	-	-	-	-
A-780	101044.	.411	1.250	14.9	.96	20.1	-	-	-	-	-	-	-	-
A-781	101044.	.438	1.250	14.9	.96	20.1	-	-	-	-	-	-	-	-
A-782	101044.	.465	1.250	14.6	.94	19.8	-	-	-	-	-	-	-	-
A-783	101044.	.492	1.250	14.1	.91	19.0	-	-	-	-	-	-	-	-
A-784	101044.	.519	1.250	13.2	.85	17.8	-	-	-	-	-	-	-	-
A-785	101044.	.546	1.250	12.1	.78	16.4	-	-	-	-	-	-	-	-
A-786	101044.	.572	1.250	11.0	.71	14.9	-	-	-	-	-	-	-	-

CHANNEL A, CENTER WALL GAP TRAVERSE, 1/4 INCH GAP SPACING.

RUN	REYNOLDS NUMBER	Z IN.	Y IN.	$\bar{U}$ FT/SEC	$\bar{U}/U$	$\bar{U}/U^*$	$u/\bar{U}$	u/U^*	$v/\bar{U}$	v/U^*	CUTOFF KHZ	Δ/D	CURVE FIT F(HZ)	σ
A-787	101044.	.305	.000	10.6	.68	14.3	.117	1.67	.074	1.05	3.00	-	-	-
A-788	101044.	.332	.000	11.7	.75	15.8	.092	1.45	.055	.87	3.00	-	-	-
A-789	101044.	.359	.000	12.7	.82	17.2	.072	1.23	.045	.78	3.00	-	-	-
A-790	101044.	.386	.000	13.4	.86	18.1	.058	1.09	.041	.74	3.00	-	-	-
A-791	101044.	.413	.000	13.6	.88	18.4	.051	.94	.040	.75	3.00	-	-	-
A-792	101044.	.440	.000	13.6	.88	18.4	.051	.94	.040	.73	3.00	-	-	-
A-793	101044.	.466	.000	13.2	.85	17.9	.062	1.10	.042	.75	3.00	-	-	-
A-794	101044.	.493	.000	12.5	.80	16.9	.080	1.35	.048	.80	3.00	-	-	-
A-795	101044.	.520	.000	11.4	.73	15.4	.104	1.60	.059	.90	3.00	-	-	-
A-796	101044.	.547	.000	10.3	.66	13.9	.121	1.68	.077	1.06	3.00	-	-	-
A-845	101044.	.016	.000	10.5	.68	14.2	.108	1.53	-	-	3.00	.22	0.	.036
A-846	101044.	.043	.000	11.8	.76	15.9	.081	1.29	-	-	3.00	.26	0.	.026
A-847	101044.	.070	.000	12.9	.83	17.5	.065	1.13	-	-	3.00	.26	0.	.025
A-848	101044.	.097	.000	13.6	.87	18.3	.056	1.03	-	-	3.00	-	-	-
A-849	101044.	.123	.000	13.8	.89	18.6	.054	1.01	-	-	3.00	-	-	-
A-850	101044.	.150	.000	13.6	.88	18.4	.058	1.07	-	-	3.00	-	-	-
A-851	101044.	.150	.000	13.6	.88	18.4	.061	1.13	-	-	10.00	-	-	-
A-852	101044.	.150	.000	13.6	.88	18.4	.056	1.04	-	-	1.00	-	-	-
A-853	101044.	.177	.000	13.0	.84	17.6	.068	1.20	-	-	3.00	-	-	-
A-854	101044.	.204	.000	12.2	.79	16.5	.082	1.34	-	-	3.00	-	-	-
A-855	101044.	.231	.000	11.0	.71	14.9	.094	1.39	-	-	3.00	-	-	-
A-856*	101044.	.258	.000	9.6	.62	12.9	.125	1.62	-	-	3.00	-	-	-

HYDRAULIC DIAMETER, D = .811 INCHES. AVERAGE VELOCITY, U = 15.5 FT/SEC. U^* = .740 FT/SEC.

* QUESTIONABLE DATA POINT. - NO DATA POINT.

TABLE 5-1 (CONT.). TABULATION OF EXPERIMENTAL DATA.

CHANNEL A, INTERIOR GAP TRAVERSE. 1/4 INCH GAP SPACING.

RUN	REYNOLDS NUMBER	Z IN.	Y IN.	$\bar{U}$ FT/SEC	$\bar{U}/U$	$\bar{U}/U^*$	$U/\bar{U}$	U/U^*	$v/\bar{U}$	v/U^*	CUTOFF KHZ	A/D	CURVE FIT F(HZ)	σ
A-857	101044.	.730	.510	6.3	.54	11.3	.136	1.54	-	-	3.00	-	-	-
A-858	101044.	.730	.515	10.4	.70	14.7	.083	1.23	-	-	3.00	-	-	-
A-859	101044.	.730	.525	12.5	.81	16.9	.076	1.29	-	-	3.00	-	-	-
A-860	101044.	.730	.535	13.4	.86	18.1	.075	1.36	-	-	3.00	-	-	-
A-861	101044.	.730	.545	14.3	.93	19.0	.071	1.34	-	-	3.00	-	-	-
A-862	101044.	.730	.565	15.0	.97	20.3	.063	1.27	-	-	3.00	-	-	-
A-863	101044.	.730	.585	15.6	1.00	21.1	.055	1.15	-	-	3.00	-	-	-
A-864	101044.	.730	.605	15.9	1.03	21.5	.052	1.11	-	-	3.00	-	-	-
A-865	101044.	.730	.625	16.1	1.04	21.8	.046	1.00	-	-	3.00	-	-	-
A-866	101044.	.730	.625	16.1	1.04	21.8	.048	1.05	-	-	10.00	-	-	-
A-867	101044.	.730	.625	16.1	1.04	21.9	.044	.97	-	-	1.00	-	-	-
A-868	101044.	.730	.645	16.2	1.04	21.9	.045	.99	-	-	3.00	-	-	-
A-869	101044.	.730	.665	16.0	1.03	21.7	.051	1.09	-	-	3.00	-	-	-
A-870	101044.	.730	.685	15.8	1.02	21.3	.053	1.13	-	-	3.00	-	-	-
A-871	101044.	.730	.705	15.3	.98	20.6	.061	1.27	-	-	3.00	-	-	-
A-872	101044.	.730	.725	14.6	.94	19.7	.063	1.25	-	-	3.00	-	-	-
A-873	101044.	.730	.735	14.0	.90	19.0	.066	1.25	-	-	3.00	-	-	-
A-874	101044.	.730	.740	13.7	.88	18.5	.073	1.34	-	-	3.00	-	-	-
A-875	101044.	.730	.745	13.4	.86	18.1	.075	1.36	-	-	3.00	-	-	-
A-876	101044.	1.983	.745	11.0	.71	14.9	.090	1.34	-	-	3.00	-	-	-
A-877	101044.	1.983	.735	12.4	.80	16.7	.082	1.36	-	-	3.00	-	-	-
A-878	101044.	1.983	.725	13.5	.87	18.2	.077	1.40	-	-	3.00	-	-	-
A-879	101044.	1.983	.705	14.7	.95	19.8	.078	1.54	-	-	3.00	-	-	-
A-880	101044.	1.983	.685	15.6	1.00	21.1	.069	1.45	-	-	3.00	-	-	-
A-881	101044.	1.983	.665	16.2	1.04	21.9	.064	1.40	-	-	3.00	-	-	-
A-882	101044.	1.983	.645	16.6	1.07	22.5	.058	1.30	-	-	3.00	-	-	-
A-883	101044.	1.983	.625	16.6	1.08	22.7	.053	1.21	-	-	3.00	-	-	-
A-884	101044.	1.983	.605	16.6	1.08	22.7	.054	1.23	-	-	3.00	-	-	-
A-885	101044.	1.983	.585	16.6	1.07	22.4	.059	1.32	-	-	3.00	-	-	-
A-886	101044.	1.983	.565	16.2	1.04	21.9	.061	1.34	-	-	3.00	-	-	-
A-887	101044.	1.983	.545	15.5	1.00	21.0	.068	1.43	-	-	3.00	-	-	-
A-888	101044.	1.983	.525	14.9	.93	19.5	.072	1.41	-	-	3.00	-	-	-
A-889	101044.	1.983	.515	13.6	.88	18.4	.076	1.40	-	-	3.00	-	-	-
A-890	101044.	1.983	.510	13.2	.85	17.9	.079	1.32	-	-	3.00	-	-	-

CHANNEL A, SIDE WALL GAP TRAVERSES, 1/4 INCH GAP SPACING.

RUN	REYNOLDS NUMBER	Z IN.	Y IN.	$\bar{U}$ FT/SEC	$\bar{U}/U$	$\bar{U}/U^*$	$U/\bar{U}$	U/U^*	$v/\bar{U}$	v/U^*	CUTOFF KHZ	A/D	CURVE FIT F(HZ)	σ
A-891	101044.	.750	1.998	10.5	.68	14.2	.067	.95	-	-	3.00	-	-	-
A-892	101044.	.750	1.988	11.3	.73	15.3	.060	.91	-	-	3.00	-	-	-
A-893	101044.	.750	1.978	11.9	.77	16.1	.061	.98	-	-	3.00	-	-	-
A-894	101044.	.750	1.958	12.9	.83	17.4	.055	.95	-	-	3.00	-	-	-
A-895	101044.	.750	1.938	13.5	.87	18.3	.047	.86	-	-	3.00	-	-	-
A-896	101044.	.750	1.918	14.0	.90	18.9	.041	.78	-	-	3.00	-	-	-
A-897	101044.	.750	1.898	14.1	.91	19.1	.039	.74	-	-	3.00	-	-	-
A-898	101044.	.750	1.878	14.1	.91	19.1	.039	.75	-	-	3.00	-	-	-
A-899	101044.	.750	1.858	13.8	.89	18.7	.047	.88	-	-	3.00	-	-	-
A-900	101044.	.750	1.838	13.4	.86	18.1	.055	.99	-	-	3.00	-	-	-
A-901	101044.	.750	1.818	12.7	.82	17.2	.065	1.12	-	-	3.00	-	-	-
A-902	101044.	.750	1.798	11.6	.75	15.7	.073	1.16	-	-	3.00	-	-	-
A-903	101044.	.750	1.788	10.8	.70	14.6	.077	1.12	-	-	3.00	-	-	-
A-904	101044.	.750	1.778	9.7	.63	13.1	.078	1.03	-	-	3.00	-	-	-
A-905	101044.	.750	1.768	8.9	.58	11.9	.089	1.02	-	-	3.00	-	-	-
A-906	101044.	2.003	1.993	11.1	.71	14.9	.072	1.08	-	-	3.00	-	-	-
A-907	101044.	2.003	1.988	12.3	.79	16.6	.066	1.10	-	-	3.00	-	-	-
A-908	101044.	2.003	1.978	13.0	.84	17.6	.067	1.17	-	-	3.00	-	-	-
A-909	101044.	2.003	1.958	14.1	.91	19.1	.063	1.20	-	-	3.00	-	-	-
A-910	101044.	2.003	1.938	14.8	.95	20.0	.053	1.07	-	-	3.00	-	-	-
A-911	101044.	2.003	1.918	15.3	.98	20.7	.047	.97	-	-	3.00	-	-	-
A-912	101044.	2.003	1.898	15.5	1.00	21.0	.043	.90	-	-	3.00	-	-	-
A-913	101044.	2.003	1.878	15.5	1.00	21.0	.047	.98	-	-	3.00	-	-	-
A-914	101044.	2.003	1.858	15.4	.99	20.8	.052	1.07	-	-	3.00	-	-	-
A-915	101044.	2.003	1.838	14.9	.96	20.1	.061	1.22	-	-	3.00	-	-	-
A-916	101044.	2.003	1.818	14.2	.92	19.2	.070	1.35	-	-	3.00	-	-	-
A-917	101044.	2.003	1.798	13.2	.85	17.9	.085	1.52	-	-	3.00	-	-	-
A-918	101044.	2.003	1.788	12.6	.81	17.0	.087	1.47	-	-	3.00	-	-	-
A-919	101044.	2.003	1.778	10.8	.70	14.6	.121	1.77	-	-	3.00	-	-	-

HYDRAULIC DIAMETER, D = .811 INCHES. AVERAGE VELOCITY, U = 15.5 FT/SEC, U^* = .740 FT/SEC.
* QUESTIONABLE DATA POINT. - NO DATA POINT.

TABLE H-1 (CONT.). TABULATION OF EXPERIMENTAL DATA.

CHANNEL 4. INTERIOR SUB REGION SUB, 1/4 INCH SUB SPACING.

RUN	REYNOLDS NUMBER	Z IN.	Y IN.	$\bar{U}$ FT/SEC	$\bar{U}/U$	$\bar{U}/U^*$	$u/\bar{U}$	u/U^*	$v/\bar{U}$	v/U^*	CUTOFF KHZ	Δ/D	CURVE FIT (HZ)	σ
A-920	101044.	.750	.745	13.4	.86	18.1	.050	1.45	-	-	3.00	-	-	-
A-921	101044.	.750	.725	14.6	.94	19.7	.048	1.34	-	-	3.00	-	-	-
A-922	101044.	.750	.705	15.3	.99	20.7	.054	1.22	-	-	3.00	-	-	-
A-923	101044.	.750	.685	15.9	1.02	21.4	.050	1.08	-	-	3.00	-	-	-
A-924	101044.	.750	.665	16.1	1.04	21.8	.047	1.02	-	-	3.00	-	-	-
A-925	101044.	.750	.645	16.2	1.05	21.9	.043	.95	-	-	3.00	-	-	-
A-926	101044.	.750	.625	16.2	1.04	21.8	.046	1.01	-	-	3.00	-	-	-
A-927	101044.	.750	.595	15.8	1.01	21.3	.054	1.19	-	-	3.00	-	-	-
A-928	101044.	.750	.565	14.9	.96	20.1	.064	1.29	-	-	3.00	-	-	-
A-929	101044.	.750	.545	13.9	.90	18.8	.069	1.31	-	-	3.00	-	-	-
A-930	101044.	.750	.525	12.3	.79	16.6	.076	1.27	-	-	3.00	-	-	-
A-931	101044.	.750	.515	10.3	.66	13.9	.083	1.16	-	-	3.00	-	-	-
A-932	101044.	.804	.745	13.5	.87	18.3	.075	1.36	-	-	3.00	-	-	-
A-933	101044.	.804	.725	14.6	.94	19.8	.070	1.39	-	-	3.00	-	-	-
A-934	101044.	.804	.705	15.5	1.00	20.9	.062	1.29	-	-	3.00	-	-	-
A-935	101044.	.804	.685	16.0	1.03	21.6	.057	1.24	-	-	3.00	-	-	-
A-936	101044.	.804	.665	16.3	1.05	22.0	.052	1.14	-	-	3.00	-	-	-
A-937	101044.	.804	.645	16.5	1.06	22.3	.049	1.09	-	-	3.00	-	-	-
A-938	101044.	.804	.625	16.4	1.06	22.2	.050	1.12	-	-	3.00	-	-	-
A-939	101044.	.804	.595	15.9	1.03	21.5	.059	1.27	-	-	3.00	-	-	-
A-940	101044.	.804	.565	15.1	.97	20.4	.071	1.49	-	-	3.00	-	-	-
A-941	101044.	.804	.545	14.1	.91	19.1	.075	1.49	-	-	3.00	-	-	-
A-942	101044.	.804	.525	12.5	.80	16.9	.076	1.27	-	-	3.00	-	-	-
A-943	101044.	.804	.515	10.6	.68	14.4	.087	1.25	-	-	3.00	-	-	-
A-944	101044.	.871	.745	14.2	.91	19.2	.076	1.49	-	-	3.00	-	-	-
A-945	101044.	.871	.725	15.2	.98	20.6	.075	1.54	-	-	3.00	-	-	-
A-946	101044.	.871	.705	16.0	1.03	21.6	.067	1.45	-	-	3.00	-	-	-
A-947	101044.	.871	.685	16.5	1.06	22.3	.063	1.40	-	-	3.00	-	-	-
A-948	101044.	.871	.665	16.8	1.08	22.7	.058	1.32	-	-	3.00	-	-	-
A-949	101044.	.871	.645	17.0	1.09	23.0	.054	1.23	-	-	3.00	-	-	-
A-950	101044.	.871	.625	16.9	1.09	22.9	.055	1.25	-	-	3.00	-	-	-
A-951	101044.	.871	.595	16.6	1.07	22.4	.060	1.35	-	-	3.00	-	-	-
A-952	101044.	.871	.565	15.8	1.02	21.4	.069	1.47	-	-	3.00	-	-	-
A-953	101044.	.871	.545	15.0	.97	20.3	.078	1.59	-	-	3.00	-	-	-
A-954	101044.	.871	.525	13.6	.88	18.4	.081	1.49	-	-	3.00	-	-	-
A-955	101044.	.871	.515	12.5	.81	16.9	.086	1.46	-	-	3.00	-	-	-
A-956	101044.	.603	.745	15.1	.97	20.4	.065	1.32	-	-	3.00	-	-	-
A-957	101044.	.603	.725	15.6	1.00	21.0	.058	1.23	-	-	3.00	-	-	-
A-958	101044.	.603	.705	16.0	1.03	21.6	.052	1.12	-	-	3.00	-	-	-
A-959	101044.	.603	.685	16.2	1.05	22.0	.047	1.03	-	-	3.00	-	-	-
A-960	101044.	.603	.665	16.4	1.05	22.1	.045	1.00	-	-	3.00	-	-	-
A-961	101044.	.603	.645	16.3	1.05	22.1	.049	1.08	-	-	3.00	-	-	-
A-962	101044.	.603	.625	16.2	1.04	21.9	.052	1.14	-	-	3.00	-	-	-
A-963	101044.	.603	.595	15.8	1.02	21.3	.061	1.31	-	-	3.00	-	-	-
A-964	101044.	.603	.565	15.1	.97	20.4	.071	1.44	-	-	3.00	-	-	-
A-965	101044.	.603	.545	14.4	.93	19.4	.078	1.52	-	-	3.00	-	-	-
A-966	101044.	.603	.525	13.6	.87	18.3	.083	1.52	-	-	3.00	-	-	-
A-967	101044.	.603	.515	13.0	.84	17.6	.089	1.57	-	-	3.00	-	-	-
A-968	101044.	.670	.745	14.1	.91	19.0	.070	1.33	-	-	3.00	-	-	-
A-969	101044.	.670	.725	14.9	.96	20.1	.067	1.35	-	-	3.00	-	-	-
A-970	101044.	.670	.705	15.6	1.00	21.1	.053	1.12	-	-	3.00	-	-	-
A-971	101044.	.670	.675	16.1	1.04	21.7	.044	.96	-	-	3.00	-	-	-
A-972	101044.	.670	.645	16.2	1.04	21.9	.043	.99	-	-	3.00	-	-	-
A-973	101044.	.670	.615	16.0	1.03	21.6	.050	1.08	-	-	3.00	-	-	-
A-974	101044.	.670	.585	15.4	.99	20.9	.059	1.24	-	-	3.00	-	-	-
A-975	101044.	.670	.565	14.9	.96	20.2	.070	1.41	-	-	3.00	-	-	-
A-976	101044.	.670	.545	14.1	.91	19.1	.071	1.35	-	-	3.00	-	-	-
A-977	101044.	.670	.525	12.6	.81	17.0	.082	1.39	-	-	3.00	-	-	-
A-978	101044.	.670	.515	11.7	.76	15.8	.084	1.33	-	-	3.00	-	-	-
A-979	101044.	.670	.510	11.3	.73	15.3	.087	1.33	-	-	3.00	-	-	-

HYDRAULIC DIAMETER, D = .911 INCHES. AVERAGE VELOCITY, U = 15.5 FT/SEC. U^* = .740 FT/SEC.
* QUESTIONABLE DATA POINT. - NO DATA POINT.

TABLE B-1 (CONT.). TABULATION OF EXPERIMENTAL DATA.

CHANNEL A. WALL AND INTERIOR CENTERLINE TRAVERSES. 1/8 INCH GAP SPACING.

RUN	REYNOLDS NUMBER	Z IN.	Y IN.	$\bar{U}$ FT/SEC	$\bar{U}/U$	$\bar{U}/U^*$	$u/\bar{U}$	u/U^*	$v/\bar{U}$	v/U^*	CUTOFF KHZ	A/D	CURVE FIT F(HZ)	σ
A1000	58247.	.067	.625	9.4	.90	17.6	.087	1.53	-	-	2.00	.51	18.	.026
A1001	58247.	.134	.625	10.7	1.02	20.0	.068	1.37	-	-	2.00	.51	9.	.019
A1002	58247.	.201	.625	11.6	1.11	21.8	.053	1.15	-	-	2.00	.50	32.	.025
A1003	58247.	.268	.625	12.0	1.15	22.5	.045	1.02	-	-	2.00	.45	35.	.059
A1004	55505.	.336	.625	12.7	1.22	23.7	.050	1.20	-	-	2.00	.55	39.	.056
A1005	55505.	.402	.625	12.5	1.19	23.3	.067	1.56	-	-	2.00	.49	40.	.023
A1006	55505.	.469	.625	11.9	1.14	22.2	.065	1.68	-	-	2.00	.31	47.	.020
A1007	55505.	.537	.625	11.3	1.08	21.0	.095	2.00	-	-	2.00	.27	47.	.008
A1008	55505.	.604	.625	10.6	1.01	19.7	.101	1.99	-	-	2.00	.24	50.	.030
A1009	55505.	.671	.625	10.0	.95	18.6	.100	1.86	-	-	2.00	.22	47.	.042
A1010	55505.	.738	.625	9.5	.91	17.7	.091	1.62	-	-	2.00	.31	45.	.027
A1011	55505.	.805	.625	9.3	.89	17.4	.060	1.39	-	-	2.00	.59	13.	.023
A1012	55505.	.872	.625	9.3	.89	17.4	.081	1.40	-	-	2.00	.51	4.	.017
A1013	55505.	.939	.625	9.7	.92	18.0	.096	1.73	-	-	2.00	.27	48.	.032
A1014	55505.	1.006	.625	10.2	.98	19.0	.100	1.90	-	-	2.00	.23	49.	.020
A1015	55505.	1.073	.625	11.0	1.05	20.4	.089	1.81	-	-	2.00	.28	47.	.017
A1016	55505.	1.140	.625	11.5	1.10	21.5	.087	1.87	-	-	2.00	.30	48.	.020
A1017	55505.	1.207	.625	12.2	1.16	22.7	.079	1.79	-	-	2.00	.37	46.	.035
A1018	55505.	1.274	.625	12.7	1.22	23.7	.067	1.60	-	-	2.00	.48	42.	.048
A1019	55505.	1.341	.625	13.2	1.26	24.6	.057	1.39	-	-	2.00	.58	34.	.038
A1020	55505.	1.408	.625	13.5	1.28	25.0	.049	1.22	-	-	2.00	.66	0.	.044
A1021	55505.	1.476	.625	13.5	1.28	25.0	.050	1.24	-	-	2.00	.65	0.	.033
A1022	55505.	1.543	.625	13.2	1.26	24.6	.056	1.37	-	-	2.00	.68	22.	.047
A1023	55505.	1.610	.625	12.9	1.23	23.9	.059	1.42	-	-	2.00	.66	32.	.067
A1024	55505.	1.677	.625	12.4	1.19	23.1	.067	1.55	-	-	2.00	.59	37.	.055
A1025	55505.	1.744	.625	12.0	1.15	22.4	.069	1.55	-	-	2.00	.47	39.	.062
A1026	55505.	1.811	.625	11.6	1.10	21.5	.074	1.59	-	-	2.00	.44	38.	.050
A1027	55505.	1.878	.625	11.0	1.05	20.4	.082	1.68	-	-	2.00	.46	33.	.053
A1028	55505.	1.945	.625	10.5	1.00	19.6	.083	1.61	-	-	2.00	.40	36.	.041
A1029	55505.	2.012	.625	10.2	.97	19.0	.080	1.51	-	-	2.00	.57	29.	.046
A1030	55505.	2.079	.625	10.1	.96	18.7	.069	1.20	-	-	2.00	.57	19.	.018
A1031	54827.	2.113	.625	10.1	.96	18.7	.058	1.09	-	-	2.00	-	-	-
A1032	54827.	2.113	.635	10.0	.95	18.5	.063	1.17	-	-	2.00	-	-	-
A1033	54827.	2.113	.645	9.9	.94	18.4	.062	1.13	-	-	2.00	-	-	-
A1034	54827.	2.113	.655	9.6	.92	17.9	.072	1.29	-	-	2.00	.59	0.	.015
A1035	54827.	2.113	.665	9.4	.90	17.4	.067	1.17	-	-	2.00	-	-	-
A1036	54827.	2.113	.675	8.9	.85	16.4	.069	1.19	-	-	2.00	.48	0.	.018
A1037	54827.	2.113	.685	9.9	.95	18.4	.065	1.20	-	-	2.00	.53	4.	.010
A1038	54827.	2.113	.605	9.7	.92	18.0	.065	1.17	-	-	2.00	-	-	-
A1039	54827.	2.113	.595	9.3	.89	17.3	.069	1.20	-	-	2.00	.58	0.	.038
A1040	54827.	2.113	.585	8.9	.85	16.6	.070	1.15	-	-	2.00	-	-	-
A1041	54827.	2.113	.580	8.5	.81	15.7	.081	1.27	-	-	2.00	.37	0.	.055
A1042*	54827.	.838	.580	5.1	.48	9.4	.292	2.75	-	-	2.00	-	-	-
A1043	54827.	.838	.585	7.6	.73	14.2	.085	1.20	-	-	2.00	.49	0.	.025
A1044	54827.	.838	.595	8.4	.80	15.6	.082	1.28	-	-	2.00	-	-	-
A1045	54827.	.838	.605	8.9	.85	16.6	.076	1.26	-	-	2.00	.55	0.	.029
A1046	54827.	.838	.615	9.2	.88	17.1	.080	1.37	-	-	2.00	-	-	-
A1047	54827.	.838	.625	9.4	.89	17.4	.079	1.37	-	-	2.00	.55	0.	.033
A1048	54827.	.838	.635	9.3	.89	17.3	.078	1.36	-	-	2.00	-	-	-
A1049	54827.	.838	.645	9.1	.87	16.9	.079	1.33	-	-	2.00	.57	0.	.031
A1050	54827.	.838	.655	8.7	.83	16.1	.082	1.32	-	-	2.00	-	-	-
A1051	54827.	.838	.665	8.0	.77	14.9	.084	1.26	-	-	2.00	.46	15.	.041
A1052	54827.	.838	.670	7.2	.69	13.4	.156	2.09	-	-	2.00	-	-	-

CHANNEL A. CORNER AND WALL CENTERLINE TRAVERSES. 3/16 INCH GAP SPACING.

RUN	REYNOLDS NUMBER	Z IN.	Y IN.	$\bar{U}$ FT/SEC	$\bar{U}/U$	$\bar{U}/U^*$	$u/\bar{U}$	u/U^*	$v/\bar{U}$	v/U^*	CUTOFF KHZ	A/D	CURVE FIT F(HZ)	σ
A1053	54827.	.067	1.906	10.2	.97	18.9	.068	1.28	-	-	2.00	.37	0.	.031
A1054	54827.	.134	1.906	11.3	1.08	21.1	.053	1.11	-	-	2.00	.38	26.	.058
A1055	54827.	.201	1.906	11.5	1.10	21.3	.057	1.22	-	-	2.00	.42	5.	.069
A1056	54827.	.268	1.906	11.4	1.08	21.1	.057	1.20	-	-	2.00	.51	0.	.039
A1057	54827.	.335	1.906	11.4	1.08	21.1	.056	1.19	-	-	2.00	.41	0.	.039
A1058	54827.	.402	1.906	11.4	1.09	21.2	.055	1.16	-	-	2.00	.40	0.	.080
A1059	54827.	.470	1.906	11.5	1.09	21.3	.048	1.01	-	-	2.00	.39	22.	.090
A1060	54827.	.537	1.906	11.4	1.08	21.1	.046	.94	-	-	2.00	.44	38.	.085
A1061	54827.	.604	1.906	11.1	1.06	20.7	.045	.99	-	-	2.00	.44	3.	.070
A1062	54827.	.671	1.906	11.0	1.05	20.5	.039	.80	-	-	2.00	.35	51.	.119
A1063	54827.	.738	1.906	10.8	1.04	20.2	.038	.77	-	-	2.00	.26	63.	.151
A1064	54827.	.805	1.906	10.8	1.03	20.0	.037	.74	-	-	2.00	.21	76.	.108
A1065	54827.	.872	1.906	10.8	1.03	20.0	.038	.76	-	-	2.00	.20	65.	.116
A1066	54827.	.939	1.906	10.9	1.04	20.3	.041	.84	-	-	2.00	.33	45.	.105
A1067	54827.	1.006	1.906	11.1	1.06	20.7	.042	.87	-	-	2.00	.44	38.	.123
A1068	54827.	1.073	1.906	11.4	1.08	21.1	.046	.98	-	-	2.00	.45	40.	.093
A1069	54827.	1.140	1.906	11.6	1.10	21.5	.051	1.09	-	-	2.00	.41	39.	.080
A1070	54827.	1.207	1.906	11.7	1.12	21.7	.055	1.19	-	-	2.00	.41	42.	.069
A1071	54827.	1.274	1.906	11.7	1.12	21.7	.058	1.27	-	-	2.00	.48	35.	.069
A1072	54827.	1.341	1.906	11.6	1.11	21.6	.063	1.35	-	-	2.00	.52	33.	.062
A1073	54827.	1.409	1.906	11.5	1.10	21.4	.065	1.38	-	-	2.00	.55	30.	.046
A1074	54827.	1.476	1.906	11.5	1.10	21.4	.064	1.36	-	-	2.00	.57	0.	.030

HYDRAULIC DIAMETER, D = .519 INCHES. AVERAGE VELOCITY, U = 10.5 FT/SEC, U^* = .538 FT/SEC.
* QUESTIONABLE DATA POINT. - NO DATA POINT.

TABLE B-1 (CONT.). TABULATION OF EXPERIMENTAL DATA.

CHANNEL A, CORNER AND WALL CENTERLINE TRAVERSES, 3/16 INCH GAP SPACING.

RUN	REYNOLDS NUMBER	Z IN.	Y IN.	$\bar{U}$ FT/SEC	$\bar{U}/U$	$\bar{U}/U^*$	$u/\bar{U}$	u/U^*	$v/\bar{U}$	v/U^*	CUTOFF KHZ	λ/D	CURVE FIT F(HZ)	CURVE FIT σ
A1075	54827.	1.543	1.906	11.6	1.11	21.6	.063	1.36	-	-	2.00	.58	0.	.061
A1076	54827.	1.610	1.906	11.6	1.11	21.6	.059	1.28	-	-	2.00	.57	0.	.046
A1077	54827.	1.677	1.906	11.6	1.11	21.6	.058	1.25	-	-	2.00	.59	28.	.054
A1078	54827.	1.744	1.906	11.5	1.10	21.4	.053	1.14	-	-	2.00	.63	24.	.050
A1079	54827.	1.811	1.906	11.2	1.07	20.8	.052	1.09	-	-	2.00	.64	26.	.046
A1080	54827.	1.878	1.906	10.9	1.04	20.2	.055	1.11	-	-	2.00	.58	29.	.051
A1081	54827.	1.945	1.906	10.5	1.00	19.6	.052	1.01	-	-	2.00	.57	29.	.065
A1082	54827.	2.012	1.906	10.3	.99	19.2	.044	.85	-	-	2.00	.51	0.	.039
A1083	54827.	2.079	1.906	10.2	.97	18.9	.039	.73	-	-	2.00	.39	0.	.027
A1084	54827.	2.113	1.906	10.2	.97	19.0	.040	.75	-	-	2.00	.39	0.	.021
A1085	54827.	2.113	1.921	10.1	.97	18.8	.040	.74	-	-	2.00	-	-	-
A1086	54827.	2.113	1.936	10.0	.95	18.5	.046	.85	-	-	2.00	-	-	-
A1087	54827.	2.113	1.951	9.6	.92	17.8	.053	.99	-	-	2.00	-	-	-
A1088	54827.	2.113	1.966	9.2	.88	17.1	.057	.97	-	-	2.00	-	-	-
A1089	54827.	2.113	1.981	8.4	.80	15.6	.059	.92	-	-	2.00	-	-	-
A1090*	54827.	2.113	1.996	4.2	.40	7.8	.345	2.68	-	-	2.00	-	-	-
A1091	54827.	2.113	1.891	10.1	.96	18.8	.043	.80	-	-	2.00	-	-	-
A1092	54827.	2.113	1.876	9.9	.94	18.3	.049	.90	-	-	2.00	-	-	-
A1093	54827.	2.113	1.861	9.5	.91	17.7	.052	.92	-	-	2.00	-	-	-
A1094	54827.	2.113	1.846	9.0	.86	16.7	.057	.96	-	-	2.00	-	-	-
A1095	54827.	2.113	1.831	8.0	.77	14.9	.073	1.09	-	-	2.00	-	-	-
A1096	56869.	.838	1.906	10.6	1.01	19.7	.036	.71	-	-	2.00	-	-	-
A1097	56869.	.838	1.891	10.5	1.00	19.5	.041	.80	-	-	2.00	-	-	-
A1098	56869.	.838	1.876	10.2	.97	19.0	.047	.89	-	-	2.00	-	-	-
A1099	56869.	.838	1.861	9.6	.94	18.4	.053	.98	-	-	2.00	-	-	-
A1100	56869.	.838	1.846	9.4	.89	17.4	.056	.97	-	-	2.00	-	-	-
A1101	56869.	.838	1.831	8.7	.83	16.3	.060	.98	-	-	2.00	-	-	-
A1102	56869.	.838	1.816	7.5	.72	14.1	.075	1.05	-	-	2.00	-	-	-
A1103	56869.	.838	1.921	10.6	1.01	19.7	.036	.71	-	-	2.00	-	-	-
A1104	56869.	.838	1.936	10.4	1.00	19.5	.041	.80	-	-	2.00	-	-	-
A1105	56869.	.838	1.951	10.1	.96	18.8	.046	.87	-	-	2.00	-	-	-
A1106	56869.	.838	1.966	9.7	.93	18.1	.052	.95	-	-	2.00	-	-	-
A1107	56869.	.838	1.981	9.1	.87	17.0	.057	.98	-	-	2.00	-	-	-
A1108	56869.	.838	1.996	8.2	.78	15.2	.061	.94	-	-	2.00	-	-	-

CHANNEL A, CORNER AND WALL CHANNEL MAP, 3/16 INCH GAP SPACING.

RUN	REYNOLDS NUMBER	Z IN.	Y IN.	$\bar{U}$ FT/SEC	$\bar{U}/U$	$\bar{U}/U^*$	$u/\bar{U}$	u/U^*	$v/\bar{U}$	v/U^*	CUTOFF KHZ	λ/D	CURVE FIT F(HZ)	CURVE FIT σ
A1109	103525.	.067	1.906	16.6	.96	19.9	.070	1.41	-	-	4.00	.36	0.	.020
A1110	103525.	.134	1.906	18.9	1.09	22.7	.048	1.08	-	-	4.00	.41	0.	.021
A1111	103525.	.201	1.906	19.2	1.11	23.0	.052	1.20	-	-	4.00	.51	0.	.031
A1112	103525.	.268	1.906	19.0	1.09	22.8	.057	1.30	-	-	4.00	.53	0.	.039
A1113	103525.	.335	1.906	19.1	1.10	22.9	.052	1.20	-	-	4.00	.50	0.	.034
A1114	103525.	.402	1.906	19.2	1.11	23.1	.047	1.08	-	-	4.00	.48	0.	.028
A1115	103525.	.469	1.906	19.2	1.11	23.0	.042	.97	-	-	4.00	.51	0.	.038
A1116	103525.	.536	1.906	19.0	1.09	22.8	.040	.92	-	-	4.00	.54	0.	.040
A1117	103525.	.603	1.906	18.7	1.08	22.4	.039	.88	-	-	4.00	.56	0.	.051
A1118	103525.	.670	1.906	18.4	1.06	22.0	.037	.81	-	-	4.00	.54	0.	.050
A1119	103525.	.737	1.906	18.1	1.04	21.7	.035	.76	-	-	4.00	.47	0.	.038
A1120	103525.	.804	1.906	18.0	1.04	21.6	.034	.73	-	-	4.00	.44	0.	.035
A1121	103525.	.871	1.906	18.1	1.04	21.7	.035	.76	-	-	4.00	.43	0.	.036
A1122	103525.	.938	1.906	18.3	1.06	22.0	.037	.82	-	-	4.00	.54	0.	.038
A1123	103525.	1.005	1.906	18.7	1.08	22.4	.039	.87	-	-	4.00	.59	0.	.037
A1124	103525.	1.072	1.906	19.1	1.10	22.9	.042	.96	-	-	4.00	.58	0.	.035
A1125	103525.	1.139	1.906	19.4	1.12	23.3	.044	1.02	-	-	4.00	.55	18.	.037
A1126	103525.	1.206	1.906	19.7	1.13	23.6	.047	1.12	-	-	4.00	.54	31.	.040
A1127	103525.	1.273	1.906	19.7	1.14	23.6	.053	1.26	-	-	4.00	.61	0.	.040
A1128	103525.	1.340	1.906	19.6	1.13	23.5	.056	1.32	-	-	4.00	.66	11.	.039
A1129	103526.	1.407	1.906	19.4	1.12	23.3	.062	1.43	-	-	4.00	.63	0.	.029
A1130	103525.	1.474	1.906	19.4	1.12	23.3	.060	1.41	-	-	4.00	.59	0.	.024
A1131	103525.	1.541	1.906	19.5	1.13	23.4	.059	1.38	-	-	4.00	.57	0.	.029
A1132	103525.	1.608	1.906	19.7	1.13	23.6	.058	1.37	-	-	4.00	.62	0.	.043
A1133	103525.	1.675	1.906	19.6	1.13	23.5	.054	1.28	-	-	4.00	.61	33.	.044
A1134	103525.	1.742	1.906	19.4	1.12	23.2	.049	1.14	-	-	4.00	.61	45.	.041
A1135	103525.	1.810	1.906	18.9	1.09	22.7	.049	1.12	-	-	4.00	.62	48.	.051
A1136	103525.	1.877	1.906	18.3	1.06	22.0	.050	1.10	-	-	4.00	.61	46.	.048
A1137	103525.	1.944	1.906	17.8	1.03	21.3	.046	.98	-	-	4.00	.56	51.	.060
A1138	103525.	2.011	1.906	17.4	1.00	20.9	.043	.90	-	-	4.00	.58	20.	.034
A1139	103525.	2.078	1.906	17.2	.99	20.6	.038	.79	-	-	4.00	.47	0.	.031
A1140	103525.	2.111	1.906	17.2	.99	20.6	.038	.78	-	-	4.00	.49	0.	.023
A1141	103525.	2.111	1.921	17.0	.98	20.4	.043	.88	-	-	4.00	-	-	-
A1142	103525.	2.111	1.936	16.6	.95	19.9	.048	.95	-	-	4.00	-	-	-
A1143	103525.	2.111	1.951	15.9	.91	19.0	.051	.97	-	-	4.00	-	-	-
A1144	103525.	2.111	1.966	14.8	.86	17.8	.060	1.06	-	-	4.00	-	-	-
A1145	103525.	2.111	1.981	13.1	.76	15.3	.062	.98	-	-	4.00	-	-	-
A1146	103525.	2.111	1.891	17.2	.99	20.6	.039	.80	-	-	4.00	-	-	-
A1147	103525.	2.111	1.876	16.9	.97	20.3	.043	.88	-	-	4.00	-	-	-
A1148	103525.	2.111	1.861	16.4	.95	19.7	.048	.95	-	-	4.00	-	-	-

HYDRAULIC DIAMETER, D = .339 INCHES. AVERAGE VELOCITY, U = 17.4 FT/SEC. U^* = .839 FT/SEC.

* QUESTIONABLE DATA POINT. - NO DATA POINT.

TABLE B-1 (CONT.). TABULATION OF EXPERIMENTAL DATA.

CHANNEL A, CORNER AND WALL CHANNEL MAPS, 3/16 INCH GAP SPACING.

RUN	REYNOLDS NUMBER	Z IN.	Y IN.	$\bar{U}$ FT/SEC	$\bar{U}/U$	$\bar{U}/U^*$	$u/\bar{U}$	v/U^*	$v/\bar{U}$	v/U^*	CUTOFF KHZ	A/D	CURVE FIT (HZ)	FIT σ
A1149	103525.	2.111	1.846	15.8	.91	18.9	.054	1.02	-	-	4.00	-	-	-
A1150	103525.	2.111	1.931	14.6	.85	17.7	.072	1.23	-	-	4.00	-	-	-
A1151*	103525.	2.111	1.416	13.6	.79	16.3	.059	.97	-	-	4.00	-	-	-
A1152	103525.	.067	1.941	17.4	1.00	20.9	.061	1.27	-	-	4.00	-	-	-
A1153	103525.	.134	1.941	18.6	1.07	22.3	.056	1.25	-	-	4.00	-	-	-
A1154	103525.	.201	1.941	18.4	1.06	22.1	.065	1.43	-	-	4.00	-	-	-
A1155	103525.	.268	1.941	18.2	1.05	21.9	.061	1.34	-	-	4.00	-	-	-
A1156	103525.	.335	1.941	18.4	1.06	22.0	.058	1.28	-	-	4.00	-	-	-
A1157	103525.	.402	1.941	18.6	1.07	22.3	.056	1.25	-	-	4.00	-	-	-
A1158	103525.	.469	1.941	18.6	1.07	22.3	.054	1.21	-	-	4.00	-	-	-
A1159	103525.	.536	1.941	18.4	1.06	22.1	.051	1.14	-	-	4.00	-	-	-
A1160	103525.	.603	1.941	18.3	1.05	21.9	.048	1.05	-	-	4.00	-	-	-
A1161	103525.	.670	1.941	18.0	1.04	21.6	.047	1.03	-	-	4.00	-	-	-
A1162	103525.	.737	1.941	17.9	1.03	21.4	.045	.96	-	-	4.00	-	-	-
A1163	103525.	.804	1.941	17.9	1.03	21.5	.042	.91	-	-	4.00	-	-	-
A1164	103525.	.871	1.941	17.7	1.02	21.2	.047	1.00	-	-	4.00	-	-	-
A1165	103525.	.938	1.941	17.8	1.03	21.3	.053	1.13	-	-	4.00	-	-	-
A1166	103525.	1.005	1.941	18.1	1.04	21.7	.055	1.19	-	-	4.00	-	-	-
A1167	103525.	1.072	1.941	18.5	1.06	22.1	.056	1.24	-	-	4.00	-	-	-
A1168	103525.	1.139	1.941	18.7	1.08	22.4	.057	1.28	-	-	4.00	-	-	-
A1169	103525.	1.206	1.941	18.9	1.09	22.7	.060	1.36	-	-	4.00	-	-	-
A1170	103525.	1.273	1.941	18.8	1.09	22.6	.064	1.45	-	-	4.00	-	-	-
A1171	103525.	1.340	1.941	18.6	1.07	22.3	.069	1.54	-	-	4.00	-	-	-
A1172	103525.	1.407	1.941	18.4	1.06	22.1	.072	1.58	-	-	4.00	-	-	-
A1173	103525.	1.474	1.941	18.4	1.06	22.1	.067	1.47	-	-	4.00	-	-	-
A1174	103526.	1.474	1.976	16.5	.95	19.8	.080	1.59	-	-	4.00	-	-	-
A1175	103525.	1.407	1.976	16.6	.95	19.8	.087	1.72	-	-	4.00	-	-	-
A1176	103525.	1.340	1.976	16.8	.97	20.1	.079	1.59	-	-	4.00	-	-	-
A1177	103525.	1.273	1.976	16.9	.98	20.3	.077	1.57	-	-	4.00	-	-	-
A1178	103525.	1.206	1.976	17.0	.98	20.3	.077	1.57	-	-	4.00	-	-	-
A1179	103525.	1.139	1.976	16.9	.97	20.2	.072	1.46	-	-	4.00	-	-	-
A1180	103525.	1.072	1.976	16.6	.96	19.9	.069	1.36	-	-	4.00	-	-	-
A1181	103525.	1.005	1.976	16.3	.94	19.6	.065	1.28	-	-	4.00	-	-	-
A1182	103525.	.938	1.976	16.1	.93	19.3	.062	1.19	-	-	4.00	-	-	-
A1183	103525.	.871	1.976	16.0	.92	19.1	.062	1.18	-	-	4.00	-	-	-
A1184	103525.	.804	1.976	16.0	.92	19.1	.061	1.16	-	-	4.00	-	-	-
A1185	103525.	.737	1.976	16.0	.92	19.2	.063	1.20	-	-	4.00	-	-	-
A1186	103525.	.670	1.976	16.1	.93	19.3	.064	1.24	-	-	4.00	-	-	-
A1187	103525.	.603	1.976	16.3	.94	19.5	.068	1.33	-	-	4.00	-	-	-
A1188	103525.	.536	1.976	16.6	.95	19.8	.070	1.39	-	-	4.00	-	-	-
A1189	103525.	.469	1.976	16.7	.96	20.0	.069	1.39	-	-	4.00	-	-	-
A1190	103526.	.402	1.976	16.7	.96	20.0	.077	1.54	-	-	4.00	-	-	-
A1191	103525.	.335	1.976	16.6	.96	19.9	.076	1.51	-	-	4.00	-	-	-
A1192	103526.	.268	1.976	16.5	.95	19.7	.077	1.51	-	-	4.00	-	-	-
A1193	103525.	.201	1.976	16.6	.96	19.9	.074	1.48	-	-	4.00	-	-	-
A1194	103525.	.134	1.976	16.7	.96	20.0	.067	1.34	-	-	4.00	-	-	-
A1195	103525.	.067	1.976	16.1	.93	19.3	.069	1.33	-	-	4.00	-	-	-
A1196	103525.	.067	1.996	17.4	1.00	20.9	.061	1.27	-	-	4.00	-	-	-
A1197	103525.	.134	1.996	18.2	1.05	21.8	.060	1.30	-	-	4.00	-	-	-
A1198	103525.	.201	1.996	17.9	1.03	21.5	.068	1.46	-	-	4.00	-	-	-
A1199	103525.	.268	1.996	17.8	1.02	21.3	.070	1.48	-	-	4.00	-	-	-
A1200	103525.	.335	1.996	18.0	1.03	21.5	.065	1.39	-	-	4.00	-	-	-
A1201	103526.	.402	1.996	18.1	1.04	21.7	.062	1.35	-	-	4.00	-	-	-
A1202	103525.	.469	1.996	18.1	1.04	21.7	.061	1.33	-	-	4.00	-	-	-
A1203	103525.	.536	1.996	18.0	1.04	21.6	.060	1.29	-	-	4.00	-	-	-
A1204	103525.	.603	1.996	17.8	1.02	21.3	.055	1.18	-	-	4.00	-	-	-
A1205	103525.	.670	1.996	17.5	1.01	21.0	.054	1.14	-	-	4.00	-	-	-
A1206	103525.	.737	1.996	17.4	1.00	20.8	.053	1.10	-	-	4.00	-	-	-
A1207	103525.	.804	1.996	17.3	1.00	20.7	.050	1.04	-	-	4.00	-	-	-
A1208	103525.	.871	1.996	17.3	1.00	20.8	.051	1.05	-	-	4.00	-	-	-
A1209	103525.	.938	1.996	17.5	1.01	21.0	.052	1.10	-	-	4.00	-	-	-
A1210	103525.	1.005	1.996	17.7	1.02	21.3	.057	1.21	-	-	4.00	-	-	-
A1211	103525.	1.072	1.996	18.1	1.04	21.7	.058	1.25	-	-	4.00	-	-	-
A1212	103525.	1.139	1.996	18.3	1.05	21.9	.062	1.37	-	-	4.00	-	-	-
A1213	103525.	1.206	1.996	18.5	1.06	22.2	.063	1.39	-	-	4.00	-	-	-
A1214	103525.	1.273	1.996	18.3	1.06	22.0	.071	1.56	-	-	4.00	-	-	-
A1215	103525.	1.340	1.996	18.2	1.05	21.8	.076	1.65	-	-	4.00	-	-	-
A1216	103525.	1.407	1.996	18.0	1.04	21.6	.074	1.60	-	-	4.00	-	-	-
A1217	103525.	1.474	1.996	18.0	1.04	21.6	.073	1.58	-	-	4.00	-	-	-
A1218	103525.	1.474	1.986	15.2	.87	18.2	.088	1.60	-	-	4.00	-	-	-
A1219	103525.	1.407	1.986	15.3	.88	18.3	.087	1.59	-	-	4.00	-	-	-
A1220	103525.	1.340	1.986	15.4	.89	18.5	.080	1.48	-	-	4.00	-	-	-
A1221	103525.	1.273	1.986	15.5	.89	18.6	.076	1.41	-	-	4.00	-	-	-
A1222	103525.	1.206	1.986	15.6	.90	18.7	.074	1.39	-	-	4.00	-	-	-
A1223	103525.	1.139	1.986	15.5	.89	18.5	.068	1.26	-	-	4.00	-	-	-
A1224	103525.	1.072	1.986	15.2	.88	18.2	.074	1.34	-	-	4.00	-	-	-
A1225	103525.	1.005	1.986	14.9	.86	17.9	.070	1.25	-	-	4.00	-	-	-
A1226	103525.	.938	1.986	14.8	.85	17.7	.063	1.11	-	-	4.00	-	-	-
A1227	103525.	.871	1.986	14.6	.84	17.5	.063	1.10	-	-	4.00	-	-	-
A1228	103525.	.804	1.986	14.7	.85	17.6	.062	1.09	-	-	4.00	-	-	-

HYDRAULIC DIAMETER, D = .539 INCHES. AVERAGE VELOCITY, U = 17.4 FT/SEC, U^* = .834 FT/SEC.

* QUESTIONABLE DATA POINT. - NO DATA POINT.

TABLE 8-1 (CONT.). TABULATION OF EXPERIMENTAL DATA.

CHANNEL A, CORNER AND WALL CHANNEL MAP, 3/16 INCH GAP SPACING.

RUN	REYNOLDS NUMBER	Z IN.	Y IN.	$\bar{U}$ FT/SEC	$\bar{U}/U$	$\bar{U}/U^*$	$u'/\bar{U}$	u'/U^*	$v'/\bar{U}$	v'/U^*	CUTOFF KHZ	A/D	CURVE FIT F(HZ)	CURVE FIT σ
A1229	103525.	.737	1.986	14.7	.85	17.6	.066	1.16	-	-	9.00	-	-	-
A1230	103525.	.670	1.986	14.9	.86	17.8	.066	1.22	-	-	9.00	-	-	-
A1231	103525.	.603	1.986	15.1	.87	18.1	.067	1.21	-	-	9.00	-	-	-
A1232	103525.	.536	1.986	15.3	.88	18.3	.068	1.25	-	-	9.00	-	-	-
A1233	103525.	.469	1.986	15.4	.89	18.5	.071	1.32	-	-	9.00	-	-	-
A1234	103525.	.402	1.986	15.4	.89	18.5	.076	1.41	-	-	9.00	-	-	-
A1235	103525.	.335	1.986	15.3	.88	18.3	.077	1.41	-	-	9.00	-	-	-
A1236	103525.	.268	1.986	15.1	.87	18.2	.079	1.43	-	-	9.00	-	-	-
A1237	103525.	.201	1.986	15.2	.87	18.2	.083	1.51	-	-	9.00	-	-	-
A1238	103525.	.134	1.986	15.2	.87	18.2	.073	1.34	-	-	9.00	-	-	-
A1239	103525.	.067	1.986	14.6	.84	17.5	.069	1.20	-	-	9.00	-	-	-
A1240	103525.	.838	1.921	18.1	1.04	21.7	.040	.88	-	-	9.00	-	-	-
A1241	103525.	.836	1.936	17.8	1.03	21.4	.045	.97	-	-	9.00	-	-	-
A1242	103525.	.838	1.951	17.4	1.00	20.8	.050	1.03	-	-	9.00	-	-	-
A1243	103525.	.838	1.966	16.6	.95	19.8	.060	1.19	-	-	9.00	-	-	-
A1244	103525.	.838	1.981	15.5	.89	18.5	.065	1.21	-	-	9.00	-	-	-
A1245	103525.	.838	1.996	13.7	.79	16.4	.067	1.10	-	-	9.00	-	-	-
A1246	103525.	.838	1.891	18.0	1.04	21.6	.041	.89	-	-	9.00	-	-	-
A1247	103525.	.838	1.876	17.6	1.02	21.1	.046	.98	-	-	9.00	-	-	-
A1248	103525.	.838	1.861	17.1	.98	20.4	.051	1.03	-	-	9.00	-	-	-
A1249	103525.	.838	1.846	16.1	.93	19.4	.058	1.13	-	-	9.00	-	-	-
A1250	103525.	.838	1.831	15.1	.87	18.1	.061	1.10	-	-	9.00	-	-	-
A1251	103525.	.838	1.821	13.5	.78	16.2	.073	1.18	-	-	9.00	-	-	-

CHANNEL A, WALL AND INTERIOR CHANNEL MAP, 1/8 INCH GAP SPACING.

RUN	REYNOLDS NUMBER	Z IN.	Y IN.	$\bar{U}$ FT/SEC	$\bar{U}/U$	$\bar{U}/U^*$	$u'/\bar{U}$	u'/U^*	$v'/\bar{U}$	v'/U^*	CUTOFF KHZ	A/D	CURVE FIT F(HZ)	CURVE FIT σ
A1252	103525.	.034	.625	15.0	.90	18.7	.101	1.89	-	-	9.00	.52	12.	.029
A1253	103525.	.101	.625	18.6	1.07	22.3	.071	1.58	-	-	9.00	.58	22.	.023
A1254	103525.	.168	.625	20.2	1.16	24.2	.056	1.36	-	-	9.00	.51	59.	.027
A1255	103525.	.235	.625	21.1	1.21	25.3	.046	1.16	-	-	9.00	.55	37.	.020
A1256	103525.	.302	.625	21.3	1.23	25.6	.050	1.29	-	-	9.00	.69	0.	.026
A1257	103525.	.369	.625	21.0	1.21	25.1	.069	1.74	-	-	9.00	.55	61.	.030
A1258	103525.	.436	.625	20.2	1.16	24.2	.086	2.08	-	-	9.00	.91	69.	.015
A1259	103525.	.503	.625	19.2	1.10	23.0	.103	2.36	-	-	9.00	.32	79.	.032
A1260	103525.	.570	.625	18.0	1.04	21.6	.106	2.29	-	-	9.00	.25	76.	.010
A1261	103525.	.637	.625	17.0	.98	20.4	.107	2.19	-	-	9.00	.30	71.	.094
A1262	103525.	.704	.625	16.0	.92	19.1	.094	1.80	-	-	9.00	.30	72.	.019
A1263	103525.	.771	.625	15.5	.89	18.6	.086	1.60	-	-	9.00	.53	41.	.022
A1264	103525.	.838	.625	15.4	.89	18.5	.081	1.50	-	-	9.00	.70	0.	.040
A1265	103525.	.905	.625	15.8	.91	18.9	.084	1.59	-	-	9.00	.99	58.	.022
A1266	103525.	.972	.625	16.5	.95	19.8	.093	1.85	-	-	9.00	.27	75.	.016
A1267	103525.	1.039	.625	17.4	1.00	20.9	.093	1.94	-	-	9.00	.25	77.	.031
A1268	103525.	1.106	.625	18.4	1.06	22.1	.092	2.03	-	-	9.00	.29	75.	.031
A1269	103525.	1.173	.625	19.5	1.12	23.3	.081	1.89	-	-	9.00	.38	73.	.040
A1270	103525.	1.240	.625	20.4	1.17	24.4	.073	1.77	-	-	9.00	.45	71.	.043
A1271	103525.	1.307	.625	21.1	1.22	25.3	.066	1.66	-	-	9.00	.59	54.	.038
A1272	103525.	1.374	.625	21.6	1.24	25.9	.055	1.43	-	-	9.00	.62	0.	.025
A1273	103525.	1.441	.625	21.8	1.25	26.1	.049	1.27	-	-	9.00	.60	0.	.033
A1274	103525.	1.508	.625	21.5	1.24	25.7	.055	1.42	-	-	9.00	.63	0.	.028
A1275	103525.	1.575	.625	20.9	1.20	25.1	.064	1.61	-	-	9.00	.60	38.	.030
A1276	103525.	1.642	.625	20.2	1.16	24.2	.068	1.65	-	-	9.00	.50	65.	.049
A1277	103525.	1.709	.625	19.5	1.12	23.4	.072	1.68	-	-	9.00	.51	61.	.036
A1278	103525.	1.776	.625	18.8	1.08	22.5	.078	1.75	-	-	9.00	.45	63.	.035
A1279	103525.	1.843	.625	18.0	1.04	21.6	.079	1.70	-	-	9.00	.91	63.	.030
A1280	103525.	1.910	.625	17.2	.99	20.6	.082	1.69	-	-	9.00	.45	59.	.023
A1281	103525.	1.977	.625	16.6	.96	19.9	.077	1.53	-	-	9.00	.49	54.	.021
A1282	103525.	2.044	.625	16.3	.94	19.5	.069	1.34	-	-	9.00	.64	0.	.019
A1283	103525.	2.078	.625	16.3	.94	19.5	.066	1.29	-	-	9.00	.60	0.	.026
A1284	103525.	2.078	.615	16.1	.93	19.3	.068	1.31	-	-	9.00	-	-	-
A1285	103525.	2.078	.605	15.7	.90	18.8	.071	1.34	-	-	9.00	-	-	-
A1286	103525.	2.078	.595	15.2	.87	18.2	.072	1.31	-	-	9.00	-	-	-
A1287	103525.	2.078	.585	14.3	.82	17.1	.078	1.34	-	-	9.00	-	-	-
A1288	103525.	2.078	.635	16.3	.94	19.6	.064	1.26	-	-	9.00	-	-	-
A1289	103525.	2.078	.645	16.3	.94	19.5	.066	1.28	-	-	9.00	-	-	-
A1290	103525.	2.078	.655	16.0	.92	19.1	.066	1.26	-	-	9.00	-	-	-
A1291	103525.	2.078	.665	15.4	.89	18.4	.068	1.25	-	-	9.00	-	-	-

HYDRAULIC DIAMETER, D = .589 INCHES. AVERAGE VELOCITY, U = 17.4 FT/SEC. U^* = .834 FT/SEC.

* QUESTIONABLE DATA POINT. - NO DATA POINT.

TABLE B-1 (CONT.). TABULATION OF EXPERIMENTAL DATA.

CHANNEL A: WALL AND INTERIOR CHANNEL MAP. 1/8 INCH GAP SPACING.

RUN	REYNOLDS NUMBER	Z IN.	Y IN.	$\bar{U}$ FT/SEC	$\bar{U}/U$	$\bar{U}/U^*$	$u/\bar{U}$	u/U^*	$v/\bar{U}$	v/U^*	CUTOFF KHZ	A/D	CURVE FIT F(KHZ)	σ
A1292	103525.	.804	.615	15.9	.89	16.5	.079	1.46	-	-	9.00	-	-	-
A1293	103525.	.804	.605	14.9	.86	17.9	.065	1.53	-	-	9.00	-	-	-
A1294	103525.	.804	.595	14.1	.81	16.9	.065	1.43	-	-	9.00	-	-	-
A1295	103525.	.804	.585	12.8	.74	15.3	.081	1.25	-	-	9.00	-	-	-
A1296	103525.	.804	.635	15.9	.88	18.9	.076	1.40	-	-	9.00	-	-	-
A1297	103525.	.804	.645	14.8	.85	17.8	.082	1.46	-	-	9.00	-	-	-
A1298	103525.	.804	.655	14.0	.81	16.8	.077	1.29	-	-	9.00	-	-	-
A1299	103525.	.804	.665	12.5	.72	15.0	.078	1.16	-	-	9.00	-	-	-
A1300	103525.	.804	.625	15.6	.90	18.7	.077	1.43	-	-	9.00	.71	0.	.037
A1301	103525.	.804	.600	15.7	.90	18.8	.097	1.82	-	-	9.00	-	-	-
A1302	103525.	.101	.600	18.7	1.08	22.4	.070	1.57	-	-	9.00	-	-	-
A1303	103525.	.168	.600	20.3	1.17	24.3	.057	1.38	-	-	9.00	-	-	-
A1304	103525.	.235	.600	21.2	1.22	25.4	.046	1.17	-	-	9.00	-	-	-
A1305	103525.	.302	.600	21.3	1.23	25.6	.048	1.22	-	-	9.00	-	-	-
A1306	103525.	.369	.600	21.0	1.21	25.2	.063	1.60	-	-	9.00	-	-	-
A1307	103525.	.436	.600	20.2	1.16	24.2	.080	1.94	-	-	9.00	-	-	-
A1308	103525.	.503	.600	19.1	1.10	22.9	.095	2.17	-	-	9.00	-	-	-
A1309	103525.	.570	.600	17.8	1.03	21.4	.096	2.10	-	-	9.00	-	-	-
A1310	103525.	.637	.600	16.5	.95	19.8	.107	2.12	-	-	9.00	-	-	-
A1311	103525.	.704	.600	15.4	.89	18.5	.098	1.82	-	-	9.00	-	-	-
A1312	103525.	.771	.600	14.7	.85	17.7	.086	1.52	-	-	9.00	-	-	-
A1313	103525.	.838	.600	14.7	.85	17.7	.084	1.49	-	-	9.00	-	-	-
A1314	103525.	.905	.600	15.3	.88	18.4	.094	1.72	-	-	9.00	-	-	-
A1315	103525.	.972	.600	16.4	.94	19.6	.097	1.90	-	-	9.00	-	-	-
A1316	103525.	1.039	.600	17.5	1.01	21.0	.095	1.99	-	-	9.00	-	-	-
A1317	103525.	1.106	.600	18.6	1.07	22.3	.089	1.99	-	-	9.00	-	-	-
A1318	103525.	1.173	.600	19.5	1.13	23.4	.083	1.94	-	-	9.00	-	-	-
A1319	103525.	1.240	.600	20.4	1.18	24.5	.077	1.87	-	-	9.00	-	-	-
A1320	103525.	1.307	.600	21.2	1.22	25.4	.064	1.62	-	-	9.00	-	-	-
A1321	103525.	1.374	.600	21.8	1.25	26.1	.055	1.43	-	-	9.00	-	-	-
A1322	103525.	1.441	.600	21.9	1.26	26.3	.062	1.63	-	-	9.00	-	-	-
A1323	103525.	1.508	.600	21.6	1.24	25.9	.056	1.46	-	-	9.00	-	-	-
A1324*	103525.	1.508	.575	20.8	1.20	24.9	.065	1.61	-	-	9.00	-	-	-
A1325*	103525.	1.441	.575	20.3	1.17	24.4	.088	2.15	-	-	9.00	-	-	-
A1326*	103525.	1.374	.575	20.5	1.18	24.5	.076	1.86	-	-	9.00	-	-	-
A1327*	103525.	1.307	.575	19.3	1.11	23.2	.124	2.87	-	-	9.00	-	-	-
A1328*	103525.	1.240	.575	19.8	1.14	23.7	.075	1.79	-	-	9.00	-	-	-
A1329	103525.	1.173	.575	19.1	1.10	22.9	.090	2.06	-	-	9.00	-	-	-
A1330	103525.	1.106	.575	18.1	1.04	21.7	.095	2.05	-	-	9.00	-	-	-
A1331	103525.	1.039	.575	17.0	.98	20.3	.101	2.05	-	-	9.00	-	-	-
A1332	103525.	.972	.575	15.2	.87	18.2	.104	1.89	-	-	9.00	-	-	-
A1333	103525.	.905	.575	13.2	.76	15.8	.098	1.55	-	-	9.00	-	-	-
A1334	103525.	.838	.575	10.9	.63	13.0	.094	1.23	-	-	9.00	-	-	-
A1335*	103525.	.771	.575	9.9	.57	11.8	.111	1.31	-	-	9.00	-	-	-
A1336	103525.	.704	.575	12.8	.74	15.3	.099	1.51	-	-	9.00	-	-	-
A1337	103525.	.637	.575	14.9	.86	17.9	.107	1.92	-	-	9.00	-	-	-
A1338	103525.	.570	.575	17.0	.98	20.4	.106	2.17	-	-	9.00	-	-	-
A1339	103525.	.503	.575	18.6	1.07	22.3	.089	1.99	-	-	9.00	-	-	-
A1340	103525.	.436	.575	19.9	1.15	23.9	.079	1.88	-	-	9.00	-	-	-
A1341	103525.	.369	.575	20.8	1.20	25.0	.063	1.57	-	-	9.00	-	-	-
A1342	103525.	.302	.575	21.3	1.22	25.5	.051	1.29	-	-	9.00	-	-	-
A1343	103525.	.235	.575	21.1	1.22	25.3	.049	1.12	-	-	9.00	-	-	-
A1344	103525.	.168	.575	20.2	1.16	24.2	.055	1.34	-	-	9.00	-	-	-
A1345	103525.	.101	.575	18.7	1.08	22.4	.069	1.55	-	-	9.00	-	-	-
A1346	103525.	.034	.575	15.7	.90	18.8	.103	1.93	-	-	9.00	-	-	-
A1347	103525.	.034	.650	16.0	.92	19.2	.093	1.79	-	-	9.00	-	-	-
A1348	103525.	.101	.650	18.9	1.09	22.7	.067	1.52	-	-	9.00	-	-	-
A1349	103525.	.168	.650	20.4	1.18	24.5	.056	1.38	-	-	9.00	-	-	-
A1350	103525.	.235	.650	21.3	1.23	25.6	.046	1.17	-	-	9.00	-	-	-
A1351	103525.	.302	.650	21.6	1.24	25.9	.047	1.21	-	-	9.00	-	-	-
A1352	103525.	.369	.650	21.1	1.22	25.3	.067	1.69	-	-	9.00	-	-	-
A1353	103525.	.436	.650	20.3	1.17	24.3	.088	2.19	-	-	9.00	-	-	-
A1354	103525.	.503	.650	19.2	1.11	23.0	.092	2.11	-	-	9.00	-	-	-
A1355	103525.	.570	.650	17.9	1.03	21.5	.101	2.16	-	-	9.00	-	-	-
A1356	103525.	.637	.650	16.6	.96	19.9	.105	2.10	-	-	9.00	-	-	-
A1357	103525.	.704	.650	15.5	.90	18.6	.099	1.84	-	-	9.00	-	-	-
A1358	103525.	.771	.650	14.9	.86	17.9	.084	1.60	-	-	9.00	-	-	-
A1359	103525.	.838	.650	14.9	.86	17.8	.085	1.62	-	-	9.00	-	-	-
A1360	103525.	.905	.650	15.5	.89	18.6	.087	1.62	-	-	9.00	-	-	-
A1361	103525.	.972	.650	16.5	.95	19.7	.098	1.93	-	-	9.00	-	-	-
A1362*	103525.	1.039	.650	17.7	1.02	21.2	.085	1.81	-	-	9.00	-	-	-
A1363	103525.	1.106	.650	18.7	1.08	22.4	.089	1.99	-	-	9.00	-	-	-
A1364	103525.	1.173	.650	19.7	1.13	23.6	.082	1.94	-	-	9.00	-	-	-
A1365	103525.	1.240	.650	20.6	1.19	24.7	.072	1.78	-	-	9.00	-	-	-
A1366	103525.	1.307	.650	21.4	1.23	25.6	.062	1.59	-	-	9.00	-	-	-
A1367	103525.	1.374	.650	21.9	1.26	26.3	.053	1.39	-	-	9.00	-	-	-
A1368	103525.	1.441	.650	22.1	1.27	26.5	.050	1.32	-	-	9.00	-	-	-
A1369	103525.	1.508	.650	21.8	1.26	26.1	.052	1.37	-	-	9.00	-	-	-
A1370	103525.	1.508	.675	21.7	1.25	26.0	.052	1.35	-	-	9.00	-	-	-
A1371	103525.	1.441	.675	22.0	1.27	26.4	.047	1.24	-	-	9.00	-	-	-

HYDRAULIC DIAMETER, D = .589 INCHES. AVERAGE VELOCITY, U = 17.4 FT/SEC. U^* = .834 FT/SEC.

* QUESTIONABLE DATA POINT. - NO DATA POINT.

TABLE B-1 (CONT.). TABULATION OF EXPERIMENTAL DATA.

CHANNEL A, WALL AND INTERIOR CHANNEL MAP, 1/8 INCH GAP SPACING.

RUN	REYNOLDS NUMBER	Z IN.	Y IN.	$\bar{U}$ FT/SEC	$\bar{U}/U$	$\bar{U}/U^*$	$u'/\bar{U}$	u'/U^*	$v'/\bar{U}$	v'/U^*	CUTOFF KHZ	Λ/D	CURVE FIT F(HZ)	CURVE FIT σ
A1372	103525.	1.374	.675	21.9	1.26	26.2	.051	1.34	-	-	9.00	-	-	-
A1373	103525.	1.307	.675	21.9	1.23	25.6	.059	1.52	-	-	9.00	-	-	-
A1374	103525.	1.240	.675	20.6	1.19	24.7	.069	1.70	-	-	9.00	-	-	-
A1375	103525.	1.173	.675	19.7	1.13	23.6	.080	1.89	-	-	9.00	-	-	-
A1376	103525.	1.106	.675	18.5	1.07	22.2	.082	1.82	-	-	9.00	-	-	-
A1377	103525.	1.039	.675	17.2	.99	20.6	.089	1.82	-	-	9.00	-	-	-
A1378	103525.	.972	.675	15.9	.89	18.5	.098	1.81	-	-	9.00	-	-	-
A1379	103525.	.905	.675	13.9	.77	16.1	.092	1.47	-	-	9.00	-	-	-
A1380	103525.	.838	.675	10.9	.63	13.0	.099	1.30	-	-	9.00	-	-	-
A1381	103525.	.771	.675	8.2	.47	9.8	.117	1.15	-	-	9.00	-	-	-
A1382	103525.	.704	.675	11.9	.68	14.2	.101	1.43	-	-	9.00	-	-	-
A1383	103525.	.637	.675	14.9	.83	17.3	.103	1.79	-	-	9.00	-	-	-
A1384	103525.	.570	.675	16.6	.96	19.9	.102	2.02	-	-	9.00	-	-	-
A1385	103525.	.503	.675	18.3	1.06	22.0	.090	1.97	-	-	9.00	-	-	-
A1386	103525.	.436	.675	19.7	1.14	23.6	.086	2.03	-	-	9.00	-	-	-
A1387	103525.	.369	.675	20.8	1.20	25.0	.067	1.66	-	-	9.00	-	-	-
A1388	103525.	.302	.675	21.4	1.23	25.7	.048	1.22	-	-	9.00	-	-	-
A1389	103525.	.235	.675	21.4	1.23	25.6	.043	1.10	-	-	9.00	-	-	-
A1390	103525.	.168	.675	20.7	1.19	24.8	.049	1.22	-	-	9.00	-	-	-
A1391	103525.	.101	.675	19.3	1.11	23.2	.073	1.68	-	-	9.00	-	-	-
A1392	103525.	.034	.675	16.9	.97	20.2	.094	1.90	-	-	9.00	-	-	-

CHANNEL A, WALL AND INTERIOR CENTERLINE TRAVERSES, 1/8 INCH GAP SPACING.

RUN	REYNOLDS NUMBER	Z IN.	Y IN.	$\bar{U}$ FT/SEC	$\bar{U}/U$	$\bar{U}/U^*$	$u'/\bar{U}$	u'/U^*	$v'/\bar{U}$	v'/U^*	CUTOFF KHZ	Λ/D	CURVE FIT F(HZ)	CURVE FIT σ
A1393	212132.	.049	.622	18.2	1.05	23.5	.101	2.37	-	-	9.00	.56	51.	.016
A1394	215039.	.136	.622	20.9	1.20	27.1	.063	1.71	-	-	9.00	.61	49.	.028
A1395	215039.	.202	.622	22.1	1.28	28.7	.049	1.42	-	-	9.00	.63	0.	.025
A1396	212132.	.269	.622	22.6	1.30	29.2	.051	1.48	-	-	9.00	.69	0.	.027
A1397	212132.	.336	.625	22.3	1.28	28.8	.072	2.08	-	-	9.00	.79	31.	.033
A1398	212132.	.402	.625	21.3	1.23	27.5	.108	2.96	-	-	9.00	.56	60.	.038
A1399	212132.	.469	.625	19.9	1.15	25.7	.130	3.39	-	-	9.00	.41	65.	.020
A1400	212132.	.536	.625	18.3	1.06	23.7	.159	3.77	-	-	9.00	.32	68.	.019
A1401	212132.	.602	.625	16.9	.97	21.8	.152	3.31	-	-	9.00	.22	71.	.015
A1402	212132.	.669	.625	15.6	.90	20.2	.151	3.06	-	-	9.00	.23	70.	.012
A1403	212132.	.735	.625	14.9	.86	19.2	.129	2.49	-	-	9.00	.36	62.	.027
A1404	212132.	.802	.625	14.5	.84	18.7	.108	2.02	-	-	9.00	.59	16.	.029
A1405	212132.	.869	.625	14.5	.83	18.7	.104	1.94	-	-	9.00	.61	0.	.037
A1406	212132.	.935	.625	14.8	.85	19.2	.106	2.04	-	-	9.00	.42	57.	.011
A1407	212132.	1.002	.625	15.5	.89	20.1	.121	2.43	-	-	9.00	.26	71.	.015
A1408	212132.	1.069	.625	16.4	.96	21.5	.115	2.46	-	-	9.00	.27	71.	.022
A1409	212132.	1.135	.625	17.7	1.02	22.8	.116	2.64	-	-	9.00	.29	71.	.033
A1410	212132.	1.202	.625	18.7	1.08	24.2	.100	2.43	-	-	9.00	.35	73.	.048
A1411	212132.	1.268	.625	19.7	1.13	25.4	.092	2.33	-	-	9.00	.43	70.	.040
A1412	212132.	1.335	.625	20.6	1.19	26.6	.080	2.13	-	-	9.00	.49	67.	.050
A1413	212132.	1.402	.625	21.2	1.22	27.4	.071	1.95	-	-	9.00	.52	36.	.031
A1414	212132.	1.468	.625	21.3	1.23	27.6	.065	1.78	-	-	9.00	.49	0.	.035
A1415	212132.	1.535	.625	21.0	1.21	27.2	.069	1.87	-	-	9.00	.56	35.	.040
A1416	212132.	1.602	.625	20.3	1.17	26.2	.083	2.19	-	-	9.00	.50	69.	.045
A1417	212132.	1.668	.625	19.5	1.12	25.2	.091	2.30	-	-	9.00	.47	66.	.045
A1418	212132.	1.735	.625	18.7	1.08	2 .2	.094	2.27	-	-	9.00	.44	65.	.046
A1419	212132.	1.801	.625	17.8	1.03	23.0	.102	2.39	-	-	9.00	.39	65.	.047
A1420	212132.	1.868	.625	16.9	.97	21.8	.104	2.26	-	-	9.00	.37	63.	.032
A1421	212132.	1.935	.625	16.1	.93	20.8	.103	2.19	-	-	9.00	.40	60.	.023
A1422	212132.	2.001	.625	15.5	.89	20.0	.092	1.89	-	-	9.00	.50	47.	.012
A1423	212132.	2.068	.625	15.2	.87	19.6	.092	1.80	-	-	9.00	.52	0.	.022
A1424	212132.	2.068	.615	14.7	.85	19.0	.096	1.83	-	-	9.00	-	-	-
A1425	212132.	2.068	.605	14.2	.82	18.3	.100	1.84	-	-	9.00	-	-	-
A1426	212132.	2.068	.595	13.3	.77	17.2	.104	1.82	-	-	9.00	-	-	-
A1427	212132.	2.068	.587	12.2	.70	15.7	.111	1.75	-	-	9.00	-	-	-
A1428	212132.	2.066	.635	15.4	.89	19.9	.083	1.65	-	-	9.00	-	-	-
A1429	212132.	2.068	.645	15.3	.88	19.8	.089	1.67	-	-	9.00	-	-	-
A1430	212132.	2.068	.655	15.1	.87	19.6	.082	1.61	-	-	9.00	-	-	-
A1431	212132.	2.068	.663	14.4	.84	18.8	.095	1.80	-	-	9.00	-	-	-
A1432	212132.	.835	.635	13.9	.80	18.0	.105	1.89	-	-	9.00	-	-	-
A1433	212132.	.835	.645	13.0	.75	16.9	.113	1.90	-	-	9.00	-	-	-
A1434	212132.	.835	.655	11.5	.66	14.9	.109	1.62	-	-	9.00	-	-	-
A1435	212132.	.835	.663	8.6	.50	11.2	.144	1.61	-	-	9.00	*	-	-
A1436	212132.	.835	.615	14.1	.81	18.2	.111	2.02	-	-	9.00	-	-	-
A1437	212132.	.835	.605	13.5	.78	17.5	.111	1.94	-	-	9.00	-	-	-
A1438	212132.	.835	.595	12.5	.72	16.2	.113	1.77	-	-	9.00	-	-	-
A1439	212132.	.835	.587	10.8	.62	14.0	.131	1.84	-	-	9.00	-	-	-

HYDRAULIC DIAMETER, D = .589 INCHES. AVERAGE VELOCITY, U = 17.4 FT/SEC, U^* = .773 FT/SEC.
* QUESTIONABLE DATA POINT. - NO DATA POINT.

TABLE B-1 (CONT.). TABULATION OF EXPERIMENTAL DATA.

CHANNEL A. CORNER AND WALL CENTERLINE TRAVERSES, 3/16 INCH GAP SPACING.

RUN	REYNOLDS NUMBER	Z IN.	Y IN.	$\bar{U}$ FT/SEC	$\bar{U}/U$	$\bar{U}/U^*$	$v/\bar{U}$	v/U^*	CUTOFF KHZ	Λ/D	CURVE FIT (HZ)	σ
A1490	212132.	.833	1.936	18.3	1.08	24.3	.058	1.40	-	-	4.00	-	-	-
A1491	212132.	.833	1.921	18.2	1.05	23.6	.069	1.62	-	-	4.00	-	-	-
A1492	212132.	.833	1.936	17.4	1.00	22.5	.079	1.78	-	-	4.00	-	-	-
A1493	212132.	.833	1.951	16.3	.94	21.1	.095	2.01	-	-	4.00	-	-	-
A1494	212132.	.833	1.966	14.7	.85	19.1	.108	2.06	-	-	4.00	-	-	-
A1495	212132.	.833	1.981	12.2	.70	15.8	.121	1.91	-	-	4.00	-	-	-
A1496	212132.	.833	1.891	19.1	1.10	24.7	.052	1.28	-	-	4.00	-	-	-
A1497	212132.	.833	1.876	19.2	1.11	24.8	.048	1.18	-	-	4.00	-	-	-
A1498	212132.	.833	1.861	19.0	1.09	24.5	.048	1.17	-	-	4.00	-	-	-
A1499	212132.	.833	1.846	18.3	1.05	23.7	.052	1.24	-	-	4.00	-	-	-
A1450	212132.	.833	1.831	17.1	.99	22.1	.058	1.28	-	-	4.00	-	-	-
A1451	212132.	2.065	1.921	17.3	1.00	22.4	.067	1.51	-	-	4.00	-	-	-
A1452	212132.	2.065	1.936	16.7	.96	21.5	.075	1.62	-	-	4.00	-	-	-
A1453	212132.	2.065	1.951	15.6	.90	20.2	.091	1.84	-	-	4.00	-	-	-
A1454	212132.	2.065	1.966	14.1	.81	18.3	.100	1.83	-	-	4.00	-	-	-
A1455	212132.	2.065	1.981	11.6	.67	15.0	.109	1.63	-	-	4.00	-	-	-
A1456	212132.	2.065	1.891	18.0	1.04	23.3	.055	1.29	-	-	4.00	-	-	-
A1457	212132.	2.065	1.876	18.0	1.04	23.2	.050	1.16	-	-	4.00	-	-	-
A1458	212132.	2.065	1.861	17.6	1.01	22.7	.056	1.27	-	-	4.00	-	-	-
A1459	212132.	2.065	1.846	16.8	.97	21.7	.059	1.29	-	-	4.00	-	-	-
A1460	212132.	2.065	1.831	15.2	.88	19.7	.062	1.22	-	-	4.00	-	-	-
A1461	212132.	2.065	1.906	17.8	1.03	23.1	.060	1.38	-	-	4.00	.47	49.	.046
A1462	212132.	1.999	1.906	18.0	1.04	23.3	.068	1.58	-	-	4.00	.53	52.	.058
A1463	212132.	1.932	1.906	18.5	1.06	23.9	.072	1.73	-	-	4.00	.53	57.	.059
A1464	212132.	1.865	1.906	19.1	1.10	24.7	.074	1.83	-	-	4.00	.55	56.	.050
A1465	212132.	1.799	1.906	19.8	1.14	25.7	.065	1.68	-	-	4.00	.55	58.	.051
A1466	212132.	1.732	1.906	20.5	1.18	26.5	.070	1.84	-	-	4.00	.56	59.	.054
A1467	212132.	1.665	1.906	21.1	1.22	27.3	.064	1.74	-	-	4.00	.59	55.	.043
A1468	212132.	1.599	1.906	21.5	1.24	27.8	.063	1.74	-	-	4.00	.61	54.	.050
A1469	212132.	1.532	1.906	21.7	1.25	28.0	.060	1.69	-	-	4.00	.54	53.	.049
A1470	212132.	1.466	1.906	21.6	1.25	28.0	.062	1.73	-	-	4.00	.51	55.	.042
A1471	212132.	1.399	1.906	21.6	1.24	27.9	.063	1.76	-	-	4.00	.54	49.	.039
A1472	212132.	1.332	1.906	21.6	1.24	27.9	.062	1.74	-	-	4.00	.49	61.	.040
A1473	212132.	1.266	1.906	21.6	1.24	27.9	.055	1.55	-	-	4.00	.49	48.	.048
A1474	212132.	1.199	1.906	21.3	1.22	27.5	.058	1.59	-	-	4.00	.57	48.	.049
A1475	212132.	1.133	1.906	20.7	1.19	26.8	.062	1.67	-	-	4.00	.58	53.	.054
A1476	212132.	1.066	1.906	20.1	1.16	26.0	.065	1.70	-	-	4.00	.61	51.	.047
A1477	212132.	.999	1.906	19.6	1.12	25.2	.067	1.70	-	-	4.00	.57	51.	.051
A1478	212132.	.933	1.906	19.1	1.10	24.7	.063	1.55	-	-	4.00	.60	30.	.038
A1479	212132.	.866	1.906	18.8	1.09	24.4	.060	1.47	-	-	4.00	.58	0.	.035
A1480	212132.	.799	1.906	18.7	1.08	24.2	.061	1.47	-	-	4.00	.54	0.	.039
A1481	212132.	.733	1.906	18.9	1.09	24.4	.062	1.51	-	-	4.00	.52	0.	.038
A1482	212132.	.666	1.906	19.4	1.11	25.0	.060	1.51	-	-	4.00	.58	0.	.039
A1483	212132.	.600	1.906	20.0	1.15	25.9	.061	1.58	-	-	4.00	.63	0.	.053
A1484	212132.	.533	1.906	20.6	1.20	26.9	.060	1.62	-	-	4.00	.72	0.	.098
A1485	212132.	.466	1.906	21.6	1.24	27.9	.052	1.44	-	-	4.00	.64	0.	.053
A1486	212132.	.400	1.906	22.1	1.27	28.5	.050	1.43	-	-	4.00	.57	0.	.059
A1487	212132.	.333	1.906	22.4	1.29	29.0	.051	1.47	-	-	4.00	.51	0.	.035
A1488	212132.	.266	1.906	22.5	1.30	29.1	.052	1.51	-	-	4.00	.49	0.	.041
A1489	212132.	.200	1.906	22.5	1.30	29.1	.054	1.57	-	-	4.00	.55	0.	.051
A1490	212132.	.133	1.906	22.2	1.28	28.8	.055	1.59	-	-	4.00	.47	0.	.031
A1491	212132.	.067	1.906	20.3	1.17	26.3	.076	2.00	-	-	4.00	.38	0.	.035

CHANNEL A. INTERIOR CHANNEL TRAVERSE, 1/8 INCH GAP SPACING

RUN	REYNOLDS NUMBER	Z IN.	Y IN.	$\bar{U}$ FT/SEC	$\bar{U}/U$	$\bar{U}/U^*$	$v/\bar{U}$	v/U^*	CUTOFF KHZ	Λ/D	CURVE FIT (HZ)	σ
A1492	103525.	.054	.625	16.9	.94	19.6	.097	1.90	-	-	4.00	.65	9.	.020
A1493	103525.	.122	.625	19.0	1.10	22.8	.072	1.65	-	-	4.00	.82	0.	.020
A1494	103525.	.188	.625	20.9	1.21	25.1	.056	1.41	-	-	4.00	.87	0.	.022
A1495	103525.	.255	.625	22.2	1.28	26.6	.044	1.16	-	-	4.00	.82	0.	.029
A1496	103525.	.322	.625	22.9	1.32	27.4	.035	.95	-	-	4.00	.86	0.	.030
A1497	103525.	.390	.625	22.9	1.32	27.4	.040	1.11	-	-	4.00	.81	35.	.028
A1498	103525.	.457	.625	22.4	1.29	26.8	.053	1.41	-	-	4.00	.63	57.	.007
A1499	103525.	.523	.625	21.6	1.24	25.8	.070	1.80	-	-	4.00	.54	59.	.007
A1500	103525.	.591	.625	20.7	1.19	24.8	.072	1.78	-	-	4.00	.67	50.	.022
A1501	103525.	.658	.625	19.7	1.13	23.6	.077	1.82	-	-	4.00	.46	63.	.026
A1502	103525.	.724	.625	18.8	1.08	22.5	.077	1.74	-	-	4.00	.48	60.	.029
A1503	103525.	.789	.625	18.1	1.04	21.7	.070	1.52	-	-	4.00	.55	53.	.019
A1504	103525.	.858	.625	17.6	1.02	21.1	.061	1.28	-	-	4.00	.75	21.	.009
A1505	103525.	.925	.625	17.7	1.02	21.3	.058	1.22	-	-	4.00	.69	20.	.021
A1506	103525.	.992	.625	18.2	1.05	21.8	.067	1.46	-	-	4.00	.51	58.	.011
A1507	103525.	1.060	.625	19.0	1.09	22.8	.071	1.62	-	-	4.00	.44	64.	.006
A1508	103525.	1.126	.625	19.9	1.14	23.8	.071	1.69	-	-	4.00	.45	66.	.006
A1509	103525.	1.193	.625	20.8	1.20	24.9	.066	1.69	-	-	4.00	.49	66.	.015
A1510	103525.	1.259	.625	21.5	1.24	25.8	.063	1.63	-	-	4.00	.56	61.	.012
A1511	103525.	1.327	.625	22.3	1.28	26.7	.057	1.54	-	-	4.00	.61	59.	.029
A1512	103525.	1.394	.625	23.0	1.33	27.6	.047	1.31	-	-	4.00	.70	44.	.032
A1513	103525.	1.462	.625	23.4	1.35	28.1	.043	1.19	-	-	4.00	.69	0.	.026
A1514	103525.	1.527	.625	23.4	1.35	28.1	.042	1.17	-	-	4.00	.74	0.	.035

HYDRAULIC DIAMETER, D = .569 INCHES. AVERAGE VELOCITY, U = 17.4 FT/SEC. U^* = .839 FT/SEC.
* QUESTIONABLE DATA POINT. - NO DATA POINT.

TABLE B-1 (CONT.). TABULATION OF EXPERIMENTAL DATA.

CHANNEL A, INTERIOR CHANNEL TRAVERSE, 1/8 INCH GAP SPACING.

RUN	REYNOLDS NUMBER	Z IN.	Y IN.	$\bar{U}$ FT/SEC	$\bar{U}/U$	$\bar{U}/U^*$	$U/\bar{U}$	U/U^*	$v/\bar{U}$	v/U^*	CUTOFF KHZ	Λ/D	CURVE FIT F(HZ)	σ
A1515	103525.	1.595	.625	23.1	1.33	27.7	.049	1.35	-	-	4.00	.76	0.	.026
A1516	103525.	1.662	.625	22.5	1.30	27.0	.055	1.46	-	-	4.00	.69	46.	.040
A1517	103525.	1.729	.625	21.8	1.26	26.1	.061	1.59	-	-	4.00	.64	55.	.027
A1518	103525.	1.796	.625	21.0	1.21	25.2	.068	1.71	-	-	4.00	.57	58.	.025
A1519	103525.	1.863	.625	20.1	1.16	24.1	.073	1.77	-	-	4.00	.54	54.	.012
A1520	103525.	1.931	.625	19.2	1.11	23.0	.079	1.82	-	-	4.00	.48	56.	.005
A1521	103525.	1.997	.625	18.3	1.05	21.9	.082	1.80	-	-	4.00	.50	53.	.009
A1522	103525.	2.064	.625	17.7	1.02	21.2	.073	1.54	-	-	4.00	.61	46.	.005
A1523	103525.	2.133	.625	17.3	1.00	20.8	.061	1.27	-	-	4.00	.80	28.	.015
A1524	103525.	2.200	.625	17.4	1.00	20.8	.061	1.26	-	-	4.00	.80	0.	.031
A1525	103525.	2.119	1.906	17.3	1.00	20.8	.035	.73	-	-	4.00	.60	0.	.028
A1526	103525.	1.984	1.906	18.0	1.03	21.5	.047	1.02	-	-	4.00	.71	41.	.035
A1527	103525.	1.848	1.906	19.1	1.10	22.9	.050	1.15	-	-	4.00	.74	42.	.032
A1528	103525.	1.714	1.906	19.9	1.14	23.8	.050	1.19	-	-	4.00	.70	35.	.038
A1529	103525.	1.583	1.906	20.0	1.15	24.0	.054	1.31	-	-	4.00	.74	0.	.018
A1530	103525.	1.448	1.906	19.9	1.15	23.9	.057	1.37	-	-	4.00	.76	0.	.021
A1531	103525.	1.314	1.906	19.9	1.15	23.8	.054	1.28	-	-	4.00	.73	1.	.023
A1532	103525.	1.180	1.906	19.2	1.10	23.0	.049	1.13	-	-	4.00	.74	33.	.033
A1533	103525.	1.048	1.906	17.9	1.03	21.5	.046	.98	-	-	4.00	.62	46.	.027
A1534	103525.	.915	1.906	17.1	.99	20.5	.033	.67	-	-	4.00	.54	0.	.022
A1535	103525.	.777	1.906	17.4	1.00	20.9	.037	.77	-	-	4.00	.64	30.	.038
A1536	103525.	.646	1.906	18.5	1.07	22.2	.042	.94	-	-	4.00	.68	42.	.035
A1537	103525.	.508	1.906	19.4	1.12	23.3	.041	.96	-	-	4.00	.69	0.	.033
A1538	103525.	.373	1.906	19.7	1.14	23.7	.046	1.09	-	-	4.00	.77	0.	.025
A1539	103525.	.241	1.906	19.9	1.15	23.9	.042	1.01	-	-	4.00	.60	0.	.033
A1540	103525.	.107	1.906	17.4	1.00	20.9	.055	1.15	-	-	4.00	.46	0.	.020

CHANNEL A, WALL CHANNEL TRAVERSE, 3/16 INCH GAP SPACING.

RUN	REYNOLDS NUMBER	Z IN.	Y IN.	$\bar{U}$ FT/SEC	$\bar{U}/U$	$\bar{U}/U^*$	$U/\bar{U}$	U/U^*	$v/\bar{U}$	v/U^*	CUTOFF KHZ	Λ/D	CURVE FIT F(HZ)	σ
A1541	220871.	.065	1.906	16.1	.93	21.0	.087	1.82	-	-	4.00	.34	0.	.020
A1542	220871.	.198	1.906	19.4	1.12	25.3	.046	1.17	-	-	4.00	.64	0.	.027
A1543	220871.	.334	1.906	19.3	1.11	25.1	.049	1.23	-	-	4.00	.67	0.	.036
A1544	220871.	.463	1.906	19.3	1.11	25.0	.042	1.06	-	-	4.00	.67	0.	.033
A1545	220871.	.597	1.906	18.5	1.07	24.1	.043	1.09	-	-	4.00	.74	39.	.033
A1546	220871.	.730	1.906	17.5	1.01	22.7	.043	.96	-	-	4.00	.67	40.	.032
A1547	220871.	.870	1.906	16.8	.97	21.8	.035	.76	-	-	4.00	.54	0.	.028
A1548	220871.	1.009	1.906	17.3	1.00	22.5	.046	1.03	-	-	4.00	.66	42.	.032
A1549	220871.	1.137	1.906	18.5	1.07	24.0	.051	1.23	-	-	4.00	.76	35.	.028
A1550	220871.	1.269	1.906	19.4	1.12	25.2	.052	1.30	-	-	4.00	.73	0.	.030
A1551	220871.	1.398	1.906	19.7	1.13	25.6	.055	1.41	-	-	4.00	.72	0.	.026
A1552	220871.	1.534	1.906	19.8	1.14	25.7	.055	1.41	-	-	4.00	.72	0.	.028
A1553	220871.	1.661	1.906	19.7	1.14	25.6	.052	1.33	-	-	4.00	.71	0.	.027
A1554	220871.	1.801	1.906	19.2	1.11	24.9	.050	1.25	-	-	4.00	.84	39.	.035
A1555	220871.	1.932	1.906	18.2	1.05	23.6	.051	1.20	-	-	4.00	.73	41.	.032
A1556	220871.	2.067	1.906	17.3	1.00	22.5	.041	.93	-	-	4.00	.77	19.	.017
A1557	220871.	2.200	1.906	17.2	.99	22.4	.041	.92	-	-	4.00	.64	0.	.019

CHANNEL A, INTERIOR CHANNEL TRAVERSE, 1/8 INCH GAP SPACING

RUN	REYNOLDS NUMBER	Z IN.	Y IN.	$\bar{U}$ FT/SEC	$\bar{U}/U$	$\bar{U}/U^*$	$U/\bar{U}$	U/U^*	$v/\bar{U}$	v/U^*	CUTOFF KHZ	Λ/D	CURVE FIT F(HZ)	σ
A1558	220871.	2.197	.625	16.4	.94	21.3	.063	1.39	-	-	4.00	.71	0.	.010
A1559	220871.	2.058	.625	16.3	.94	21.2	.070	1.47	-	-	4.00	.64	41.	.016
A1560	220871.	1.928	.625	18.4	1.06	23.8	.075	1.79	-	-	4.00	.59	48.	.010
A1561	220871.	1.799	.625	20.2	1.17	26.3	.070	1.83	-	-	4.00	.60	54.	.028
A1562	220871.	1.665	.625	21.8	1.26	28.3	.055	1.55	-	-	4.00	.66	46.	.023
A1563	220871.	1.530	.625	22.7	1.31	29.4	.041	1.21	-	-	4.00	.68	0.	.025
A1564	220871.	1.405	.625	22.4	1.29	29.0	.047	1.37	-	-	4.00	.72	27.	.012
A1565	220871.	1.269	.625	21.0	1.21	27.3	.060	1.63	-	-	4.00	.57	59.	.022
A1566	220871.	1.129	.625	19.2	1.11	24.9	.073	1.73	-	-	4.00	.52	59.	.019
A1567	220871.	.997	.625	16.7	.96	21.7	.073	1.58	-	-	4.00	.52	52.	.021
A1568	220871.	.868	.625	14.8	.85	19.2	.063	1.20	-	-	4.00	.68	0.	.011
A1569	220871.	.732	.625	16.2	.94	21.1	.074	1.55	-	-	4.00	.49	52.	.019
A1570	220871.	.599	.625	19.3	1.11	25.0	.075	1.86	-	-	4.00	.59	53.	.020
A1571	220871.	.459	.625	21.6	1.24	28.0	.055	1.55	-	-	4.00	.62	53.	.031
A1572	220871.	.330	.625	22.5	1.30	29.2	.035	1.03	-	-	4.00	.59	0.	.028
A1573	220871.	.202	.625	21.3	1.23	27.7	.048	1.32	-	-	4.00	.69	0.	.023
A1574	220871.	.069	.625	17.3	1.00	22.5	.091	2.09	-	-	4.00	.60	0.	.022

HYDRAULIC DIAMETER, D = .589 INCHES. AVERAGE VELOCITY, U = 17.4 FT/SEC. U^* = .773 FT/SEC.
* QUESTIONABLE DATA POINT. - NO DATA POINT.

TABLE B-1 (CONT.). TABULATION OF EXPERIMENTAL DATA.

CHANNEL B, INTERIOR CHANNEL TRAVERSE, 1/4 INCH GAP SPACING.

RUN	REYNOLDS NUMBER	Z IN.	Y IN.	$\bar{U}$ FT/SEC	$\bar{U}/U$	$\bar{U}/U^*$	$v/\bar{U}$	u/U^*	$v/\bar{U}$	v/U^*	CUTOFF KHZ	A/D	CURVE FIT F(HZ)	σ
B 1	103010.	.630	.625	22.9	1.38	29.5	.034	1.01	-	-	10.00	-	-	-
B 2	103010.	.630	.625	22.8	1.37	29.4	.034	.99	-	-	5.00	-	-	-
B 3	103010.	.630	.625	22.8	1.37	29.4	.031	.90	-	-	2.00	-	-	-
B 4	103010.	.630	.625	22.8	1.37	29.4	.029	.85	-	-	1.00	-	-	-
B 5	100010.	.026	.625	14.2	.86	18.3	.117	2.15	-	-	1.00	-	-	-
B 6	100010.	.093	.625	17.8	1.07	22.9	.063	1.44	-	-	1.00	.91	0.	.026
B 7	100010.	.160	.625	19.4	1.16	24.9	.045	1.13	-	-	1.00	-	-	-
B 8	100010.	.227	.625	20.1	1.21	25.9	.044	1.15	-	-	1.00	.99	0.	.022
B 9	100010.	.294	.625	20.7	1.25	26.7	.043	1.14	-	-	1.00	-	-	-
B 10	100010.	.361	.625	21.3	1.28	27.4	.042	1.14	-	-	1.00	.99	0.	.009
B 11	100010.	.428	.625	21.8	1.31	28.1	.039	1.08	-	-	1.00	-	-	-
B 12	100010.	.495	.625	22.2	1.34	28.7	.035	1.01	-	-	1.00	.90	0.	.021
B 13	100010.	.562	.625	22.6	1.36	29.1	.031	.91	-	-	1.00	-	-	-
B 14	103010.	.630	.625	22.8	1.37	29.4	.029	.86	-	-	1.00	.38	0.	.021
B 15	100010.	.697	.625	22.6	1.36	29.2	.033	.95	-	-	1.00	-	-	-
B 16	100010.	.764	.625	22.3	1.34	28.7	.037	1.07	-	-	1.00	.39	0.	.021
B 17	10001C.	.831	.625	21.7	1.31	28.0	.043	1.19	-	-	1.00	-	-	-
B 18	100010.	.898	.625	21.2	1.28	27.4	.043	1.19	-	-	1.00	.92	0.	.012
B 19	100010.	.965	.625	20.7	1.25	26.7	.046	1.23	-	-	1.00	-	-	-
B 20	100010.	1.032	.625	20.2	1.21	26.0	.048	1.25	-	-	1.00	.95	0.	.025
B 21	103010.	1.099	.625	19.6	1.18	25.2	.046	1.16	-	-	1.00	-	-	-
B 22	100010.	1.167	.625	18.2	1.09	23.5	.060	1.41	-	-	1.00	.34	0.	.029
B 23	100010.	1.234	.625	14.6	.88	18.9	.125	2.36	-	-	1.00	-	-	-

CHANNEL B, CENTER GAP TRAVERSE, 1/4 INCH GAP SPACING.

RUN	REYNOLDS NUMBER	Z IN.	Y IN.	$\bar{U}$ FT/SEC	$\bar{U}/U$	$\bar{U}/U^*$	$v/\bar{U}$	u/U^*	$v/\bar{U}$	v/U^*	CUTOFF KHZ	A/D	CURVE FIT F(HZ)	σ
B 24	101329.	.690	.000	18.8	1.13	24.2	.042	1.01	-	-	10.00	-	-	-
B 25	101329.	.690	.000	18.8	1.13	24.2	.041	.99	-	-	5.00	-	-	-
B 26	101329.	.690	.000	18.8	1.13	24.2	.038	.93	-	-	2.00	-	-	-
B 27	101329.	.690	.000	18.8	1.13	24.2	.036	.87	-	-	1.00	-	-	-
B 28	101329.	.690	.000	18.8	1.13	24.2	.042	1.01	-	-	7.00	-	-	-
B 29	101329.	.690	.000	18.8	1.13	24.2	.040	.98	-	-	9.00	-	-	-
B 30	101329.	.690	.000	18.8	1.13	24.2	.039	.95	-	-	3.00	-	-	-
B 31	101329.	.690	.000	18.8	1.13	24.2	.036	.88	-	-	1.00	-	-	-
B 32	101329.	.518	.000	16.1	.97	20.8	.076	1.58	-	-	1.00	-	-	-
B 33	101329.	.532	.000	16.6	1.00	21.5	.068	1.47	-	-	1.00	-	-	-
B 34	101329.	.545	.000	17.2	1.03	22.2	.061	1.35	-	-	1.00	.99	0.	.016
B 35	101329.	.558	.000	17.6	1.06	22.8	.055	1.25	-	-	1.00	-	-	-
B 36	101329.	.585	.000	18.3	1.10	23.7	.045	1.07	-	-	1.00	.99	0.	.019
B 37	101329.	.612	.000	18.7	1.13	24.2	.037	.89	-	-	1.00	-	-	-
B 38	101329.	.639	.000	18.8	1.13	24.3	.037	.90	-	-	1.00	.91	0.	.031
B 39	101329.	.666	.000	18.6	1.12	24.0	.041	.99	-	-	1.00	.92	0.	.021
B 40	101329.	.693	.000	18.0	1.08	23.2	.052	1.21	-	-	1.00	-	-	-
B 41	101329.	.719	.000	17.2	1.04	22.2	.062	1.37	-	-	1.00	.38	0.	.024
B 42	101329.	.733	.000	16.7	1.00	21.6	.073	1.58	-	-	1.00	-	-	-
B 43	101329.	.746	.000	16.2	.97	20.9	.079	1.65	-	-	1.00	.29	0.	.025
B 44*	100010.	.760	.000	15.8	.95	20.4	.089	1.81	-	-	1.00	-	-	-
B 45*	100010.	.760	.000	15.8	.95	20.4	.108	2.20	-	-	6.00	-	-	-
B 46	100010.	.746	.000	16.2	.97	20.8	.097	2.02	-	-	6.00	.32	0.	.039
B 47	100010.	.733	.000	16.6	1.00	21.4	.083	1.78	-	-	6.00	-	-	-
B 48	100010.	.720	.000	17.1	1.03	22.1	.072	1.58	-	-	6.00	.37	0.	.029
B 49	100010.	.693	.000	18.0	1.08	23.3	.056	1.29	-	-	6.00	-	-	-
B 50	100010.	.666	.000	18.6	1.12	24.0	.045	1.08	-	-	6.00	.37	0.	.022
B 51	100010.	.639	.000	18.8	1.13	24.3	.041	1.00	-	-	6.00	.39	0.	.024
B 52	100010.	.612	.000	18.8	1.13	24.2	.043	1.04	-	-	6.00	-	-	-
B 53	100010.	.585	.000	18.4	1.11	23.7	.048	1.15	-	-	6.00	.53	0.	.009
B 54	100010.	.558	.000	17.7	1.07	22.9	.059	1.35	-	-	6.00	-	-	-
B 55	100010.	.545	.000	17.3	1.04	22.3	.069	1.54	-	-	6.00	.91	0.	.035

HYDRAULIC DIAMETER, D = .759 INCHES. AVERAGE VELOCITY, U = 16.6 FT/SEC, U^* = .776 FT/SEC.
* QUESTIONABLE DATA POINT. - NO DATA POINT.

TABLE B-1 (CONT.). TABULATION OF EXPERIMENTAL DATA.

CHANNEL B, INTERIOR CHANNEL MAP, 1/4 INCH GAP SPACING.

RUN	REYNOLDS NUMBER	Z IN.	Y IN.	$\bar{U}$ FT/SEC	$\bar{U}/U$	$\bar{U}/U^*$	$u'/\bar{U}$	u'/U^*	$v'/\bar{U}$	v'/U^*	CUTOFF KHZ	Λ/D	CURVE F(HZ)	FIT σ
B 56	100010.	.502	.007	16.8	1.01	21.7	.076	1.64	-	-	6.00	-	-	-
B 57	100010.	.489	.007	16.3	.98	21.0	.080	1.68	-	-	6.00	-	-	-
B 58	100010.	.026	.510	11.6	.70	15.0	.152	2.29	-	-	6.00	-	-	-
B 59	100010.	.093	.510	13.4	.81	17.3	.093	1.62	-	-	6.00	.37	0.	.027
B 60	100010.	.160	.510	15.6	.94	20.2	.086	1.73	-	-	6.00	-	-	-
B 61	100010.	.227	.510	17.5	1.05	22.5	.081	1.82	-	-	6.00	.51	0.	.026
B 62	100010.	.294	.510	18.8	1.13	24.3	.077	1.87	-	-	6.00	-	-	-
B 63	100010.	.361	.510	19.8	1.19	25.5	.073	1.86	-	-	6.00	.53	0.	.035
B 64	100010.	.428	.510	20.6	1.24	26.6	.063	1.69	-	-	6.00	-	-	-
B 65	100010.	.495	.510	21.5	1.29	27.7	.051	1.42	-	-	6.00	.37	0.	.022
B 66	100010.	.562	.510	22.1	1.33	28.4	.048	1.37	-	-	6.00	-	-	-
B 67	100010.	.630	.510	22.4	1.35	28.9	.040	1.16	-	-	6.00	.34	47.	.035
B 68	100010.	.630	.565	22.7	1.37	29.3	.035	1.03	-	-	6.00	-	-	-
B 69	100010.	.562	.565	22.4	1.35	28.9	.039	1.12	-	-	6.00	.38	0.	.018
B 70	100010.	.495	.565	21.9	1.32	28.3	.047	1.33	-	-	6.00	-	-	-
B 71	100010.	.428	.565	21.4	1.28	27.5	.052	1.43	-	-	6.00	.55	0.	.011
B 72	100010.	.361	.565	20.7	1.25	26.7	.057	1.53	-	-	6.00	-	-	-
B 73	100010.	.294	.565	20.2	1.21	26.0	.058	1.51	-	-	6.00	.41	0.	.028
B 74	100010.	.227	.565	19.4	1.17	25.0	.062	1.54	-	-	6.00	-	-	-
B 75	100010.	.160	.565	18.5	1.11	23.8	.069	1.63	-	-	6.00	.42	0.	.026
B 76	100010.	.093	.565	17.2	1.04	22.2	.072	1.61	-	-	6.00	-	-	-
B 77	100010.	.026	.565	14.9	.90	19.2	.110	2.12	-	-	6.00	.32	0.	.029
B 78	102656.	.629	.565	22.4	1.35	29.0	.039	1.14	-	-	6.00	-	-	-
B 79	102656.	.629	.625	22.4	1.35	29.0	.039	1.13	-	-	6.00	.36	0.	.019
B 80	102656.	.562	.625	22.4	1.35	28.9	.039	1.13	-	-	6.00	-	-	-
B 81	102656.	.495	.625	22.1	1.33	28.5	.044	1.26	-	-	6.00	.34	0.	.016
B 82	102656.	.428	.625	21.6	1.30	27.9	.048	1.35	-	-	6.00	-	-	-
B 83	102656.	.361	.625	21.1	1.27	27.3	.050	1.37	-	-	6.00	.36	0.	.020
B 84	102656.	.294	.625	20.6	1.24	26.7	.052	1.39	-	-	6.00	-	-	-
B 85	102656.	.227	.625	20.1	1.21	25.9	.056	1.45	-	-	6.00	.40	30.	.093
B 86	102656.	.160	.625	19.4	1.17	25.1	.056	1.41	-	-	6.00	-	-	-
B 87	102656.	.093	.625	18.3	1.10	23.6	.066	1.56	-	-	6.00	.34	0.	.022
B 88	102656.	.026	.625	15.0	.90	19.4	.128	2.47	-	-	6.00	-	-	-
B 89	102656.	.026	.685	15.4	.93	19.9	.106	2.11	-	-	6.00	.36	0.	.026
B 90	102656.	.093	.685	17.6	1.06	22.7	.079	1.68	-	-	6.00	-	-	-
B 91	102656.	.160	.685	18.5	1.11	23.9	.072	1.72	-	-	6.00	.45	0.	.030
B 92	102656.	.227	.685	19.4	1.16	25.0	.067	1.69	-	-	6.00	-	-	-
B 93	102656.	.294	.685	20.1	1.21	26.0	.063	1.64	-	-	6.00	.33	0.	.029
B 94	102656.	.361	.685	20.7	1.25	26.8	.061	1.63	-	-	6.00	-	-	-
B 95	102656.	.428	.685	21.3	1.28	27.6	.053	1.47	-	-	6.00	.43	0.	.029
B 96	102656.	.495	.685	21.8	1.31	28.2	.049	1.38	-	-	6.00	-	-	-
B 97	102656.	.562	.685	22.2	1.34	28.7	.041	1.18	-	-	6.00	.40	0.	.013
B 98	102656.	.629	.685	22.3	1.34	28.8	.043	1.22	-	-	6.00	-	-	-
B 99	102656.	.629	.740	21.9	1.32	28.3	.046	1.29	-	-	6.00	.37	0.	.020
B100	102656.	.562	.740	21.8	1.31	28.1	.048	1.35	-	-	6.00	-	-	-
B101	102656.	.495	.740	21.3	1.28	27.5	.057	1.58	-	-	6.00	.48	0.	.018
B102	102656.	.428	.740	20.6	1.24	26.7	.067	1.78	-	-	6.00	-	-	-
B103	102656.	.361	.740	19.9	1.20	25.7	.076	1.96	-	-	6.00	.55	0.	.034
B104	102656.	.294	.740	19.0	1.14	24.6	.082	2.00	-	-	6.00	-	-	-
B105	102656.	.227	.740	17.8	1.07	23.1	.088	2.04	-	-	6.00	.37	0.	.030
B106	102656.	.160	.740	16.3	.98	21.1	.096	2.03	-	-	6.00	.35	0.	.020
B107	102656.	.093	.740	14.7	.88	19.0	.105	2.00	-	-	6.00	-	-	-
B108	102656.	.026	.740	13.3	.80	17.1	.118	2.02	-	-	6.00	.78	0.	.037

CHANNEL B, SIDE GAP TRAVERSE, 1/4 INCH GAP SPACING.

RUN	REYNOLDS NUMBER	Z IN.	Y IN.	$\bar{U}$ FT/SEC	$\bar{U}/U$	$\bar{U}/U^*$	$u'/\bar{U}$	u'/U^*	$v'/\bar{U}$	v'/U^*	CUTOFF KHZ	Λ/D	CURVE F(HZ)	FIT σ
B109	102656.	.506	1.330	14.7	.88	18.9	.108	2.05	-	-	6.00	-	-	-
B110	102656.	.519	1.330	15.2	.91	19.7	.097	1.90	-	-	6.00	-	-	-
B111	102656.	.533	1.330	15.9	.96	20.6	.082	1.69	-	-	6.00	.29	0.	.024
B112	102656.	.560	1.330	17.0	1.03	22.0	.069	1.51	-	-	6.00	-	-	-
B113	102656.	.587	1.330	17.8	1.07	23.0	.055	1.27	-	-	6.00	.40	0.	.020
B114	102656.	.607	1.330	18.1	1.09	23.4	.048	1.12	-	-	6.00	-	-	-
B115	102656.	.627	1.330	18.4	1.10	23.7	.045	1.06	-	-	6.00	.30	0.	.029
B116	102656.	.654	1.330	18.2	1.09	23.5	.048	1.12	-	-	6.00	.33	0.	.043
B117	102656.	.680	1.330	17.7	1.07	22.9	.060	1.37	-	-	6.00	-	-	-
B118	102656.	.707	1.330	16.9	1.02	21.9	.073	1.60	-	-	6.00	.34	0.	.024
B119	102656.	.721	1.330	16.3	.98	21.0	.085	1.79	-	-	6.00	-	-	-
B120	102656.	.734	1.330	15.6	.94	20.2	.095	1.91	-	-	6.00	.29	0.	.029
B121	102656.	.748	1.330	15.0	.93	19.5	.112	2.19	-	-	6.00	-	-	-

HYDRAULIC DIAMETER, D = .759 INCHES. AVERAGE VELOCITY, U = 16.6 FT/SEC. U^* = .773 FT/SEC.
* QUESTIONABLE DATA POINT. - NO DATA POINT.

TABLE B-1 (CONT.). TABULATION OF EXPERIMENTAL DATA.

CHANNEL B, SIDE CHANNEL MAP, 1/4 INCH GAP SPACING.

RUN	REYNOLDS NUMBER	Z IN.	Y IN.	$\bar{U}$ FT/SEC	$\bar{U}/U$	$\bar{U}/U^*$	$u'/\bar{U}$	u'/U^*	$v'/\bar{U}$	v'/U^*	CUTOFF KHZ	A/D	CURVE FIT F(HZ)	CURVE FIT σ
B122	103990.	.627	1.755	19.6	1.18	25.9	.034	.97	-	-	9.00	.39	0.	.029
B123	103990.	.560	1.755	19.9	1.17	25.1	.040	1.02	-	-	9.00	-	-	-
B124	103990.	.493	1.755	18.9	1.19	24.5	.045	1.10	-	-	9.00	.33	0.	.013
B125	103990.	.425	1.755	18.2	1.10	23.6	.051	1.21	-	-	9.00	-	-	-
B126	103990.	.358	1.755	17.3	1.09	22.3	.061	1.37	-	-	9.00	.96	0.	.022
B127	103990.	.291	1.755	16.0	.96	20.8	.066	1.38	-	-	9.00	-	-	-
B128	103990.	.224	1.755	14.5	.87	18.8	.077	1.46	-	-	9.00	.90	0.	.023
B129	103990.	.157	1.755	13.1	.79	16.9	.081	1.37	-	-	9.00	-	-	-
B130	103990.	.090	1.755	11.7	.70	15.1	.083	1.22	-	-	9.00	.22	0.	.031
B131	103990.	.023	1.755	10.2	.61	13.1	.125	1.69	-	-	9.00	-	-	-
B132	103990.	.023	1.815	11.2	.67	14.5	.125	1.81	-	-	9.00	-	-	-
B133	103990.	.090	1.815	13.9	.83	17.9	.076	1.36	-	-	9.00	-	-	-
B134	103990.	.157	1.815	15.3	.92	19.8	.061	1.20	-	-	9.00	.29	0.	.016
B135	103990.	.224	1.815	16.2	.98	21.0	.059	1.23	-	-	9.00	-	-	-
B136	103990.	.291	1.815	17.1	1.03	22.2	.052	1.16	-	-	9.00	.33	0.	.020
B137	103990.	.358	1.815	17.9	1.07	23.1	.050	1.15	-	-	9.00	-	-	-
B138	103990.	.425	1.815	18.4	1.11	23.8	.047	1.11	-	-	9.00	.36	0.	.019
B139	103990.	.493	1.815	18.7	1.12	24.2	.049	1.19	-	-	9.00	-	-	-
B140	103990.	.560	1.815	18.8	1.13	24.4	.054	1.32	-	-	9.00	.47	0.	.047
B141	103990.	.627	1.815	19.0	1.19	24.6	.051	1.25	-	-	9.00	-	-	-
B142	103990.	.627	1.875	17.8	1.07	23.1	.062	1.43	-	-	9.00	.45	0.	.038
B143	103990.	.560	1.875	17.7	1.06	22.9	.064	1.46	-	-	9.00	-	-	-
B144	103990.	.493	1.875	17.6	1.06	22.8	.063	1.43	-	-	9.00	.63	0.	.029
B145	103990.	.425	1.875	17.6	1.06	22.8	.057	1.29	-	-	9.00	-	-	-
B146	103990.	.358	1.875	17.3	1.04	22.4	.055	1.29	-	-	9.00	.96	0.	.041
B147	103990.	.291	1.875	16.8	1.01	21.8	.055	1.21	-	-	9.00	-	-	-
B148	103990.	.224	1.875	16.3	.98	21.1	.053	1.13	-	-	9.00	.39	0.	.025
B149	103990.	.157	1.875	15.5	.94	20.1	.053	1.07	-	-	9.00	-	-	-
B150	103990.	.090	1.875	13.7	.83	17.8	.086	1.52	-	-	9.00	.38	0.	.025
B151	103990.	.023	1.875	10.3	.62	13.3	.137	1.83	-	-	9.00	-	-	-
B152	102656.	.627	1.875	17.8	1.07	23.0	.064	1.46	-	-	9.00	-	-	-
B153	102656.	.627	1.935	16.3	.98	21.1	.078	1.69	-	-	9.00	-	-	-
B154	102656.	.560	1.935	16.2	.97	20.9	.080	1.67	-	-	9.00	.88	0.	.012
B155	102656.	.493	1.935	16.2	.97	21.0	.078	1.64	-	-	9.00	-	-	-
B156	102656.	.425	1.935	16.2	.97	21.0	.075	1.58	-	-	9.00	.58	0.	.019
B157	102656.	.358	1.935	16.0	.96	20.7	.075	1.55	-	-	9.00	-	-	-
B158	102656.	.291	1.935	15.5	.94	20.1	.076	1.53	-	-	9.00	.32	0.	.037
B159	102656.	.224	1.935	15.0	.90	19.4	.078	1.51	-	-	9.00	-	-	-
B160	102656.	.157	1.935	14.6	.88	18.9	.077	1.46	-	-	9.00	.36	0.	.025
B161	102656.	.090	1.935	13.9	.83	17.9	.080	1.49	-	-	9.00	-	-	-
B162	102656.	.023	1.935	11.7	.71	15.2	.130	1.97	-	-	9.00	-	-	-
B163	102656.	.627	1.985	14.2	.85	18.3	.084	1.55	-	-	9.00	-	-	-
B164	102656.	.560	1.985	14.0	.84	18.1	.084	1.52	-	-	9.00	-	-	-
B165	102656.	.493	1.935	14.0	.84	18.1	.084	1.52	-	-	9.00	-	-	-
B166	102656.	.425	1.985	14.0	.84	18.1	.082	1.48	-	-	9.00	-	-	-
B167	102656.	.358	1.985	13.8	.83	17.8	.081	1.43	-	-	9.00	-	-	-
B168	102656.	.291	1.985	13.3	.80	17.1	.083	1.43	-	-	9.00	-	-	-
B169	102656.	.224	1.985	12.8	.77	16.5	.079	1.31	-	-	9.00	-	-	-
B170	102656.	.157	1.985	12.5	.75	16.1	.081	1.30	-	-	9.00	-	-	-
B171	102656.	.090	1.985	11.9	.71	15.4	.081	1.25	-	-	9.00	-	-	-
B172	102656.	.023	1.985	10.7	.64	13.8	.102	1.40	-	-	9.00	-	-	-

CHANNEL C, CENTER GAP TRAVERSE, 1/4 INCH GAP SPACING.

RUN	REYNOLDS NUMBER	Z IN.	Y IN.	$\bar{U}$ FT/SEC	$\bar{U}/U$	$\bar{U}/U^*$	$u'/\bar{U}$	u'/U^*	$v'/\bar{U}$	v'/U^*	CUTOFF KHZ	A/D	CURVE FIT F(HZ)	CURVE FIT σ
C 1*	102357.	.757	.000	17.3	.90	19.5	.099	1.93	-	-	9.00	-	-	-
C 2	102357.	.744	.000	17.9	.93	20.2	.092	1.66	-	-	9.00	-	-	-
C 3	102357.	.730	.000	18.4	.96	20.8	.073	1.53	-	-	9.00	.91	0.	.020
C 4	102357.	.717	.000	18.8	.98	21.3	.069	1.46	-	-	9.00	-	-	-
C 5	102357.	.690	.000	19.8	1.03	22.4	.051	1.13	-	-	9.00	.96	0.	.025
C 6	102357.	.663	.000	20.4	1.06	23.0	.041	.95	-	-	9.00	-	-	-
C 7	102357.	.636	.000	20.6	1.07	23.3	.036	.85	-	-	9.00	.99	0.	.041
C 8	102357.	.609	.000	20.4	1.06	23.1	.039	.89	-	-	9.00	-	-	-
C 9	102357.	.582	.000	20.0	1.04	22.6	.046	1.04	-	-	9.00	.98	0.	.037
C 10	102357.	.556	.000	19.1	1.00	21.7	.056	1.22	-	-	9.00	-	-	-
C 11	102357.	.542	.000	18.6	.97	21.1	.064	1.35	-	-	9.00	.45	0.	.020
C 12	102357.	.529	.000	18.1	.94	20.5	.071	1.45	-	-	9.00	-	-	-
C 13	102357.	.515	.000	17.5	.91	19.8	.079	1.58	-	-	9.00	.35	0.	.020

HYDRAULIC DIAMETER, D = .056 INCHES. AVERAGE VELOCITY, U = 19.2 FT/SEC. U^* = .883 FT/SEC.

* QUESTIONABLE DATA POINT. - NO DATA POINT.

TABLE B-1 (CONT.). TABULATION OF EXPERIMENTAL DATA.

CHANNEL C, SIDE GAP TRAVERSE, 1/4 INCH GAP SPACING.

RUN	REYNOLDS NUMBER	Z IN.	Y IN.	$\bar{U}$ FT/SEC	$\bar{U}/U$	$\bar{U}/U^*$	$u/\bar{U}$	u/U^*	$v/\bar{U}$	v/U^*	CUTOFF KHZ	Λ/D	CURVE FIT F(HZ)	σ
C 14	102357.	.511	1.250	17.2	.90	19.5	.089	1.73	-	-	4.00	.34	0.	.021
C 15	102357.	.525	1.250	17.9	.93	20.3	.078	1.58	-	-	4.00	-	-	-
C 16	102357.	.538	1.250	18.6	.97	21.1	.068	1.43	-	-	4.00	.49	0.	.009
C 17	102357.	.552	1.250	19.2	1.00	21.7	.059	1.26	-	-	4.00	-	-	-
C 18	102357.	.578	1.250	20.1	1.05	22.7	.049	1.12	-	-	4.00	.44	0.	.015
C 19	102357.	.605	1.250	20.7	1.08	23.4	.042	.98	-	-	4.00	-	-	-
C 20	102357.	.632	1.250	20.9	1.09	23.6	.037	.87	-	-	4.00	.51	0.	.032
C 21	102357.	.659	1.250	20.7	1.08	23.4	.041	.97	-	-	4.00	-	-	-
C 22	102357.	.686	1.250	20.1	1.05	22.8	.048	1.10	-	-	4.00	.46	0.	.022
C 23	102357.	.713	1.250	19.2	1.00	21.7	.066	1.43	-	-	4.00	-	-	-
C 24	102357.	.726	1.250	18.7	.97	21.1	.071	1.50	-	-	4.00	.36	0.	.026
C 25	102357.	.740	1.250	18.1	.94	20.5	.083	1.70	-	-	4.00	-	-	-
C 26*	102357.	.753	1.250	17.6	.92	19.9	.094	1.87	-	-	4.00	-	-	-

CHANNEL C, INTERIOR CHANNEL MAP. 1/4 INCH GAP SPACING.

RUN	REYNOLDS NUMBER	Z IN.	Y IN.	$\bar{U}$ FT/SEC	$\bar{U}/U$	$\bar{U}/U^*$	$u/\bar{U}$	u/U^*	$v/\bar{U}$	v/U^*	CUTOFF KHZ	Λ/D	CURVE FIT F(HZ)	σ
C 27	102357.	.638	.505	24.9	1.30	28.2	.044	1.23	-	-	4.00	.38	0.	.019
C 28	102357.	.570	.505	24.4	1.27	27.6	.052	1.45	-	-	4.00	-	-	-
C 29	102357.	.503	.505	23.7	1.24	26.8	.058	1.57	-	-	4.00	.59	0.	.032
C 30	102357.	.436	.505	22.9	1.20	26.0	.065	1.69	-	-	4.00	-	-	-
C 31	102357.	.369	.505	22.1	1.15	25.0	.074	1.85	-	-	4.00	.58	0.	.020
C 32	102357.	.302	.505	21.0	1.10	23.8	.076	1.87	-	-	4.00	-	-	-
C 33	102357.	.235	.505	19.5	1.02	22.1	.084	1.86	-	-	4.00	.52	0.	.025
C 34	102357.	.168	.505	17.5	.91	19.8	.094	1.86	-	-	4.00	-	-	-
C 35	102357.	.101	.505	15.9	.83	18.0	.080	1.49	-	-	4.00	.34	0.	.026
C 36	102357.	.034	.505	15.0	.78	17.0	.115	1.96	-	-	4.00	-	-	-
C 37	102357.	.034	.565	16.6	.87	18.8	.142	2.68	-	-	4.00	.26	0.	.026
C 38	102357.	.101	.565	19.4	1.01	21.9	.074	1.63	-	-	4.00	-	-	-
C 39	102357.	.168	.565	20.9	1.09	23.7	.065	1.59	-	-	4.00	.52	0.	.015
C 40	102357.	.235	.565	21.9	1.14	24.7	.063	1.56	-	-	4.00	-	-	-
C 41	102357.	.302	.565	22.6	1.18	25.6	.060	1.53	-	-	4.00	.49	0.	.028
C 42	102357.	.369	.565	23.3	1.21	26.4	.057	1.51	-	-	4.00	-	-	-
C 43	102357.	.436	.565	23.9	1.25	27.1	.051	1.39	-	-	4.00	.57	0.	.029
C 44	102357.	.503	.565	24.5	1.28	27.8	.049	1.37	-	-	4.00	-	-	-
C 45	102357.	.570	.565	25.0	1.30	28.3	.043	1.21	-	-	4.00	.59	0.	.026
C 46	102357.	.638	.565	25.3	1.32	28.6	.039	1.13	-	-	4.00	-	-	-
C 47	102357.	1.242	.625	17.6	.92	19.9	.120	2.39	-	-	4.00	-	-	-
C 48	102357.	1.174	.625	20.7	1.08	23.4	.062	1.44	-	-	4.00	.41	0.	.032
C 49	102357.	1.107	.625	22.0	1.15	24.9	.049	1.23	-	-	4.00	-	-	-
C 50	102357.	1.040	.625	22.7	1.18	25.7	.050	1.29	-	-	4.00	.58	0.	.011
C 51	102357.	.973	.625	23.3	1.21	26.4	.050	1.31	-	-	4.00	-	-	-
C 52	102357.	.906	.625	23.8	1.24	27.0	.049	1.32	-	-	4.00	.46	0.	.019
C 53	102357.	.839	.625	24.4	1.27	27.7	.044	1.22	-	-	4.00	-	-	-
C 54	102357.	.772	.625	25.0	1.30	28.3	.040	1.19	-	-	4.00	.52	0.	.027
C 55	102357.	.705	.625	25.4	1.32	28.7	.035	1.01	-	-	4.00	-	-	-
C 56	102357.	.638	.625	25.4	1.33	28.8	.035	1.00	-	-	4.00	.60	0.	.069
C 57	102357.	.570	.625	25.2	1.32	28.6	.037	1.06	-	-	4.00	-	-	-
C 58	102357.	.503	.625	24.8	1.29	28.0	.042	1.17	-	-	4.00	.55	0.	.035
C 59	102357.	.436	.625	24.2	1.26	27.4	.043	1.19	-	-	4.00	-	-	-
C 60	102357.	.369	.625	23.7	1.23	26.8	.046	1.23	-	-	4.00	.54	0.	.023
C 61	102357.	.302	.625	23.0	1.20	26.1	.050	1.30	-	-	4.00	-	-	-
C 62	102357.	.235	.625	22.4	1.17	25.4	.048	1.21	-	-	4.00	.58	0.	.024
C 63	102357.	.168	.625	21.6	1.12	24.4	.051	1.24	-	-	4.00	-	-	-
C 64	102357.	.101	.625	19.5	1.02	22.1	.076	1.69	-	-	4.00	.43	0.	.059
C 65	102357.	.034	.625	16.0	.83	18.1	.144	2.60	-	-	4.00	-	-	-
C 66	102357.	.034	.685	16.3	.85	18.4	.119	2.19	-	-	4.00	-	-	-
C 67	102357.	.101	.685	19.1	.99	21.6	.066	1.42	-	-	4.00	-	-	-
C 68	102357.	.168	.685	20.6	1.07	23.3	.061	1.42	-	-	4.00	-	-	-
C 69	102357.	.235	.685	21.5	1.12	24.3	.063	1.52	-	-	4.00	-	-	-
C 70	102357.	.302	.685	22.3	1.16	25.3	.063	1.51	-	-	4.00	-	-	-
C 71	102357.	.369	.685	23.1	1.20	26.1	.055	1.46	-	-	4.00	-	-	-
C 72	102357.	.436	.685	23.8	1.24	27.0	.051	1.37	-	-	4.00	-	-	-
C 73	102357.	.503	.685	24.5	1.28	27.7	.045	1.24	-	-	4.00	-	-	-
C 74	102357.	.570	.685	25.1	1.31	28.4	.043	1.13	-	-	4.00	-	-	-
C 75	102357.	.638	.685	25.4	1.32	28.7	.039	.99	-	-	4.00	-	-	-
C 76	102357.	.638	.745	25.0	1.30	28.3	.037	1.04	-	-	4.00	.48	0.	.046
C 77	102357.	.570	.745	24.7	1.29	27.9	.045	1.26	-	-	4.00	.71	0.	.036
C 78	102357.	.503	.745	24.3	1.25	27.1	.050	1.35	-	-	4.00	-	-	-
C 79	102357.	.436	.745	23.0	1.20	26.1	.054	1.50	-	-	4.00	.57	0.	.025
C 80	102357.	.369	.745	22.3	1.15	24.9	.066	1.65	-	-	4.00	-	-	-
C 81	102357.	.302	.745	20.4	1.08	23.5	.075	1.76	-	-	4.00	.67	0.	.018
C 82	102357.	.235	.745	19.2	1.00	21.8	.079	1.73	-	-	4.00	-	-	-
C 83	102357.	.168	.745	17.3	.90	19.6	.082	1.61	-	-	4.00	.53	0.	.025
C 84	102357.	.101	.745	15.4	.80	17.4	.070	1.22	-	-	4.00	-	-	-
C 85	102357.	.034	.745	14.1	.73	15.9	.108	1.71	-	-	4.00	.48	0.	.022

HYDRAULIC DIAMETER, D = .656 INCHES. AVERAGE VELOCITY, U = 19.2 FT/SEC. U^* = .883 FT/SEC.
* QUESTIONABLE DATA POINT. - NO DATA POINT.

TABLE B-1 (CONT.). TABULATION OF EXPERIMENTAL DATA.

CHANNEL C, SIDE CHANNEL MAP, 1/4 GAP SPACING.

RUN	REYNOLDS NUMBER	Z IN.	Y IN.	$\bar{U}$ FT/SEC	$\bar{U}/U$	$\bar{U}/U^*$	$u/\bar{U}$	v/U^*	$v/\bar{U}$	$\overline{vv}/U^{*2}$	CUTOFF KHZ	Δ/D	CURVE FIT F(HZ)	σ
C 86	99716.	.635	1.755	22.8	1.19	25.7	.037	.99	-	-	9.00	.99	0.	.051
C 87	99718.	.568	1.755	22.6	1.18	25.5	.039	.99	-	-	9.00	-	-	-
C 88	99718.	.501	1.755	22.1	1.15	25.0	.043	1.08	-	-	9.00	.51	0.	.053
C 89	99716.	.434	1.755	21.5	1.12	24.3	.053	1.20	-	-	9.00	-	-	-
C 90	99716.	.366	1.755	20.6	1.07	23.2	.058	1.35	-	-	9.00	.99	0.	.029
C 91	99718.	.299	1.755	19.3	1.01	21.8	.071	1.55	-	-	9.00	-	-	-
C 92	99718.	.232	1.755	17.6	.92	19.8	.080	1.59	-	-	9.00	.37	0.	.029
C 93	99718.	.165	1.755	15.7	.82	17.7	.085	1.51	-	-	9.00	-	-	-
C 94	99718.	.098	1.755	14.1	.73	15.9	.084	1.33	-	-	9.00	.27	0.	.034
C 95	99718.	.031	1.755	12.4	.65	14.0	.128	1.78	-	-	9.00	-	-	-
C 96	99718.	.031	1.815	13.9	.73	15.7	.121	1.91	-	-	9.00	-	-	-
C 97	99718.	.098	1.815	17.0	.87	19.2	.070	1.35	-	-	9.00	-	-	-
C 98	99718.	.165	1.815	18.3	.95	20.7	.066	1.36	-	-	9.00	.37	0.	.019
C 99	99718.	.232	1.815	19.4	1.01	21.9	.059	1.28	-	-	9.00	-	-	-
C100	99718.	.299	1.815	20.4	1.06	23.0	.051	1.16	-	-	9.00	.99	0.	.021
C101	99718.	.366	1.815	21.2	1.10	23.9	.047	1.11	-	-	9.00	-	-	-
C102	99718.	.434	1.815	21.6	1.13	24.4	.047	1.16	-	-	9.00	.99	0.	.053
C103	99718.	.501	1.815	22.0	1.14	24.8	.048	1.18	-	-	9.00	-	-	-
C104	99718.	.568	1.815	22.2	1.16	25.0	.050	1.25	-	-	9.00	.60	0.	.050
C105	99718.	.635	1.815	22.2	1.16	25.1	.049	1.29	-	-	9.00	-	-	-
C106	99718.	.635	1.875	21.0	1.10	23.8	.062	1.48	-	-	9.00	.62	0.	.036
C107	99718.	.568	1.875	21.0	1.10	23.7	.062	1.48	-	-	9.00	-	-	-
C108	99718.	.501	1.875	20.9	1.09	23.6	.062	1.46	-	-	9.00	.99	0.	.029
C109	99716.	.434	1.875	20.8	1.08	23.5	.059	1.38	-	-	9.00	-	-	-
C110	99718.	.366	1.875	20.4	1.06	23.0	.060	1.38	-	-	9.00	.57	0.	.053
C111	99718.	.299	1.875	19.9	1.04	22.5	.060	1.35	-	-	9.00	-	-	-
C112	99718.	.232	1.875	19.4	1.01	21.9	.057	1.25	-	-	9.00	.99	0.	.034
C113	99718.	.165	1.875	18.7	.98	21.1	.054	1.14	-	-	9.00	-	-	-
C114	99718.	.098	1.875	17.0	.89	19.2	.080	1.64	-	-	9.00	.92	0.	.040
C115	99718.	.031	1.875	12.9	.67	14.6	.137	2.00	-	-	9.00	-	-	-
C116	99718.	.031	1.935	13.5	.71	15.3	.123	1.88	-	-	9.00	-	-	-
C117	99718.	.098	1.935	16.6	.87	18.8	.071	1.33	-	-	9.00	-	-	-
C118	99718.	.165	1.935	17.9	.91	19.6	.072	1.42	-	-	9.00	.97	0.	.021
C119	99718.	.232	1.935	17.6	.92	19.9	.080	1.60	-	-	9.00	-	-	-
C120	99718.	.299	1.935	18.1	.95	20.5	.079	1.62	-	-	9.00	.51	0.	.030
C121	99718.	.366	1.935	18.8	.98	21.2	.076	1.62	-	-	9.00	-	-	-
C122	99718.	.434	1.935	19.1	1.00	21.6	.079	1.70	-	-	9.00	.61	0.	.047
C123	99718.	.501	1.935	19.3	1.01	21.8	.078	1.71	-	-	9.00	-	-	-
C124	99718.	.568	1.935	19.3	1.01	21.8	.081	1.77	-	-	9.00	.70	0.	.039
C125	99718.	.635	1.935	19.4	1.01	21.9	.079	1.73	-	-	9.00	-	-	-
C126	99718.	.635	1.985	16.7	.87	18.9	.096	1.81	-	-	9.00	-	-	-
C127	99718.	.568	1.985	16.7	.87	18.9	.094	1.77	-	-	9.00	-	-	-
C128	99718.	.501	1.985	16.7	.87	18.8	.092	1.73	-	-	9.00	-	-	-
C129	99718.	.434	1.985	16.5	.86	18.6	.098	1.83	-	-	9.00	-	-	-
C130	99718.	.366	1.935	16.2	.84	18.3	.093	1.70	-	-	9.00	-	-	-
C131	99718.	.299	1.935	15.6	.81	17.6	.093	1.64	-	-	9.00	-	-	-
C132	99716.	.232	1.985	15.1	.79	17.0	.088	1.50	-	-	9.00	-	-	-
C133	99718.	.165	1.985	14.8	.77	16.7	.095	1.58	-	-	9.00	-	-	-
C134	99718.	.098	1.985	14.4	.75	16.2	.087	1.41	-	-	9.00	-	-	-
C135	99718.	.031	1.985	12.6	.66	14.2	.100	1.43	-	-	9.00	-	-	-

CHANNEL C, CENTER GAP TRAVERSE, VARIABLE CUTOFF FREQUENCY, 1/4 INCH GAP SPACING.

RUN	REYNOLDS NUMBER	Z IN.	Y IN.	$\bar{U}$ FT/SEC	$\bar{U}/U$	$\bar{U}/U^*$	$u/\bar{U}$	u/U^*	$v/\bar{U}$	v/U^*	CUTOFF KHZ	Δ/D	CURVE FIT F(HZ)	σ
C136*	101034.	.495	.000	15.8	.83	17.9	.115	2.07	-	-	10.00	-	-	-
C137*	101034.	.495	.000	15.8	.83	17.9	.110	1.97	-	-	7.00	-	-	-
C138*	101034.	.495	.000	15.8	.83	17.9	.104	1.85	-	-	4.00	-	-	-
C139*	101034.	.495	.000	15.8	.83	17.9	.093	1.66	-	-	2.00	-	-	-
C140*	101034.	.495	.000	15.8	.83	17.9	.082	1.47	-	-	1.00	-	-	-
C141*	101034.	.495	.000	15.8	.83	17.9	.072	1.29	-	-	.50	-	-	-
C142	101034.	.509	.000	16.4	.86	18.5	.101	1.87	-	-	10.00	-	-	-
C143	101034.	.509	.000	16.4	.86	18.5	.098	1.81	-	-	7.00	-	-	-
C144	101034.	.509	.000	16.4	.86	18.5	.093	1.73	-	-	4.00	-	-	-
C145	101034.	.509	.000	16.4	.86	18.5	.087	1.61	-	-	2.00	-	-	-
C146	101034.	.509	.000	16.4	.86	18.5	.082	1.52	-	-	1.00	-	-	-
C147	101034.	.509	.000	16.4	.86	18.5	.073	1.35	-	-	.50	-	-	-
C148	101034.	.536	.000	17.8	.93	20.1	.076	1.52	-	-	10.00	-	-	-
C149	101034.	.536	.000	17.8	.93	20.1	.075	1.50	-	-	7.00	-	-	-
C150	101034.	.536	.000	17.8	.93	20.1	.073	1.46	-	-	4.00	-	-	-
C151	101034.	.536	.000	17.8	.93	20.1	.068	1.37	-	-	2.00	-	-	-
C152	101034.	.536	.000	17.8	.93	20.1	.064	1.28	-	-	1.00	-	-	-
C153	101034.	.536	.000	17.8	.93	20.1	.059	1.19	-	-	.50	-	-	-
C 154	101034.	.562	.000	19.0	.99	21.4	.060	1.28	-	-	10.00	-	-	-
C 155	101034.	.562	.000	19.0	.99	21.4	.059	1.24	-	-	7.00	-	-	-
C 156	101034.	.562	.000	19.0	.99	21.4	.057	1.21	-	-	4.00	-	-	-
C 157	101034.	.562	.000	19.0	.99	21.4	.054	1.17	-	-	2.00	-	-	-
C 158	101034.	.562	.000	19.0	.99	21.4	.051	1.09	-	-	1.00	-	-	-

HYDRAULIC DIAMETER, D = .656 INCHES. AVERAGE VELOCITY, $\bar{U}$ = 19.2 FT/SEC. U^* = .885 FT/SEC.
* QUESTIONABLE DATA POINT. - NO DATA POINT.

TABLE B-1 (CONT.). TABULATION OF EXPERIMENTAL DATA.

CHANNEL C, CENTER GAP TRAVERSE, VARIABLE CUTOFF FREQUENCY, 1/4 INCH GAP SPACING.

RUN	REYNOLDS NUMBER	Z IN.	Y IN.	$\bar{U}$ FT/SEC	$\bar{U}/U$	$\bar{U}/U^*$	$u'/\bar{U}$	u'/U^*	$v'/\bar{U}$	v'/U^*	CUTOFF KHZ	Δ/D	CURVE FIT F(HZ)	σ
C 159	101034.	.562	.000	19.0	.99	21.9	.046	1.02	-	-	.50	-	-	-
C 160	101034.	.589	.000	19.7	1.03	22.3	.051	1.14	-	-	10.00	-	-	-
C 161	101034.	.589	.000	19.7	1.03	22.3	.050	1.12	-	-	7.00	-	-	-
C 162	101034.	.589	.000	19.7	1.03	22.3	.048	1.08	-	-	4.00	-	-	-
C 163	101034.	.589	.000	19.7	1.03	22.3	.046	1.03	-	-	2.00	-	-	-
C 164	101034.	.589	.030	19.7	1.03	22.3	.044	.98	-	-	1.00	-	-	-
C 165	101034.	.589	.000	19.7	1.03	22.3	.040	.89	-	-	.50	-	-	-
C 166	101034.	.616	.000	20.2	1.05	22.8	.043	.97	-	-	10.00	-	-	-
C 167	101034.	.616	.000	20.2	1.05	22.8	.043	.99	-	-	7.00	-	-	-
C 168	101034.	.616	.000	20.2	1.05	22.8	.040	.91	-	-	4.00	-	-	-
C 169	101034.	.616	.000	20.2	1.05	22.8	.037	.85	-	-	2.00	-	-	-
C 170	101034.	.616	.000	20.2	1.05	22.8	.036	.81	-	-	1.00	-	-	-
C 171	101034.	.616	.000	20.2	1.05	22.8	.032	.73	-	-	.50	-	-	-
C 172	101034.	.693	.000	20.2	1.05	22.8	.043	.97	-	-	10.00	-	-	-
C 173	101034.	.693	.000	20.2	1.05	22.8	.041	.99	-	-	7.00	-	-	-
C 174	101034.	.693	.000	20.2	1.05	22.8	.040	.91	-	-	4.00	-	-	-
C 175	101034.	.693	.000	20.2	1.05	22.8	.038	.87	-	-	2.00	-	-	-
C 176	101034.	.693	.000	20.2	1.05	22.8	.034	.78	-	-	1.00	-	-	-
C 177	101034.	.693	.000	20.2	1.05	22.8	.031	.71	-	-	.50	-	-	-
C 178	101034.	.670	.000	19.9	1.04	22.5	.049	1.10	-	-	10.00	-	-	-
C 179	101034.	.670	.000	19.9	1.04	22.5	.048	1.08	-	-	7.00	-	-	-
C 180	101034.	.670	.000	19.9	1.04	22.5	.047	1.05	-	-	4.00	-	-	-
C 181	101034.	.670	.000	19.9	1.04	22.5	.044	1.00	-	-	2.00	-	-	-
C 182	101034.	.670	.000	19.9	1.04	22.5	.042	.94	-	-	1.00	-	-	-
C 183	101034.	.670	.000	19.9	1.04	22.5	.037	.84	-	-	.50	-	-	-
C 184	101034.	.697	.000	19.1	1.00	21.6	.062	1.35	-	-	10.00	-	-	-
C 185	101034.	.697	.000	19.1	1.00	21.6	.061	1.32	-	-	7.00	-	-	-
C 186	101034.	.697	.000	19.1	1.00	21.6	.059	1.28	-	-	4.00	-	-	-
C 187	101034.	.697	.000	19.1	1.00	21.6	.056	1.21	-	-	2.00	-	-	-
C 188	101034.	.697	.000	19.1	1.00	21.6	.052	1.13	-	-	1.00	-	-	-
C 189	101034.	.697	.000	19.1	1.00	21.6	.048	1.04	-	-	.50	-	-	-
C 190	101034.	.723	.000	18.2	.95	20.5	.077	1.57	-	-	10.00	-	-	-
C 191	101034.	.723	.000	18.2	.95	20.5	.075	1.54	-	-	7.00	-	-	-
C 192	101034.	.723	.000	18.2	.95	20.5	.072	1.48	-	-	4.00	-	-	-
C 193	101034.	.723	.000	18.2	.95	20.5	.070	1.43	-	-	2.00	-	-	-
C 194	101034.	.723	.000	18.2	.95	20.5	.065	1.33	-	-	1.00	-	-	-
C 195	101034.	.723	.000	18.2	.95	20.5	.060	1.22	-	-	.50	-	-	-
C 196	101034.	.750	.000	16.8	.88	19.0	.095	1.81	-	-	10.00	-	-	-
C 197	101034.	.750	.000	16.8	.88	19.0	.093	1.77	-	-	7.00	-	-	-
C 198	101034.	.750	.000	16.8	.88	19.0	.089	1.70	-	-	4.00	-	-	-
C 199	101034.	.750	.000	16.8	.88	19.0	.082	1.55	-	-	2.00	-	-	-
C 200	101034.	.750	.000	16.8	.88	19.0	.077	1.47	-	-	1.00	-	-	-
C 201*	101034.	.769	.000	16.8	.88	19.0	.067	1.27	-	-	.50	-	-	-
C 202*	101034.	.769	.000	16.1	.84	18.2	.117	2.12	-	-	10.00	-	-	-
C 203*	101034.	.769	.000	16.1	.84	18.2	.115	2.08	-	-	7.00	-	-	-
C 204*	101034.	.769	.000	16.1	.84	18.2	.111	2.01	-	-	4.00	-	-	-
C 205*	101034.	.769	.000	16.1	.84	18.2	.100	1.83	-	-	2.00	-	-	-
C 206*	101034.	.769	.000	16.1	.84	18.2	.088	1.61	-	-	1.00	-	-	-
C 207	101034.	.769	.000	16.1	.84	18.2	.080	1.46	-	-	.50	-	-	-
C 208	101034.	.616	.000	20.2	1.05	22.8	.042	.97	-	-	10.00	.34	0.	.057
C 209	101034.	.616	.000	20.2	1.05	22.8	.042	.96	-	-	7.00	.33	0.	.056
C 210	101034.	.616	.000	20.2	1.05	22.8	.041	.93	-	-	4.00	.32	0.	.061
C 211	101034.	.616	.000	20.2	1.05	22.8	.038	.86	-	-	2.00	.36	0.	.061
C 212	101034.	.616	.000	20.2	1.05	22.8	.035	.80	-	-	1.00	.38	0.	.049
C 213	101034.	.616	.000	20.2	1.05	22.8	.032	.73	-	-	.50	.49	0.	.031

HYDRAULIC DIAMETER, D = .656 INCHES. AVERAGE VELOCITY, U = 19.2 FT/SEC, U^* = .885 FT/SEC.

* QUESTIONABLE DATA POINT. - NO DATA POINT.

TABLE B-1 (CONT.). TABULATION OF EXPERIMENTAL DATA.

CHANNEL D, GAP TRAVERSE, 1/9 INCH GAP SPACING.

RUN	REYNOLDS NUMBER	Z IN.	T IN.	$\bar{U}$ FT/SEC	$\bar{U}/U$	$\bar{U}/U^*$	$u'/\bar{U}$	u'/U^*	$v'/\bar{U}$	v'/U^*	CUTOFF KHZ	A/D	CURVE F(HZ)	FIT σ
D-1*	52625.	.476	.000	11.6	.92	18.6	.110	2.04	.076	1.45	1.00	-	-	-
D-2	52625.	.503	.000	12.2	.97	19.7	.083	1.68	.044	.86	1.00	.35	0.	.036
D-3	52625.	.530	.000	13.0	1.03	20.9	.070	1.46	.037	.77	1.00	-	-	-
D-4	52625.	.557	.000	13.8	1.09	22.1	.059	1.30	.031	.68	1.00	.47	0.	.029
D-5	52625.	.584	.000	14.4	1.14	23.2	.042	.97	.025	.59	1.00	-	-	-
D-6	52625.	.611	.000	14.8	1.17	23.8	.033	.79	.022	.52	1.00	.98	0.	.040
D-7	52625.	.637	.000	14.9	1.17	23.9	.032	.77	.022	.53	1.00	-	-	-
D-8	52625.	.664	.000	14.7	1.16	23.6	.039	.92	.023	.55	1.00	.96	0.	.039
D-9	52625.	.691	.000	14.2	1.12	22.8	.051	1.17	.027	.62	1.00	-	-	-
D-10	52625.	.718	.000	13.5	1.07	21.7	.068	1.47	.033	.72	1.00	.99	0.	.036
D-11	52625.	.745	.000	12.6	1.00	20.3	.085	1.73	.042	.85	1.00	-	-	-
D-12*	52625.	.772	.000	12.0	.95	19.3	.105	2.02	.071	1.36	1.00	-	-	-
D-13*	107953.	.496	.000	22.7	.90	20.2	.092	1.86	.041	.82	1.00	-	-	-
D-14	107953.	.523	.000	24.7	.98	21.9	.070	1.54	.028	.62	1.00	-	-	-
D-15	107953.	.550	.000	26.6	1.05	23.6	.055	1.30	.023	.53	1.00	.69	7.	.010
D-16	107953.	.577	.000	28.0	1.11	24.9	.042	1.03	.019	.47	1.00	-	-	-
D-17	107953.	.604	.000	28.9	1.14	25.6	.031	.79	.017	.44	1.00	-	-	-
D-18	107953.	.631	.000	29.2	1.15	25.8	.027	.70	.016	.43	1.00	.69	0.	.033
D-19	107953.	.657	.000	28.8	1.14	25.5	.032	.83	.018	.46	1.00	-	-	-
D-20	107953.	.684	.000	28.1	1.11	24.9	.043	1.07	.019	.48	1.00	.63	0.	.024
D-21	107953.	.711	.000	26.6	1.05	23.5	.055	1.29	.022	.53	1.00	-	-	-
D-22	107953.	.738	.000	24.6	.97	21.8	.075	1.64	.031	.67	1.00	.59	0.	.019
D-23*	107953.	.765	.000	22.5	.89	19.9	.095	1.89	.045	.90	1.00	-	-	-
D-24*	221023.	.491	.000	21.9	.86	21.4	.096	2.05	.048	1.02	1.00	-	-	-
D-25	221023.	.518	.000	24.1	.95	23.5	.076	1.78	.030	.71	1.00	.56	0.	.010
D-26	221023.	.545	.000	26.0	1.03	25.4	.059	1.49	.025	.63	1.00	-	-	-
D-27	221023.	.571	.000	27.6	1.09	26.9	.047	1.27	.021	.57	1.00	-	-	-
D-28	221023.	.598	.000	28.4	1.12	27.8	.036	1.01	.020	.55	1.00	.69	0.	.027
D-29	221023.	.625	.000	28.7	1.14	28.1	.029	.82	.019	.53	1.00	-	-	-
D-30	221023.	.651	.000	28.5	1.13	27.9	.033	.92	.019	.54	1.00	.58	0.	.026
D-31	221023.	.678	.000	27.4	1.08	26.7	.041	1.11	.021	.56	1.00	-	-	-
D-32	221023.	.705	.000	26.1	1.03	25.5	.057	1.45	.027	.68	1.00	-	-	-
D-33	221023.	.731	.000	24.4	.96	23.8	.071	1.69	.029	.70	1.00	-	-	-
D-34*	221023.	.758	.000	22.5	.89	22.0	.087	1.92	.042	.92	1.00	-	-	-

HYDRAULIC DIAMETER, D = .499 INCHES. AVERAGE VELOCITY, U = 25.3 FT/SEC. U^*=1.023 FT/SEC.

* QUESTIONABLE DATA POINT. - NO DATA POINT.

TABLE B-1 (CONT.). TABULATION OF EXPERIMENTAL DATA.

CHANNEL E, GAP TRAVERSE, 1/4 INCH GAP SPACING.

RUN	REYNOLDS NUMBER	Z IN.	Y IN.	$\bar{U}$ FT/SEC	$\bar{U}/U$	$\bar{U}/U^*$	$U/\bar{U}$	U/U^*	$V/\bar{U}$	V/U^*	CUTOFF KHZ	Λ/D	CURVE FIT F(HZ)	σ
E-1*	52791.	.963	.000	9.5	.86	17.7	.112	1.98	-	-	1.00	.15	0.	.060
E-2*	52791.	.976	.000	9.8	.88	18.3	.095	1.74	-	-	1.00	-	-	-
E-3*	52791.	.997	.000	10.2	.91	18.9	.089	1.68	-	-	1.00	.29	0.	.098
E-4	52791.	.530	.000	10.9	.98	20.3	.065	1.32	-	-	1.00	-	-	-
E-5	52791.	.569	.000	11.6	1.04	21.5	.051	1.10	-	-	1.00	.90	0.	.032
E-6	52791.	.597	.000	12.0	1.08	22.4	.035	.78	-	-	1.00	-	-	-
E-7	52791.	.631	.000	12.2	1.09	22.7	.031	.70	-	-	1.00	.90	0.	.039
E-8	52791.	.669	.000	12.0	1.08	22.4	.038	.84	-	-	1.00	-	-	-
E-9	52791.	.698	.000	11.5	1.03	21.4	.053	1.13	-	-	1.00	.93	0.	.039
E-10	52791.	.731	.000	10.7	.96	19.9	.072	1.43	-	-	1.00	-	-	-
E-11*	52791.	.765	.000	9.8	.88	18.3	.090	1.64	-	-	1.00	.29	0.	.093
E-12*	52791.	.778	.000	9.5	.85	17.6	.100	1.76	-	-	1.00	-	-	-
E-13*	52791.	.785	.000	9.3	.84	17.4	.113	1.97	-	-	1.00	-	-	-
E-14*	52714.	.496	.000	9.9	.89	18.5	.108	2.00	.079	1.36	1.00	.27	0.	.055
E-15	52714.	.523	.000	10.6	.96	19.8	.078	1.55	.043	.85	1.00	-	-	-
E-16	52714.	.557	.000	11.5	1.04	21.5	.060	1.30	.034	.73	1.00	.91	0.	.031
E-17	52714.	.590	.000	12.1	1.10	22.8	.040	.90	.026	.59	1.00	-	-	-
E-18	52714.	.629	.000	12.4	1.13	23.3	.032	.74	.023	.55	1.00	.39	0.	.050
E-19	52714.	.656	.000	12.3	1.11	23.0	.039	.91	.025	.58	1.00	-	-	-
E-20	52714.	.691	.000	11.8	1.07	22.1	.052	1.15	.029	.63	1.00	.91	0.	.030
E-21	52714.	.725	.000	10.9	.99	20.5	.070	1.43	.041	.84	1.00	-	-	-
E-22*	52714.	.751	.000	10.1	.91	18.9	.096	1.80	.059	1.12	1.00	.28	0.	.093
E-23	105455.	.506	.000	19.4	.87	19.7	.085	1.67	.050	.99	1.00	-	-	-
E-24	105455.	.533	.000	21.3	.94	21.4	.067	1.43	.033	.71	1.00	.99	0.	.025
E-25	105455.	.560	.000	22.4	1.00	22.8	.051	1.17	.027	.62	1.00	-	-	-
E-26	105455.	.586	.000	23.5	1.05	23.8	.038	.92	.023	.55	1.00	.52	0.	.029
E-27	105455.	.613	.000	23.9	1.07	24.3	.032	.78	.022	.53	1.00	-	-	-
E-28	105455.	.640	.000	24.0	1.07	24.3	.032	.78	.022	.52	1.00	.50	0.	.092
E-29	105455.	.667	.000	23.6	1.05	23.9	.038	.91	.022	.54	1.00	-	-	-
E-30	105455.	.694	.000	22.7	1.01	23.0	.049	1.12	.025	.57	1.00	.54	0.	.027
E-31	105455.	.721	.000	21.3	.95	21.7	.063	1.37	.031	.68	1.00	-	-	-
E-32	105455.	.747	.000	19.8	.89	20.2	.080	1.61	.046	.93	1.00	-	-	-
E-33*	216260.	.989	.000	18.9	.92	20.5	.094	1.94	.098	.98	1.00	-	-	-
E-34	216260.	.515	.000	20.2	.91	22.6	.067	1.52	.030	.69	1.00	.50	0.	.018
E-35	216260.	.542	.000	21.6	.97	24.3	.056	1.37	.026	.64	1.00	-	-	-
E-36	216260.	.569	.000	23.0	1.03	25.7	.042	1.08	.022	.55	1.00	-	-	-
E-37	216260.	.595	.000	23.6	1.06	26.4	.033	.87	.020	.54	1.00	.59	0.	.020
E-38	216260.	.622	.000	23.9	1.07	26.8	.029	.76	.019	.50	1.00	-	-	-
E-39	216260.	.649	.000	23.8	1.07	26.6	.031	.83	.019	.50	1.00	-	-	-
E-40	216260.	.675	.000	23.2	1.04	26.0	.039	1.03	.020	.52	1.00	.57	0.	.027
E-41	216260.	.702	.000	22.3	1.00	24.9	.050	1.24	.024	.59	1.00	-	-	-
E-42	216260.	.729	.000	21.1	.94	23.5	.061	1.44	.026	.61	1.00	-	-	-
E-43*	216260.	.756	.000	19.4	.87	21.7	.076	1.66	.034	.75	1.00	-	-	-
E-44*	216260.	.769	.000	18.9	.85	21.2	.081	1.72	.044	.93	1.00	-	-	-

HYDRAULIC DIAMETER, D = .565 INCHES. AVERAGE VELOCITY, U = 22.4 FT/SEC, U^* = .894 FT/SEC.

* QUESTIONABLE DATA POINT. - NO DATA POINT.

TABLE B-2. Tabulation of Pressure Drop Data

Channel	Flow (gpm)	Temp. (°F)	P_3-P_4 (a)	f_{34}	P_4-P_5 (a)	f_{45}	Re	$\bar{f}$
A	167.3	100.	1.60	.0199	1.58	.0196	69180.	.0197
	250.3	99.	3.22	.0179	3.17	.0176	102402.	.0177
1" Dia Rods	334.1	99.	5.57	.0173	5.43	.0169	136687.	.0171
	417.6	99.	8.40	.0167	8.50	.0169	170848.	.0168
	556.8	99.	13.98	.0157	13.77	.0154	229019.	.0155
	683.4	99.	20.40	.0152	19.95	.0148	281091.	.0150
	250.0	83.	8.09	.0199	7.79	.0191	79501.	.0195
A	300.0	84.	11.19	.0191	10.69	.0182	96546.	.0187
1 1/8" Dia Rods	403.0	82.	19.49	.0184	18.44	.0174	126625.	.0179
	503.0	82.	28.47	.0173	26.96	.0164	158045.	.0168
	600.0	83.	38.90	.0166	36.99	.0158	190802.	.0162
B	45.5	44.	1.08	.0235	1.14	.0248	22763.	.0241
	63.0	44.	1.95	.0221	2.00	.0227	31517.	.0224
	80.2	47.	2.97	.0208	3.05	.0213	42081.	.0211
	101.0	47.	4.47	.0197	4.60	.0203	52995.	.0200
	136.5	47.	7.65	.0185	7.85	.0190	71622.	.0187
	172.0	47.	11.60	.0176	11.80	.0179	90249.	.0178
	203.5	45.	15.70	.0171	16.00	.0174	104277.	.0172
	234.0	45.	20.15	.0166	20.68	.0170	119905.	.0168
C	58.5	44.	3.60	.0209	3.75	.0218	35363.	.0213
	62.0	44.	4.05	.0209	4.10	.0212	37178.	.0211
	81.4	46.	6.40	.0192	6.75	.0202	50802.	.0197
	87.0	47.	7.35	.0193	7.53	.0198	54727.	.0195
	121.3	46.	12.95	.0175	13.67	.0184	75703.	.0180
	124.0	47.	13.87	.0179	14.15	.0183	78002.	.0181
	146.1	45.	18.50	.0172	19.00	.0177	89743.	.0174
	113.0	71.	10.60	.0165	11.00	.0171	101026.	.0168
	170.3	45.	24.45	.0167	25.10	.0172	104609.	.0170
	170.5	46.	23.65	.0162	25.30	.0173	106409.	.0167
	210.5	46.	35.77	.0160	36.75	.0165	131373.	.0163
	219.3	46.	37.30	.0154	40.10	.0166	136865.	.0160
D	14.8	78.	1.07	.0267	1.01	.0252	18281.	.0259
	19.5	78.	1.74	.0250	1.60	.0230	24087.	.0240
	30.2	78.	3.76	.0225	3.34	.0200	37304.	.0213
	40.3	78.	6.12	.0206	5.43	.0183	49779.	.0194
	49.6	78.	8.76	.0195	7.70	.0171	61267.	.0183
	69.6	78.	16.11	.0182	14.00	.0158	85971.	.0170
	89.6	78.	25.49	.0173	21.99	.0150	110676.	.0162
E	15.2	70.	.96	.0246	.94	.0241	19613.	.0244
	30.3	70.	3.25	.0210	3.01	.0194	39097.	.0202
	39.9	70.	5.20	.0194	4.78	.0178	51484.	.0186
	49.4	70.	7.67	.0186	7.03	.0171	63742.	.0179
	65.4	70.	12.20	.0169	11.17	.0155	84388.	.0162
	77.2	70.	16.83	.0167	15.39	.0153	99613.	.0160

(a) Inches of 2.95 specific gravity oil

No. of Copies	Offsite
1	AEC Advisory Committee for Reactor Safeguards Washington, D.C. M. C. Gaskr
1	AEC Chicago Patent Office, Washington, D.C. G. H. Lee
7	AEC Directorate of Licensing, Washington, D.C. E. G. Case (3) V. Stello T. Novak D. Ross G. M. Lauben
2	AEC Directorate of Reactor Standards, Washington, D.C.
1	AEC Office of Assistant General Counsel for Patents Washington, D.C. R. A. Anderson
2	AEC Technical Information Center
20	AEC Division of Reactor Development and Technology Washington, D.C. Assistant Director, Reactor Technology Chief, Special Technology Branch Chief, Reactor Physics Branch Assistant Director, Reactor Engineering Chief, Core Design Branch Chief, Fuel Engineering Branch Assistant Director, Nuclear Safety Chief, Fast Reactor Safety Branch Chief, Thermal Reactor Safety Branch Chief, Analysis and Evaluation Branch Assistant Director, Plant Engineering Assistant Director, Program Analysis Chief, Water Projects Branch Chief, LMFBR Projects Branch E. Davidson F. Goldner R. Impara T. Speis R. M. Scroggins (2)

No. of Copies	Offsite
2	Argonne National Laboratory H. Fauske R. P. Stein
1	Atomic Energy Commission Brussels Office U.S. Mission to the European Communities APO, New York, N. Y. 09667
1	Atomic Energy of Canada, Limited Chalk River, Ontario, Canada G. A. Wikhammer
5	Atomics International P.O. Box 591, Canoga Park, California 91305 Louis Bernath Donald T. Eggan David C. Fulton H. Morowitz W. B. Wolfe
2	Babcock and Wilcox Company P.O. Box 1260 Lynchburg, Virginia 24502 R. E. Willard C. Morgan
2	Babcock and Wilcox Alliance Research Center 1562 Beeson Street Alliance, Ohio 44601 J. S. Gellerstadt G. D. Lindstrom
1	Brookhaven National Laboratory O. E. Dwyer
2	Chicago Operations Office Richard J. Bariboldi
1	Columbia University Department of Chemical Engineering J. E. Casterline

No. of Copies	Offsite
2	Combustion Engineering, Inc. F. Bevilacqua P. Zamola
1	duPont Company, Wilmington, Delaware 19898 J. S. Neill
1	Gulf-General Atomic P.O. Box 608 San Diego 12, California 92112 R. Katz
1	General Electric Company, San Jose (Trumbull) BRDO, Sunnyvale, California P. Magee
4	General Electric Company, San Jose Earl Janssen R. T. Lahey S. Levy W. Sutherland
1	Georgia Institute of Technology Novak Zuber
2	Idaho Nuclear, Inc. Idaho Falls, Idaho C. Solbrig L. Ybarrando
2	Jersey Nuclear Corp. Bellevue, Washington L. Bupp G. A. Sofer
1	Knolls Atomic Power Laboratory General Electric Company Schenectady, New York G. H. Halsey
1	Union Carbide Corporation (ORNL) Floyd L. Culler

No. of Copies	Offsite
1	Nuclear Fuel Services Rockville, Md. R. T. Berringer
1	Union Carbide Corp. (ORNL-Y-12) M. Fontana H. W. Hoffman
1	Gulf United Nuclear Fuels Corporation Grasslands Road Elmsford, New York H. S. Chung
1	University of Minnesota Department of Chemical Engineering Minneapolis, Minnesota 55455 H. S. Isbin
1	Westinghouse Bettis Atomic Power Laboratory S. Green
2	Westinghouse Electric Corporation H. Chelemer L. S. Tong
2	Westinghouse Electric Corporation Waltz Mill Site P.O. Box 158 Madison, Pa. E. Novendstern R. Markley
	Onsite-Hanford
1	AEC Chicago Patent Group R. M. Poteat
2	RDT Sr. Site Representative F. Standerfer

No. of Copies	Onsite-Hanford
54	Battelle-Northwest
	D. T. Aase
	R. T. Allemann
	N. E. Carter
	P. D. Cohn
	D. L. Condotta
	J. C. Fox
	S. Goldsmith
	B. M. Johnson
	C. W. Lindenmeier
	T. I. McSweeney
	C. A. Oster
	L. T. Pedersen
	D. S. Rowe (30)
	A. M. Sutey
	D. S. Trent
	C. L. Wheeler
	W. C. Wolkenhauer
	F. R. Zaloudek
	Technical Information Files (5)
	Technical Publications (1)
2	Douglas United Nuclear
	R. Shoemaker
	R. Baars
10	Westinghouse-Hanford
	R. E. Collingham
	J. M. Creer
	W. M. Gajewski
	J. W. Hagan
	K. M. Horst
	J. Muroaka
	R. E. Peterson
	J. F. Wett
	J. M. Yatabe